SCUOLA DOTTORALE IN

GEOLOGIA DELL'AMBIENTE E DELLE RISORSE

(SDIGAR)

Sezione Geologia delle Risorse Naturali

Ciclo XXVIII

GEOCHEMISTRY AND GEOCHRONOLOGY OF TRAVERTINE FROM THE INTERNAL APENNINE CHAIN (SOUTHERN TUSCANY): IMPLICATION FOR THE HYDROTHERMAL SETTING IN A POST-OROGENIC DOMAIN

Gabriele Berardi

A thesis submitted for the degree of Doctor of Philosophy at Università degli Studi Roma Tre

Academic Year 2015-2016

Supervisor:

Prof. Michele Soligo

Co-supervisors:

Dr. Andrea Billi

Prof. Federico Rossetti

Dr. Gianluca Vignaroli

Geochemistry and geochronology of travertine from the internal Apennine chain (Southern Tuscany): implication for the hydrothermal setting in a post-orogenic domain.

by

Gabriele Berardi

Abstract

Thermogene travertines form through precipitation of $CaCO_3$ from supersaturated fluids usually generated and discharged in volcano-tectonic settings, often deposited in proximity of active geothermal springs or along open fissures. This dissertation includes three main chapters presenting a multiscale and multidisciplinary study on the Quaternary travertine deposits from the Albegna basin, Southern Tuscany, Italy, with the main aim of understanding their spatio-temporal distribution and define the feedback relationships and controlling factors on their deposition. The Albegna basin is an excellent area for studying feedback relationships between travertine deposition tectonics, active geothermal systems and climate due to the coexistence of active and fossil travertine deposition, few kilometers south of the Mt. Amiata geothermal field. In the northern section of the Albegna basin, travertines are deposited at different altitudes along a N-S-striking alignment about 18 km long, comprised between the Semproniano village (to the north) and the Saturnia village (to the south). This work integrates geological-structural investigations, geochronological analyses, and geochemical investigations on travertines and associated mineralizations, focusing on the hydrothermal circulation at the scale of the basin and on selected single travertine deposits.

At the scale of the basin, the main novelty is that it was possible to reconstruct the 4D tectonic-hydrothermal system evolution over a distance of about 30 km and a time span of over 600 ka, through the spatio-temporal distribution of thermogene travertine deposits and other $CaCO_3$ mineralizations as well as their morphological, geological, structural, and geochemical characters. In particular, this work show a general rejuvenation of the travertine deposition, a cooling of the parental fluid

temperature and a lowering of the depositional altitude moving southward in the Albegna basin, moving away from the Mt. Amiata volcano. The Pleistocene travertine deposition of the Albegna basin was assisted by active tectonics, modulated by paleoclimate, within a region of positive geothermal anomaly to the south of the Mt. Amiata volcanic district. Wet climate conditions regulated the abundance of water, tectonic activity provided the permeability pathways, and the geothermal anomaly provided the ascension energy (heat) for convective hydrothermal circulation of percolating meteoric fluid(s) that interacted at depth with the carbonate reservoir.

At the scale of the single deposit, the modes and rates for the growth of the Semproniano fissure ridge and the relationships between travertine fissure ridges and plateaus were investigated, as well as the implications in terms of the CO_2 release, and the possible relationships between banded travertine formation and Quaternary paleoclimate-hydrological oscillations. Banded travertine of the Semproniano fissure ridge is the thickest continuous vein documented in the literature (50 m), and its thickness appears to be connected with its probable shallow emplacement and with the unusual longevity of the hydrothermal activity, longer than any other fissure ridge in literature (between at least 650 and 85 ka). The epithermal fluid supply feeding the Semproniano giant vein is not directly connected with the main volcanic paroxysmal activity of the Mt. Amiata volcano (which is younger than the early growth of the vein), rather with the positive geothermal anomaly associated with its pre eruptive stages through structurally-controlled fluid pathways which created and maintained active convection and supply of CO_2-enriched meteoric fluids. This work provide also an estimation of the long-term release of CO_2 from the Semproniano giant vein to improve our knowledge on the CO_2 cycle in the past in geothermal/volcanic provinces. Finally, in two travertine quarries in the Albegna basin, syn-diagenetic non-tectonic folding caused by progressive hydrothermal veining were recognized. Those presented are the first records of syn-diagenetic non-tectonic contractional deformations in thermogene travertines. The changes of some pristine rock properties such as fabric, porosity, stratigraphic-chronological sequence, and rheology, if disregarded or unrecognized, may significantly impact paleoclimate, neotectonics, paleohydrology, and hydrocarbon reservoirs.

Aknowledgments

During the last years I had the luck to be supported and believed in by many people which I would like to thank. I owe an enormous gratitude to my supervisor, prof. Michele Soligo and co-supervisors, dott. Andrea Billi, prof. Federico Rossetti, dott. Gianluca Vignaroli for their great support, scientific help, ideas, stimulating discussions, and for believing in me also when I didn't. It was a real pleasure and honour to work and learn with you.

I wish to thank the many good scientists which whom I had the fortune to work with during this study. Dr. Giuditta Fellin is thanked for her patience and assistance at ETH Zurich, with you I learned a lot. Dr. Sándor Kele is thanked for his assistance and friendship in and outside lab in Zurich, and for the great scientific collaboration. Prof. Stefano Bernasconi is thanked for letting me use the facilities of Stable Isotopes Lab at ETH Zurich and for revising my manuscripts. Thanks to Dott. Francesca Tecce for the time I spent in the Fluid Inclusions lab; it was a a real pleasure to work with you and to learn great technique. Prof. River and Dr. Oruç Baykara are thanked for the help with the U/Th ages in Taiwan. Prof. Francesca Castorina is thanked for her work on Sr, Nd isotopes and REE investigations. I want to thank Saturnia Travertini s.r.l. and Terme di Saturnia s.p.a. for the logistic help in the field. Infinite thanks go to my family and close friends for being with me during this journey, in particular to my sister Ginevra.

Table of Contents

Chapter 1

Introduction

Thermogene travertines form through precipitation of $CaCO_3$ from supersaturated fluids generated and discharged in regions often affected by recent tectonic and/or volcanic activity (Pentecost, 1995; Ford and Pedley, 1996; Hancock et al., 1996; Crossey et al., 2006). These deposits are usually associated with hot springs and are widely diffused in areas characterized by positive geothermal anomalies (Pentecost, 1995; Ford and Pedley, 1996; Minissale et al., 2002) representing therefore a marker for understanding the evolution of geothermal systems.

The importance of studying the travertine deposits resides in different aspects:

- Travertines have been shown to be reliable indicators of paleoclimate oscillations (i.e., glacial vs. interglacial and dry vs. wet periods), with obvious inferences on paleohydrogeological circuits (Rihs et al., 2000; Faccenna et al., 2008). Generally, Quaternary travertine deposition is correlated with warm and wet (interglacial) conditions (e.g., Dramis et al., 1999; Frank et al., 2000; Rihs et al., 2000; Soligo et al., 2002; Luque and Julià, 2007; Faccenna et al., 2008; Kampman et al., 2012; Priewisch et al. 2014), where high-stand levels of the water table supply huge amounts of fluids for the growth of travertine deposits. On the other hand, travertine formation in dry glacial periods (low-stand of the water table) has been documented and used to emphasize the importance of tectonic activity, rather than climate, to facilitate control travertine precipitation (e.g., Uysal et al., 2009; Brogi et al., 2010; Özkul et al., 2013).
- Thermogene travertine deposits have been studied for providing constraints on tectonic activity and earthquake occurrence in regions of active tectonism (e.g., Hancock et al., 1999, Uysal et al., 2007, 2009; Brogi and Capezzuoli, 2009; Brogi et al., 2010; De Filippis et al., 2013; Ricketts et al., 2014). In particular, deformation structures associated with

travertine deposition (i.e., fault and fracture networks), as well as the spatial distribution of peculiar travertine deposits (e.g., fissure ridge) can be correlated with state of tectonic stress used to constrain structurally-controlled fluid flow in geothermal areas.

- Travertine deposits have been investigated for constraining the palaeohydrological regimes (Crossey et al., 2006; Priewisch et al., 2014). In particular, a widespread travertine deposition can be related to an interplay between wet climate and high hydrothermal pressures, with fluids circulating through complex artesian aquifer systems and profoundly affected by endogenic.
- Travertine deposits have been also used as potential analogs of long-term outflow from artificial CO_2 storages (Shipton et al., 2004; Burnside et al., 2013; Bickle and Kampman, 2013). In particular, travertine deposits have been used to estimate past rates of CO_2 outgassing and the partitioning between CO_2 dissolved in carbonate minerals and direct escaped to the surface.

Southern Tuscany (central Italy; Fig. 1.1) is a key area for studying feedback relationships between travertine deposition tectonics, active geothermal systems and climate (e.g. Brogi et al., 2010; 2012). Southern Tuscany belongs to the inner sector of the Tertiary Apennines chain, an area characterized by an attenuated crustal section and diffuse fossil and active hydrothermalism associated with highly-productive geothermal areas (Batini et al., 2003; Buonasorte et al., 2007). Larderello-Travale and Mt. Amiata fields represents the most important geothermal areas of Italy, with an annual electrical production of more than 5300 GWh (Bertani, 2005). Geothermal anomalies and hydrothermalism in southern Tuscany are intimately connected to the Neogene post-orogenic extensional collapse of the Apennines chain and associated widespread Neogene-Quaternary magmatism all along the Tyrrhenian Sea margin (Innocenti et al., 1992; Marinelli et al., 1993; Serri et al., 1993; Carmignani et al., 1994; Jolivet et al., 1998). Here, high positive geothermal anomalies fed (and still feed) vigorous hydrothermal fluid circulation in Mesozoic reservoir carbonates, favoring

the deposition of widespread travertines at the surface in correspondence of tectonically-controlled settings (e.g., Minissale, 2004).

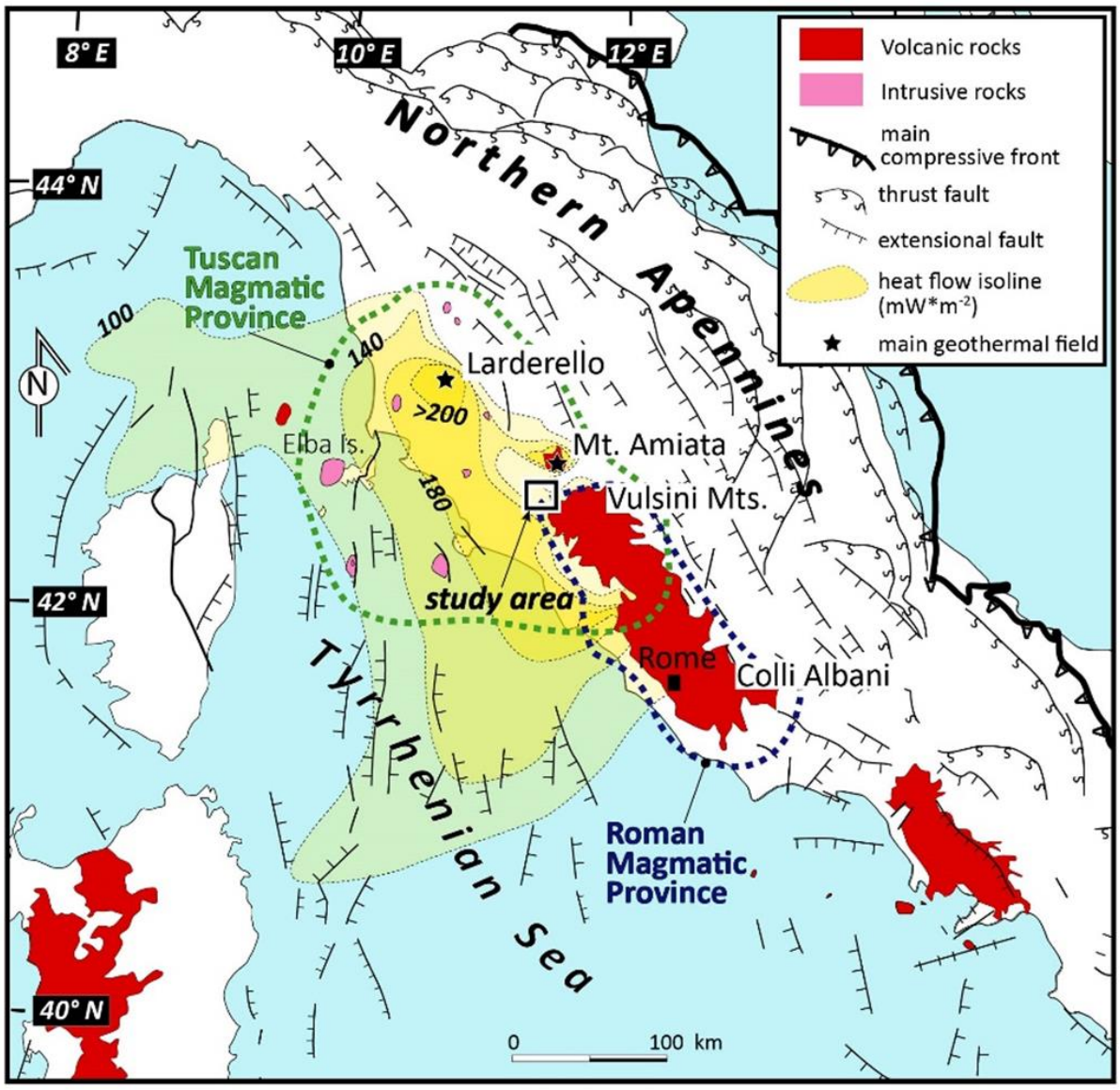

Figure 1.1 – Structural map of the Northern Apennines (Italy) showing main extensional fault systems, magmatic provinces (Tuscan Magmatic Province and Roman Magmatic Province, after Peccerillo, 2003 and Buttinelli et al., 2014), heat flow isolines (after Della Vedova et al., 2001), and geothermal fields. The study area near the Mt. Amiata and Vulsini Mts. volcanic districts is also shown.

During the last decades, multidisciplinary approaches have been addressed to the study of several travertine deposits of the southern Tuscany such as Rapolano (e.g. Guo and Riding, 1999; Brogi and Capezzuoli, 2009; Brogi et al., 2010), Sarteano (Brogi et al., 2012), Castelnuovo dell'Abate (Rimondi et al., 2015).

A poorly studied hydrothermal setting is represented by the Albegna basin, a morphotectonic depression localized few kilometers south of the Mt. Amiata geothermal field (Fig. 1.2). The Albegna basin, due to the coexistence of fossil and active travertine deposition (e.g. Bosi et al., 1996) and the presence of different travertine morphotypes (plateau and fissure ridge travertine) is an excellent area for studying the relationships between hydrothermalism, tectonics and paleoclimate, as well as their space-time evolution.

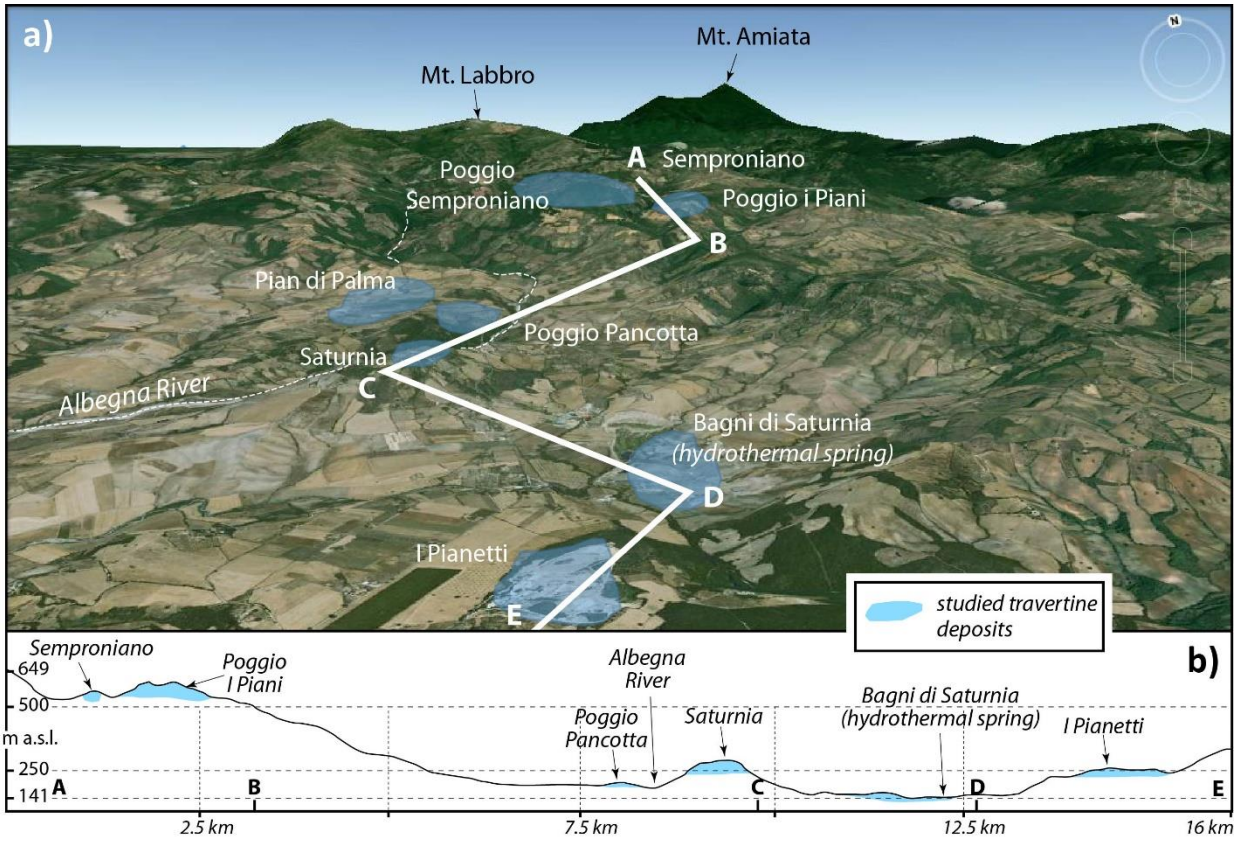

Figure 1.2 – (a) Northward panoramic view (Google Earth image) with localization of the studied travertine deposits in the Albegna basin. (b) Topographic profile illustrating the elevation of the main travertine deposits. The travertine elevation decreases from north (Sempronian) to south (Saturnia), where some hydrothermal manifestations and thermogene travertine deposition are active. See the A-B-C-D-E profile track in Figure 1.2(a).

This PhD thesis deals with the travertine deposition occurring in the northern portion of the Albegna basin. In particular, I focused my attention on a series of travertine deposits forming a N-S-striking alignment about 18 km long, comprised between the Sempronian village (to the north) and the Saturnia village (to the south) (Fig. 1.2a).

The main aims of this PhD work are: (1) to recognize different travertine morphotypes (e.g., fissure ridge vs. plateau) and to document their main geometrical properties (width, thickness), their spatial orientation, and their internal fabric (banded vs. bedded fabric); (2) to characterize the structural setting of the travertine deposits and their geometrical-structural relationships with adjacent units, with particular documentation of the tectonic-related structures (faults and associated fracture networks, calcite-filled veins) cut-crossing both the travertines and the other units; (3) to provide ages of deposition of the travertine deposits and the associated structures (calcite-filled veins, speleothems); (4) to geochemically characterize the travertine deposits by integrating different geochemical approaches.

All these specific aims provide insights addressed at the scale of the single travertine deposit, at the scale of the whole Albegna basin hydrothermal setting, at the regional scale, as well as general implication can be also provided. Results from this PhD work are finalized: (1) to determine the modes and growth rates of the travertine deposits, with particular attention to the fissure ridge in the Semproniano village; (2) to highlight the changes of the original travertine properties (sedimentary fabric, porosity, stratigraphic chronological sequence, and rheology) due to syn-diagenetic processes; (3) to reconstruct the spatio-temporal evolution of a hydrothermal system in a tectonically-controlled area; (4) to define the hydrothermal-hydrogeological circuit feeding the travertine-depositing thermal springs; (5) to provide constraints on the Quaternary tectonics of the Tuscany region, with implication on the neotectonics of the Tyrrhenian margin of the Apennines chain; (6) to understand the influences of Quaternary paleoclimate and hydrological oscillations on the travertine deposition.

Results from this research are reported in the following chapters and finalized in the conclusions chapter. This PhD thesis includes three main chapters that address different aspects of travertine deposition and growth using multiscale and multisciplinary approaches. These three chapters are all independent works with the common theme of hydrothermal circulation and travertine deposition in the Albegna valley. Each chapter has been written in the form of scientific paper for publication, therefore repetition of some material is necessary. Each chapter is composed by its own abstract,

introduction, methodologies, results, discussions, conclusions, references, and appendix sections. To accomplish these results using a multidisciplinary approach, I collaborated with several scientists and laboratories listed at the beginning of each chapter. I conducted the majority of field work, structural geology and geomorphologic survey, sampling and sampling strategy, U/Th dating (α spectrometry), C- and O- isotope analyses, and fluid inclusion microthermometry. I collaborated in performing and interpreting U/Th dating (MC-ICP-MS), Sr- and Nd- isotopes and REE data.

Chapter 2 deals with the relationships between hydrothermalism, tectonics, and paleoclimate during Quaternary time. In the Albegna basin, the occurrence of both fossil and active travertine deposits provides the opportunity to elucidate the evolution, both spatially and temporally, of a hydrothermal system in a tectonically-controlled area. Moreover, the Albegna basin is a case of hydrothermal setting located along the Tyrrhenian margin of the Apennines belt, where neotectonic fault systems are recognized to be oriented transversally to the belt trend. This study provides original, multidisciplinary, and multiscale results that can be generalized within the broad interest for tectonic-hydrothermal systems in areas of geothermal interest.

Chapter 3 deals with the relationships between hydrothermalism and tectonics during Quaternary time by investigating a giant carbonate vein (≥50 m thick; fissure ridge travertines) and nearby travertine plateaus in the Semproniano area (Mt. Amiata geothermal field). Our results can provide a progress in understanding the development of such uncommon geological structure (the thickest continuous vein hitherto documented in the literature found within a fissure ridge travertine) in very shallow crustal environment, and the convective fluid circulation attaining in hydrothermal-tectonic settings.

Chapter 4 deals with the syn-diagenetic non-tectonic folding caused by progressive hydrothermal veining recognized in two travertine quarries in the Albegna basin. Those presented are the first records of syn-diagenetic non-tectonic contractional deformations in thermogene travertines. The identification of these structures and related changes of rock properties is relevant for the frequent

use of thermogene travertines as proxy in paleoclimate, neotectonic, paleohydrological, paleoseismic, and hydrocarbon or CO_2 reservoir/storage studies.

Chapter 5 summarizes the conclusions obtained in the whole PhD work providing considerations and open problems for future research.

The general conclusion of this work is that the travertine deposits of the Albegna basin excellently document the feedback relationships between travertine deposition, hydrothermal fluid circulation, the Quaternary tectonics, and the paleoclimate oscillations.

References

Batini F., Brogi A., Lazzarotto A., Liotta D., Pandeli E. 2003. Geological features of the Larderello–Travale and Monte Amiata geothermal areas (southern Tuscany, Italy). Episodes, 26, 239-244.

Bertani R., 2005. World geothermal power generation in the period 2001–2005. Geothermics, 34, 651-690.

Bickle M., Kampman N., 2013. Lessons in carbon storage from geological analogues. Geology, 41, 525-526.

Bosi C., Messina P., Rosati M., Sposato A., 1996. Età dei travertini della Toscana meridionale e relative implicazioni neotettoniche. Memorie della Società Geologica Italiana, 51, 293-304.

Brogi A., 2008. The structure of the Monte Amiata volcano-geothermal area (Northern Apennines, Italy): Neogene-Quaternary compression versus extension. International Journal of Earth Sciences, 97, 677-703. DOI 10.1007/s00531-007-0191-1.

Brogi A., Capezzuoli E., 2009. Travertine deposition and faulting: the fault-related travertine fissure-ridge at Terme S. Giovanni, Rapolano Terme (Italy). International Journal of Earth Sciences (Geologische Rundschau), 98, 931–947.

Brogi A., Capezzuoli E., Ague R., Branca M., Voltaggio M., 2010. Studying travertines for neotectonics investigations: middle–late Pleistocene syn-tectonic travertine deposition at Serre di Rapolano (Northern Apennines, Italy). International Journal of Earth Sciences, 99, 1382–1398.

Brogi A., Capezzuoli E., Buracchi E., Branca M., 2012. Tectonic control on travertine and calcareous tufa deposition in a low-temperature geothermal system (Sarteano, Central Italy). Journal of the Geological Society, 169, 461–476.

Buonasorte G., Cataldi R., Ceccarelli A., Costantini A., D'Offizi S., Lazzarotto A., Ridolfi A., Baldi P., Barelli A., Bertini G., Bertrami R., Calamai A., Cameli G., Corsi R., D'Acquino C., Fiordelisi A., Gezzo A., Lovari F., 1988. Ricerca ed esplorazione nell'area geotermica di Torre Alfina (Lazio – Umbria). Bollettino della Società Geologica Italiana, 107, 265-337.

Buonasorte G., Cataldi R., Passaleva G., 2007. Geothermal Development In Italy: From Present To Future. Proceedings European Geothermal Congress 2007, Unterhaching, Germany, 30 May-1 June 2007.

Burnside N.M., Shipton Z.K., Dockrill B., Ellam R.M., 2013. Man-made versus natural CO_2 leakage: A 400 k.y. history of an analogue for engineered geological storage of CO_2. Geology, 41, 471–474.

Buttinelli M., Chiarabba C., Anselmi M., Bianchi I., De Rita D., Quattrocchi F., 2014. Crustal structure of Northern Latium (central Italy) from receiver functions analysis: New evidences of a post-collisional back-arc margin evolution. Tectonophysics, 621, 148-158.

Cadoux, A. and D.L. Pinti, 2009. Hybrid character and pre-eruptive events of Mt Amiata volcano (Italy) inferred from geochronological, petro-geochemical and isotopic data. Journal of Volcanology and Geothermal Research, 179, 169-190.

Carmignani L., Decandia F.A., Fantozzi P.L., Lazzarotto A., Liotta D., Meccheri M. 1994. Tertiary extensional tectonics in Tuscany (Northern Apennines, Italy). Tectonophysics, 238, 295-315.

Carmignani L., Conti P., Cornamusini G., Pirro A. 2013. Geological map of Tuscany (Italy). Journal of Maps, 9:4, 487-497, DOI: 10.1080/17445647.2013.820154.

Costantini A., Ghezzo C. & Lazzarotto A., 1984. Carta geologica dell'area geotermica di Torre Alfina (prov. Di Siena-Viterbo-Terni). ENEL, Unità Nazionale Geotermica – Pisa. Cartografia S.EL.C.A., Firenze.

Crossey L.J., Fischer T.P., Patchett P.J., Karlstrom K.E., Hilton D.R., Newell D.L., Huntoon P., Reynolds A.C., de Leeuw G.A.M., 2006. Dissected hydrologic system at the Grand Canyon: interaction between deeply derived fluids and plateau aquifer waters in modern springs and travertine. Geology, 34, 25-28.

De Filippis L., Faccenna C., Billi A., Anzalone E., Brilli M., Soligo M., Tuccimei P., 2013. Plateau versus fissure ridge travertines from Quaternary geothermal springs of Italy and Turkey: Interactions and feedbacks between fluid discharge, paleoclimate, and tectonics. Earth-Science Reviews, 123, 35-52.

Della Vedova B., Bellani S., Pellis G., Squarci P., 2001. Deep temperatures and surface heat flow distribution. In: Vai G.B. and Martini I.P. (Eds.): Anatomy of an Orogen: the Apennines and Adjacent Mediterranean Basins. Kluwer Academic Publisher, 65–76.

Dramis F., Materazzi M., Cilla G., 1999. Influence of climatic changes on freshwater travertine deposition: A new hypothesis. Physics and Chemistry of the Earth, Part A: Solid Earth and Geodesy, 24, 893-897, doi: 1127 10.1016/S1464-1895(99)00132-5.

Faccenna C., Soligo M., Billi A., De Filippis L., Funiciello R., Rossetti C., Tuccimei P., 2008. Late Pleistocene depositional cycles of the Lapis Tiburtinus travertine (Tivoli, central Italy): possible influence of climate and fault activity. Global and Planetary Change, 63, 299–308.

Ford T.D., Pedley H.M., 1996. A review of tufa and travertine deposits of the world. Earth-Science Reviews, 41, 117–175.

Frank N., Braum M., Hambach U., Mangini A., Wagner G., 2000. Warm period growth of travertine during the last 1150 interglaciation in Southern Germany. Quaternary Research, 54, 38–48. doi:10.1006/qres.2000.2135.

Guo L., Riding R., 1999. Rapid facies changes in Holocene fissure ridge hot spring travertines, Rapolano Terme, Italy. Sedimentology, 46, 1145-1158. doi:10.1046/j.1365-3091.1999.00269.x

Hancock P.L., Chalmers R.M.L., Altunel E., Çakir Z., 1999. Travitonics: using travertine in active fault studies. Journal of Structural Geology, 21, 903–916.

Innocenti F., Serri G., Ferrara G., Manetti P., Tonarini S., 1992. Genesis and classification of the rocks of the Tuscan Magmatic Province: thirty years after the Marinelli's model. Acta Vulcanology, 2, 247-265.

Jolivet L., Faccenna C., Goffé B., Mattei M., Rossetti F., Brunet C., et al., 1998. Midcrustal shear zones in post-orogenic extension: example from the northern Tyrrhenian Sea (Italy). Journal of Geophysical Research, 103, 12123–12160.

Kampman N., Burnside N.M., Shipton Z.K., Chapman H.J., Nicholl J.A., Ellam R.M., Bickle M.J., 2012. Pulses of carbon dioxide emissions from intracrustal faults following climatic warming. Nature Geoscience, 5, 352-358.

Luque J.A. and Julià R., 2007. U/Th dating of Quaternary travertines at the middle River Llobregat (NE Iberian Peninsula, Northwestern Mediterranean). Correlation with sea-level changes. Geologica Acta, 5, 109-117.

Marinelli G., Barberi F., Cioni R., 1993. Sollevamenti neogenici e intrusioni acide della Toscana e del Lazio settentrionale. Memorie della Società Geologica Italiana, 49, 279-288.

Martelli L., Moratti G., Sani F., 1989. Analisi strutturale dei travertini della Toscana meridionale (Valle dell'Albegna). Bollettino della Società Geologica Italiana, 108, 197-205.

Minissale A., Kerrick D.M., Magro G., Murrell M.T., Paladini M., Rihs S., Sturchio N.C., Tassi F., Vaselli O., 2002. Geochemistry of Quaternary travertines in the region north of Rome (Italy): structural, hydrologic, and paleoclimatic implications, Earth and Planetary Science Letters, 203, 709-728.

Minissale A., 2004. Origin, transport and discharge of CO_2 in central Italy. Earth-Science Reviews, 66, 89-141.

Özkul M., Kele S., Gökgöz, A., Shen C.C., Jones B., Baykara M.O., Fórizs I., Nemeth T., Chang Y.-W., Alçiçek M.C., 2013. Comparison of the Quaternary travertine sites in the Denizli Extensional Basin based on their depositional and geochemical data. Sedimentary Geology, 294, 179–204.

Peccerillo A., 2003. Plio-Quaternary magmatism in Italy. Episodes, 26, 222-226.

Pentecost A., 1995. The Quaternary travertine deposits of Europe and Asia Minor. Quaternary Science Reviews, 14, 1005–1028.

Priewisch A., Crossey L.J., Karlstrom K.E., Polyak V.J., Asmerom Y., Nereson A., Ricketts J.W., 2014. U-series geochronology of large-volume Quaternary travertine deposits of the southeastern Colorado Plateau: Evaluating episodicity and tectonic and paleohydrologic controls. Geosphere, 10, 401-423.

Rihs S., Condomines M., Poidevin J.L., 2000. Long-term behaviour of continental hydrothermal systems: U-series study of hydrothermal carbonates from the French Massif Central (Allier Valley). Geochimica et Cosmochimica Acta, 64 (18), 3189-3199.

Ricketts J.W., Karlstrom K.E., Priewisch A., Crossey L.J., Polyak V.J., Asmerom Y., 2014. Quaternary extension in the Rio Grande rift at elevated strain rates recorded in travertine deposits, central New Mexico. Lithosphere, 6, 3–16.

Rimondi V., Costagliola P., Ruggieri G., Benvenuti M., Boschi C., Brogi A., Capezzuoli E., Morelli G., Gasparon M., Liotta D., 2015. Investigating fossil hydrothermal systems by means of fluid inclusions and stable isotopes in banded travertine: an example from Castelnuovo dell'Abate (southern Tuscany, Italy). International Journal of Earth Sciences, 1-21.

Serri, G., Innocenti, F., Manetti, P., 1993. Geochemical and petrological evidence of the subduction of delaminated Adriatic continental lithosphere in the genesis of the Neogene-Quaternary magmatism in central Italy. Tectonophysics, 223, 117-147.

Shipton Z.K., Evans J.P., Kirchner D., Kolesar P.T., Williams A.P., Heath J., 2004. Analysis of CO_2 leakage through "low-permeability" faults from natural reservoirs in the Colorado Plateau, southern Utah. Geological Society, London, Special Publications, 233, 43-58.

Soligo M., Tuccimei P., Barberi R., Delitala M.C., Miccadei E., Taddeucci A., 2002. U/Th dating of freshwater travertine from Middle Velino Valley (Central Italy): paleoclimatic and geological implications. Palaeogeography, Palaeoclimatology, Palaeoecology, 184, 147-161.

Uysal I.T., Feng Y., Zhao J.X., Altunel E., Weatherley D., Karabacak V., Cengiz O., Golding S.D., Lawrence M.G., Collerson K.D., 2007. U-series dating and geochemical tracing of late Quaternary travertine in co-seismic fissures: Earth and Planetary 1068 Science Letters, 257 (3–4), 450–462.

Uysal I.T., Feng Y., Zhao J.X., Isik V., Nuriel P., Golding S.D., 2009. Hydrotermal CO_2 degassing in seismically active zones during the late Quaternary. Chemical Geology, 265, 442–454.

Vignaroli G., Pinton A., De Benedetti A.A., Giordano G., Rossetti F., Soligo M., Berardi G., 2013. Structural compartmentalisation of a geothermal system, the Torre Alfina field (central Italy). Tectonophysics, 608, 482-498

Chapter 2

This chapter consists of a paper submitted to Litosphere (Vignaroli G., Berardi G., Billi A., Kele S., Rossetti F., Soligo M., Bernasconi S.M. "Tectonics, hydrothermalism, and paleoclimate recorded by Quaternary travertines and their spatio-temporal distribution in the Albegna basin, central Italy: insights on the Tyrrhenian margin neotectonics"), focusing on the relationships between hydrothermalism, tectonics and paleoclimate during Quaternary time in the Albegna basin of southern Tuscany (central Italy), with a final overview on the Tyrrhenian margin neotectonics.

Tectonics, hydrothermalism, and paleoclimate recorded by Quaternary travertines and their spatio-temporal distribution in the Albegna basin, central Italy: insights on the Tyrrhenian margin neotectonics

Abstract

The Neogene-Quaternary Albegna basin (southern Tuscany, central Italy), located to the south of the active geothermal field of Monte Amiata, hosts fossil and active thermogene travertine deposits, which are used in this work to reconstruct the spatio-temporal evolution of the feeding hydrothermal system. Travertine deposition interferes with regional tectonics that operated through distributed N-S- and ~E-W-striking transtensional fault arrays. The geochronological dataset ($^{230}Th/^{234}U$, Uranium-series disequilibrium) indicates a general rejuvenation (from >350 to <40 ka) of the travertine deposits moving from north to south and from higher to lower elevations. The recognized negative $\delta^{13}C$ and positive $\delta^{18}O$ correlations with younger deposition ages and lower depositional elevations provide evidence for a change in space and time of the hydrothermal fluid supply, suggesting a progressive dilution of the endogenic fluid sources due to continuous meteoric inputs. Comparison with paleoclimate records suggests increased travertine deposition during (humid) interglacial periods characterized by high-stands of the water table. In conclusion, the travertine deposits of the Albegna basin have recorded the interactions and feedbacks between tectonics, hydrothermalism, and paleoclimate within a region of positive geothermal anomaly during the Quaternary. These results shed also light on the neotectonic evolution of the Tyrrhenian margin of central Italy, where

hydrothermalism is distributed along margin-transverse structures during Pleistocene-Holocene times. It is hypothesized that originally upper-crustal, margin-transverse transfer faults have evolved to througoing crustal features during Quaternary times, providing structurally-controlled pathways for hydrothermal otwlow in the region. We suggests this was the consequence of a change in the relative magnitude of the principal stress vectors in the hinterland domain of the Apennine chain that occurred under a regional stress field dominated by a continuos NE-SW-direct maximum extension direction.

2.1. Introduction

Hydrothermal settings are common in many tectonically-active continental regions (Browne, 1978; Bibby et al., 1995; Rae et al., 2003; Newell et al., 2005; Crossey et al., 2006; Uysal et al., 2009; Cas et al., 2011; Mazzini et al., 2012; Baillieux et al., 2013; Karlstrom et al., 2013; Ricketts et al., 2014; Sella et al., 2014), where active faulting and fracturing provide viable pathways for circulation and mixing of endogenic and meteoric fluids, leading to diffuse mineralization and hydrothermal outflow (Curewitz and Karson, 1997; Cox et al., 2001; Rowland and Sibson, 2004; Billi et al., 2007; Gudmundsson, 2011; Bigi et al., 2015; Crossey et al., 2015; Vignaroli et al., 2015).

In hydrothermal settings where carbonate-enriched fluids circulate within calcareous reservoirs, thermogene travertine is the common $CaCO_3$ sinter precipitated from thermal springs (Pentecost, 1995; Ford and Pedley, 1996; Pentecost, 2005). Thermogene travertine deposits have been documented to represent important markers for the mode and style of tectonic activity within hydrothermal settings (e.g., Altunel and Hancock, 1993; Hancock et al., 1999; Altunel and Karabacak, 2005; Uysal et al., 2007; Faccenna et al., 2008; Brogi and Capezzuoli, 2009; Brogi et al., 2010a; De Filippis and Billi, 2012; De Filippis et al., 2013b; Frery et al., 2015). Moreover, thermogene travertine has been used as a reliable indicator of paleoclimatic oscillations (Rihs et al., 2000; Soligo et al., 2002; Faccenna et al., 2008; Uysal et al., 2009; De Filippis et al., 2013; Toker et al., 2015) and palaeohydrological regimes (Crossey et al., 2006; Crossey and Karlstrom, 2012; Priewisch et al., 2014).

The region of Tuscany in central Italy (Fig. 2.1) is characterized by diffuse fossil and active hydrothermalism associated with highly productive geothermal areas of the Larderello-Travale and Mt. Amiata fields (Batini et al., 2003; Buonasorte et al., 2007). These geothermal fields are characterized by heat flux higher than 600 $mW \cdot m^{-2}$ (Della Vedova et al., 2001) and collectively provide an annual electrical production of more than 5300 GWh (Bertani, 2005). Hydrothermalism in Tuscany is originated by high heat flow due to Miocene-Quaternary post-orogenic thinning of the central Apennines chain (present-day crustal thickness is about 22-24 km; Locardi and Nicolich,

1988; Billi et al., 2006) and associated emplacement of dominantly anatectic products of the Late Miocene-Pleistocene Tuscan Magmatic Province (Innocenti et al., 1992; Marinelli et al., 1993; Serri et al., 1993; Carmignani et al., 1994; Jolivet et al., 1998). Active hydrothermal springs and gas manifestations, including active travertine-depositing springs (e.g., Minissale, 2004; Barazzuoli et al., 2013; Capezzuoli, 2013), are the main present-day features of ongoing hydrothermal activity, particularly in southern Tuscany (Figs. 2.1 and 2.2). Recent studies of travertine and hydrothermal ore deposits have documented structurally-controlled fluid flow in the region (e.g., Bellani et al., 2004; Brogi and Fabbrini, 2009; Brogi et al., 2010a; Liotta et al., 2010; Rossetti et al., 2007, 2011, Rimondi et al., 2015). In particular, Plio-Pleistocene faulting played a primary role into the endogenic fluid circulation that fed and still feeds some geothermal fields and $CaCO_3$-rich springs in the Mt. Amiata geothermal area (Brogi et al., 2012). This geological setting makes Tuscany an excellent area for studying the relationships between hydrothermalism and tectonics, and their spatio-temporal evolution, through thermogene travertine deposits.

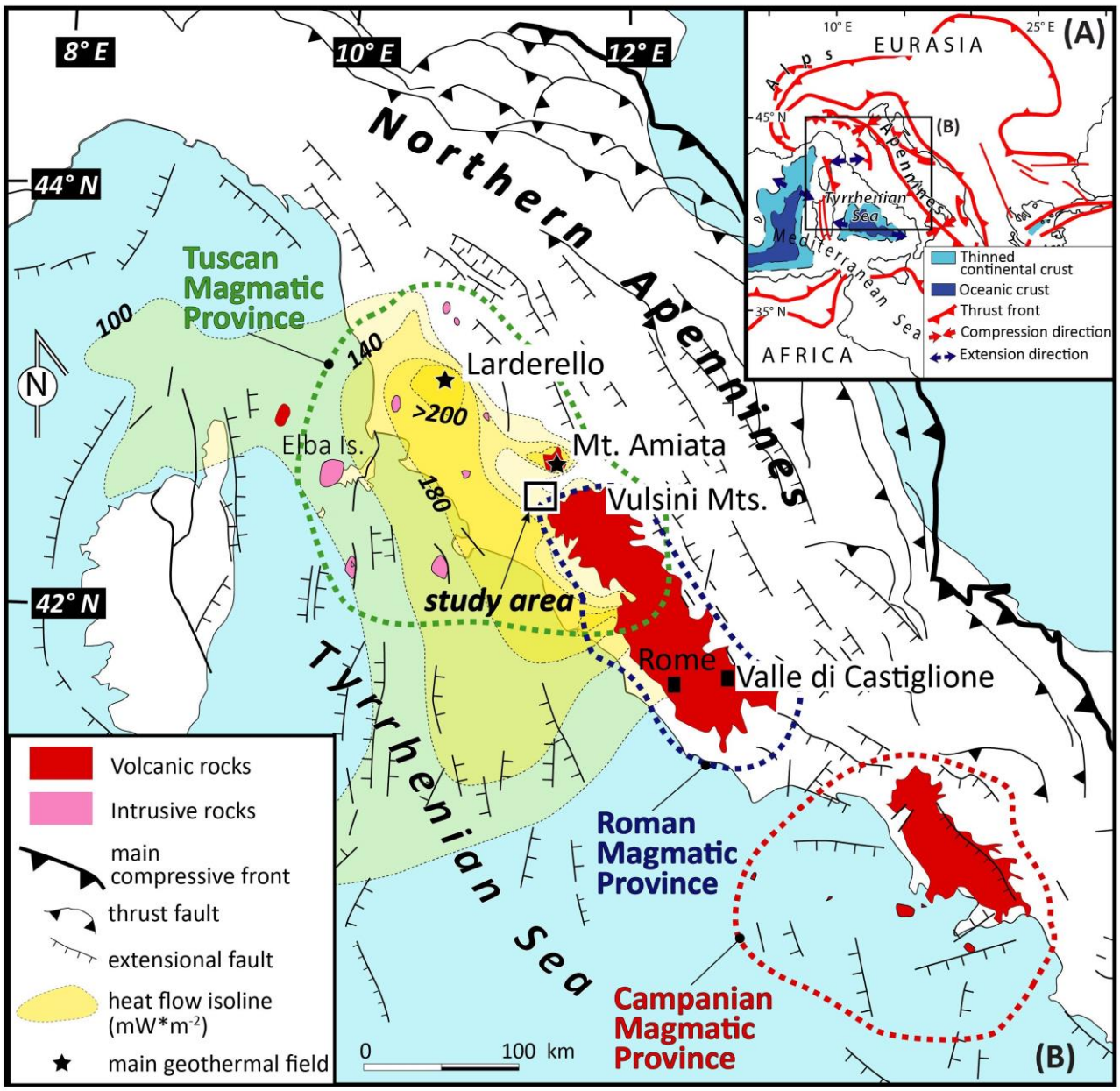

Figure 2.1 – (A) Schematic tectonic map of the central Mediterranean region illustrating the trend of the main thrust fronts and the location of back-arc extensional domains (modified after Jolivet et al., 1998); (B) Geological map of the Northern Apennines (Italy) showing main extensional fault systems, magmatic provinces (Tuscan Magmatic Province and Roman Magmatic Province, after Peccerillo, 2003 and Buttinelli et al., 2014), heat flow isolines (after Della Vedova et al., 2001), and geothermal fields. The study area near the Mt. Amiata and Vulsini Mts. volcanic districts is also shown.

This paper addresses the relationships between Quaternary hydrothermalism, tectonics, and paleoclimatic evolution in the Neogene-Quaternary Albegna basin of southern Tuscany (Fig. 2.2). Our multidisciplinary approach integrates structural investigations, geochronological analyses ($^{230}Th/^{234}U$, Uranium-series disequilibrium), and stable isotope ($\delta^{13}C$ and $\delta^{18}O$) systematics on

selected carbonate structures (bedded and banded travertines and calcite-filled veins). The main objectives are (1) to reconstruct the spatio-temporal evolution of a hydrothermal system in a tectonically-controlled area of geothermal interest, and (2) to discuss possible implications on the neotectonic regime along the Tyrrhenian margin in central Italy.

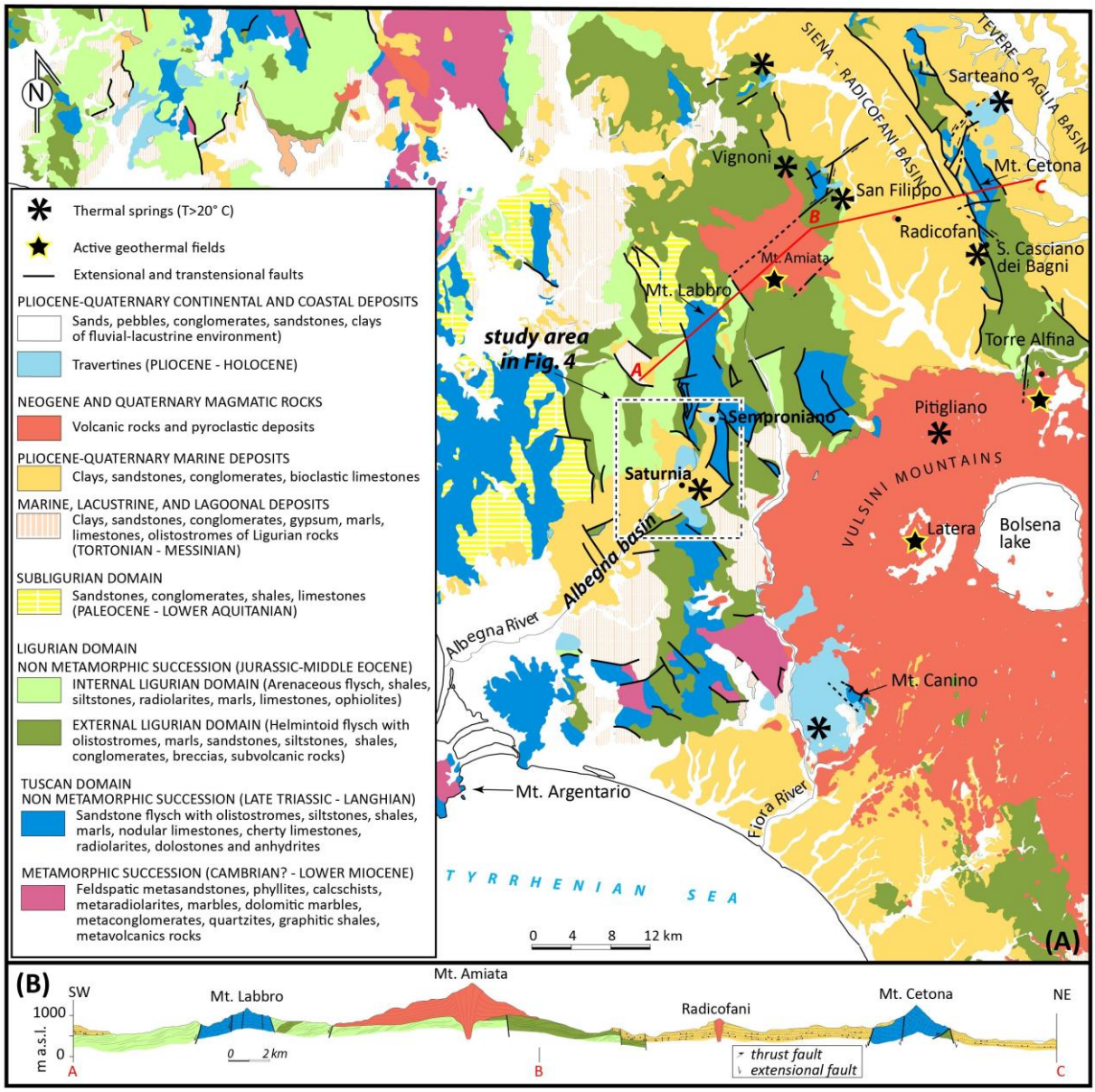

Figure 2.2 – (A) Geological-structural map of southern Tuscany showing main post-orogenic fault zones and travertine deposits (partially redrawn and adapted after Carmignani et al., 2013). The location of the study area is indicated with a dashed rectangle. Tectonic structures are from Costantini et al. (1984), Buonasorte et al. (1988), Martelli et al. (1989), Brogi (2008), Brogi et al. (2010, 2012), Carmignani et al. (2013), and Vignaroli et al. (2013). The map also shows main geothermal fields and thermal springs (after Minissale, 2004). (B) Geological cross-section through the Mt. Amiata volcanic district (redrawn and readapted after Jacobacci et al., 1967) showing post-orogenic structures such as faults, sedimentary basins, and volcanic districts. See the A-B-C cross-section track in Figure 2.2A.

2.2. Geological setting

Southern Tuscany is part of the hinterland domain (on the Tyrrhenian Sea) of the Paleogene-Quaternary northern Apennines chain (Fig. 2.1). The Apennines orogenic construction has resulted from the Meso-Cenozoic tectonic convergence between the European and African plates (e.g. Dewey et al., 1989; Boccaletti et al., 1990; Wortel & Spakman, 2002). The convergence has been characterized by Cenozoic eastward retreating subduction of the African subducting plate (Royden et al., 1987; Doglioni, 1991; Faccenna et al., 2004; Rosenbaum & Lister, 2004) inducing (i) a general eastward migration of thrust fronts and foredeep basins in a classic piggy-back sequence toward the foreland (e.g., Patacca et al., 1990; Cipollari and Cosentino, 1995; Massoli et al., 2006) and (ii) crustal-scale extension in the hinterland (Tyrrhenian Sea) (e.g. Malinverno and Ryan, 1986; Jolivet et al., 1998).

In southern Tuscany (Fig. 2.2A), Miocene-to-Quaternary post-orogenic sedimentary sequences (Martini and Sagri, 1993; Liotta, 1994; Pascucci et al., 2006; Brogi and Liotta, 2008; Brogi, 2011; Brogi et al., 2013; 2014) unconformably overlie a tectonic nappe-stack composed of, from top to bottom (Carmignani et al., 2013 and references therein): (i) oceanic-derived units of the Ligurian Domain, consisting of marly-arenaceous flysch-type and discontinuous ophiolitic sequences (Lower Cretaceous to Upper Eocene in age) and (ii) continental-derived units of the Tuscan Domain, including a non-metamorphic succession (Mesozoic carbonate and Cenozoic marly and siliciclastic sedimentary sequences of the Tuscan Nappe) and the underlying metamorphic units of the Tuscan Metamorphic Domain. These units are presently exposed in NNW-SSE- (as in the Mt. Cetona area) and N-S- (as in the Mt. Labbro area) trending elongate structural highs bounded by extensional and transtensional faults (e.g., Brogi, 2004a; Bonciani et al., 2005; Brogi and Fabbrini, 2009; Carmignani et al., 2013; Fig. 2.2B).

There are two opposing interpretations of the Neogene-Quaternary tectonics of southern Tuscany. The most common interpretation favors a post-orogenic extensional regime acting at the rear (west) of the eastward-migrating compressional front (e.g., Carmignani et al., 1994; Keller et al.,

1994; Lavecchia et al. 1994; Faccenna et al. 1997; Barchi et al., 1998; Jolivet et al., 1998; Martini et al., 2001; Collettini et al., 2006). This regime has led to the formation of orogen-parallel extensional basins, where NW-striking basin-boundary faults have been dissected by transverse transfer zones, the latter accommodating differential rates and amounts of extension between adjacent extensional compartments (Liotta, 1991; Faccenna et al., 1994; Acocella and Funiciello, 2002; 2006; Liotta et al., 2015). Alternatively, a Miocene-Pliocene shortening regime has been described as having being active in Tuscany, causing basement duplexing and out-of-sequence thrusting (e.g., Boccaletti et al., 1997; Cerrina Feroni et al., 2006; Musumeci and Vaselli, 2012; Bonini et al., 2014). In this latter interpretation, extensional and strike-slip faulting would represent the most recent mode of deformation in Tuscany.

Late Miocene-Quaternary magmatism is localized along the Tyrrhenian margin (e.g., Peccerillo, 2003; Conticelli et al., 2015) (Fig. 2.1) and characterized in Tuscany by acidic intrusive and volcanic products with associated HT metamorphism (e.g., Innocenti et al., 1992; Serri et al., 1993; Acocella and Rossetti, 2002; Rocchi et al., 2002; Dini et al., 2005; Rossetti et al., 2007; 2008; Farina et al., 2010; Cifelli et al, 2012). The Tuscan Magmatic Province hosts fossil and active hydrothermal systems. Endogenic fluid circulation within hydrothermal systems has been dominantly channelized by possibly-active extensional faults (e.g., Barberi et al., 1994; Buonasorte et al., 1988; Chiarabba et al., 1995; Gianelli et al., 1997; Batini et al., 2003; Bellani et al., 2004; Annunziatellis et al., 2008; Brogi, 2008; Liotta et al., 2010; Rossetti et al., 2008; 2011; Brogi et al., 2015).

The Mesozoic carbonate units of the Tuscan Nappe has exerted a pivotal role in the functioning of the entire geothermal-hydrothermal setting of Tuscany. At the surface and shallow levels, these rocks provide the recharge areas where meteoric waters infiltrate to depth thanks to the well-developed fault-fracture permeability network. At depth, the carbonate rocks constitute the reservoirs where meteoric and endogenic fluids circulate and mix before ascending to feed surface thermal springs and CO_2 emission centers (e.g., Batini et al., 2003; Minissale, 2004). Active and fossil travertine deposits occur with variable size and shape in proximity of the exposed Mesozoic

carbonates and at the peripheries of the main volcanic centers (Mt. Amiata and Vulsini Mountains in Fig. 2.2A). As explained above, these travertine deposits originated from the long-term interaction between faults, fractures, and hydrothermal fluids during the Quaternary (Brogi, 2004b; Brogi et al., 2012).

The Albegna basin is a tectonic depression striking NE-SW in its southern portion and turning to N-S in its northern portion (Fig. 2.2A), thus oriented oblique-to-perpendicular to the strike of the major extensional NW-SE basin-boundary faults. The Albegna basin is delimited to the north by the Mt. Amiata volcanic district (300-190 ka; Cadoux and Pinti, 2009; Laurenzi et al., 2015; Marroni et al., 2015) and to the south-east by the Vulsini Mountains volcanic district (590-127 ka; Nappi et al., 1995). The Albegna basin is filled by marine and transitional sediments, which are late Miocene to Quaternary in age. These deposits consist of marine clays, regressive sands, gravels, and conglomerates covered by aeolian sands and fluvial clays (Zanchi and Tozzi, 1987; Bettelli et al., 1990; Bonazzi et al., 1992; Bossio et al., 1993; Bossio et al., 2003). Steeply-dipping N-S- and E-W-striking tectonic structures, mainly consisting of extensional and oblique-to-strike-slip faults, dissect both the basin-filling deposits and the substratum (Zanchi and Tozzi, 1987; Brogi, 2004a; Bellani et al., 2005; Brogi and Fabbrini, 2009). In particular, N-S-striking extensional faults bound the Mesozoic carbonate units exposed in the northern portion of the basin, along the Mt. Labbro structural high (e.g., Bettelli et al., 1990; Brogi, 2004a; Carmignani et al., 2013; Fig. 2.2A).

Both regional uplift (related both to regional tectonics and to the Mt. Amiata volcanic bulging) and eustatic fluctuations contributed to the morphological shaping of the Albegna basin during the Pleistocene-Holocene period (Piccini et al., 2015). In fact, marine Pliocene sediments presently occur up to about 600 m a.s.l. and multiple Quaternary alluvial terraces occur at different elevations between 50 and 300 m a.s.l. The present landscape of low rolling hills is dominated by the alternation of morphological depressions (mostly filled by Quaternary deposits) and positive morphotypes, both being affected by well-pronounced escarpments and canyon incisions.

As demonstrated by the geochemistry of numerous thermal springs, the hydrogeological setting of the Albegna basin and surrounding areas is mainly conditioned by the deep aquifer occurring within the Mesozoic carbonate units of the Tuscan Nappe (e.g., Baldi et al., 1973; Duchi et al., 1992; Chiodini et al., 1995; Minissale, 2004). This aquifer has experienced important vertical oscillations during the Quaternary, as also shown by the occurrence of speleogenic markers and landscape changes (Piccini et al., 2015). Presently, the general southward drainage is toward the Saturnia thermal springs (Fig. 2.2A), where gas emissions and travertine deposition are still active (Minissale, 2004).

In the northern part of the Albegna basin, a series of travertine deposits lies unconformably on top of the Neogene sediments (Zanchi and Tozzi, 1987; Bosi et al., 1996; Barilaro et al., 2012). Some of these travertine deposits are affected by faults with associated damage zones and joint networks. These deformations have been considered as resulting from either Pliocene-Pleistocene extensional tectonics (Zanchi and Tozzi, 1987), or alternating contractional and extensional tectonic phases active in southern Tuscany during the Late Pleistocene (Martelli et al., 1989). Based on morphological and stratigraphic characters of the Albegna travertine deposits, Bosi et al. (1996) proposed discrete phases of travertine deposition over a long time interval between Messinian and Holocene times. So far, the only available radiometric age (218 +39/-27 ka) available for the Albegna travertine deposits was determined on a travertine sample collected in a quarry located immediately to south of the Saturnia village (Taddeucci and Voltaggio, 1987). Additional radiometric age dating are thus required to constrain (1) the ages of these travertine deposits and (2) their possible relationships with the hydrothermal, tectonic, and climatic conditions within the Albegna basin and the greater Tuscan region.

2.3. Workflow, methods, and nomenclature

Structural investigations have been carried out along a N-S trending transect in the northern part of the Albegna basin, where a series of travertine deposits are exposed. From north to south,

these deposits are named: Semproniano ridge, Poggio Semproniano, Poggio i Piani, Pian di Palma, Poggio Pancotta, Saturnia village, Bagni di Saturnia, and I Pianetti (Fig. 2.3A and Table 2.1). Field observations have been focused on the recognition of: (i) the different travertine morphotypes (plateau *vs*. fissure ridge travertines), (ii) the different styles of travertine deposition and precipitation (bedded *vs*. banded travertines), (iii) the geometric relationships between the travertine deposits and the surrounding units, and (iv) the structural features (fault and fracture systems) post-dating travertine deposition. Fault and fracture systems have been studied in terms of their geometry (attitude, spacing, aperture, persistence, and crosscutting relationships) and kinematics. Results of our field investigations (Table 2.2) are synthesized in the geological-structural map of Figure 2.4.

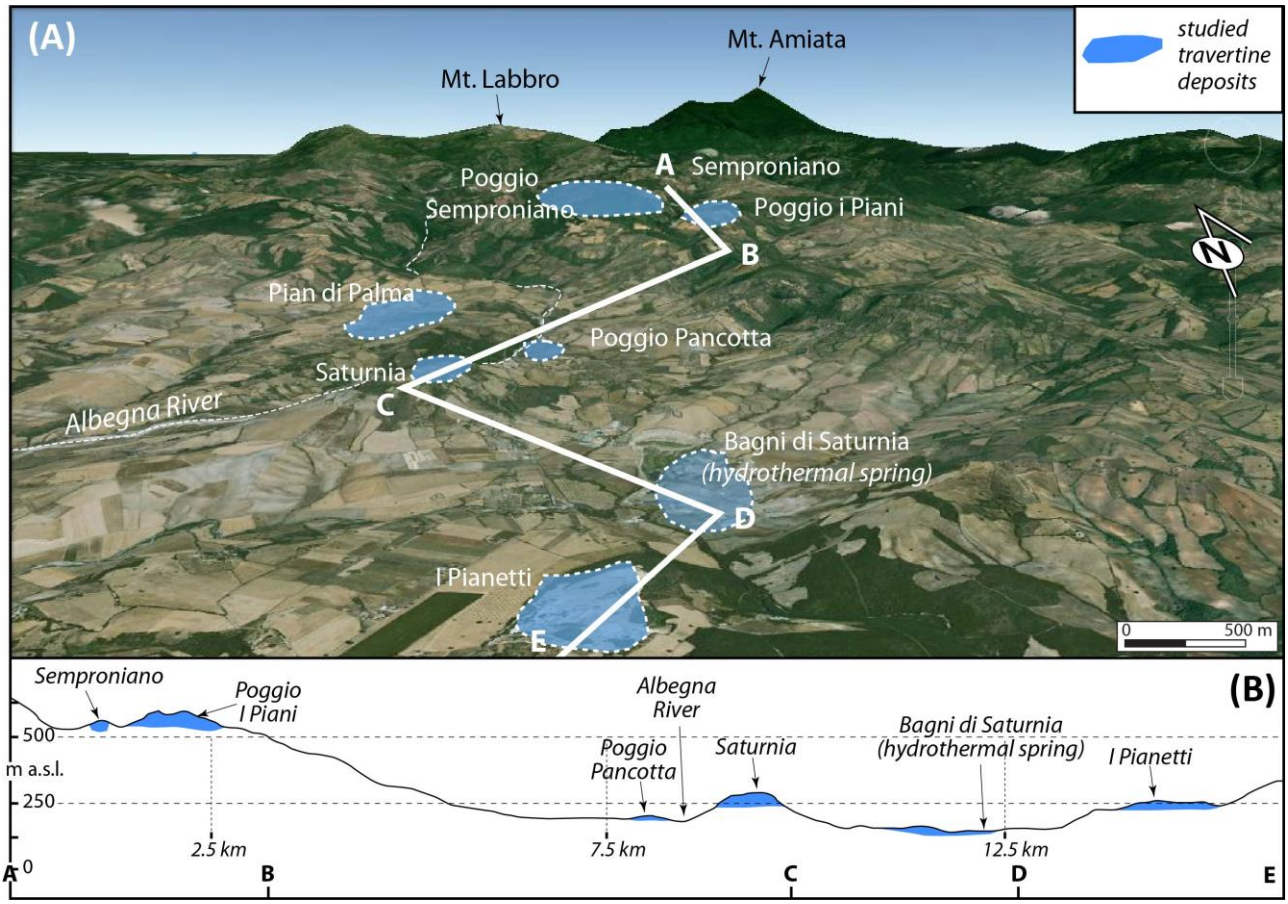

Figure 2.3 - (A) Northward panoramic view (Google Earth image) with localization of the studied travertine deposits in the Albegna basin. (B) Topographic profile illustrating the elevation of the main travertine deposits. The travertine elevation decreases from north (Semproniano) to south (Saturnia), where some hydrothermal manifestations and thermogene travertine deposition are active. See the A-B-C-D-E profile track in Figure 2.3A.

Fissure ridges are defined as elongate mound-shaped travertine deposit, straight or curved in map view, with a main crestal fissure, and length spanning from a few meters to several hundreds of meters (e.g., Hancock et al. 1999; Altunel and Karabacak, 2005; Brogi and Capezzuoli, 2009; De Filippis and Billi, 2012; De Filippis et al., 2013). Travertine plateaus are defined as travertine deposit characterized by centimeter-thick, subhorizontal bedding. Usually, travertine plateaus form tabular body wider than fissure ridge, and sometimes producing a prominent topography.

Table 2.1 - Main characteristics of the travertine deposits in the Albegna basin.

Travertine deposit	**Lat. Long.**	**Elevation (m.a.sl.)**	**Estimated thickness (m)**	**Travertine morphotype**	**Travertine type**
Semproniano village	42°43’51’’ N 11°32’25’’ E	570-620	30	Fissure ridge	Banded
Poggio Semproniano	42°43’25’’ N 11°31’46’’ E	500-700	200	Plateau, positive morphostructure	Bedded
Poggio I Piani	42°43’19’’ N 11°32’38’’ E	590-640	50	Plateau, positive morphostructure	Bedded
Pian di Palma	42°41’21’’ N 11°29’58’’ E	250-230	20	Plateau, depressed morphostructure	Bedded
Poggio Pancotta	42°40’28’’ N 11°30’42’’ E	200-260	20	Plateau, positive morphostructure	Bedded
Saturnia village	42°39’51’’ N 11°30’14’’ E	260-300	40	Plateau, positive morphostructure	Bedded with local banded
Bagni di Saturnia	42°38’53’’ N 11°30’43’’ E	142		Depressed morphostructure	Bedded
I Pianetti	42°38’01’’ N 11°30’34’’ E	260-220	40	Plateau, depressed morphostructure	Bedded with intrusive veins

Bedded travertines are the primary travertine strata formed during open air $CaCO_3$ precipitation from saturated H_2O solutions. Banded travertine are the $CaCO_3$ precipitates filling fractures that cut through the bedded travertines (and also other host rocks) or develop in a sill-like

fashion along the travertine beds themselves. These structures are usually filled by sparitic and variably-colored bands of $CaCO_3$ precipitated in a non-open air (intralithic) environment (e.g., Uysal et al., 2007; De Filippis et al., 2013a). We use the term veins only for fractures filled by non-banded sparry calcite with maximum thickness of a few centimeters.

Bedded and banded travertines, veins, and speleothem-like concretions have been systematically sampled across the study area for geochronological and isotopic analyses. Samples have been dated through the $^{230}Th/^{234}U$ method (Ivanovich and Harmon, 1992), which is based on the fractionation of the parent isotopes ^{238}U and ^{234}U from their long-lived daughter ^{230}Th. This technique assumes that Thorium is not included in the crystal lattice of the carbonate at the time of deposition, being easily hydrolyzed and precipitated or adsorbed on detritic fraction, whereas Uranium is soluble in the surface and near-surface environments co-precipitating with $CaCO_3$ on exsolution of CO_2. A $^{230}Th/^{234}U$ ratio close to one indicates that ^{230}Th and ^{234}U have reached secular equilibrium and therefore give an older than the ca. 350 ka limit of the $^{230}Th/^{234}U$ dating method. The $^{13}C/^{12}C$ ($\delta^{13}C$) and the $^{18}O/^{16}O$ ($\delta^{18}O$) ratios of samples have been investigated to distinguish between thermogene and meteogene carbonates and to characterize the origin and properties of the parental fluids (Friedman, 1970; Manfra et al., 1974; Fouke et al., 2000; Pentecost, 2005; Kele et al., 2011). In thermogene travertines, CO_2 mainly derives from deep magmatic fluids and from their interaction with carbonate rocks. Conversely, CO_2 in meteogene travertines mainly derives from the atmosphere and shallow deposits such as soils (Turi, 1986; Kele et al., 2003; Pentecost 2005). These distinct CO_2 sources are reflected in the $\delta^{13}C$ values, with thermogene travertines being characterized by $\delta^{13}C$ values comprised between -3 to +8‰ and meteogene travertines being characterized by average $\delta^{13}C$ values around -10‰ (Pentecost, 2005). Eventually, from the $\delta^{18}O$ values, we calculated the temperature of the travertine and vein parental fluids using the equation of Kele et al. (2015).

2.4. Results

2.4.1. Travertine types

The Albegna basin is characterized by an articulate structural setting of extensional faults oriented N-S, NW-SE and NE-SW, bounding the Pliocene-Quaternary basinal deposits (e.g., Brogi, 2004a; Bonciani et al., 2005; Brogi and Fabbrini, 2009; Carmignani et al., 2013; Fig. 2.2A). Both E-W- and NE-SW-striking strike slip faults intersect the pre-existing N-S-striking extensional ones (e.g., Brogi et al., 2010b; 2012). In particular, the overall structural architecture of the study area (Fig. 2.4A) is controlled by post-orogenic e extensional and strike-slip fault systems, cutting across the travertine deposits (see below) and the surrounding host units (Fig. 2.4B).

Fossil and active travertine deposits of the Albegna basin are exposed at different elevations (Fig. 2.3B) and roughly N-S-aligned along a transect of about 18 km (Fig. 2.4A). The northernmost travertine deposits are represented by the isolated fissure ridge forming the bedrock of the Semproniano village at about 550 m a.s.l. and two thick plateaus (Poggio Semproniano and Poggio i Piani) forming positive morphological structures at about 600-700 m a.s.l. Moving toward the south, an additional travertine deposit is exposed in a morphological depression in the Pian di Palma locality (about 230 m a.s.l.) on the northwest side of the Albegna River. On the southeast side, two travertine deposits form tabular positive morphological features in the Poggio Pancotta (about 200 m a.s.l.) and Saturnia (250-290 m a.s.l.). The southernmost travertine deposit, which is exposed at I Pianetti (about 230 m a.s.l.), forms a roughly tabular feature filling a morphological depression. Active hydrothermalism and travertine deposition occur at about 140 m a.s.l. at Bagni di Saturnia. This travertine deposit is the lowest one in elevation in the study area.

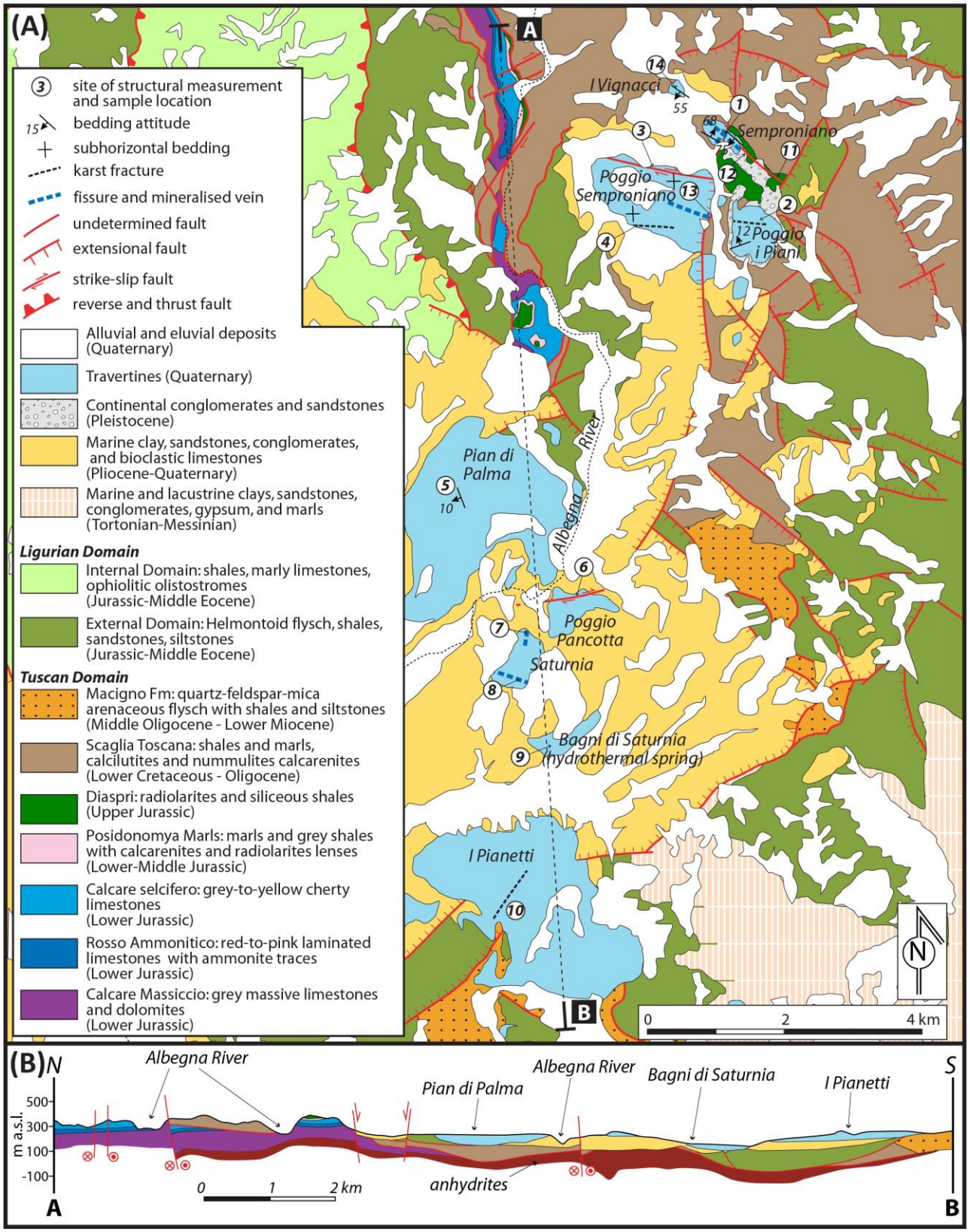

Figure 2.4 – (A) Structural map of the study area with structural measurement sites shown with numbers within circles (see Table 1). The map is based on the geological map at the 1:10,000 scale available online at http://www.regione.toscana.it/-/geologia. (B) N-S geological cross-section (redrawn and readapted after Guastaldi et al., 2014) illustrating the geometric-structural relationships between the studied travertine deposits and the underlying units.

Below, with reference to the sites of structural measurements shown in Fig. 2.4A, we analyze the travertine morphological characters to understand the travertine morphotypes and their internal fabrics. The Semproniano travertine (site 1) consists of a NW-SE-striking fissure-ridge structure located 500 m to the north of the Poggio i Piani and Poggio Semproniano travertine plateaus (sites 2 and 4, respectively; Fig. 2.5A). The exposed ridge is ca. 700 m long in the NW-SE direction and 400 m wide in the perpendicular direction. In the north-western part, the ridge is in contact with Lower Cretaceous-Oligocene shales and marls of the Scaglia Toscana Fmt. (Tuscan Nappe) and Pliocene-Quaternary marine clays and sandstones (Fig. 2.5B). In the south-eastern part, the ridge is in contact with Upper Jurassic radiolarites and siliceous shales (Diaspri Fmt of the Tuscan Nappe; see also Gelmini et al., 1967). The structural relationships between the travertine deposit and the surrounding units are not clear due to the coverage provided by Quaternary cover and anthropic backfill. The internal fabric of the travertine fissure ridge in the Semproniano village consists of a wide (50 m at least) vertical to sub-vertical banded travertine (Figs. 2.5C and 2.5D) extensively exposed below the Aldobrandeschi Fortress. The banded travertine consists of alternating centimeter-thick white bands (with calcite crystals growing perpendicular to the wall) and grey-colored finer grained bands. These bands are generally parallel to one another and strike parallel to the fissure ridge (average strike N315º), dipping toward NE or SW (Fig. 2.5D). In places, intersecting bands create v-shaped geometries (Fig. 2.5C). Poorly preserved remnants of sub-horizontal bedded travertine are exposed on the distal part of the south-western flank of the fissure ridge. This bedded travertine consists of plano-parallel brown-colored centimeter-thick beds (Fig. 2.5E). Unlike the banded travertine, which is characterized by non-porous sparry calcium carbonate, the bedded travertine is characterized by calcite shrubs, laminations, and millimeter-to-centimeter-sized syn-depositional cavities of depositional and post-depositional (karst) origin (Fig. 2.5F). The contact between the banded and bedded travertines is not clearly visible.

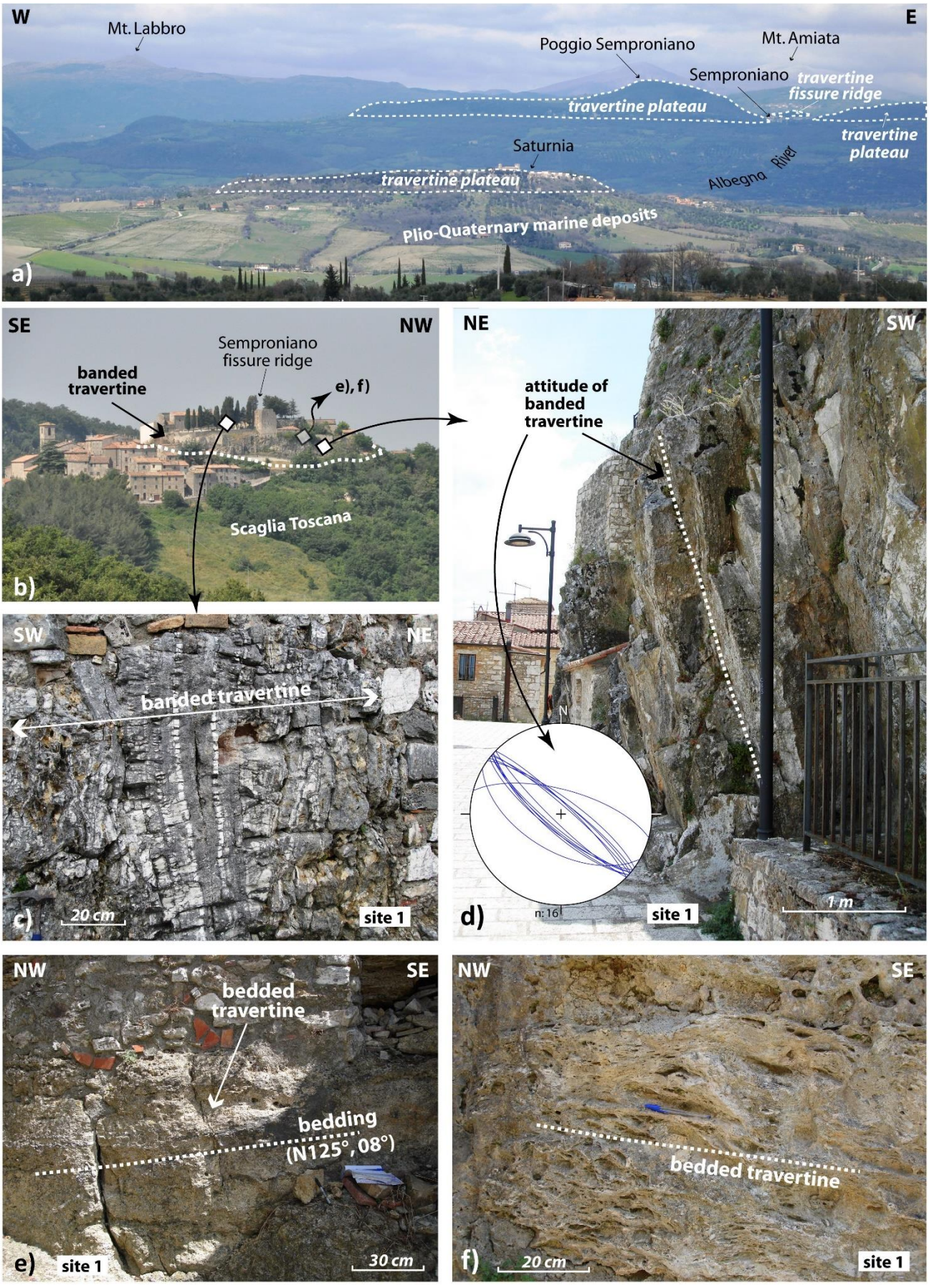
W
E
Mt. Labbro
Poggio Sempronian
Mt. Amiata
Sempronian
travertine fissure ridge
travertine plateau
travertine plateau
Saturnia
travertine plateau
Albegna River
Plio-Quaternary marine deposits
a)
SE
NW
Sempronian fissure ridge
banded travertine
e), f)
Scaglia Toscana
b)
NE
SW
attitude of banded travertine
N
n: 16
site 1
1 m
d)
SW
NE
banded travertine
20 cm
site 1
c)
NW
SE
bedded travertine
bedding (N125°, 08°)
site 1
30 cm
e)
NW
SE
bedded travertine
20 cm
site 1
f)

Figure 2.5 - (a) Northeastward panoramic view of the study area showing the Mt. Amiata volcanic district, the Meso-Cenozoic carbonate reservoir exposed in the Mt. Labbro area, and the studied travertine deposits. Travertine plateaus occur at Saturnia, Poggio Semproniano, and Poggio i Piani. The northernmost travertine deposit corresponds to the huge fissure ridge cropping out in the Semproniano village. (b) View of the fissure ridge travertine extensively exposed below the fortress of the Aldobrandeschi family (X Century) in the Semproniano village. The host units are represented by the Pliocene deposits belonging to the post-orogenic depositional cycle. (c) The central part of the fissure ridge (Semproniano) is characterized by a thick vein of banded travertine consisting of a rhythmic sequence of centimeter-thick crystallised levels of sparry calcite. (d) The banded travertine (Semproniano) is mainly oriented NW-SE and characterized by high dip values (see the stereoplot; stereographic projection, Schmidt net, lower hemisphere). (e) Sub-horizontal, bedded travertine exposed in the south-western flank of the fissure ridge (Semproniano). (f) Detail from the bedded travertine (Semproniano) with peculiar fabric defined by lamination, shrubs, and karst-dissolution cavities.

About 1 km to the north-west of Semproniano, an isolated deposit of travertine is exposed in the I Vignacci locality (site 14). The internal fabric of this deposit consists of banded travertine with high-dipping (*ca*. 55°) NW-SE-striking bands (Fig. S2.1), dipping at high angle with respect to the adjacent sub-horizontal Pliocene-Quaternary sequence. The orientation of this banded travertine is very similar to the one observed in Semproniano (average strike: N145°). This evidence suggests a structural and geometric continuity between I Vignacci and Semproniano village banded travertines.

At Poggio Semproniano and Poggio i Piani, the travertine plateaus are sub-horizontal (Figs. 2.5A and 2.6A) and lie on top of the Pliocene-Quaternary marine sequence or of the Scaglia Toscana. They consist of plano-parallel (Fig. 2.6B), centimeter-thick beds of white-colored lime-mudstone with heterogeneous porosity due to the presence of microbialites and millimeters-to-centimeters-sized karst-dissolution cavities (Fig. 2.6C). Bedding is generally horizontal (Fig. 2.6C) although locally complicated by fault-related tilting (see below).

The Pian di Palma (site 5) and I Pianetti (site 10) deposits consist of sub-horizontal travertine plateaus filling local depressions. The Pian di Palma plateau has a horseshoe-like shape of ca. 6 km^2 in areal extension. About 20 m of this travertine is exposed in an abandoned quarry at Pian di Palma (Fig. 2.6D). The travertine is characterized by thick beds (average thickness between 20 and 50 cm) affected by numerous post-depositional features such as calcite veins, sub-horizontal karst cavities, and vertical karst-conduits. The stratigraphic-structural relationships between this travertine plateau

and the adjacent units are not well exposed. The travertine is laterally in contact with (and probably lies on top of) the Pliocene-Quaternary marine sequence, whose architecture is controlled by NW-SE-striking and N-S-striking extensional faults (Fig. 2.4).

The travertine plateau at I Pianetti has a sub-circular shape, a maximum thickness of about 30 m, and it is visible in a large active quarry. The travertine is characterized by decimeter-thick plano-parallel beds, which, in places, form complex convoluted (non-tectonic) geometries.

At Saturnia (sites 7 and 8) and Bagni di Saturnia (site 9), the travertine deposits lie on top of the Pliocene-Quaternary marine sediments and mainly consist of bedded travertine boundstone with homogeneous primary porosity and millimeter-to-centimeter-sized karst-dissolution cavities. At the travertine-active site of Bagni di Saturnia, different depositional facies are distinguished including cascades, pools, and terraced slopes (Figs. 2.6E and 2.6F).

Figure 2.6 - (a) Panoramic view of the Poggio Sempronianо travertine plateau lying on top of the Plio-Quaternary marine deposits and bounded, toward the east, by a major N-S-striking extensional fault. In the fault footwall, the Scaglia Toscana unit (belonging to the non-metamorphic succession of the Tuscan Domain) is exposed. (b) Sub-horizontal, meter-thick bedding of the travertine deposit forming the plateau of Poggio Sempronianо. (c) Close-up view of the bedded travertine occurring at Poggio i Piani. (d) Bedded travertine exposed within the abandoned quarry of the Pian di Palma locality. The travertine deposit is characterized by sub-horizontal beds affected by karst cavities. (e) Travertine terraces with active deposition from $CaCO_3$-rich thermal waters near the public thermal center in Saturnia. (f) Recent fossil travertine waterfalls near Saturnia.

2.4.2. Post-depositional structures

Post-depositional structures affecting the travertine deposits have been studied in order to understand their geometry, spatial distribution, and tectonic and/or hydrothermal significance.

(i) Faults. The travertine deposits are affected by two main sub-vertical fault systems: one striking between E-W and ENE-WSW at the northern side of Poggio Semproniano (site 3) and at Poggio Pancotta (site 6), and one striking N-S at the eastern side of Poggio Semproniano. These fault systems are composed of damage zones (e.g. Caine et al., 1996; Fig. 2.7A) a few meters thick at the most. Fault planes dip steeply (> 50°) to the NW or SE. Most slickenlines and abrasive striations on fault planes (Figs. 2.7B and 2.7E) are characterized by a pitch smaller than 15° or greater than 165° (see the stereographic projections in Fig. 2.7), providing evidence for strike-slip-dominated kinematics. Synthetic shear fractures (Riedel shears) and lunate-cuspate morphologies on the striated fault planes (Figs. 2.7C and 72.D), consistently point to right-lateral shear. N-S-striking faults affecting travertine deposits are comparatively rare. At Semproniano village (site 1), a N184°-striking fault develops 0.5 m-wide damage zone within the banded travertine (Fig. 2.8A). Slickenlines on the fault surfaces are very difficult to determine. Very close to this N-S-striking fault, centimeters thick (average thickness: 7-10 centimeters), NNE-SSW-striking fractures filled by light brown speleothem-like concretions cut through the banded travertine (Figs. 2.8B and 2.8C). Geometrical relationships between fault surface and these speleothem-filled fractures (here interpreted as tension fractures) are consistent with a left-lateral shear. This N-S-striking fault is probably the northern culmination of the extensional fault system that marks the contact between the Pliocene-Quaternary sedimentary deposits and the Tuscan Nappe units south of the Semproniano village (Fig. 2.4A).

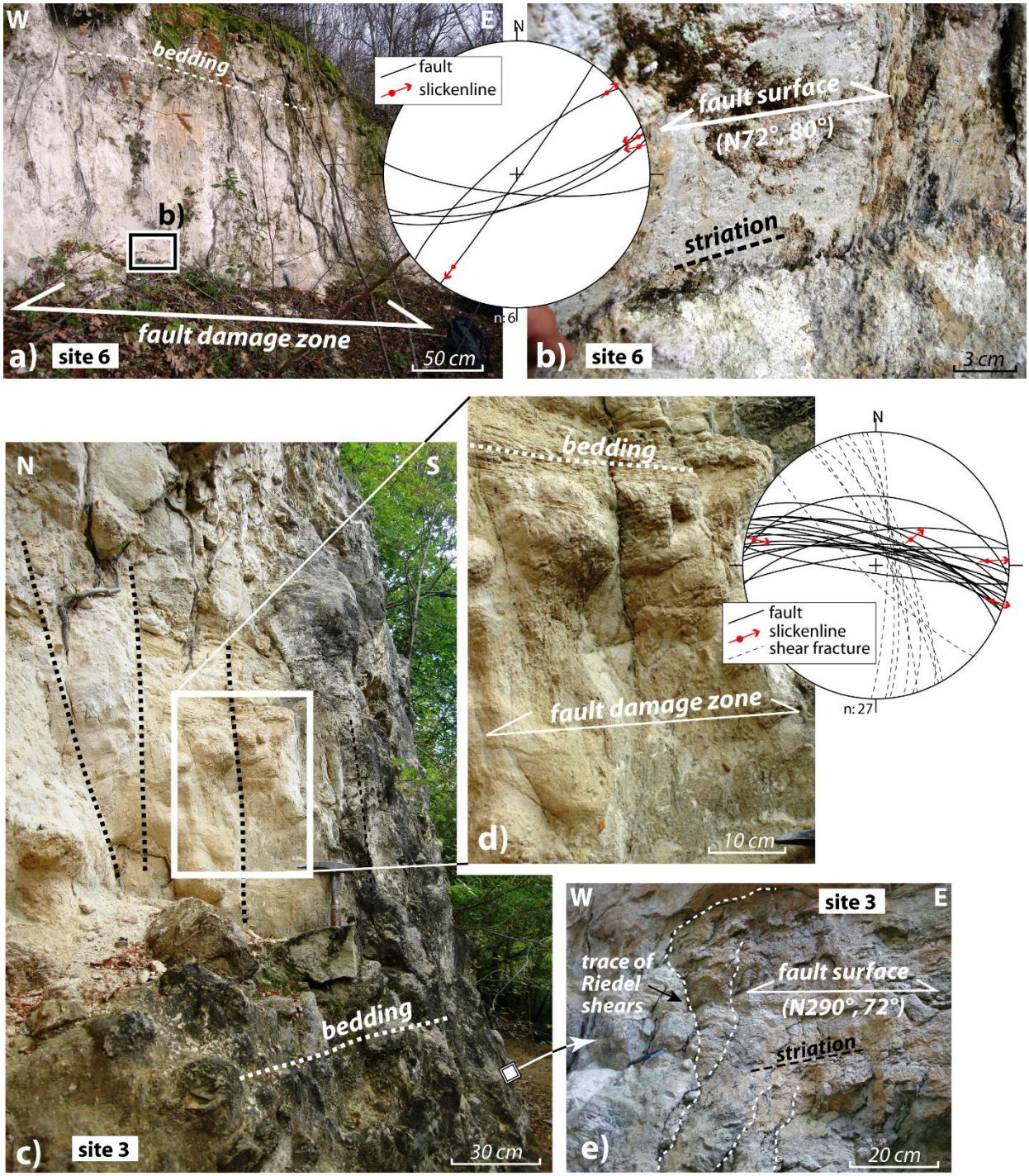

Figure 2.7 - E-W-striking right-lateral strike-slip faults affecting the bedded travertine at (a-b) Poggio Pancotta and (c-e) Poggio Semproniano. (a) At Poggio Pancotta, a metre-width fault damage zone and narrowly-spaced (in the order of a few decimeters) fault surfaces occur. (b) Fault surfaces are equipped with oblique- to strike-slip striations (pitch is generally higher than 160° or lesser than 20°; see the stereoplot). (c) Fault damage zone across travertine beds at Poggio Semproniano are characterized by highly-dipping surfaces (see the stereoplot). (d) Metre-width fault cataclastic bands consisting of severely fractured travertine blocks and decimeter-spaced fault surfaces. (e) Fault systems include curvilinear shear surfaces making an angle of 20–25° with the strike of the main fault surface and interpreted as Riedel shears within a right-lateral strike-slip kinematics.

Faults affecting the host rocks of the travertine deposits are not well exposed in the study area. NW-SE-striking faults have been recognized affecting the Pleistocene continental deposits exposed to the southeast of Semproniano (site 12). These faults consist of fault segments (Fig. S2.1B) with spacing of a few decimeters and displacement of a few centimeters at the most. When present, fault striations show a pitch around 160° (Fig. S2.1B) indicating oblique strike-slip kinematics. Subsidiary Riedel shears are consistent with fault right-lateral motions. Furthermore, this fault set is aligned along the strike of a main strike-slip fault zone exposed in an abandoned quarry within the Diaspri Fm. (site 11; Fig. S2.1C). This NW-SE striking fault zone is characterized by near-vertical fault surfaces, which form negative flower structure, close to which bedding is severely undulated and verticalized.

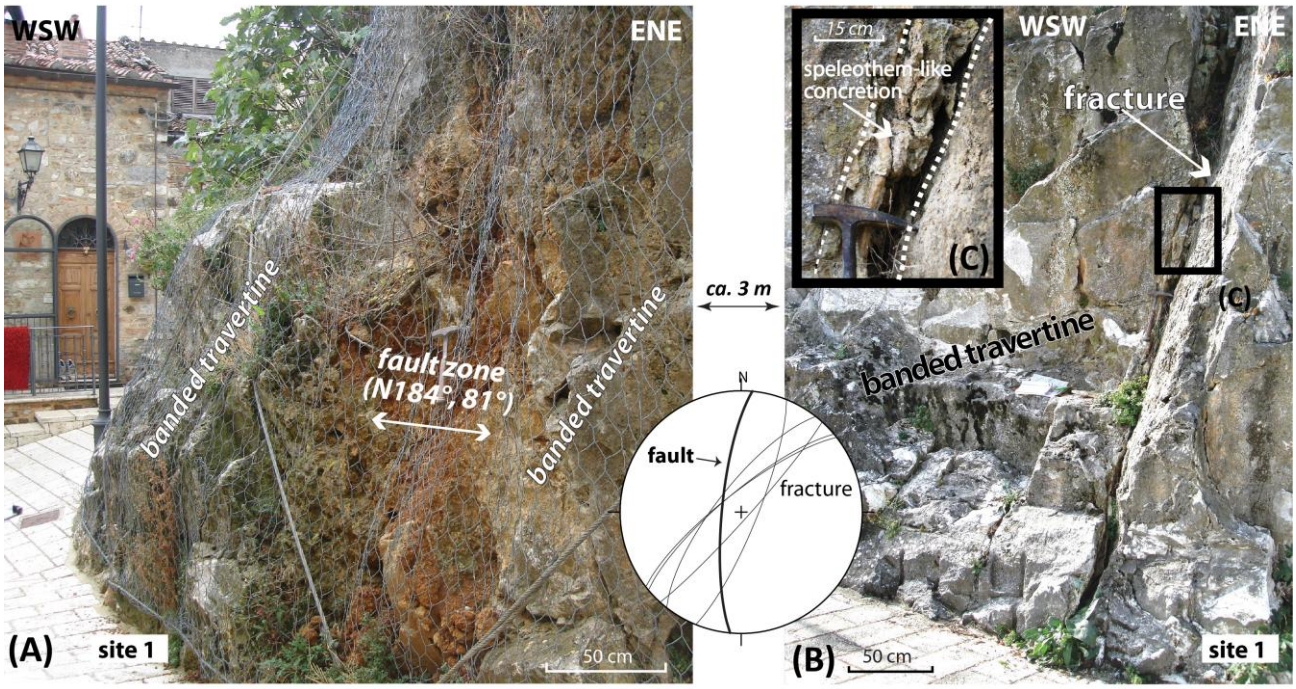

Figure 2.8 – (A) N-S-striking fault across the banded travertine of the Semproniano village. The fault is characterized by a half-meter-wide damage zone. (B) NE-SW-striking fractures, correlated to the N-S-striking fault, cut through the banded travertine. (C) Fractures are filled by speleothem-like concretions. Geometrical relationships between fault surface and speleothem-filled fractures suggest left-lateral shear (see the stereoplot, stereographic projection, Schmidt net, lower hemisphere).

(ii) Calcite-filled veins. At Poggio Semproniano (site 13), calcite-filled veins occur as a systematic set cutting through the bedded travertine and the underlying Scaglia Toscana Fmt. These

veins are a few centimeters thick (average thickness between 2 and 5 centimeters), with variable spacing between about 0.1 and 1 m (Fig. 2.9A). The veins consist of monogenic filling of white crystalline calcite or rhythmic millimeter-thick white-and-grey layering (Fig. 9B and 9C). At Poggio Semproniano, this vein set strikes NW-SE (average strike: N129°), with a high dip angle > 70° toward SW (Fig. 2.9A).

(iii) Fractures. At Semproniano (site 1), Poggio i Piani (site 2), Poggio Semproniano (site 4), and Pian di Palma (site 10), travertine deposits are affected by networks of fractures, some of which are strongly karstified (Fig. 2.4A). Fractures consist of decimeter-wide mechanical discontinuities within the travertine beds with either curvilinear or planar geometries. Fractures are commonly identified around (several meters) from the main fault systems cutting through the travertine bodies. At Poggio Semproniano and Poggio i Piani, these features strike from ESE-WNW to ENE-WSW, with dip angles close to 90° (Fig. S2.1D). Evidence of karst weathering is common along the fracture surfaces and consists of a main central crack and several secondary anastomosing irregular fractures. The edge of these fractures is karstified with a typical jigsaw profile. In the I Pianetti quarry, the karst-fractures strike in the NE-SW direction. These features are meters-to-decameters long with a mean spacing of 5-10 m (Fig. 2.9D). Karstified fractures are often connected, upward or downward, with large sub-horizontal cavities. Locally, these fractures host speleothems formed by sparry and globular calcite (Fig. 2.9E).

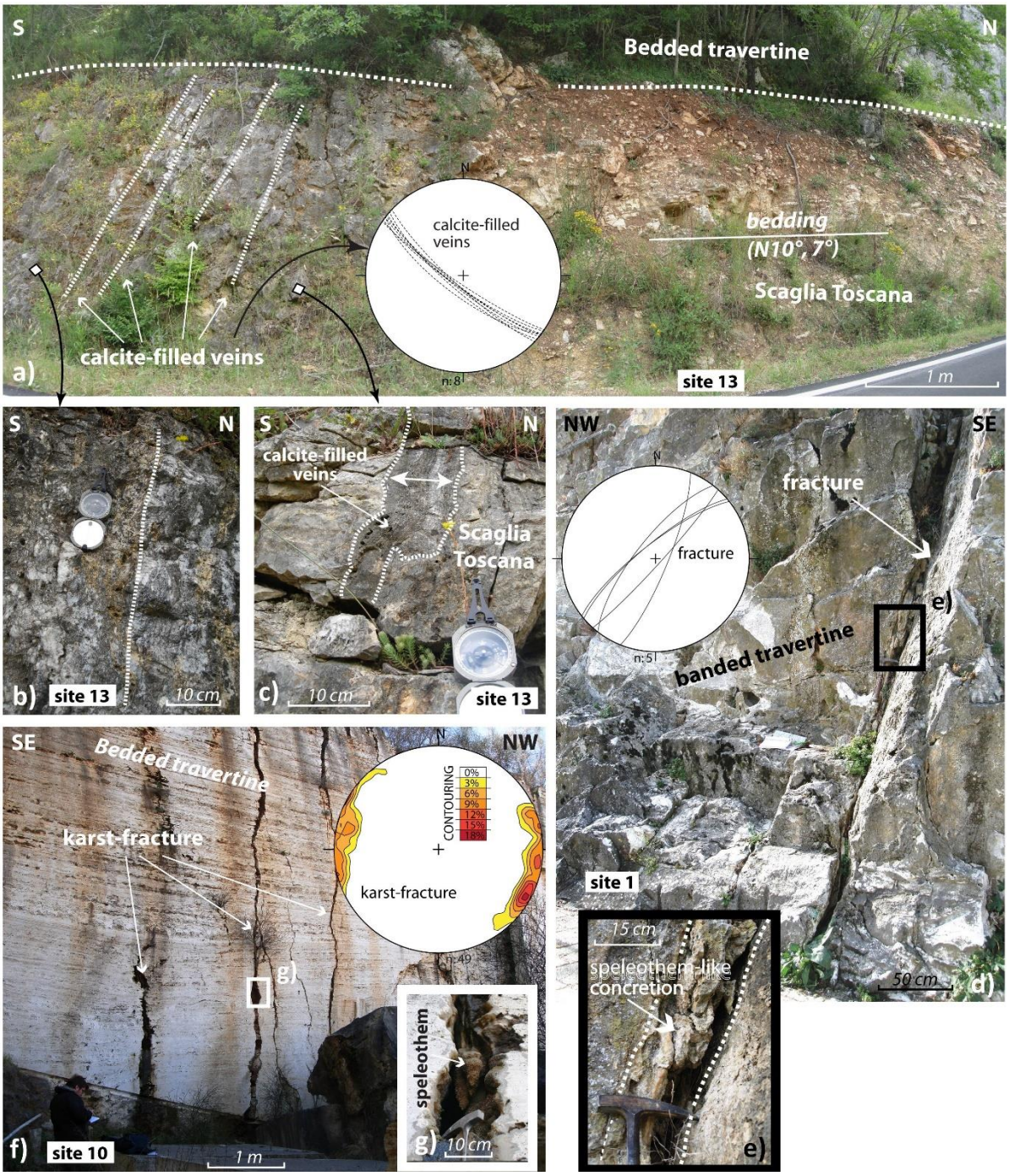

Figure 2.9 – (A) Set of calcite-filled steep veins cutting through the sub-horizontal Scaglia Toscana units lying below the bedded travertine of Poggio Semproniano. The veins strike NW-SE and dip toward the SW (see the stereoplot, stereographic projection, Schmidt net, lower hemisphere). These features consist of both (B) centimeter-thick monogenic calcite-filled veins and (C) decimeter-thick rhythmic layering of white-and-grey levels. (D) NNE-SSW-striking (see the stereoplot, stereographic projection, Schmidt net, lower hemisphere) karstified fractures across bedded travertine exposed in the I Pianetti quarry. (E) Close-up view of the previous photograph showing a speleothem occurring within a karstified fracture.

(iv) Banded travertine through travertine beds. At Saturnia (site 8), an exposed steeply-dipping 0.5-m-thick banded travertine cuts through the sub-horizontal travertine beds (Fig. 2.10A).

The banded travertine forms an inclined (about 33°) tabular body striking N282° and consists of fine-grained white carbonate concretion forming centimeter-thick bands parallel to the contact with the host travertine beds (Fig. 2.7B). Similar geometrical and cross-cutting relationships have been observed within the travertine exposed to the north of the Saturnia village (site 7), where a meter-thick banded travertine characterized by undulated bands cuts through the bedded travertine (Fig. S2.1E).

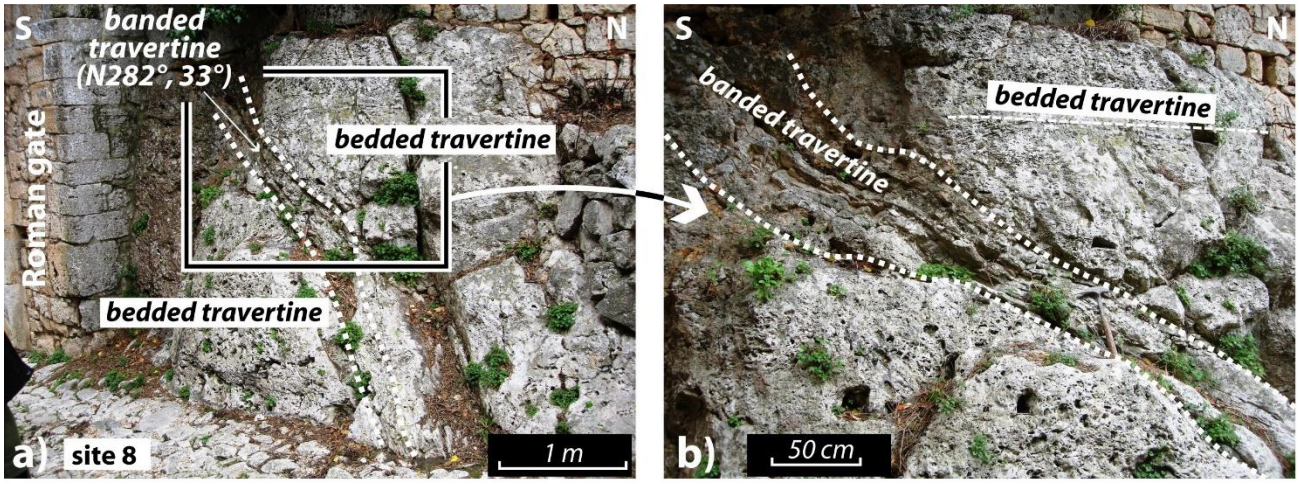

Figure 2.10 – (a) Banded-bedded travertine relationships observed in the Saturnia travertine plateau near the Roman gate (Saturnia village, site 8). (b) A decimeter-thick banded travertine cross-cuts the sub-horizontal bedded travertine (Saturnia village, site 8).

Table 2.2 - Summary of the main structural features observed during the field survey**.**

Structural measurement site	**Lat.** **Long.**	**Location**	**Lithology**	**Structures**	**Figure**
1	42°43’51’’ N 11°32’25’’ E	Semproniano village	Travertine	Fissure ridge, banded travertine, secondary fracture and N-S faulting	Fig. 2.5, Fig. 2.8, Fig. S2.1
2	42°43’25’’ N 11°31’46’’ E	Poggio i Piani	Travertine	Bedding, karst-fracture network	Fig. 2.6, Fig. S2.1
3	42°43’32’’ N 11°31’52’’ E	Poggio Semproniano (northern side)	Travertine	Bedding, E-W striking dextral strike slip fault zone	Fig. 2.6, Fig. 2.9
4	42°43’13’’ N 11°31’42’’ E	Poggio Semproniano (southern side)	Travertine	Bedding, karst-fracture network	Fig. 2.6
5	42°41’21’’ N 11°29’58’’ E	Pian di Palma	Travertine	Bedding, sub-horizontal karst-cavities	Fig. 2.6
6	42°40’28’’ N 11°30’42’’ E	Poggio Pancotta	Travertine	ENE-WSE striking dextral strike slip fault zone	Fig. 2.9
7	42°40’18’’ N 11°30’22’’ E	North of Saturnia village	Travertine	Bedded-banded relationships	Fig. S2.1
8	42°39’51’’ N 11°30’15’’ E	Saturnia village (Roman gate)	Travertine	Bedded-banded relationships	Fig. 2.7
9	42°38’53’’ N 11°30’43’’ E	Bagni di Saturnia	Travertine	Bedding, depositional facies	Fig. 2.6
10	42°38’01’’ N 11°30’34’’ E	I Pianetti	Travertine	Karst-fracture network, bedding	Fig. 2.8
11	42°43’29’’ N 11°32’58’’ E	SE of Semproniano (abandoned quarry)	Diaspri (Tuscan Domain)	NW-SE striking strike slip fault zone, bedding	Fig. S2.1
12	42°43’32’’ N 11°32’46’’ E	SE of Semproniano (public road)	Pleistocene continental deposits	NW-SE striking strike slip fault zone, bedding	Fig. S2.1
13	42°43’09’’ N 11°32’18’’ E	Poggio Semproniano (eastern side)	Scaglia Toscana (Tuscan Domain) and Travertine	Calcite-filled veins, bedding	Fig. 2.8
14	42°44’14’’ N 11°32’07’’ E	I Vignacci	Travertine	Fissure ridge, banded travertine	Fig. S2.1

2.4.3. $^{230}Th/^{234}U$ geochronology

Eighteen banded and bedded travertine samples, calcite-filled veins, and speleothem-like concretions have been analyzed to constrain the age of hydrothermal circulation in the Albegna basin.

Samples have been analyzed at the Laboratory of Environmental and Isotopic Geochemistry (Department of Sciences, Roma Tre University, Italy). Samples have been cut with a diamond saw and ultrasonically washed in deionized water. About 60 g of each prepared sample have been dissolved in 7 N HNO_3 and filtered to separate the leachates from the insoluble residue. The leachates have been heated at 200 °C after adding a few milliliters of hydrogen peroxide to annihilate the organic matter, and then spiked them with a $^{228}Th/^{232}U$ tracer. The isotopic complexes of U and Th have been extracted according to the procedure described in Edwards et al. (1986), and then analyzed through alpha-counting, using high-resolution ion-implanted Ortec silicon-surface barrier detectors. The age of samples has been determined with a $^{230}Th/^{232}Th$ activity ratio higher than 80, free from non-radiogenic ^{230}Th, using the $^{230}Th/^{234}U$ and $^{234}U/^{238}U$ activity ratio of the analysed calcite samples. In contrast, ages obtained for samples with a $^{230}Th/^{232}Th$ activity ratio less than or equal to 80 for the presence of non-radiogenic ^{230}Th related to detrital ^{232}Th required a correction performed assuming that all detrital Th had an average $^{230}Th/^{232}Th$ activity ratio of 0.85 ± 0.36 (Wedepohl, 1995). Eventually, the ages have been calculated using ISOPLOT (Ludwig, 2003) with errors expressed as $\pm 1\sigma$.

Our $^{230}Th/^{234}U$ geochronological data are reported in Table 3. All samples show a very low U concentration ranging from 3 to 208 ppb with a $^{234}U/^{238}U$ activity ratio between 0.978 and 1.585. The $^{230}Th/^{232}Th$ activity ratio, which is an indicator of the detrital contamination in the analyzed samples, ranges between 1.2 and 289. Results from the samples characterized by a $^{230}Th/^{232}Th$ activity ratio lower than 80 have been corrected using the $^{230}Th/^{232}Th$ activity ratio of 0.85 ± 0.36 (Wedepohl, 1995), which is the crustal thorium mean composition. Determined ages span within the 33-214 ka interval. Moreover, three ages resulted older than the limit (c. 350 ka) of the dating method (Table 2.3).

Table 2.3. Fabric type, uranium abundance, uranium and thorium activity ratios, and ages of samples (travertine and calcite-filled veins) from the Albegna Valley. *The ($^{230}Th/^{234}U$) was corrected using the crustal thorium mean composition, 0.85 ± 0.36 (Wedephol, 1995), for samples with a $^{230}Th/^{232}Th$ activity ratio lower than 80.

Location	Sample	Rock type	U (ppm)	$^{230}Th/^{232}Th$	$^{234}U/^{238}U$	$^{230}Th/^{234}U$	($^{230}Th/^{234}U$) corrected*	Age (ka)
Sempronian Village	**SP1**	banded travertine	0.0124 ± 0.0009	23.746 ± 2.639	1.138 ± 0.107	1.014 ± 0.087		**>350**
Sempronian Village	**SP8**	banded travertine	0.0152 ± 0.0004	14.516 ± 1.511	0.980 ± 0.034	1.016 ± 0.043		**>350**
Sempronian Village	**SPV1**	speleothem-like	0.145 ± 0.004	125.34 ± 45.73	1.003 ± 0.028	0.588 ± 0.034		**97 ± 9**
Sempronian Village	**SP11**	bedded travertine	0.0 53 ± 0.002	7.148 ± 0.251	1.094 ± 0.026	0.892 ± 0.027	0.878 ± 0.051	**214 +50/-37**
Vignacci	**VI1**	banded travertine	0.0770 ± 0.0006	2.277 ± 0.112	1.012 ± 0.071	1.578 ± 0.093		**>350**
Poggio Sempronian	**SP10**	calcite vein	0.032 ± 0.002	110.353 ± 20.338	0.978 ± 0.061	0.299 ± 0.023		**39 ± 4**
Poggio Sempronian	**PO2**	bedded travertine	0.053 ± 0.002	169.884 ± 26.205	1.198 ± 0.036	0.818 ± 0.039		**171 ± 19**
Poggio i Piani	**PP1**	bedded travertine	0.077 ± 0.003	171.43 ± 23.82	1.112 ± 0.031	0.857 ± 0.028		**198 ± 18**
Pian di Palma Quarry	**USI13 1-7**	bedded travertine	0.031 ± 0.002	107.279 ± 80.071	1.403 ± 0.125	0.263 ± 0.026		**33 ± 4**
Pian di Palma Quarry	**USI1**	bedded travertine	0.0121 ± 0.0007	21.875 ± 5.503	1.449 ± 0.104	0.378 ± 0.034	0.369 ± 0.093	**49 ± 15**
Saturnia Village	**SA1**	bedded travertine	0.129 ± 0.014	289 ± 175	1.125 ± 0.053	0.736 ± 0.045		**140 ± 17**
Saturnia Village	**SA14-05**	bedded travertine	0.208 ± 0.005	26.373 ± 1.568	1.133 ± 0.020	0.749 ± 0.023	0.742 ± 0.060	**142 ± 23**
Saturnia Village	**SA14-01**	banded travertine	0.018 ± 0.001	21.830 ± 3.061	1.565 ± 0.056	0.613 ± 0.024	0.603 ± 0.078	**94 ± 18**
Saturnia Village	**SA2**	banded travertine	0.0130 ± 0.0009	87.275 ± 12.583	1.585 ± 0.098	0.696 ± 0.053		**118 ± 15**

Bagni di Saturnia	**SA6**	bedded travertine	0.01000 ± 0.0006	1.234 ± 0.106	1.531 ± 0.116	0.490 ± 0.039	0.312 ± 0.047	**40 ± 7**
I Pianetti Quarry	**ST4**	bedded travertine	0.022 ± 0.002	1.226 ± 0.081	1.361 ± 0.073	0.785 ± 0.041	0.648 ± 0.056	**107 ± 15**
I Pianetti Quarry	**ST1**	bedded travertine	0.045 ± 0.003	5.823 ± 0.482	1.196 ± 0.035	0.746 ± 0.037	0.716 ± 0.072	**130 ± 23**
I Pianetti Quarry	**CP13-1-4**	bedded travertine	0.0095 ± 0.0005	3.186 ± 0.209	1.307 ± 0.063	0.681 ± 0.029	0.629 ± 0.049	**103 ± 13**

2.4.4. C- and O-isotopes and calculated paleofluids temperatures

C- and O-isotopes ($\delta^{13}C$ and $\delta^{18}O$) analyses on 38 samples have been performed to constrain the chemistry of the parental hydrothermal fluid. The isotopic composition of carbonate has been measured according to the method described in detail in Breitenbach and Bernasconi (2011). Approximately 100 µg of powder has been filled in 12 ml Exetainers, (Labco, High Wycombe, UK) and flushed with pure Helium. The samples have been reacted with 3-5 drops of 100% phosphoric acid at 70°C with a ThermoFisher GasBench device connected to a ThermoFisher Delta V mass spectrometer. The average long term reproducibility of the measurements (i.e., based on replicated standards) is ±0.05‰ for $\delta^{13}C$ and ±0.06‰ for $\delta^{18}O$. The instrument is calibrated with the international standards NBS19 ($\delta^{13}C$= 1.95 and $\delta^{18}O$ = -2.2‰) and NBS18 ($\delta^{13}C$ = -5.01 and $\delta^{18}O$ = -23.01‰). Results are expressed in ‰ against Vienna Pee Dee Belemnite standard (V-PDB) for both $\delta^{13}C$ and $\delta^{18}O$. Formation temperatures of the travertines have been determined with the equation of Kele et al. (2015) which is based on travertine vent and pool samples. As benchmark (i.e., $\delta^{18}O_{fluid}$) we used the modern $\delta^{18}O$ of the Bagni di Saturnia hydrothermal spring waters (-6.4‰ V-SMOW), which are characterized by a constant temperature of 37 °C (e.g., Minissale, 2004). In doing so, the oxygen isotope composition of the travertine precipitating water is assumed that was similar to that of the presently-active spring at Bagni di Saturnia. Stable isotope composition and calculated paleotemperatures are reported in Table 2.4 and Figure 2.11.

Selected samples include banded travertines, bedded travertines, calcite-filled veins, and speleothem-like concretions. With the exception of light brown speleothem-like concretions in secondary fractures occurring at Semproniano (SPV1 and SPV2, Fig. 2.8C), all travertines and associated mineralizations show positive $\delta^{13}C$ values between 2.8 and 10.5‰ (mean value 6.7‰), indicating a thermogene origin (Pentecost, 2005). The $\delta^{18}O$ values are comprised in a wide range from -12.7 to -5.1‰ (V-PDB) with a mean value -8.64‰ (Figs. 2.11A and 2.11B).

Calculated paleotemperatures range between a minimum of 22 to a maximum of 60 °C (Table 4). Samples characterized by the highest calculated paleotemperatures belong to Semproniano village fissure ridge banded travertines, whereas the lowest ones belongs to bedded travertines from Pian di Palma quarry. This evidence attests for a decreasing paleotemperature trend moving from highest to lowest elevations and from North to South in the study area (Figs. 2.11C and 2.11D). Banded travertines are generally characterized by mean calculated paleotemperatures of around 10 °C higher than the associated bedded travertine.

Table 2.4 - Stable oxygen and carbon isotope composition, and paleotemperature of banded travertine, bedded travertine, and calcite veins from the Albegna basin. Isotope compositions are expressed in ‰ against Vienna Pee Dee Belemnite standard (V-PDB). Temperature of parental fluids derive from $\delta^{18}O$ through the equation of Kele et al. (2015).

Sample	Location	Rock Type	$\delta^{13}C$ (‰ V-PDB)	$\delta^{18}O$ (‰ V-PDB)	$\delta^{18}O$ (‰ V-SMOW)	$T_{calculated}$ (°C)
SP1	Semproniano Village	banded travertine	9.5	-12.7	17.8	60
SP5	Semproniano Village	banded travertine	8.9	-10.8	19.8	49
SP6	Semproniano Village	banded travertine	10.0	-12.2	18.3	57
SP7	Semproniano Village	banded travertine	10.5	-11.6	19.0	53
SP8	Semproniano Village	banded travertine	9.7	-12.3	18.2	57
SP11	Semproniano Village	bedded travertine	9.9	-8.2	22.2	36
SP14/06	Semproniano Village	bedded travertine	5.3	-9.8	20.9	44
SP14/05	Semproniano Village	bedded travertine	5.8	-9.7	20.9	44
SPV1	Semproniano Village	Speleothem-like	-9.4	-6.0	25.6	n.c.
SPV2	Semproniano Village	Speleothem-like	-9.7	-5.6	23.7	n.c.
PP1	Poggio i Piani	bedded travertine	6.5	-11.6	19.0	53

PS 1	Poggio Semproniano	bedded travertine	6.9	-10.2	20.4	46
PS 3	Poggio Semproniano	bedded travertine	5.8	-10.1	20.5	46
SP9	Poggio Semproniano	bedded travertine	6.8	-9.6	21.0	43
PO1	Poggio Semproniano	bedded travertine	5.6	-11.4	19.2	53
PO2	Poggio Semproniano	bedded travertine	7.1	-9.8	20.8	44
SP10	Poggio Semproniano	Calcite vein	8.4	-10.7	19.9	49
SP3	Poggio Semproniano	Calcite vein	7.1	-11.5	19.0	53
SA1	Saturnia Village	bedded travertine	7.3	-7.5	23.2	33
SA14/05	Saturnia Village	bedded travertine	6.4	-8.0	22.6	36
SA14/01	Saturnia Village	banded travertine	7.5	-9.1	21.6	41
SA2	Saturnia Village	banded travertine	7.7	-9.1	21.6	41
SA5	Saturnia Spring	bedded travertine	2.8	-8.7	22.0	38
SA6	Saturnia Spring	bedded travertine	3.1	-6.6	24.1	29
SA7	Saturnia Spring	bedded travertine	3.3	-8.1	22.6	36
USI13-1-1	Pian di Palma quarry	bedded travertine	7.4	-5.2	25.6	22
USI13-1-2	Pian di Palma quarry	bedded travertine	7.4	-5.2	25.6	22
USI13-1-3	Pian di Palma quarry	bedded travertine	5.8	-5.8	24.9	25
USI13-1-4	Pian di Palma quarry	bedded travertine	6.2	-5.4	25.3	24
USI13-1-5	Pian di Palma quarry	bedded travertine	6.2	-5.4	25.4	23
USI13-1-6	Pian di Palma quarry	bedded travertine	7.1	-5.1	25.6	22
CP 13-1-1	I Pianetti quarry	bedded travertine	6.5	-6.1	24.6	26
CP 13-1-2	I Pianetti quarry	bedded travertine	6.2	-6.3	24.4	27
CP 13-1-3	I Pianetti quarry	bedded travertine	6.4	-6.2	24.6	27
CP 13-1-4	I Pianetti quarry	bedded travertine	6.2	-6.8	23.9	30
CP18-01	I Pianetti quarry	bedded travertine	6.5	-7.9	22.8	35
CP18-02	I Pianetti quarry	bedded travertine	5.1	-8.0	22.7	35
CP18-03	I Pianetti quarry	bedded travertine	6.1	-7.9	22.8	35

V-PDB, Vienna Pee Dee Belemnite standard; V-SMOW, Vienna Standard Mean Ocean Water; n.c., not calculated.

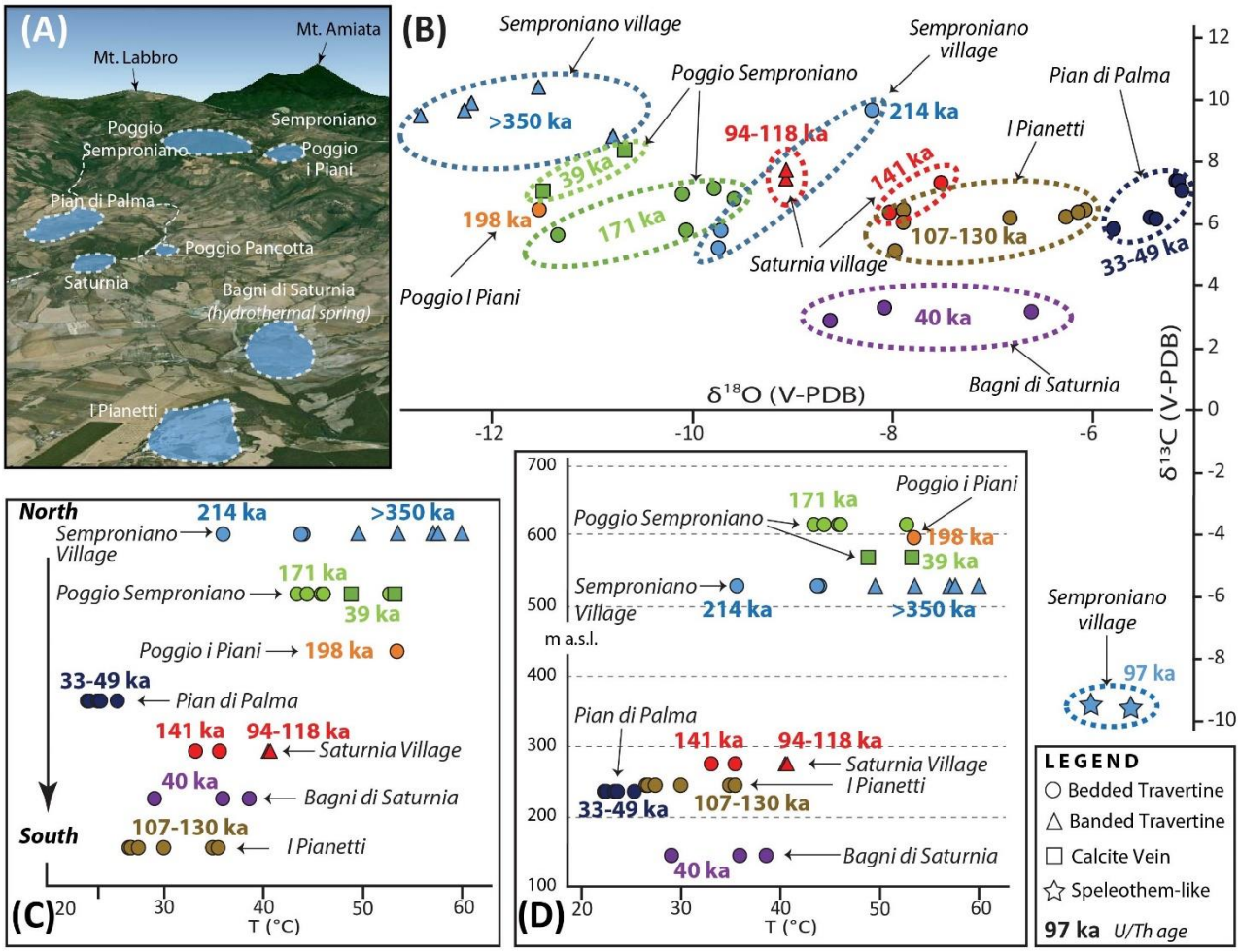

Figure 2.11 – (a) Northward panoramic view (Google Earth image similar to Figure 2.3a) with localization of the studied travertine deposits. (b) Combined plot of $\delta^{13}C$ (‰ V-PDB) and $\delta^{18}O$ (‰ V-PDB) isotope values obtained for the samples of bedded and banded travertines, calcite veins, and speleothem-like concretions. Isotope values are correlated with the corresponding U/Th ages (Tables 2.3 and 2.4). (c) Parental fluid temperatures (parental fluids of the studied travertine deposits) plotted versus the geographic location of the corresponding travertine deposits and correlated with the corresponding U/Th ages (Tables 2.3 and 2.4). (d) Parental fluid temperatures (parental fluids of the studied travertine deposits) plotted versus the elevation of the corresponding travertine deposits and correlated with the corresponding U/Th ages.

2.5. Discussion

2.5.1. Tectonic synthesis

Our structural analysis documents that the main travertine deposits within the Albegna basin are aligned N-S (Fig. 2.4A) and located along major N-S-striking faults and at fault intersection (at Semproniano village, Poggio Semproniano, Poggio I Piani). Some travertine deposits are cut cross by right-lateral strike-slip faults oriented E-W and WNW-ESE (at Poggio Semponiano and Poggio

Pancotta; Fig. 2.7). Moreover, the N-S-striking fault at Semproniano village cut through the fissure ridge with a (left-lateral) strike-slip shear. This fault pattern of N-S- and E-W-striking faults is similar from nearby hydrothermal areas in southern Tuscany (e.g., Brogi et al., 2010a; 2012; Rimondi et al., 2015) and along the Tyrrhenian margin (see below).

Our geochronological data allow dating the tectonic-hydrothermal processes as active from >350 ka to the present time. The oldest travertines and veins are older than the dating method range (ca. 350 ka), whereas the youngest one is about 33 ka old. Moreover, the Albegna basin hydrothermal system and associated travertine deposition are still active at the Bagni di Saturnia thermal spring. Integrating our chronological data with previous ones from nearby similar hydrothermal settings (Taddeucci and Voltaggio 1987; Brogi et al., 2012; Rimondi et al., 2015), we can constrain the onset of hydrothermalism in southern Tuscany at the middle Pleistocene, concurrently with the main phases of crustal uplift and emplacement of magmatic bodies in the region (Barberi et al., 1994), with the volcanic activity of the Mt. Amiata (300-190 ka; Cadoux and Pinti, 2008) and Vulsini Mountains (590-127 ka; Nappi et al., 1995), and with hypogenic speleogenesis (69-19 ka; Piccini et al., 2015). This hydrothermal scenario is consistent with the occurrence of a regional thermal anomaly below the Tuscan Magmatic Province, producing long-lived convective circulation of endogenic fluids during the Pleistocene (Minissale, 2004).

Our geochronological data, together with the observed relationships between travertine deposition and development of fault-fracture systems, can be used to constrain the minimum age of faulting in the region. E-W striking right-lateral fault at Poggio Semproniano cut through the bedded travertine dated at 171 ± 19 ka, whereas the N-S striking fault cut through the banded travertine at Semproniano fissure ridge dated as >350 ka. Tension fractures at Semproniano fissure ridge are filled by speleothem-like concretions dated 97 ± 9 ka. The karstified fractures at Poggio I Piani and I Pianetti cut through bedded travertine dated 198 ± 18 ka and 107 ± 15, respectively. These ages constrain at the Upper Pleistocene the tectonic activity in the Albegna basin.

In synthesis, our structural data show that the growth of the studied travertines occurred concurrently with fault activity and can thus be considered as syn-tectonic depositional units. If integrated with ages from recent studies (e.g., Brogi, 2008; Brogi et al., 2010a, 2014), our U-Th data show that faulting in the southern Tuscany is significantly younger than previously thought and has worked simultaneously with long-lived convective circulation of hydrothermal fluids in the Tuscan Magmatic Province.

2.5.2. Hydrothermalism

In our dataset (Table 2.4 and Fig. 2.10), only the speleothem-like concretions sampled in some fractures (SPV1 and SPV2) are characterized by negative $\delta^{13}C$ values (i.e., -9.4 and -9.7‰). These negative values are probably due to the high contribution of atmospheric and soil-zone CO_2 dissolved in the parental fluids of these carbonates. These values are indicative of a meteoric origin (Pentecost, 2005), suggesting that these carbonate mineralizations were formed by percolation of meteoric waters within cracks. This evidence suggests that the Semproniano fissure ridge was probably fully formed at 97 ka, which is the time of deposition of the analyzed speleothem-like concretions. On the other hand, the travertine and veins are characterized by positive $\delta^{13}C$ values (Table 2.4), which are indicative of a hydrothermal fluid source derived by the mixing of deep magmatic fluids and meteoric waters with CO_2 originated from limestone decarbonation (Gonfiantini et al., 1968; Guo et al., 1996). Our $\delta^{13}C$ and $\delta^{18}O$ values are comparable with those reported in previous studies (e.g., Minissale, 2004 and references therein) and are in the range typical of thermogene travertines deposited by present-day thermal springs of central Italy (Minissale, 2004; Gandin and Capezzuoli, 2008). Travertines belonging to Semproniano village fissure ridge are characterized by $\delta^{13}C$ values more positive than usual thermogene values probably as results of downstream CO_2 degassing, producing an increase in $\delta^{13}C$ (Özkul et al., 2013).

Some differences can be found when comparing our isotopic dataset with that of nearby hydrothermal settings along the Tyrrhenian margin. The continental carbonates of the Sarteano

system (southern Tuscany) yielded $\delta^{13}C$ values ranging between 1.6 and −2.5‰ (Brogi et al. 2012), which are indicative of a larger meteoric component. The isotope data for the Tivoli travertine (Latium) are concentrated in a small range ($8.31 < \delta^{13}C < 10.77$ and $-4.76 < \delta^{18}O < -7.18$‰) and attributed to a strong process of diagenesis that obliterated the original oxygen isotopic signature (Manfra et al., 1974; De Filippis et al., 2013a). The variability of oxygen and carbon isotope compositions observed in the travertines of the Albegna basin has analogies with that of travertine samples from the Denizli basin (Turkey) and Mammoth Hot Spring (Yellowstone Park, USA). For the Denizli basin, the travertine formation is largely attributed to variable interaction between the meteoric waters and the deep hydrothermal fluids (e.g., Dilsiz, 2006; Uysal et al., 2007; De Filippis et al., 2013a). In contrast, the travertine deposition at Mammoth Hot Spring is attributed to high extent of CO_2 degassing during diagenesis processes (e.g., Fouke et al., 2000; Chafetz and Guidry, 2003). Based on C- and O-isotope data, travertines of the Albegna basin can be interpreted as forming during a dominant circulation of CO_2-enriched hydrothermal fluids with variable contribution of colder shallow aquifer mainly recharged by meteoric precipitation.

Estimated temperatures for parental fluids span between about 60 °C for the banded travertine from the Semproniano village and about 22 °C for the bedded travertine from the Pian di Palma quarry (Table 2.4 and Figs. 2.11C and 2.11D). There are no analogous datasets for parental fluids from fossil hydrothermal settings along the Tyrrhenian margin in central Italy, but our estimated temperatures are comparable with the temperatures of present-day thermal springs in this region (i.e., T >20° C; Minissale, 2004).

A comparison with previously-studied thermogene travertine systems can be drawn on the depositional longevity as constrained by U-Th data. We do not know the longevity of single travertine deposits and structures in the Albegna basin but, based on the radiometric dating data, we can assess the longevity of the entire Albegna hydrothermal-travertine system to be >350 ka. This activity is longer than estimated activities for travertine deposition at Rapolano (Tuscany, Italy; about 133 ka; Brogi et al. 2010a), at Sarteano (Tuscany, Italy; about 250 ka; Brogi et al. 2012), at Tivoli (Latium,

central Italy; about 100 ka; Faccenna et al., 2008), at Limagne Graben (Massif central, France; about 250 ka; Rihs et al. 2000), and at the Ebro basin (Spain; about 239 ka; Luque and Julià, 2007). Longer activities have indeed been documented for travertine deposition in the Denizli basin (Turkey; at least 600 ka; Engin et al., 1999; Altunel and Karabacak, 2005; Uysal et al., 2007; De Filippis et al., 2012; De Filippis et al., 2013a; Özkul et al., 2013; Lebatard et al., 2014; Toker et al., 2015), and in the Rio Grande rift (USA; about 660 ka; Priewisch et al., 2014).

To conclude, the overall $CaCO_3$-rich hydrothermal circulation in the Albegna basin has been active longer than other hydrothermal systems along the Tyrrhenian margin (i.e., compare with the Rapolano, Sarteano, and Tivoli travertines). During late Quaternary times, a $CaCO_3$-rich hydrothermal longevity of a few hundreds of thousands of years seems characteristic of the Albegna basin and further large travertine depositional basins occurring in continental tectonically-controlled settings around the world (e.g., Denizli basin, Limagne Graben, Rio Grande rift, and Llobregat travertines in the Ebro basin).

2.5.3. Spatio-temporal hydrothermal evolution

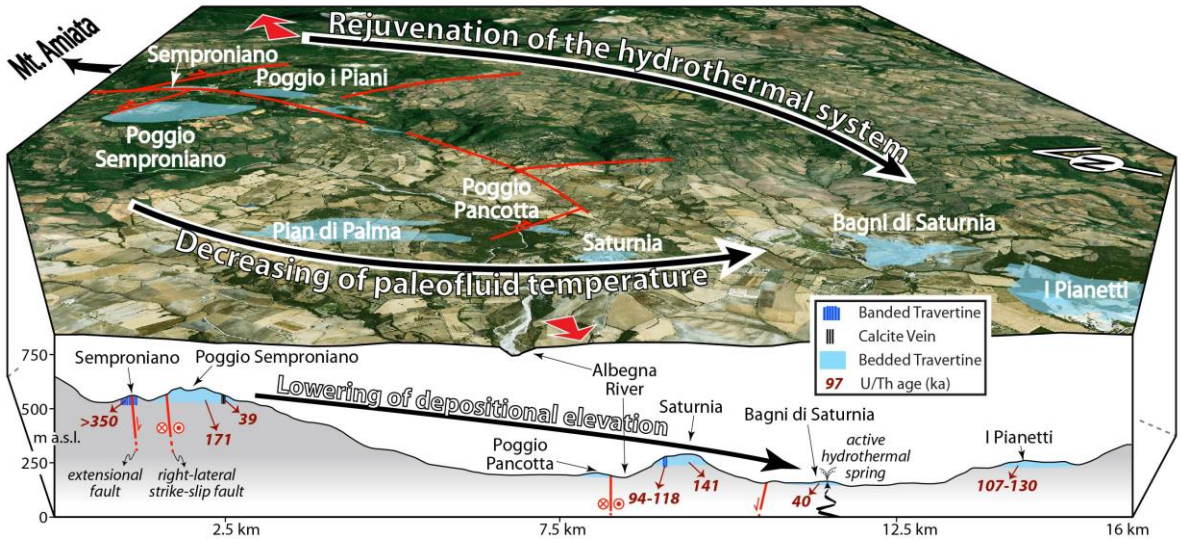

We can interpret the travertine deposits of the Albegna basin as a marker of a hydrothermal activity

that evolves in space and time along a N-S structural alignment. The following main features have been recognized and documented in this paper for the Albegna basin:

a) a general southward rejuvenation of the hydrothermal system, i.e. the travertine deposition becomes younger moving from north to south. The Semproniano deposits have ages >350 ka, whereas the youngest dated deposit (c. 40 ka) and the active springs occurs toward the south in the Bagni di Saturnia locality;

b) a lowering of travertine deposition elevations. At Semproniano and Poggio Semproniano, the deposits lie at about 600-700 m a.s.l., whereas toward the south in the Bagni di Saturnia and I Pianetti localities, the deposits lie at about 140-220 m a.s.l. The parallel altimetric and chronological gradients (from north to south) indicate a rapid lowering of the water table toward the south (i.e., toward the Tyrrhenian Sea) during Pleistocene time in the order of 1 mm yr^{-1} (Piccini et al., 2015);

c) a change in isotopic signature. Along the N-S profile (Figure 2.11a), the correlation between isotopic data and U-Th ages indicates a general decreasing trend of $\delta^{13}C$ and increasing trend of $\delta^{18}O$ from older to younger travertine deposits (Fig. 2.11B). The highest $\delta^{13}C$ values belong to the oldest travertines (the Semproniano fissure ridge), whereas the lowest $\delta^{13}C$ values are found in the active thermal spring of Bagni di Saturnia. The only exception is represented by the calcite-filled veins occurring at Poggio Semproniano, which developed synchronously with the bedded travertine of Bagni di Saturnia and Pian di Palma localities. $\delta^{18}O$ values show a wide range with the most negative values corresponding to older travertines (Semproniano village, Poggio Semproniano and Poggio I Piani) and the less negative values belonging to the travertines of Pian di Palma quarry (the youngest deposit);

d) a decrease of the paleofluid temperatures. The gradient of $\delta^{18}O$ values from north to south corresponds to a decrease of precipitation temperatures (Fig. 2.11C). This decreasing trend is also confirmed when considering the temperatures versus elevations of the travertine

deposits (Fig. 2.11D). This evidence corroborates the hypothesis of an increasing contribution of meteoric waters with time.

Summarizing, we interpret the Albegna basin as a long-lived hydrothermal-tectonic setting with a progressive southward migration of the fluid circulation, moving away from the geothermal center of the Mt. Amiata, located to the north of the Albegna basin. In Figure 2.12, we document the spatio-temporal migration of this hydrothermal system. The main travertine-depositing center changed its position horizontally (along the N-S structural alignment) and vertically (lowering of the depositional elevations), reaching the present-day deposition center at the Bagni di Saturnia locality. The travertines show decreasing $\delta^{13}C$ and increasing of the $\delta^{18}O$ consistently with increasing dilution of endogenic fluids by meteoric fluids. Main extensional and strike-slip fault systems provided the necessary hydraulic pathways for infiltration of meteoric waters to depth of the carbonate reservoir, the possible connection and mixing between different hydrogeological-hydrothermal circuits (e.g., Curewitz and Karson, 1997; Cox et al., 2001; Rowland and Sibson, 2004; Gudmundsson, 2011), and the subsequent ascension to surface of $CaCO_3$-rich hydrothermal fluids. Mixing with meteoric fluids resulted in a decrease of fluid temperatures down to the present value of 37° C at the Bagni di Saturnia springs (Minissale, 2004).

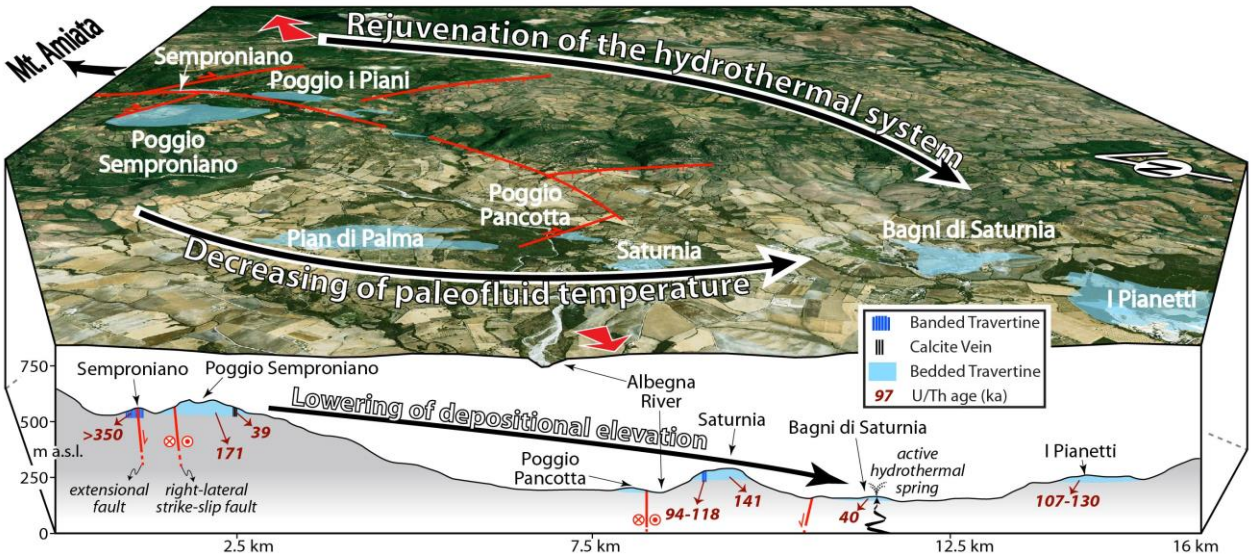

Figure 2.12 – Spatio-temporal evolution of the hydrothermal system in the Albegna basin as constrained by the geological, geochronological, and geochemical datasets provided in this study (see also Piccini et al., 2015). The spatio-temporal evolution is characterized by younger travertines moving from north to south and from upper to lower elevations. The temperature of the travertine parental fluids decreases with time and space moving toward younger deposits, toward the south, and toward lower elevations of deposition. As explained in the text, also $\delta^{13}C$ and $\delta^{18}O$ values tend to change with space and time from north to south, from upper to lower elevations, and from older to younger deposits. Location of the travertine deposits and travertine-related structures is also shown together with the fault pattern.

2.5.4. The contribution of paleoclimate

Our geochronological data can contribute to the understanding of the feedback relationships between thermogene travertine deposition and paleoclimate in the Albegna basin. In the last decades, many studies have been devoted to the correlation between travertine deposition and paleoclimate oscillations. There is a general consensus in considering warm and wet (interglacial) conditions as the most favorable for travertine deposition during late Quaternary time (e.g., Dramis et al., 1999; Frank et al., 2000; Rihs et al., 2000; Soligo et al., 2002; Pentecost, 2005; Luque and Julià, 2007; Faccenna et al., 2008; Kampman et al., 2012; Priewisch et al. 2014). Intuitively, high-stand conditions of the water table during wet periods can favor the supply of fluids for the growth of travertine deposits. Nevertheless, travertine formation in dry glacial periods (low-stand of the water table) has been documented and used to emphasize the importance of tectonic activity, rather than climate, to control travertine precipitation (e.g., Uysal et al., 2009; Brogi et al., 2010; Özkul et al., 2013). Finally, a complete interaction and feedback between fluid discharge, paleoclimate, and tectonics has been proposed by De Filippis et al. (2013a) to control morphologically and volumetrically the different travertine deposits (travertine plateaus and fissure ridges).

We compared our radiometric age data (Table 2.3) with major Quaternary paleoclimate indicators and events determined both at the global and regional scales (Fig. 2.13). We used, in particular, paleoclimate records extracted from the deep sea oxygen isotope trend (Zachos et al., 2001) integrated with the pollen dataset from Valle di Castiglione (located about 150 km to the south of the Albegna basin; see location in Fig. 2.1). Although our travertine dating data are affected by rather large error bars, we observe that the majority of our travertine ages falls within the interglacial

periods. This is particularly true for the travertine ages younger than 130 ka, including data from bedded travertine, banded travertine, calcite-filled veins, and speleothem-like concretions. This evidence suggests that the travertines and travertine-related structures preferentially formed during warm (and humid) climate periods characterized by high-stand conditions of the water table. Nevertheless, our data also document that large volumetric amount of travertine deposits in the Albegna basin (bedded travertine plateaus at Poggio Semproniano and at Saturnia village) are coeval with a glacial period at about 130-180 ka, which is also a non-humid time as demonstrated by the pollen curve from Valle di Castiglione (Fig. 2.13). This evidence probably testifies for an important contribution of endogenic fluid supply to travertine deposition during the low-stand (and non-humid) conditions of the water table (see also Toker et al., 2015). In other words, the endogenic fluid supply may have partly compensated the lowering of the water table during the glacial low-stand periods.

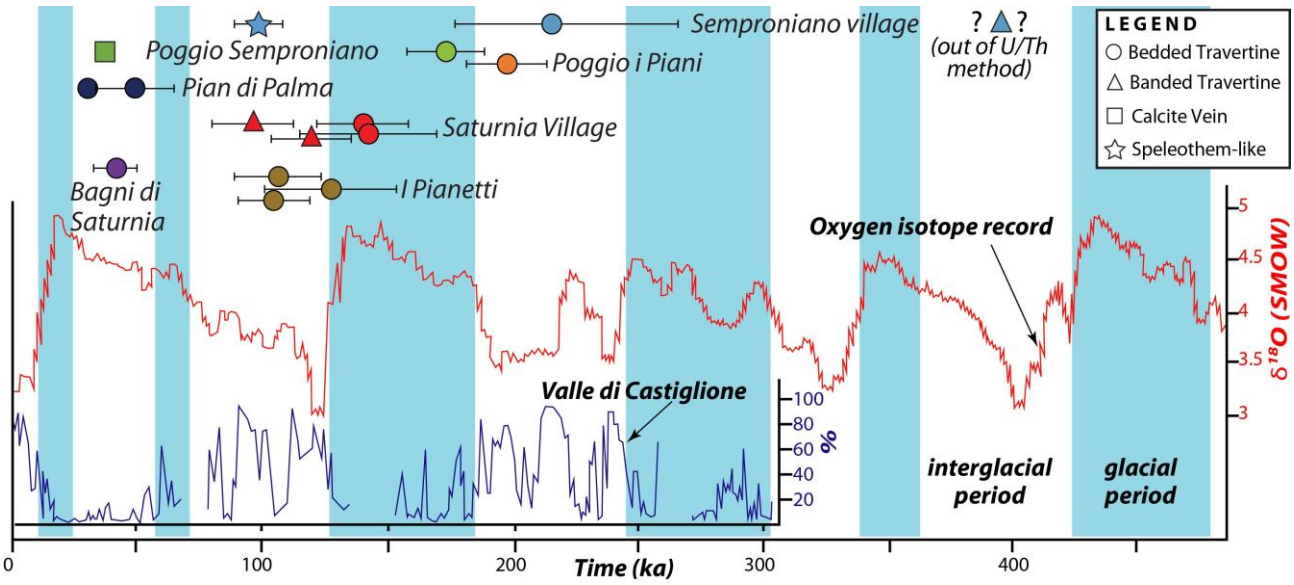

Figure 2.13 – Comparison between U/Th ages of CaCO3 samples (bedded and banded travertines, calcite-filled veins, and speleothem-like concretions) from the Albegna basin and major paleoclimate indicators represented by the deep sea oxygen isotope trend (Zachos et al., 2001) and the pollen dataset from Valle di Castiglione (Tzedakis et al., 2001). Glacial/interglacial periods are redrawn and modified after Priewisch et al. (2014). Valle di Castiglione is located in central Italy (see location in Fig. 2.1) only about 200 km from the Albegna basin.

2.5.5. Implications for the Tyrrhenian margin neotectonics

The recognized structural pattern of the Albegna basin is compatible with the post-orogenic regional extensional tectonic regime described for the Tyrrhenian margin, where main NW-SE-striking extensional faults (i.e. parallel to the trend of the Apennines belt) and related sedimentary basins developed in Pliocene-Quaternary times (Malinverno & Ryan, 1986; Patacca et al., 1990; Bossio et al., 1993; Martini and Sagri, 1993; Bartole, 1995; Jolivet et al., 1998; Cavinato and De Celles, 1999; Pauselli et al., 2006; Billi and Tiberti, 2009; Brogi et al., 2014). Within this scenario, the strike-slip to transtensional faults oriented transversally to the NW-SE oriented extensional boundary faults are interpreted as transfer systems accommodating different stretching rates within the extending crust (Faccenna et al., 1994; Aiello et al., 2000; Acocella and Funiciello, 2002; Acocella and Funiciello, 2006; Liotta et al., 2015). It is worth nothing that many of these transverse faults have acted as preferential pathways for hydrothermal outflow and controlled distribution of volcanism along the Tyrrhenian margin at least since late Pleistocene time. On this regard, we report, from NW to SE along the Tyrrhenian margin, ten main instances (see Fig. 2.14A) where recent or active hydrothermal activity is localized along transverse faults (i.e., NE-SW and N-S), as is the case of the Albegna basin (this study): (1) Rapolano, Tuscany (Brogi and Capezzuoli, 2009), (2) Sarteano, Tuscany (Brogi et al., 2012), (3) Torre Alfina, Latium (Vignaroli et al., 2013), (4) Roman Plain, Latium (Sella et al., 2014; Bigi et al., 2014; Frepoli et al., 2010), (5) Viterbo, Latium (Baldi et al., 1974; Chiocchini et al., 2010), (6) Sutri, Latium (Corrado et al., 2014), (7) Tivoli, Latium (Gasparini et al., 2002; Faccenna et al., 2008; De Filippis et al., 2013), (8) Zolforata di Pomezia, Latium (Vignaroli et al., 2015), (9) Zannone Island, Latium (Ingrassia et al., 2015), and (10) Mt Massico-Roccamonfina,

Transfer faults are known as compartmental non-Andersonian faults restricted to shallow levels, i.e., in the hanging wall of extensional faults (Gibbs, 1984; Van der Pluijm and Marshak, 2003). As such, transfer faults are not expected to act as pathways for endogenic (deep) hydrothermal fluids as is the case of the Albegna basin and elsewhere along the Tyrrhenian margin. We conclude

that the structures that nucleated and initially grew as transfer zones transversally to the Apennines trend (Neogene) have probably evolved as through-going crustal faults in recent times (Quaternary) so to allow the upflow of endogenic fluids stored in geothermal reservoirs of the region. (1) In a first stage (Neogene; Fig. 2.14B), the post-orogenic extensional tectonics acted on the Tyrrhenian margin of the Apennines operated through major NW-SE-striking extensional faults. The orientation of the paleo-stress axes followed the Anderson's theory of extensional faulting with a vertical σ_1 (maximum compression) and σ_2 and σ_3 (intermediate and minimum compression, respectively) lying on a horizontal plane. The vertical σ_1 was the consequence of far-field (slab retrat) and near-field (Apennines crustal thickening) stress regimes acting at the back of the eastward migrating compressional system. Within this setting, transfer zones developed in a non-Andersonian mode in the hanging walls of the NW-SE-striking normal faults to separate differently-stretched adjacent compartments (e.g., Gibbs, 1984). (2) As the extension progressed (late Quaternary; Fig. 2.14B), vigorous crustal thinning and erosion reduced the lithostatic load (σ_1), providing a new stress regime probably characterized by a vertical σ_2 axis (switch between σ_1 and σ_2) and horizontal σ_1 and σ_3. At this stage, the NW-SE-striking extensional faults became less effective, whereas the former shallow transfer zones switched to strike-slip crustal-scale faults. Both the pre-existing NE-SW- and some newly-generated N-S-striking strike-slip to transtensional faults responded to a horizontal $\sigma 1$ and propagated downward into the crust so to reach the endogenic fluid accumulation at depth and offer them a viable pathway for surficial uprising and mixing with meteoric waters.

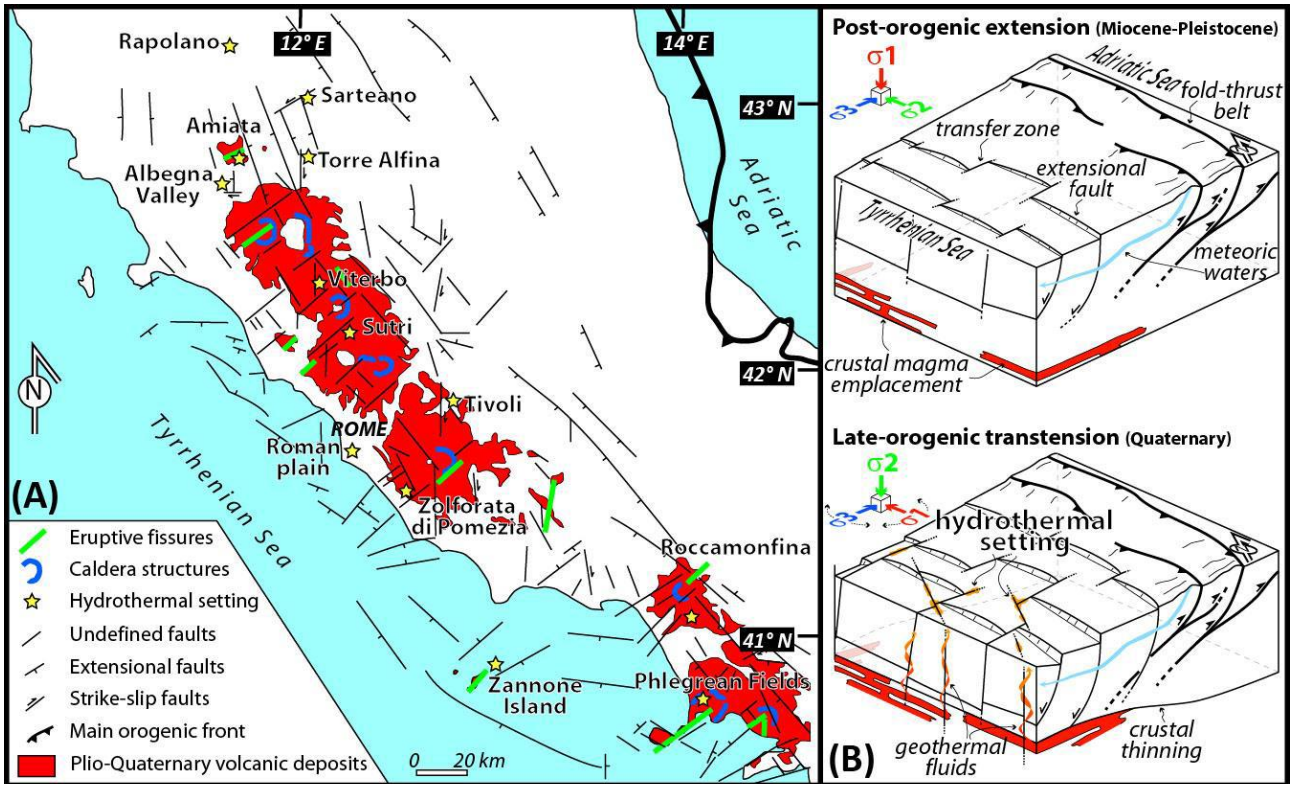

Figure 2.14 – (A) Simplified structural map of the Tyrrhenian margin showing the main fault systems, the Plio-Quaternary volcanoes, and the principal hydrothermal-tectonic systems (redrawn and modified after Acocella and Funiciello, 2006 and Conticelli et al., 2015). (B) Two-stage scenario (based on the model of Acocella and Funiciello, 2006) illustrating the structural control of the originally-shallow transfer zones on the localisation of hydrothermal fields. During post orogenic extension (above) the margin-transverse structures acted as non-Andersonian transfer zones restricted to shallow levels. Subsequently (below), due to the change in the stress tensor induced by crustal thinning (i.e., switch between σ1 and σ2 paleostress axes), these originally-shallow faults were re-activated and enhanced so to rupture downward into the crust and generate the pathway for hydrothermal fluid ascension.

2.6. Conclusions

(1) The Quaternary travertine deposition in the Albegna basin in central Italy was assisted by interaction and feedback between hydrothermalism, active tectonics, and paleoclimate, within a region of positive geothermal anomaly. While hydrothermalism provided the feeding fluids and the ascension energy (heat), tectonics provided the permeable pathways and paleoclimate modulated the abundance and elevations of groundwaters that buffered and mixed with the endogenic fluids.

(2) The origin of the discussed southward and downward migration of the thermogene travertine depositional system remains to be explained. As such, the Albegna basin remains an interesting

topic to be further studied for a better understanding of additional causes, e.g., eustatism, morphological molding, and groundwater level changes as influenced by climate oscillations and endogenic fluid supply.

(3) The reconstructed spatio-temporal tectonic-hydrothermal evolution of the Albegna basin sheds light on the neotectonic and hydrothermal activity along many faults transverse to the Tyrrhenian margin, where, due to the change in the stress tensor induced by post-orogenic crustal thinning, these originally-shallow faults were re-activated and enhanced so to propagate rupture downward into the crust and generate the effective pathway for hydrothermal outflow.

2.7. Appendix

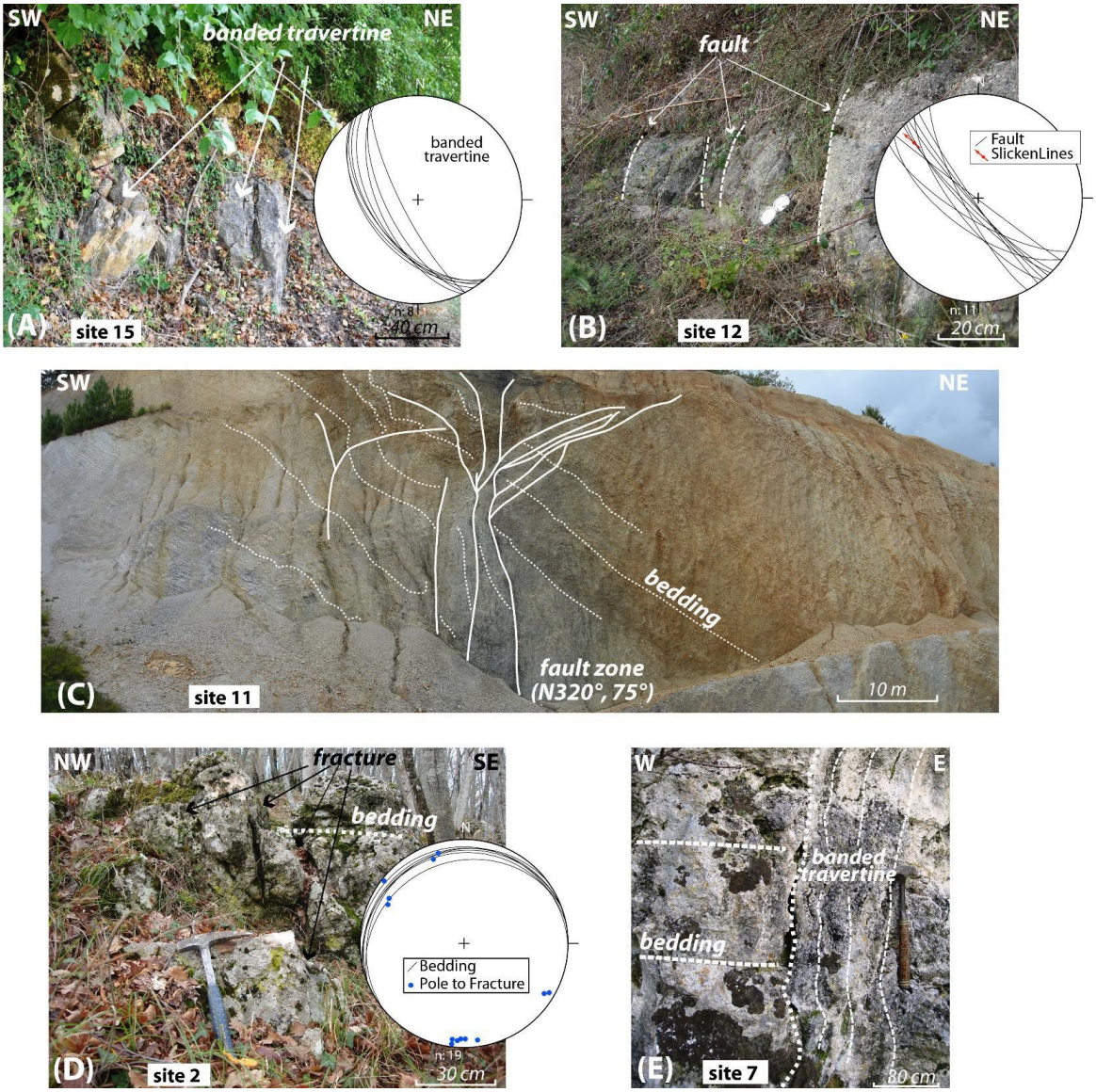

Figure S2.1 – (A) NW-SE-striking banded travertine exposed in the I Vignacci locality (see the stereoplot, stereographic projection, Schmidt net, lower hemisphere). The travertine attitude suggests a structural continuity with the NW-SE-striking banded travertine forming the fissure ridge of the Semproniano village, which is located a few hundreds of meters from I Vignacci. (B) Decimetre-spaced faults affecting the Quaternary continental deposits exposed to the southeast of Semproniano village (see the stereoplot, stereographic projection, Schmidt net, lower hemisphere). These fault surfaces strike NW-SE, i.e., parallel to the fissure ridge banded travertine of Semproniano. In one case, we found evidence of right-lateral displacement along this fault set. (C) NW-SE-striking fault zone exposed in an abandoned quarry located to the southeast of the Semproniano village. Faults affect and deform beds of radiolarites and siliceous shales belonging to the Tuscan Nappe. The fault architecture consists of fault surfaces forming a negative flower structure (in cross-sectional view). This fault system aligns along the NW-SE trend of the travertine fissure ridge (see also the geological map in Fig. 2.4A). (D) Karstified fractures cutting through the bedded travertine that forms the plateau of Poggio i Piani (see the stereoplot, stereographic projection, Schmidt net, lower hemisphere). (E) Bedded travertine exposed immediately to the north of the Saturnia village. The bedded travertine is cut by a metre-thick subvertical banded travertine.

2.8. References

Acocella V. and Funiciello R., 2002. Transverse structures and volcanic activity along the Tyrrhenian margin of central Italy. Bollettino della Società Geologica Italiana, special vol. 1, 739-747.

Acocella V. and Funiciello R., 2006. Transverse systems along the extensional Tyrrhenian margin of central Italy and their influence on volcanism. Tectonics 25, TC2003. http://dx.doi.org/10.1029/2005TC001845.

Acocella, V. and Rossetti, F., 2002. The role of extensional structures on pluton ascent and emplacement: the case of southern Tuscany (Italy). Tectonophysics, 354, 71-83.

Aiello G, Marsella E., Sacchi M., 2000. Quaternary structural evolution of Terracina and Gaeta basins (Eastern Tyrrhenian margin, Italy). Rend. Fis. Acc. Lincei, 11, 41-58.

Altunel E. and Hancock P.L., 1993. Morphology and structural setting of Quaternary travertines at Pamukkale, Turkey. Geological Journal, 28, 335-346.

Altunel E. and Karabacak V., 2005. Determination of horizontal extension from fissure-ridge travertines: a case study from the Denizli Basin, southwestern Turkey. Geodinamica Acta, 18/3-4, 333-342.

Annunziatellis A., Beaubien S.E., Bigi S., Ciotoli G., Coltella M., Lombardi S., 2008. Gas migration along fault systems and through the vadose zone in the Latera caldera (central Italy): implications for CO2 geological storage. Int. J. Greenhouse Gas Control, 2, 353-372.

Aucelli P.P.C., Amato V., Budillon F., Senatore M.R., Amodio S., D'Amico C., Da Prato S., Ferraro L., Pappone G., Russo Ermolli E., 2012. Evolution of the Sele River coastal plain (southern Italy) during the Late Quaternary by inland and offshore stratigraphical analyses. Rend. Fis. Acc. Lincei, 23, 81-102, doi 10.1007/s12210-012-0165-5.

Baillieux P., Schill E., Edel J.B., Mauri G., 2013. Localization of temperature anomalies in the Upper Rhine Graben: insights from geophysics and neotectonic activity. International Geology Review, DOI:10.1080/00206814.2013.794914.

Baldi P., Ferrara G.C., Masselli L., Pieretti G., 1973. Hydrogeochemistry of the region between Monte Amiata and Rome. Geothermics, 2, 124-128.

Baldi P., Decandia F.A., Lazzarotto A., Calamai A., 1974. Studio geologico del sub-strato della copertura vulcanica Laziale nella zona dei laghi di Bolsena, Vico e Bracciano. Memorie della Società Geologica Italiana, 13, 575-606.

Barazzuoli P., Capacci F., Migliorini J., Rigati R., 2013. Termalismo e travertini in Toscana meridionale. In: Acque e Travertini, Eds: Billi A., De Filippis L., Ubertini L., ISSN 2035-8088. Rendiconti Online della Società Geologica Italiana, 27, 42-53, doi: 10.3301/ROL.2013.19.

Barazzuoli P., Nocchi M., Rigati R., Salleolini M., 2008. A conceptual and numerical model for groundwater management: a case study on a coastal aquifer in southern Tuscany, Italy. Hydrogeology Journal, 16, 1557-1576.

Barbagli, A., Brogna F.N.A., Callegari I., Guastaldi E., Liali G., Marsico N., Rezza C., Trotta M., 2013. Multi-isotope and hydrogeochemical approach for characterizing Saturnia thermal groundwater (Grosseto, Italy). Italian Journal of Groundwater, AS07029, 025-040.

Barberi F., Innocenti F., Ricci C.A., 1971. Il magmatismo dell'Appennino Centro Settentrionale. Rend. Soc. It Minerl. Petrol., 27, 169-210.

Barberi, F., Buonasorte, G., Cioni, R., Fiordelisi, A., Foresi, L., Iaccarino, S., Laurenzi, M.A., Sbrana, A., Vernia, L., Villa, I.M., 1994. Plio-Pleistocene geological evolution of the geothermal area of Tuscany and Latium. Mem. Descr. Carta Geol. Ital. 49, 77–133.

Barchi M., Minelli G., Pialli G., 1997. The CROP-03 profile: a synthesis of results on deep structures of the Northern Apennines. Memorie della Società Geologica Italiana, 52, 383-400.

Barilaro F., Della Porta G., Capezzuoli E., 2012. Depositional geometry and fabric types of hydrothermal travertine deposits (Albegna Valley, Tuscany, Italy). Rend. Online Soc. Geol. It., 21, 1024-1025.

Bartole R., 1995. The North Tyrrhenian-Northern Apennines post-collisional system: Constraint for a geodynamic model. Terra Nova, 7, 7-30.

Batini F., Brogi A., Lazzarotto A., Liotta D. & Pandeli E. (2003) - Geological features of the Larderello–Travale and Monte Amiata geothermal areas (southern Tuscany, Italy). Episodes, 26, 239-244.

Bellani, S., Brogi, A., Lazzarotto, A., Liotta, D., Ranalli, G., 2004. Heat flow, deep temperatures and extensional structures in the Larderello geothermal field (Italy). Constraints on geothermal fluid flow. J. Volcanol. Geoth. Res. 132, 15–29.

Bertani R., 2005. World geothermal power generation in the period 2001–2005. Geothermics, 34, 651-690.

Bettelli G., Bonazzi U., Fazzini P., Fontana D., Gasperi G., 1990. Carta geologica del bacino del F. Albegna. Ist. Geol. Univ. Modena, S.EL.CA. Firenze, 1990.

Bibby H.M., Caldwell T.G., Davey F.J., Webb T.H., 1995. Geophysical evidence on the structure of the Taupo Volcanic Zone and its hydrothermal circulation. Journal of Volcanology and Geothermal Research, 68, 29-58.

Bigi, S., Beaubien, S.E., Ciotoli, G., D'Ambrogi, C., Doglioni, C., Ferrante, V., Lombardi, S., Milli, S., Orlando, L., Ruggiero, L., Tartarello, M.C., and Sacco, P., 2014, Mantle-derived CO2

migration along active faults within an extensional basin margin (Fiumicino, Rome, Italy). Tectonophysics, 637, 137–149, doi: 10.1016/j.tecto.2014.10.001.

Billi A., Bosi V., De Meo A., 1997. Caratterizzazione strutturale del rilievo del Monte Massico nell'ambito dell'evoluzione quaternaria delle depressioni costiere dei fiumi Garigliano e Volturno (Campania settentrionale). Il Quaternario, Italian Journal of Quaternary Sciences, 10, 15-26.

Billi A., Valle A., Brilli M., Faccenna C., Funiciello R., 2007. Fracture-controlled fluid circulation and dissolutional weathering in sinkhole-prone carbonate rocks from central Italy. Journal of Structural Geology, 29, 385-395.

Billi A. and Tiberti M.M., 2009. Possible causes of arc development in the Apennines, central Italy. Geological Society of America Bulletin, 121, 1409-1420, doi:10.1130/b26335.1.

Billi A., Tiberti M.M., Cavinato G.P., Cosentino D., Di Luzio E., Keller J.V.A., Kluth C., Orlando L., Parotto M., Praturlon A., Romanelli M., Storti F., Wardell N., 2006. First results from the CROP-11 deep seismic profile, central Apennines, Italy: evidence of mid-crustal folding. Journal of Geological Society London, 163, 583-586.

Boccaletti M., Calamita F., Deiana G., Gelati R., Massari F., Moratti G., Ricci Lucchi F., 1990, Migrating foredeep-thrust belt systems in the northern Apennines and southern Alps: Palaeogeography, Palaeoclimatology, Palaeoecology, v. 77, p. 3-14.

Boccaletti M., Gianelli G., Sani F., 1997. Tectonic regime, granite emplacement and crustal structure in the inner zone of the Northern Apennines (Tuscany, Italy): a new hypothesis. Tectonophysics, 270, 127-143.

Bonazzi U., Fazzini P., Gasperi G., 1992. Note alla carta geologica del Bacino del Fiume Albegna. Bollettino della Società Geologica Italiana, 111, 341-354.

Bonciani F., Callegari I., Conti P., Cornamusini G., Carmignani L., 2005. Neogene post-collisional evolution of the internal Northern Apennines: insights from the upper Fiora and Albegna valleys (Mt. Amiata geothermal area, southern Tuscany). Boll. Soc. Geol. It., Volume Speciale n. 3 (2005), 103-118.

Bonini M., Sani F., Stucchi E.M., Moratti G., Benvenuti M., Menanno G., Tanini C., 2014. Late Miocene shortening of the Northern Apennines back-arc. Journal of Geodynamics, 74, 1-31.

Bosi, C., P. Messina, M. Rosati and A. Sposato, 1996. Età dei travertini della Toscana meridionale e relative implicazioni neotettoniche. Memorie della Società Geologica Italiana, 51: 293-304.

Bossio A., Costantini A., Lazzarotto A., Liotta D., Mazzanti R., Mazzei R., Salvatorini G., Sandrelli F., 1993. Rassegna delle conoscenze sulla stratigrafiad el NeautoctonoToscano. Memorie della Società Geologica Italiana, 49, 17-98.

Bossio A., Foresi L.M., Mazzei R., Salvatorini G., Sandrelli F., Bilotti M., Colli A., Rossetto R., 2003. Geology and stratigraphy of the southern sector of the Neogene Albegna River Basin (Grosseto, Tuscany, Italy): Geologica Romana, 37, 165-173.

Breitenbach S.F:M. and Bernasconi S.M., 2011. Carbon and oxygen isotope analysis of small carbonate samples (20 to 100 µg) with a GasBench II preparation device. Rapid Communications in Mass Spectrometry, 25, 1910-1914.

Brogi A., 2004a. Miocene extension in the inner Northern Apennines: the Tuscan Nappe megaboudins in the Mt. Amiata geothermal area and their influence on Neogene sedimentation. Bollettino della Società Geologica Italiana, 123, 513-529.

Brogi, A. 2004b. Faults linkage, damage rocks and hydrothermal fluid circulation: tectonic interpretation of the Rapolano Terme travertines (southern Tuscany, Italy) in the context of the Northern Apennines Neogene–Quaternary extension. Eclogae Geologicae Helveticae, 97, 307–320.

Brogi A., 2008. The structure of the Monte Amiata volcano-geothermal area (Northern Apennines, Italy): Neogene-Quaternary compression versus extension. International Journal of Earth Sciences, 97, 677-703. DOI 10.1007/s00531-007-0191-1

Brogi A., 2011. Bowl-shaped basin related to low-angle detachment during continental extension: The case of the controversial Neogene Siena Basin (central Italy, Northern Apennines). Tectonophysics, 499, 54-76.

Brogi A. and Capezzuoli E., 2009. Travertine deposition and faulting: the fault-related travertine fissure-ridge at Terme S. Giovanni, Rapolano Terme (Italy). International Journal of Earth Sciences, 98, 931-947, DOI 10.1007/s00531-007-0290-z.

Brogi, A., Capezzuoli, E., Aquè, R., Branca, M. & Voltaggio, M. 2010a. Studying travertines for neotectonics investigations: Middle–Late Pleistocene syn-tectonic travertine deposition at Serre di Rapolano (Northern Apennines, Italy). International Journal of Earth Sciences, 99, 1383–1398.

Brogi A., Capezzuoli E., Buracchi E., Branca M., 2012. Tectonic control on travertine and calcareous tufa deposition in a low-temperature geothermal system (Sarteano, Central Italy). Journal of the Geological Society, 169, 461–476, doi: 10.1144/0016-76492011-137.

Brogi A., Capezzuoli E., Liotta D., Meccheri M., 2015. The Tuscan Nappe structures in the Monte Amiata geothermal area (central Italy): a review. Italian Journal of Geosciences, 134, 219-236, doi: 10.3301/IJG.2014.55.

Brogi A., Capezzuoli E., Martini I., Picozzi M., Sandrelli F., 2014. Late Quaternary tectonics in the inner Northern Apennines (Siena Basin, southern Tuscany, Italy) and their seismotectonic implication. Journal of Geodynamics, 76, 25-45.

Brogi A. and Fabbrini L., 2009. Extensional and strike-slip tectonics across the Monte Amiata–Monte Cetona transect (Northern Apennines, Italy) and seismotectonic implications. Tectonophysics, 476, 195-209.

Brogi A., Fidolini F., Liotta D., 2013. Tectonic and sedimentary evolution of the Upper Valdarno Basin: new insights from the lacustrine S. Barbara Basin. Ital. J. Geosci. (Boll. Soc. Geol. It.), 132/1, 81-97, doi: 10.3301/IJG.2012.08).

Brogi A. and Liotta D. (2008) - Highly extended terrains, lateral segmentation of the substratum, and basin development: The middle-late Miocene Radicondoli Basin (inner northern Apennines, Italy). Tectonics, VOL. 27, TC5002, doi:10.1029/2007TC002188.

Brogi A., Liotta D., Meccheri M., Fabbrini L., 2010b. Transtensional shear zones controlling volcanic eruptions: the Middle Pleistocene Mt Amiata volcano (inner Northern Apennines, Italy). Terra Nova, 22, 137-146, doi: 10.1111/j.1365-3121.2010.00927.x.

Browne P.R.L., 1978. Hydrothermal alteration in active geothermal fields. Ann. Rev Earth Planet. Sci., 6, 229-250.

Buonasorte G., Cataldi R., Ceccarelli A., Costantini A., D'Offizi S., Lazzarotto A., Ridolfi A., Baldi P., Barelli A., Bertini G., Bertrami R., Calamai A., Cameli G., Corsi R., D'Acquino C., Fiordelisi A., Gezzo A. & Lovari F., 1988. Ricerca ed esplorazione nell'area geotermica di Torre Alfina (Lazio – Umbria). Boll. Soc. Geol. It., 107, 265-337.

Buonasorte G., Cataldi R., Passaleva G., 2007. Geothermal Development In Italy: From Present To Future. Proceedings European Geothermal Congress 2007, Unterhaching, Germany, 30 May-1 June 2007.

Buttinelli M., Chiarabba C., Anselmi M., Bianchi I., De Rita D., Quattrocchi F., 2014. Crustal structure of Northern Latium (central Italy) from receiver functions analysis: New evidences of a post-collisional back-arc margin evolution. Tectonophysics, 621, 148-158.

Cadoux, A. and D.L. Pinti, 2009. Hybrid character and pre-eruptive events of Mt Amiata volcano (Italy) inferred from geochronological, petro-geochemical and isotopic data. Journal of Volcanology and Geothermal Research, 179, 169-190.

Caine J.S., Evans J.P. & Forster C.B., 1996. Fault zone architecture and permeability structure. Geology, 24, 1025-1028.

Capezzuoli E., 2013. Il patrimonio di travertini e calcareous tufa in Toscana. In: Acque e Travertini, Eds: Billi A., De Filippis L., Ubertini L., ISSN 2035-8088. Rendiconti Online della Società Geologica Italiana, 27, 31-41, doi: 10.3301/ROL.2013.18.

Carmignani L., Conti P., Cornamusini G., Pirro A. (2013) - Geological map of Tuscany (Italy). Journal of Maps, 9:4, 487-497, DOI:10.1080/17445647.2013.820154

Carmignani L., Decandia F.A., Fantozzi P.L., Lazzarotto A., Liotta D. & Meccheri M. (1994) - Tertiary extensional tectonics in Tuscany (Northern Apennines, Italy). Tectonophysics, 238, 295-315.

Cas, R.A.F., Giordano, G., Esposito, A., Balsamo, F., Lo, Mastro S., 2011. Hydrothermal breccia textures and processes: Lisca Bianca Islet, Panarea, Eolian Islands, Italy. Economic Geology, 106, 437-450.

Cavinato G.P. and De Celles P.G., 1999. Extensional basins in the tectonically bimodal central Apennines fold-thrust belt, Italy: response to corner flow above a subducting slab in retrograde motion. Geology, 27, 955-958.

Cerrina Feroni A., Bonini M., Martinelli P., Moratti G., Sani F., Montanari D., Del Ventisette C., 2006. Lithological control on thrust-related deformation in the Sassa-Guardistallo Basin (Northern Apennines hinterland, Italy). Basin Research, 18, 301-321, doi: 10.1111/j.1365-2117.2006.00295.x.

Chafetz H.S. and Guidry S.A., 2003. Deposition and diagenesis of Mammoth HotSprings travertine, Yellowstone National Park,Wyoming, U.S.A. Canadian Journal of Earth Sciences, 40, 1515-1529, doi: 10.1139/E03-051.

Chafetz H.S. and Lawrence J.R., 1994. Stable isotopic variability within modern travertines. Géographie Phys. et Quatern., 48(3), 257-273.

Chiocchini U., Castaldi F., Barbieri M., Eulilli V., 2010. A stratigraphic and geophysical approach to studying the deepcirculating groundwater and thermal springs, and their recharge areas, in Cimini Mountains–Viterbo area, central Italy. Hydrogeology Journal, 18, 1319-1341, doi 10.1007/s10040-010-0601-5.

Chiodini G., Frondini F., Ponziani F., 1995. Deep structures and Carbon dioxide degassing in Central Italy. Geothermics, 24, 81-94.

Cifelli F., Minelli L., Rossetti F., Urru G., Mattei M., 2012. The emplacement of the Late Miocene Monte Capanne intrusion (Elba Island, Central Italy): constraints from magnetic fabric analyses. International Journal of Earth Sciences, 101, 787-802, doi 10.1007/s00531-011-0701-z.

Cipollari P. and Cosentino D., 1995. Miocene unconformities in the Central Apennines: geodynamic significance and sedimentary basin evolution. Tectonophysics, 252, 375-389.

Collettini, C., De Paola, N., Holdsworth, R.E., Barchi, M.R., 2006. The development and behavior of low-angle normal faults during Cenozoic asymmetric extension in the Northern Apennines, Italy. J. Struct. Geol., 28, 333-352.

Conticelli S., Boari E., Burlamacchi L., Cifelli F., Moscardi F., Laurenzi M.A., Ferrari Pedraglio L., Francalanci L., Benvenuti M.G., Braschi E., Manetti P., 2015. Geochemistry and Sr-Nd-Pb isotopes of Monte Amiata Volcano, Central Italy: evidence for magma mixing between high-K calc-alkaline and leucititic mantle-derived magmas. Italian Journal of Geosciences, 134, 266-290, doi: 10.3301/IJG.2015.12.

Corniello A., Cardellicchio N., Cavuoto G., Cuoco E., Ducci D., Minissale A., Mussi M., Petruccione E., Pelosi N., Rizzo E., Polemico M., Tamburino S.2, Tedesco D., Tiano P., Iorio M., 2015. Hydrogeological Characterization of a Geothermal system: the case of the thermo-mineral area of Mondragone (Campania, Italy). International Journal of Environmental Research, 9, 523-534.

Corrado S., Aldega L., Celano A.S., De Benedetti A.A., Giordano G., 2014. Cap rock efficiency and fluid circulation of natural hydrothermalsystems by means of XRD on clay minerals (Sutri, Northern Latium, Italy). Geothermics, 50, 180-188.

Costantini A., Ghezzo C. & Lazzarotto A., 1984. Carta geologica dell'area geotermica di Torre Alfina (prov. Di Siena-Viterbo-Terni). ENEL, Unità Nazionale Geotermica – Pisa. Cartografia S.EL.C.A., Firenze.

Cox, S.F., Knackstedt, M.A., Braun, J., 2001. Principles of structural controls on permeability and fluid flow in hydrothermal systems. Rev. Econ. Geol. 14, 1–24.

Crossey L.J., Fischer T.P., Patchett P.J., Karlstrom K.E., Hilton D.R., Newell D.L., Huntoon P., Reynolds A.C., de Leeuw G.A.M., 2006. Dissected hydrologic system at the Grand Canyon: interaction between deeply derived fluids and plateau aquifer waters in modern springs and travertine. Geology, 34, 25-28.

Crossey L.J. and Karlstrom K.E., 2012. Travertines and travertine springs in eastern Grand Canyon: What they tell us about groundwater, paleoclimate, and incision of Grand Canyon. In: Timmons J.M. and Karlstrom K.E. (Eds.), Grand Canyon Geology: Two Billion Years of Earth's History. Geological Society of America Special Paper, 489, 131-143, doi:10.1130/2012.2489(09).

Crossey, L.C., Karlstrom, K.E., Dorsey, R., Pearce, J., Wan, E., Beard, L.S., Asmerom, Y., Polyak, V., Crow, R.S., Cohen, A., Bright, J., Pecha, M.E., 2015. Importance of groundwater in

propagating downward integration of the 6–5 Ma Colorado River system: Geochemistry of springs, travertines, and lacustrine carbonates of the Grand Canyon region over the past 12 Ma. Geosphere, 11, 1–23, doi:10.1130/GES01073.1.

Curewitz D. and Karson J.A., 1997. Structural settings of hydrothermal outflow: Fracture permeability maintained by fault propagation and interaction. Journal of Volcanology and Geothermal Research, 79, 149-168.

De Filippis L. and Billi A., 2012. Morphotectonics of fissure ridge travertines from geothermal areas of Mammoth Hot Springs (Wyoming) and Bridgeport (California). Tectonophysics, 548-549, 34-48.

De Filippis L., Faccenna C., Billi A., Anzalone E., Brilli M., Soligo M., Tuccimei P., 2013a. Plateau versus fissure ridge travertines from Quaternary geothermal springs of Italy and Turkey: Interactions and feedbacks between fluid discharge, paleoclimate, and tectonics. Earth-Science Reviews, 123, 35-52.

De Filippis L., Anzalone E., Billi A., Faccenna C., Poncia P.P., Sella P., 2013b. The origin and growth of a recently-active fissure ridge travertine over a seismic fault, Tivoli, Italy. Geomorphology, 195, 13-26.

Della Vedova B., Bellani S., Pellis G., Squarci P., 2001. Deep temperatures and surface heat flow distribution. In: Vai G.B. and Martini I.P. (Eds.): Anatomy of an Orogen: the Apennines and Adjacent Mediterranean Basins. Kluwer Academic Publisher, 65–76.

Dewey J.F., Helman M.L., Knott S.D., Turco E., Hutton D.H.W., 1989, Kinematics of the western Mediterranean: Geological Society of London Special Publications, 45, 265-283.

Dilsiz C., 2006. Conceptual hydrodynamic model of the Pamukkale hydrothermal field, southwestern Turkey, based on hydrochemical and isotopic data. Hydrogeology Journal, 14, 562-572.

Dini A., Granelli G., Puxeddu M. & Ruggirei G. (2005) - Origin and evolution of Pliocene–Pleistocene granites from the Larderello geothermal field (Tuscan Magmatic Province, Italy). Lithos, 81, 1-31.

Doglioni C., 1991, A proposal for the kinematic modelling of W-dipping subductions; possible applications to the Tyrrhenian-Apennines system: Terra Nova, 3, 423-434.

Dramis F., Materazzi M., Cilla G., 1999. Influence of climatic changes on freshwater travertine deposition: A new hypothesis. Physics and Chemistry of the Earth, Part A: Solid Earth and Geodesy, 24, 893-897, doi: 10.1016/S1464-1895(99)00132-5.

Duchi V., Minissale A., Paolieri M., Prati F., Valori A., 1992. Chemical relationship between discharging fluids in the Siena-Radicofani Graben and the deep fluids produced by the

geothermal fields of the Mt. Amiata, Torre Alfina and Latera (central Italy). Geothermics, 21, 401-413.

Edwards R.L., Chen J.H., Wasserburg G.J., 1988. 238U–234U–230Th systematics and the precise measurement of time over the last 500,000 years. Earth and Planetary Science Letters 81, 175–192.

Engin B., Güven O., Köksal F., 1999. Electron spin resonance age determination of a travertine sample from the southwestern part of Turkey. Applied Radiation and Isotopes, 51, 689-699.

Faccenna C., Funiciello R., Bruni A., Mattei M., Sagnotti L., 1994. Evolution of a transfer-related basin: the Ardea basin (Latium, central Italy). Basin Research, 6, 35-46.

Faccenna C., Mattei M., Funiciello R., Jolivet L., 1997. Styles of back-arc extension in the Central Mediterranean. Terra Nova, 9, 126-130.

Faccenna C., Piromallo C., Crespo-Blanc A., Jolivet L., Rossetti F., 2004, Lateral slab deformation and the origin of the western Mediterranean arcs: Tectonics, v. 23, TC1012, doi:10.1029/2002TC001488.

Faccenna C., Soligo M., Billi A., De Filippis L., Funiciello R., Rossetti C., Tuccimei P., 2008. Late Pleistocene depositional cycles of the Lapis Tiburtinus travertine (Tivoli, central Italy): possible influence of climate and fault activity. Global and Planetary Change, 63, 299-308. http://dx.doi.org/10.1016/J.Gloplacha.2008.06.006.

Farina F., Dini A., Innocenti F., Rocchi S., Westerman D.S., 2010. Rapid incremental assembly of the Monte Capanne pluton (Elba Island, Tuscany) by downward stacking of magma sheets. Geological Society of America Bulletin, 122, 1463-1479.

Ford T.D. and Pedley H.M., 1996. A review of tufa and travertine deposits of the world. Earth-Sci. Rev., 41, 117-175.

Fouke B.W., Farmer J.D., Des Marais D.J., Pratt L., Sturchio N.C., Burns P.C., Discipulo M.K., 2000. Depositional facies and aqueous-solid geochemistry of travertine-depositing hot spring (Angel Terrace, Mammoth Hot Spring, Yellowstone National Park, U.S.A.). Journal of Sedimentary Research, 70(3), 565-585.

Frank N., Braum M., Hambach U., Mangini A., Wagner G., 2000. Warm period growth of travertine during the last interglaciation in Southern Germany. Quaternary Research, 54, 38–48. doi:10.1006/qres.2000.2135.

Frepoli A.F., Marra C., Maggi A., Marchetti A., Nardi N., Pagliuca M., Pirro M., 2010. Seismicity, seismogenic structures, and crustal stress fields in the greater Rome area (central Italy). Journal of Geophysical Research, 115, B12303. http://dx.doi.org/10.1029/2009JB006322.

Frery E., Gratier J.P., Ellouz-Zimmerman N., Loiselet C., Braun J., Deschamps P., Blamart D., Hamelin B., Swennen R., 2015. Evolution of fault permeability during episodic fluid circulation: Evidence for the effects of fluid–rock interactions from travertine studies (Utah–USA). Tectonophysics, http://dx.doi.org/10.1016/j.tecto.2015.03.018.

Friedman I., 1970. Some investigation of the deposition of travertine from Hot Springs, I. The isotopic chemistry of a travertine-depositing spring. Geochimica and Cosmochimica Acta, 34, 1303-1315.

Gandin, A. and Capezzuoli, E., 2008. Travertine versus Calcareous tufa: distinctive petrologic features and related stable isotopes signature. Il Quaternario Italian Journal of Quaternary Science, 21, 125-136.

Gasparini C., Di Maro R., Pagliuca N., Pirro M., Marchetti A., 2002. Recent seismicity of the "Acque Albule" travertine basin. Annals of Geophysics, 45, 537-550.

Gelmini R., Mantovani P., Mucchi A.M., 1967. La serie a facies Toscana del Fiume Albegna presso Semproniano (già Semprugnano – Grosseto). Memorie della Società Geologica Italiana, 6, 359-378.

Gianelli G., Manzella A., Puxeddu M., 1997. Crustal models of the geothermal areas of southern Tuscany (Italy). Tectonophysics, 281, 221-239.

Gibbs A.D., 1984. Structural evolution of extensional basin margins. Journal of Geological Society London, 141, 609-620.

Gonfiantini, R., Panichi, C. and Tongiorgi, E., 1968. Isotopic disequilibrium in travertine deposition. Earth and Planetary Science Letters, 5, 55-58.

Guastaldi E., Graziano L., Liali G., Nunzio F., Brogna A., Barbagli A., 2014. Intrinsic vulnerability assessment of Saturnia thermal aquifer by means of three parametric methods: SINTACS, GODS and COP. Environmental Earth Sciences, DOI 10.1007/s12665-014-3191-z.

Gudmundsson A., 2011. Rock Fractures in Geological Processes. Cambridge University Press, 592 pp.

Guo, L., Andrews, J., Riding, R., Dennis, P. and Dresser, Q., 1996. Possible microbial effects on stable carbon isotopes in hot travertine. Journal of Sedimentary Research, 66, 468-473.

Hancock P.L., Chalmers R.M.L., Altunel E., çakir Z., 1999. Travitonics: using travertines in active fault studies. Journal of Structural Geology, 21, 903-916.

Ingrassia M., Martorelli E., Bosman A., Macelloni L., Sposato A., Chiocci F.L., 2015. The Zannone Giant Pockmark: First evidence of a giant complex seeping structure in shallow-water, central Mediterranean Sea, Italy. Marine Geology, 363, 38-51.

Innocenti F., Serri G., Ferrara G., Manetti P., Tonarini S., 1992. Genesis and classification of the rocks of the Tuscan Magmatic Province: thirty years after the Marinelli's model. Acta Vulcanology, 2, 247-265.

Ivanovich, M., Harmon, R.S., 1992. Uranium-series Disequilibrium: Applications to Earth, Marine, and Environmental Sciences. Clarendon Press, Oxford.

Jacobacci A., Martelli G., Nappi G., 1967. Note illustrative della Carta Geologica d'Italia alla scala 1:100.000, Foglio 129, S. Fiora. La Litograf, Roma.

Jolivet L., Faccenna C., Goffé B. et al. (1998) - Midcrustal shear zones in post-orogenic extension: Example from the northern Tyrrhenian Sea (Italy). Journal of Geophysical Research, 103, 12123-12160.

Kampman N., Burnside N.M., Shipton Z.K., Chapman H.J., Nicholl J.A., Ellam R.M., Bickle M.J., 2012. Pulses of carbon dioxide emissions from intracrustal faults following climatic warming. Nature Geoscience, 5, 352-358.

Karlstrom K.E., Crossey L.J, Hilton D.R., Barry P.H., 2013. Mantle 3He and CO2 degassing in carbonic and geothermal springs of Colorado and implications for neotectonics of the Rocky Mountains. Geology, 41, 495-498, doi:10.1130/G34007.1.

Keller, J.V.A., Minelli, G., Pialli, G., 1994. Anatomy of a late orogenic extension: the Northern Apennines case. Tectonophysics, 238, 275–294. http://dx.doi.org/10.1016/0040-1951(94)90060-4.

Kele S., Vaselli O., Szabó C., Minissale A., 2003. Stable isotope geochemistry of Pleistocene travertine from Budakalász (Buda Mts, Hungary). Acta Geologica Hungarica, 46/2, 161-175.

Kele S., Özkul M., Fórizs I., Gökgöz A., Baykara M.O. and Alçiçek M.C., 2011. Stable isotope geochemical study of Pamukkale travertines: New evidences of low-temperature non-equilibrium calcite-water fractionation. Sedimentary Geology, 238, 191-212.

Kele S., Breitenbach S.F.M., Capezzuoli E., Nele Meckler A., Ziegler M., Millan I.M., Kluge T., Deák J., Hanselmann K., John C.M., Yan H., Liu Z., Bernasconi S.M., 2015. Temperature dependence of oxygen- and clumped isotope fractionation in carbonates: a study of travertines and tufas in the 6-95°C temperature range. Geochimica et Cosmochimica Acta, doi:10.1016/j.gca.2015.06.032.

Laurenzi M.A., Braschi E., Casalini M., Conticelli S., 2015. New 40Ar-39Ar dating and revision of the geochronology of the Monte Amiata Volcano, Central Italy. Italian Journal of Geosciences, 134, 255-265, doi: 10.3301/IJG.2015.11.

Lavecchia G., Brozzetti F., Barchi M., Menichetti M., Keller J.V.A., 1994. Seismotectonic zoning in east-central Italy deduced from an analysis of the Neogene to present deformations and related stress fields. Geological Society of America Bulletin, 106, 1107-1120.

Lebatard A.E., Alçiçek A.C., Rochette P., Khatib S., Vialet A., Boulbes N., Bourlès D.L., Demory F., Guipert G., Mayda S., Titov V.V., Vidal L., de Lumley H., 2014. Dating the Homo erectus bearing travertine from Kocabas (Denizli, Turkey) at at least 1.1 Ma. Earth and Planetary Science Letters 390, 8-18.

Ludwig, K.R., 2003. Isoplot/Ex version 3.00, A Geochronological Toolkit for Microsoft Excel. Berkeley Geochronology Center Special Publication 4.

Liotta D., 1991, The Arbia-Val Marecchia Line, northern Apennines: Eclogae Geologicae Helvetiae, 84(2), 413-430.

Liotta D., 1994. Structural features of the Radicofani Basin along the Piancastagnaio (Mt. Amiata) – S. Casciano dei Bagni (Mt. Cetona) cross section. Memorie della Società Geologica Italiana, 48, 401-408.

Liotta, D., Ruggieri, G., Brogi, A., Fulignati, P., Dini, A., Cardini, I., 2010. Migration of geothermal fluids in extensional terrains: the ore deposits of the Boccheggiano-Montieri area (southern Tuscany, Italy). Int. J. Earth Sci. 99, 623–644.

Liotta D., Brogi A., Meccheri M., Dini A., Bianco C., Ruggieri G., 201., Coexistence of low-angle normal and high-angle strike- to oblique-slip faults during Late Miocene mineralization in eastern Elba Island (Italy): Tectonophysics, 660, 17-34.

Locardi E. and Nicolich R.1988. Geodinamica del Tirreno e dell'Appennino centro-meridionale: La nuova carta della Moho. Memorie della Società Geologica Italiana,41, 121-140.

Luque J.A. and Julià R., 2007. U/Th dating of Quaternary travertines at the middle River Llobregat (NE Iberian Peninsula, Northwestern Mediterranean). Correlation with sea-level changes. Geologica Acta, 5, 109-117.

Malinverno A. and Ryan W., 1986. Extension in the Tyrrhenian sea and shortening in the Apennines as result of arc migration driven by sinking of the lithosphere. Tectonics, 5, 227-245.

Manfra L., Masi U., Turi B., 1974. Effetti isotopici nella diagenesi dei travertini. Geologica Romana, 13, 147-155.

Marinelli G., Barberi F., Cioni R., 1993. Sollevamenti neogenici e intrusioni acide della Toscana e del Lazio settentrionale. Memorie della Società Geologica Italiana, 49, 279-288.

Marroni M., Moratti G., Costantini A., Conticelli S., Benvenuti M.G., Pandolfi L., Bonini M., Cornamusini G., Laurenzi M.A., 2015. Geology of the Monte Amiata region, Southern

Tuscany, Central Italy. Italian Journal of Geosciences, 134, 171-199, doi: 10.3301/IJG.2015.13.

Martelli L., Moratti G., Sani F., 1989. Analisi strutturale dei travertini della Toscana meridionale (Valle dell'Albegna). Bollettino della Società Geologica Italiana, 108, 197-205.

Martini I.P. and Sagri M. (1993) - Tectono-sedimentary characteristics of late Miocene-Quaternary extensional basins of the northern Apennines, Italy. Earth Science Reviews, 34, 197 – 233, doi:10.1016/0012-8252(93)90034-5.

Martini I.P., Sagri M., Colella A., 2001. Neogene—Quaternary basins of the inner Apennines and Calabrian arc. In: Vai G.B. and Martini I.P. (Eds): Anatomy of an orogen: the Apennines and adjacent Mediterranean basins. Kluwer academic publisher, 375-400.

Massoli D., Koyi H.A., Barchi M.R., 2006. Structural evolution of a fold and thrust belt generated by multiple décollements: Analogue models and natural examples from the Northern Apennines (Italy). Journal of Structural Geology, 28, 185-199.

Mazzini A., Etiope G., Svensen H., 2012. A new hydrothermal scenario for the 2006 Lusi eruption, Indonesia. Insights from gas geochemistry. Earth and Planetary Science Letters, 317-318, 305-318.

Minissale A., 2004. Origin, transport and discharge of CO2 in central Italy. Earth-Science Reviews, 66, 89-141.

Minissale A., Evans W.C., Magro G., Vaselli O., 1997. Multiple source components in gas manifestations from north-central Italy. Chemical Geology, 142, 175-192-

Minissale, A., Kerrick, D.M., Magro, G., Murrell, M.T., Paladini, M., Rihs, S., Sturchio, N.C., Tassi, F., Vaselli, O., 2002. Geochemistry of Quaternary travertines in the region north of Rome (Italy): structural, hydrologic and paleoclimatic implications. Earth and Planetary Science Letters, 203, 709-728.

Musumeci G. and Vaselli L., 2012. Neogene deformation and granite emplacement in the metamorphic units of northern Apennines (Italy): Insights from mylonitic marbles in the Porto Azzurro pluton contact aureole (Elba Island). Geosphere, 8, 470-490, doi:10.1130/GES00665.1.

Nappi G., A. Renzulli, P. Santi and P.Y. Gillot, 1995. Geological evolution and geochronology of the Vulsini Volcano District (Central Italy). Bollettino della Società Geologica Italiana, 114, 599-613.

Newell D.L., Crossey L.J., Karlstrom K.E., Fischer T.P., Hilton D.R., 2005. Continental-scale links between the mantle and groundwater systems of the western United States: Evidence from

travertine springs and regional He isotope data. GSA Today, 15, n°12, doi: 10.1130/1052-5173(2005)015<4:CSLBTM>2.0.CO;2

Özkul M., Kele S., Gökgöz A., Shen C.C., Jones B., Baykara M.O., Fórizs I., Nemeth T., Chang Y.-W., Alçiçek M.C., 2013. Comparison of the Quaternary travertine sites in the Denizli Extensional Basin based on their depositional and geochemical data: Sedimentary Geology, 294, 179-204.

Pascucci, V., A. Costantini, I. P. Martini, and R. Dringoli (2006), Tectono-sedimentary analysis of a complex, extensional, Neogene basin formed on thrust-faulted, Northern Apennines hinterland: Radicofani Basin, Italy, Sediment. Geol., 183(1–2), 71–97, doi:10.1016/j.sedgeo.2005.09.009.

Patacca E., Sartori R., Scandone P., 1990. Tyrrhenian basin and Apenninic arcs: kinematic relation since late Tortonian times. Memorie della Società Geologica Italiana, 45, 425-451.

Pauselli C., Barchi M.R., Federico C., Magnani B., Minelli G., 2006. The crustal structure of the Northern Apennines (central Italy): an insight by the CROP03 seismic line. American Journal of Science, 306, 428-450.

Peccerillo A., 2003. Plio-Quaternary magmatism in Italy. Episodes, 26, 222-226.

Pentecost A., 1995. The Quaternary travertine deposits of Europe and Asia Minor. Quaternary Science Reviews, 14, 1005-1028.

Pentecost A., 2005. Travertine. Springer-Verlag, Berlin Heidelberg (445 pp.).

Piccini L., DeWaele J., Galli E., Polyak V.J., Bernasconi S.M., Asmeromd Y., 2015. Sulphuric acid speleogenesis and landscape evolution: Montecchio cave, Albegna river valley (Southern Tuscany, Italy). Geomorphology, 229, 134-143.

Priewisch A., Crossey L.J., Karlstrom K.E., Polyak V.J., Asmerom Y., Nereson A., Ricketts J.W., 2014. U-series geochronology of large-volume Quaternary Traverine deposits of the southestern Colorado Plateau: evaluating episodicity and tectonic and paleohydrologic controls. Geosphere, 10(2), 401-423.

Rae A.J., Cooke D.R., Phillips D., Yeats C., Ryan C., Hermoso D., 2003. Spatial and temporal relationships between hydrothermal alteration assemblages at the Palinpinon Geothermal Field, Philippines – Implications for porphyry and epithermal ore deposits. Economic Gelogists, Special Publication, 10, 223-246.

Ricketts J.W., Karlstrom K.E., Priewisch A., Crossey L.J., Polyak V.J., Asmerom Y., 2014. Quaternary extension in the Rio Grande rift at elevated strain rates recorded in travertine deposits, central New Mexico. Lithosphere, 6(1), 3-16.

Rihs, S., Condomines, M., Poidevin, J.L., 2000. Long-term behaviour of continental hydrothermal systems: U-series study of hydrothermal carbonates from the French Massif Central (Allier Valley). Geochimica et Cosmochimica Acta, 64 (18), 3189-3199.

Rimondi V., Costagliola P.,·Ruggieri G., Benvenuti M., Boschi C., Brogi A., Capezzuoli E., Morelli G., Gasparon M., Liotta D., 2015. Investigating fossil hydrothermal systems by means of fluid inclusions and stable isotopes in banded travertine: an example from Castelnuovo dell'Abate (southern Tuscany, Italy). International Journal of Earth Sciences, DOI 10.1007/s00531-015-1186-y.

Rocchi S., Westerman D.S., Dini A., Innocenti F., Tonarini S., 2002. Two-stage growth of laccoliths at Elba Island, Italy. Geology, 30, 983-986.

Rosenbaum G., and Lister G.S., 2004, Neogene and Quaternary rollback evolution of the Tyrrhenian Sea, the Apennines, and the Sicilian Maghrebides: Tectonics, v. 23, TC1013, doi: 10.1029/2003TC001518.

Rossetti, F., Tecce, F., Billi, A., Brilli, M., 2007. Patterns of fluid flow in the contact aureole of the late Miocene Monte Capanne pluton (Elba Island, Italy): the role of structures and rheology. Contributions to Mineralogy and Petrology, 153, 743-760.

Rossetti F., Balsamo F., Villa I.M., Bouybaouenne M., Faccenna C., Funiciello R., 2008. Pliocene–Pleistocene HT–LP metamorphism during multiple granitic intrusions in the southern branch of the Larderello geothermal field (southern Tuscany, Italy). Journal of the Geological Society, London, 165, 247-262.

Rossetti F., Aldega L., Tecce F., Balsamo F., Billi A., Brilli M., 2011. Fluid flow within the damage zone of the Boccheggiano extensional fault (Larderello–Travale geothermal field, central Italy): structures, alteration and implications for hydrothermal mineralization in extensional settings. Geological Magazine, 148 (4), 558–578.

Rowland, J.V. and Sibson, R.H., 2004. Structural controls on hydrothermal flow in a segmented rift system, Taupo Volcanic Zone, New Zealand. Geofluids 4, 259–283.

Royden L., Patacca E., Scandone P., 1987, Segmentation and configuration of subducted lithosphere in Italy: an important control on thrust belt and foredeep-basins evolution: Geology, v. 15, p. 714-717.

Sella P., Billi A., Mazzini I., De Filippis L., Pizzino L., Sciarra A., Quattrocchi F., 2014. A newly-emerged (August 2013) artificially-triggered fumarole near the Fiumicino airport, Rome, Italy. Journal of Volcanology and Geothermal Research, 280, 53-66.

Serri, G., Innocenti, F., Manetti, P., 1993. Geochemical and petrological evidence of the subduction of delaminated Adriatic continental lithosphere in the genesis of the Neogene-Quaternary magmatism in central Italy. Tectonophysics 223, 117-147.

Soligo M., Tuccimei P., Barberi R., Delitala M.C., Miccadei E., Taddeucci A., 2002. U/Th dating of freshwater travertine from Middle Velino Valley (Central Italy): paleoclimatic and geological implications. Palaeogeography, Palaeoclimatology, Palaeoecology, 184, 147-161.

Sturchio N.C., Pierce K.L., Murrell M.T., Sorey M.L., 1994. Uranium-series ages of travertines and timing of the last glaciation in the northern Yellowstone area, Wyoming–Montana. Quaternary Research, 41, 265-277.

Taddeucci, A. and Voltaggio, M., 1987. Th-230 dating of the travertines connected to the Vulsini Mts. volcanism (Northern Latium Italy): neotectonics and hydrogeology. Per. Mineral., 56, 295–302.

Toker, E., Kayser-Özer, M.S., Özkul, M., Kele, S., 2015. Depositional system and palaeoclimatic interpretations of Middle to Late Pleistocene travertines: Kocabas, Denizli, south-west Turkey. Sedimentology, 62, 1360-1383.

Turi B., 1986. Stable isotope geochemistry of travertines. In: P. Fritz and J.C. Fontes (Eds) - Handbook of Environmental Isotope Geochemistry. 2. Terrestrial Environment, B. Elsevier, Amsterdam, 207-238.

Tzedakis P.C., Andrieu V., de Beaulieu J.-L., Birks H.J.B., Crowhurst S., Follieri M., Hooghiemstra H., Magri D., Reille M., Sadori L., Shackleton N.J., Wijmstra T.A., 2001. Establishing a terrestrial chronological framework as a basis for biostratigraphical comparisons. Quaternary Science Reviews, 20, 1583-1592.

Uysal I.T., Feng Y., Zhao J.X., Altunel E., Weatherley D., Karabacak V., Cengiz O., Golding S.D., Lawrence M.G., Collerson K.D., 2007. U-series dating and geochemical tracing of late Quaternary travertine in co-seismic fissures. Earth and Planetary Science Letters, 257 (3-4), 450-462.

Uysal I.T., Feng Y., Zhao J.X., Isik V., Nuriel P., Golding S.D., 2009. Hydrotermal CO2 degassing in seismically active zones during the late Quaternary. Chemical Geology, 265, 442-454.

Van der Pluijm B.A. and Marshak S., 2003. Earth Structure (2° edition). Ed. W.W. Norton &Company (New York-London), 673 pp.

Vignaroli, G., Aldega, L., Balsamo, F., Billi, A., De Benedetti, A.A., De Filippis, L., Giordano, G., Rossetti, F., 2015. A way to hydrothermal paroxysm, Colli Albani Volcano, Italy. Geological Society of America Bulletin, 127, 672–687, doi: 10.1130/B31139.1.

Vignaroli G., Pinton A., De Benedetti A.A., Giordano G., Rossetti F., Soligo M., Berardi G., 2013. Structural compartmentalisation of a geothermal system, the Torre Alfina field (central Italy). Tectonophysics, 608, 482-498.

Wedepohl, K., 1995. The composition of the continental crust. Geochim. Cosmochim. Acta 59, 1217–1239.

Wortel M.J.R., and Spakman W., 2000, Subduction and slab detachment in the Mediterranean-Carpathian region: Science, v. 290, p. 1910-1917.

Zanchi, A., Tozzi, M., 1987. Evoluzione paleogeografica e strutturale recente del bacino del fiume Albegna (Toscana meridionale). Geologica Romana, 26, 305–325.

Zachos J., Pagani M., Sloan L., Thomas E., Billups K., 2001. Trends, rhythms, and aberrations in global climate 65 Ma to present. Science, 292, 686-693, doi:10.1126/science.1059412.

Chapter 3

This chapter consists of a paper submitted to Tectonophysics (Berardi G., Vignaroli G., Billi A.,, Rossetti F., Soligo M., Kele S., Baykara M.O., Bernasconi S.M., Castorina F., Tecce F., Shen C.C. "Growth of a Pleistocene giant carbonate vein and nearby thermogene travertine deposits at Semproniano, southern Tuscany, Italy"), focusing on the relationships between hydrothermalism and tectonics during Quaternary time in southern Tuscany (central Italy), by investigating a giant carbonate vein (≥50 m thick; fissure ridge travertines) and nearby travertine plateaus in the Semproniano area (Mt. Amiata geothermal field).

Growth of a Pleistocene giant carbonate vein and nearby thermogene travertine deposits at Semproniano, southern Tuscany, Italy

Abstract

A giant carbonate vein (≥50 m thick; fissure ridge travertines) and nearby travertine plateaus in the Semproniano area (Mt. Amiata geothermal field, southern Tuscany, Italy) are investigated through a multidisciplinary approach, including field and laboratory geochemical analyses (U/Th geochronology, C, Nd, O and Sr isotope systematics, REE abundances, and fluid inclusion microthermometry). The main aim of this work is to understand: (1) modes and rates for the growth of the giant vein and nearby travertine deposits within a Quaternary volcano-tectonic domain; (2) implications in terms of the CO_2 release; and (3) possible relationships with Quaternary paleoclimate and hydrological oscillations. Results show that the giant vein was the inner portion of a large fissure ridge travertine and grew asymmetrically and ataxially through repeated shallow fluid injections between >650 and 85 ka, with growth rates in the order of 10^{-2} and 10^{-3} mm a^{-1}. The giant vein developed mainly during warm humid (interglacial) periods, partially overlapping with the growth of

nearby travertine plateaus. Estimated values of CO_2 leakage connected with the vein precipitation are between about $5x10^6$ and $3x10^7$ mol a^{-1} km^{-2}, approximately representing one millionth of the present global CO_2 leakage from volcanic areas. Temperatures estimates as obtained from O-isotopes and fluid inclusion microthermometry indicate epithermal conditions (90-50 °C) for the circulating fluid during the giant vein growth, with only slight evidence of cooling with time. Geochemical and isotope data document that the travertine deposits have developed mainly during Pleistocene warm humid periods, within a tectonically-controlled convective fluid circuit fed by meteoric infiltration and maintained by the regional geothermal anomaly hosted by the carbonate reservoir of the Mt. Amiata field.

3.1. Introduction

Thermogene travertines form through precipitation of $CaCO_3$ from supersaturated fluids usually generated and discharged in volcano-tectonic settings, often deposited in proximity of active geothermal springs or along open fissures (Pentecost, 1995; Ford and Pedley, 1996; Pentecost, 2005; Crossey et al., 2006). In addition to being important decorative and construction stones since at least the Roman time (Calvo and Regueiro, 2010), a renewed world-wide interest for thermogene travertine deposits resides in their importance to be potential analogs of long-term outflow from artificial CO_2 storages (Shipton et al., 2004; Bickle and Kampman, 2013; Burnside et al., 2013; Frery et al., 2015). Moreover, recent discoveries of large hydrocarbon reserves in subsalt porous microbial and travertine-like rocks along the Brazilian and Angolan margins of the Atlantic Ocean place thermogene travertines among the best exposed analogs of these hydrocarbon-reservoir rocks, which are hitherto known only from seismic data and well cores (e.g., Beasley et al., 2010; Rezende and Pope, 2015; Ronchi and Cruciani, 2015; Soete et al., 2015).

Travertines can show various deposit morphologies such as cascades, terrace mounds, fissure ridges, plateaus, and towers (Chafetz and Folk, 1984; Altunel and Hancock, 1993a, b; Pentecost, 1995; Pentecost, 2005). These morphologies are only partially dependent on the topography over which the travertines precipitate. Other factors such as (neo)tectonics (Altunel and Hancock, 1996; Hancock et al., 1999; Brogi, 2004a; Brogi and Capezzuoli, 2009; Brogi et al., 2010, 2012; De Filippis et al., 2013a; Ricketts et al., 2014; Maggi et al., 2015), climate oscillations (Sturchio et al., 1994, Rihs et al., 2000; Faccenna et al., 2008, De Filippis et al., 2012), earthquakes (Uysal et al., 2007, 2009; Brogi et al., 2014; Gradziński et al., 2014), and hydrological regimes (Priewisch et al., 2014; Crossey et al., 2015) have been proposed to influence travertine growth and morphology; however, the way how these and other factors control the travertine development and shape is still uncertain. It is, in particular, unclear what are the factors controlling travertine deposits, that are completely different in morphology and volume such as travertine fissure ridges and plateaus, which can, nonetheless, form in close proximity during the same time span (e.g., De Filippis et al., 2013b).

In this paper, we address the growth of travertine fissure ridges and plateaus. Fissure ridges are deposits of travertines with an elongate mound shape characterized by a length between a few meters and over 2000 m, and a main crestal fissure from which the travertine-feeding fluids gush out (Chafetz and Folk 1984; Altunel and Hancock, 1993a,b, 1996; Çakır, 1999; Hancock et al., 1999; Uysal et al., 2007, 2009; De Filippis et al., 2012, 2013a). Fissure ridges are usually formed by two main travertine types: (1) the bedded travertine, which consists of a porous and stratified deposit constituting the flanks (often clinostratified) and the bulk of the fissure ridge and (2) the banded travertine, which consists of subvertical bands of sparry nonporous carbonate (usually calcite, aragonite, or both) filling large veins that intrude the axial region of the fissure ridge. In places, these veins can also develop as sill-like structures along the beds of the bedded travertine or host rocks (Uysal et al., 2007; Gratier et al., 2012). Travertine plateaus, in contrast, are characterized by massive and large deposits consisting of sub-horizontal to gently-clinostratified travertine beds usually filling a tectonic or morphological depression and producing no prominent topography (Faccenna et al., 2008; De Filippis et al., 2013a).

Tuscany (Fig. 3.1), central Italy, is a region characterized by Neogene-Quaternary formation of extensional basins, widespread magmatism, associated contact metamorphism, hydrothermalism and ore mineralization, and also numerous thermogene travertine deposits (Marinelli et al., 1993; Serri et al., 1993; Barberi et al., 1994; Carmignani et al., 1994; Dini et al., 2005; Gandin and Capezzuoli, 2008; Brogi and Capezzuoli, 2009; Rossetti et al., 2008, 2011). Travertine deposition in Tuscany has occurred near highly-productive geothermal areas (Larderello-Travale and Mt. Amiata; Batini et al., 2003), where endogenous fluids permeate Meso-Cenozoic carbonate reservoirs and mix before feeding thermal springs and CO_2 emission centers (e.g., Minissale, 2004). Both travertine fissure ridges and plateaus are documented in Tuscany. In particular, studied fissure ridges are exposed in the Rapolano Terme (e.g., Brogi and Capezzuoli, 2009; Guo and Riding, 1999) and Castelnuovo dell'Abate (Rimondi et al., 2015) localities (Fig. 3.1b), where banded travertine forms centimeters-to-meters thick veins within meters-sized elongate mounds accreted over a restricted time interval between Pleistocene and Holocene times.

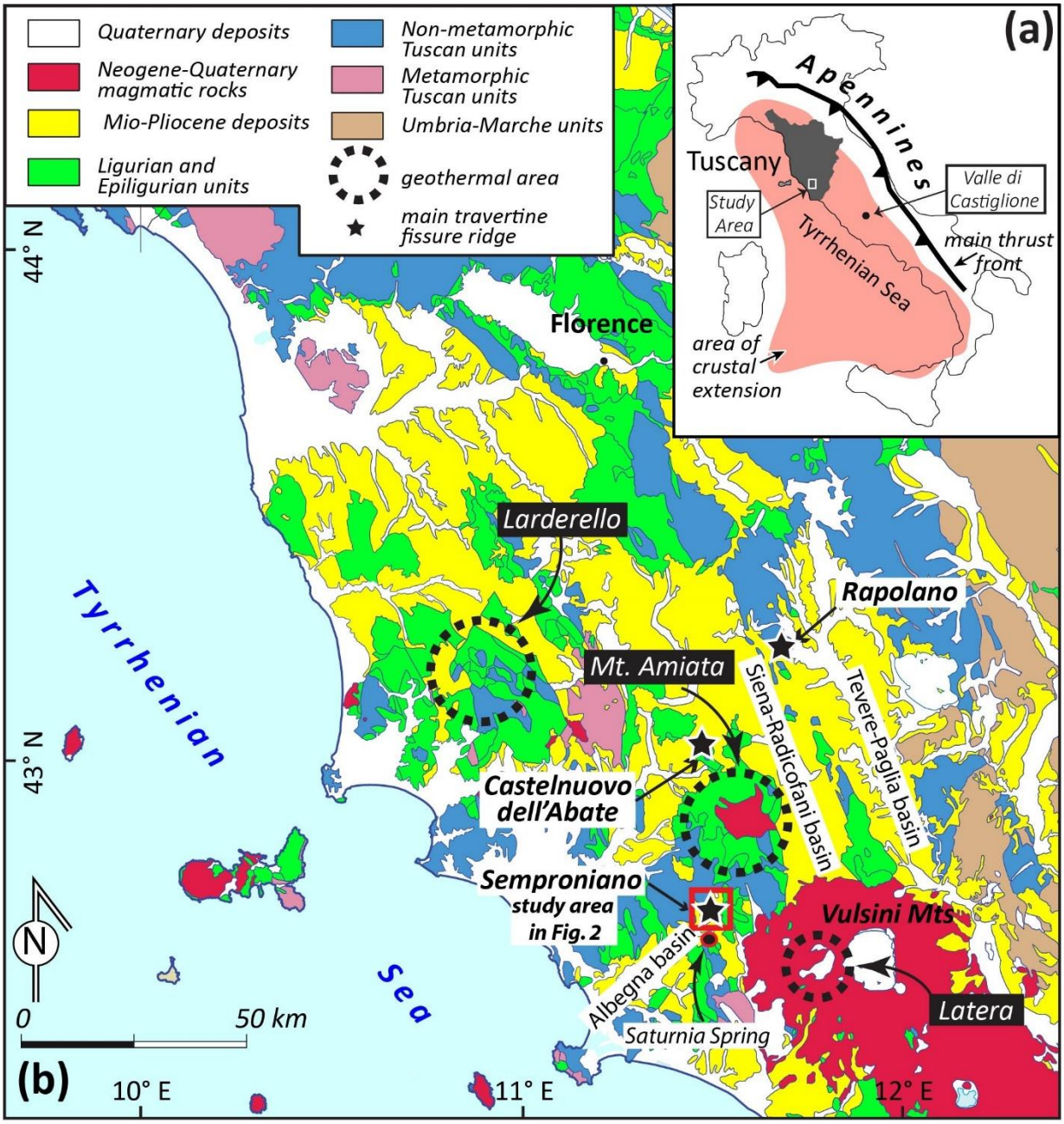

Figure 3.1 - (a) Schematic map of Italy showing the Apennines fold-thrust belt and the area affected by crustal extension at the rear (west) of the belt. This latter area includes Tuscany, where the study area (Sempronian, upper Albegna basin, southern Tuscany) is located. (b) Geological map of the southern Tuscany and northern Latium regions showing the main geothermal fields and travertine deposits (including fissure ridges).

We focus our study on travertines exposed in the village of Sempronian (northern Albegna basin), which is built on top of a hill at an altitude of 620 m. Sempronian is located only about 15 km southward of the Mt Amiata Pleistocene volcanic district and 9 km from the Saturnia thermal spring (Figs. 3.1 and 3.2), where active travertine deposition still occurs. The Sempronian village

lies on a travertine fissure ridge, a composite carbonate vein (≥50-m-thick) consisting of subvertical banded travertine (Capezzuoli et al., 2013), which crops up from the surrounding host carbonate rocks (Paleogene). Other travertine deposits or carbonate mineralizations, including travertine plateaus, small veins, and bedded travertines, are exposed within a few kilometers from the Semproniano village (Fig. 3.3a). The origin and growth modes of these deposits and mineralizations in the Semproniano area are unknown and the main driving factors (e.g., tectonics, paleohydrology, paleoclimate, etc.) as well. Moreover, absolute dating of these travertines is missing, thus making very difficult the regional correlation among these deposits as well as between the deposits themselves and the dated tectonic, volcanic, and paleoclimate events in the region.

The coexistence of different nearby $CaCO_3$-mineralizations and travertine deposits in a region of recent tectonic and volcanic activity makes the Semproniano area an excellent case study to understand the nature of those carbonates deposits. Using a multidisciplinary approach consisting of geological, structural, geomorphologic, and geochemical methods (including fieldwork, remote observations, U/Th dating, C- Nd- O- and Sr-isotope systematics, rare Earth element (REE) abundances, and fluid inclusion microthermometry), this study is aimed at understanding the development of the different travertine bodies (vein and plateau type), their mutual relationships, and the feedback relationships between travertine deposition and driving factors such as tectonics, volcanisms, and paleoclimate. The main novelty of this work concerns growth modes and rates of the Semproniano fissure ridge and implications for the associated CO_2 leakage. In addition, our results provide insights at regional scale concerning the late Quaternary hydrothermal and tectonic activity of southern Tuscany.

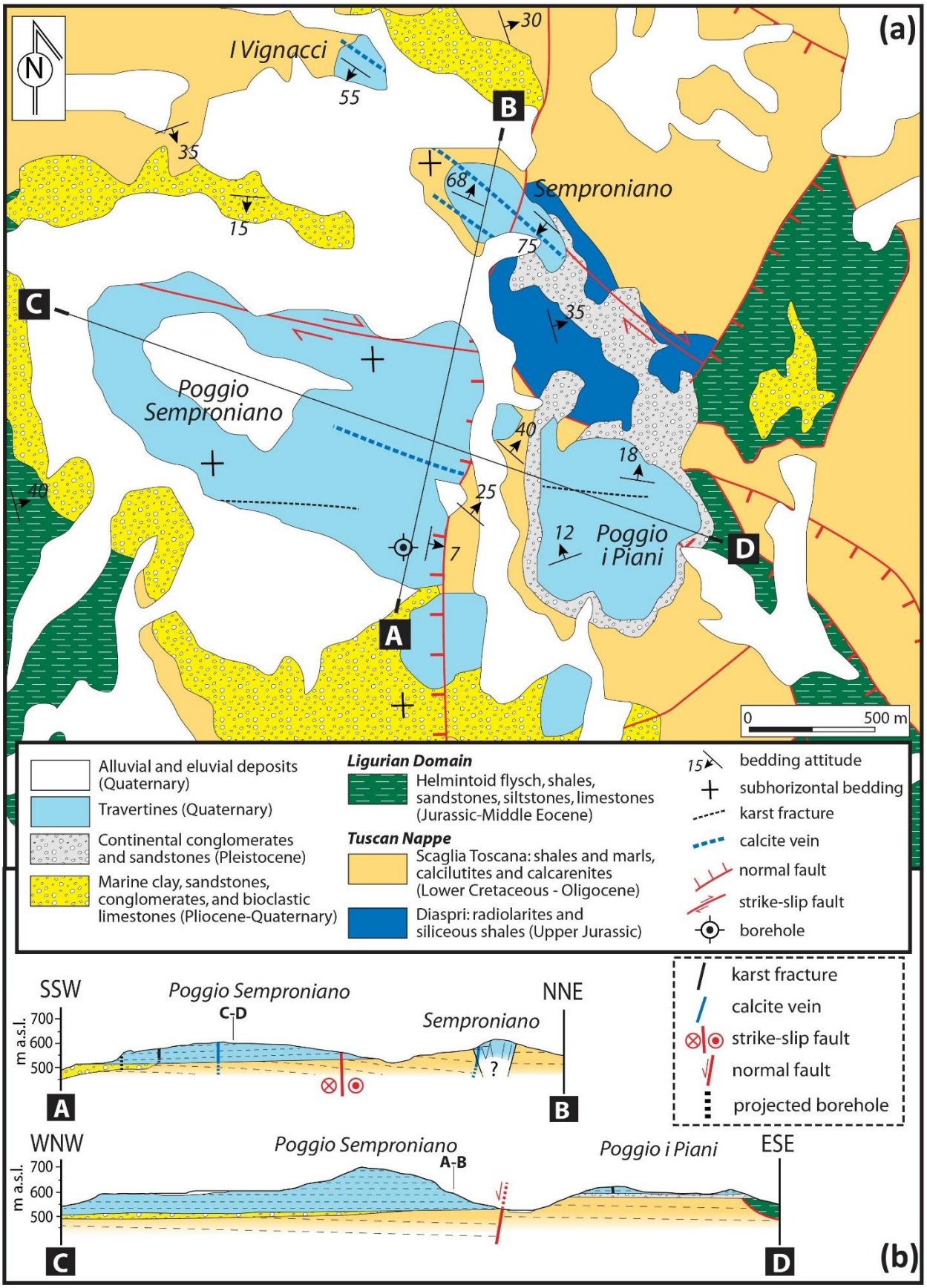

Figure 3.2 - (a) Structural geological map of the study area (Sempronianо area in the upper Albegna basin) and (b) related geological cross-sections. The map is based on and partly redrawn from the geological map at the 1:10,000 scale available online at www.regione.toscana.it/-/geologia.

3.2. Geological setting

Southern Tuscany is located in the inner sector (western) side of the northern Apennine chain (Fig. 3.1), which is a Cenozoic NW-SE-trending orogenic belt developed through a general eastward migration of thrust sheets in a classical piggy back sequence toward the Adriatic foreland (e.g., Patacca et al., 1990; Cipollari and Cosentino, 1995; Massoli et al., 2006). In Tuscany, post-orogenic extension and collapse of the previously formed orogenic belt started in late Miocene time, while, toward the east, the belt was still under a compressional regime (e.g., Malinverno & Ryan, 1986; Dewey 1988; Jolivet et al., 1998; Cavinato and De Celles, 1999; Pauselli et al., 2006). The extensional process generated normal faults that dismantled the previously-formed fold-thrust belt (e.g. Carmignani et al., 1994; Keller et al., 1994; Barchi et al., 1998; Jolivet et al., 1998; Collettini et al., 2006) and produced significant crustal thinning (present-day crust thickness is about 22-24 km; Locardi and Nicolich, 1988; Billi et al., 2006) as well as the development of sedimentary basins, magmatic provinces, and diffuse volcanism (Serri et al., 1993; Serri, 1997; Peccerillo, 2003). Fossil and active, structurally-controlled hydrothermal mineralizations are widespread evidence of the interaction between hydrothermal systems and extensional faults (e.g., Barberi et al., 1994; Buonasorte et al., 1988; Chiarabba et al., 1995; Gianelli et al., 1997; Batini et al., 2003; Bellani et al., 2004; Annunziatellis et al., 2008; Brogi, 2008; Liotta et al., 2010; Rossetti et al., 2011; Vignaroli et al., 2013).

Southern Tuscany (Fig. 3.1) is characterized by main NW-SE-trending and minor NE-SW-trending Miocene-to-Quaternary sedimentary basins formed during post-orogenic extensional processes and bounded by extensional-to-transtensional structures (Martini and Sagri, 1993; Liotta, 1994; Pascucci et al., 2006; Brogi and Liotta, 2008; Brogi, 2011; Brogi et al., 2013; 2014; 2015; Marroni et al., 2015). These structures include the Tevere-Paglia, Siena-Radicofani, and Albegna basins. The Semproniano thick vein and surrounding travertine deposits are located in the Albegna basin, which consists of a NE-SW-trending tectonic depression bounded to the north and southeast by the volcanic districts of the Mt Amiata and Vulsini Mts, respectively (Fig. 3.1). The magmatic

activity (or part of it) of the Mt Amiata district is dated to 300-190 ka according to Cadoux and Pinti (2009) and to 300-225 ka according to Laurenzi et al. (2015), whereas the activity (or part of it) of the Vulsini Mts district is dated to 590-127 ka according to Nappi et al. (1995).

The geological setting of the Albegna basin is characterized by the presence of metamorphic and non-metamorphic tectonic units stacked during the formation of the Apennines fold-thrust belt. From bottom to top, these units are as follows (e.g., Carmignani et al., 2013): (1) low-grade metamorphic rocks of the Tuscan Metamorphic Complex; (2) Upper Triassic to Oligocene kilometers-thick sedimentary succession composed by basal evaporites followed by shelf carbonates and marls (Tuscan Nappe); (3) Jurassic to Eocene ophiolite-derived clays and marls succession (Ligurian Domain); and (4) Upper Miocene to Pleistocene terrigenous post-orogenic deposits. The latter consist of fluvio-lacustrine deposits and marine clays that deposited in subsiding areas concomitantly with the regional tectonic extension (Zanchi and Tozzi, 1987; Bonazzi et al., 1992; Bossio et al., 2004).

In the Albegna basin, travertine deposits unconformably lie on top of the Neogene-Pleistocene deposits (Zanchi and Tozzi, 1987; Martelli et al., 1989; Bosi et al., 1996). The travertine deposition occurred in distinct phases and over a long time interval (Bosi et al., 1996). In particular, based on the travertine morphological and stratigraphic characters, Bosi et al. (1996) proposed a travertine deposition spanning from Messinian to Holocene times. In particular, Bosi et al. (1996) suggested that the travertines of the Semproniano area deposited during Pliocene time, whereas other authors considered them as early Pleistocene in age (Zanchi and Tozzi, 1987). The lack of absolute radiometric ages restricts the full understanding of these travertine deposits and their relationships with the hydrothermal and tectonic activity in the Albegna basin.

3.3. Methods and Results

3.3.1. Geology and geomorphology

We performed a field-based study on the geology, geomorphology, and structural setting of the travertine deposits located in the Semproniano area, namely: the (1) Semproniano ridge, (2) I

Vignacci, (3) Poggio Sempronianο, and (4) Poggio i Piani deposits (Figs. 3.2-3.5). We focused this study on the recognition of different travertine morphotypes (e.g., plateaus vs. fissure ridge travertines), on the relationships between travertine deposits and host rocks, and on the deformation features affecting the travertine deposits.

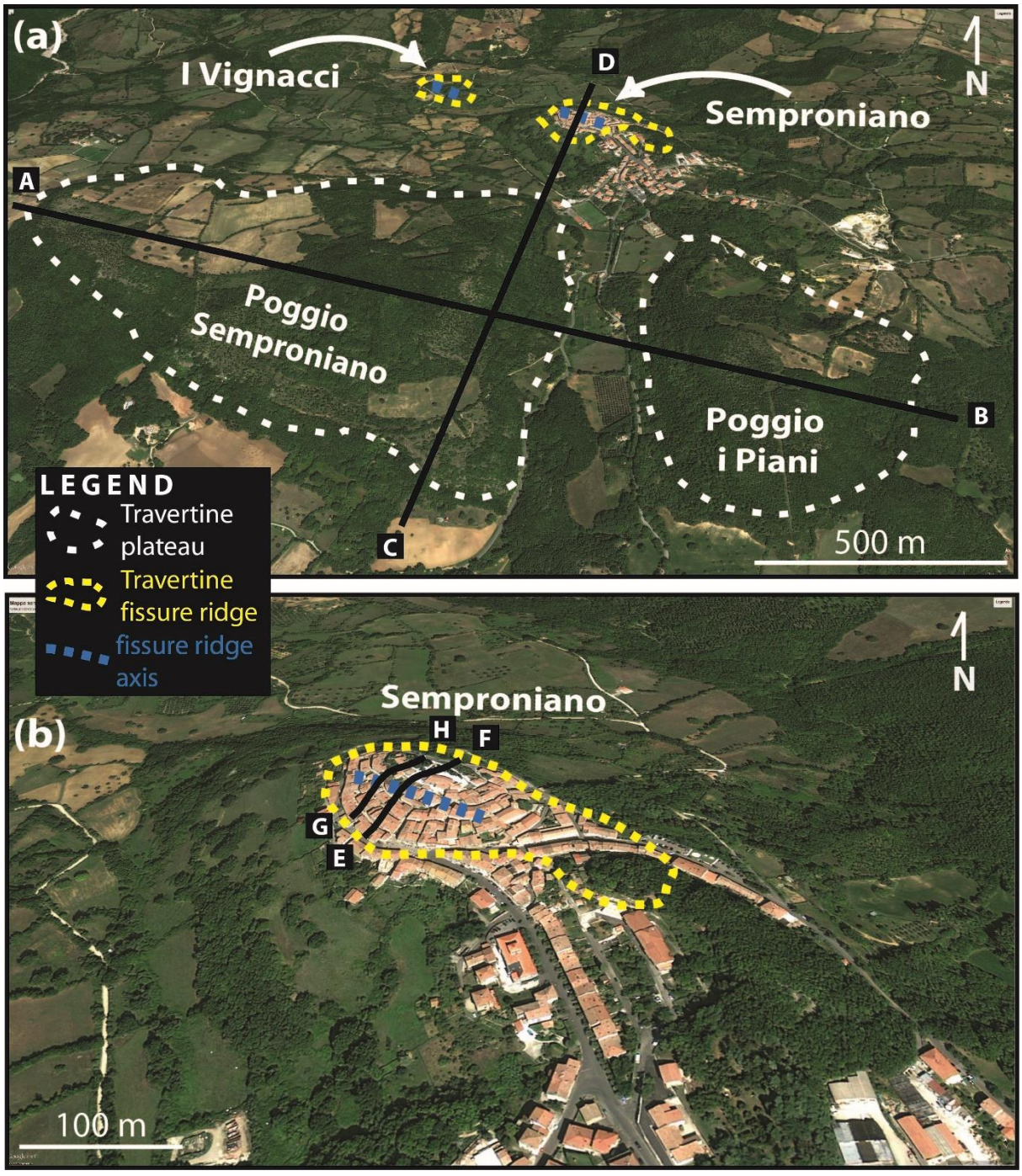

Figure 3.3 - (a) Northward panoramic view of the study area with localization of the studied travertine deposits that are differentiated by morphology. (b) Northward panoramic view of the Sempronianο ridge (i.e., Sempronianο giant vein). Tracks of geological cross-sections (Figs. 3.2b and 3.6) are also shown.

The study area is characterized by a set of post-orogenic Pliocene-Quaternary continental and marine sedimentary deposits (including the studied travertines) that unconformably rest on top of the Apennine stacked units (e.g., Bonciani et al., 2005; Brogi, 2008; Brogi and Fabbrini, 2009). The travertine plateaus (Poggio Semproniano and Poggio i Piani), in particular, unconfomably lie over Pliocene-Quaternary deposits and over the Scaglia Toscana Fmt. of the underlying Tuscan Nappe (Fig. 3.4a) which host the Semproniano fissure ridge (Fig. 3.2). The Poggio Semproniano deposit occupies the top portion of a triangular hill that is almost 700 m high (Fig. 3.3). The hill is tabular with a terrace-like top surface marked by a peripheral rim that runs all around the terraced deposit and delimits the terrace itself from the steep flanks of the hill. At the foot of these escarpments, the contact between the travertine deposit and the surrounding units is often covered by debris constituted by alluvial and eluvial deposits. The travertine body has dimensions of around 1300 m in the NW-SE direction and 700 m in the N-S direction, and has a maximum vertical thickness of about 200 m (Figs. 3.2 and 3.3). The travertine depositional fabric consists of piano-parallel centimeters-thick beds of whitish lime-mudstone with homogeneous porosity due to the presence of microbialites. Millimeter to centimeter-sized karst dissolution cavities are also present (Fig. 3.4c). On the eastern flank, the travertine beds of the Poggio Semproniano plateau and the underlying marly deposits of the Tuscan Nappe are pervaded by a set of cm-thick subvertical veins striking NW-SE, filled by white sparry carbonate.

The Poggio i Piani deposit is very similar to the one of Poggio Semproniano. Poggio i Piani is a terraced triangular hill with maximum elevation around 630 m. Also here, the travertine deposit is characterized by an outer sharp rim that runs all around the terraced deposit and delimits the terrace itself with the steep flanks of the hill. The deposit is tabular and sub-horizontal with sedimentary features similar to the ones described for Poggio Semproniano (Figs. 3.4c, d, e). The dimensions of the Poggio i Piani travertine plateau are about 500 m in the NW-SE direction and 450 m in the N-S direction with a maximum thickness of 35 m (Fig. 3.2). A narrow N10°-trending valley with a

minimum elevation of about 500 m separates the Poggio Semproniano and Poggio i Piani hills (Fig. 3.3).

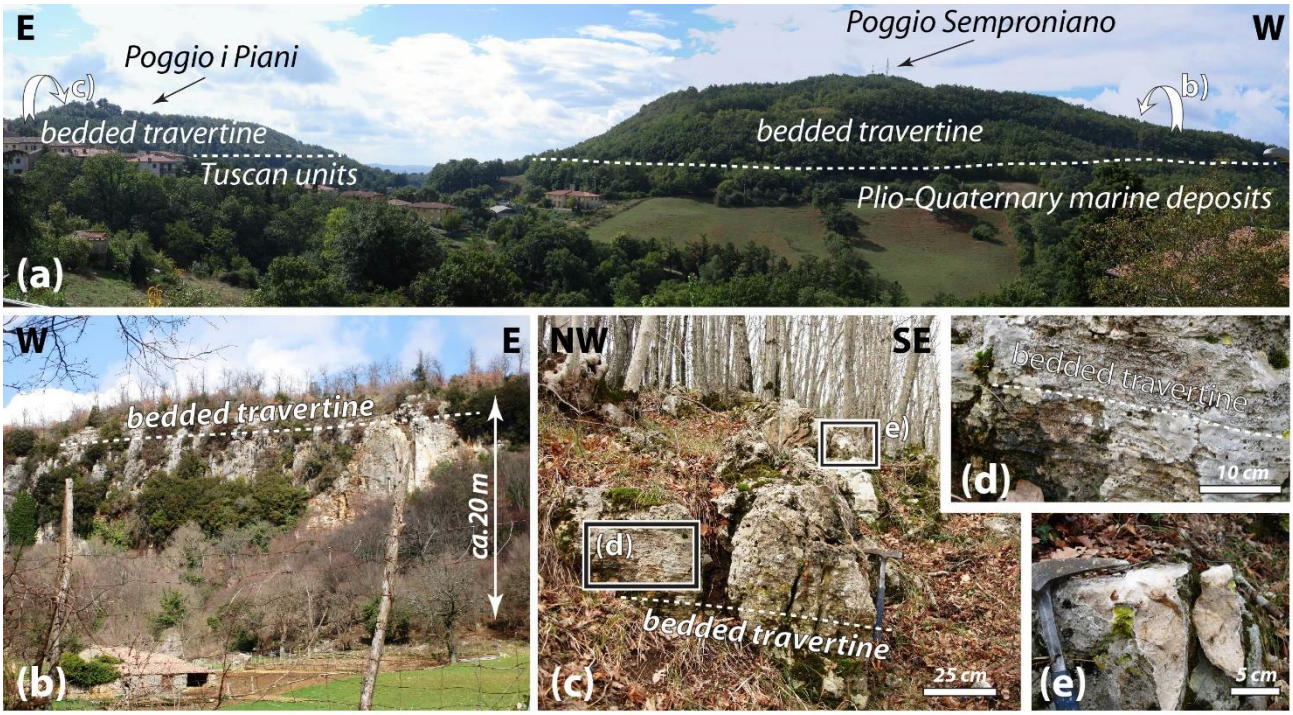

Figure 3.4 - (a) Southward panoramic view of Poggio i Piani and Poggio Semproniano travertine plateaus. The Poggio i Piani plateau lies on top of the Scaglia Toscana Fmt. (belonging to the non-metamorphic succession of the Tuscan Domain) whereas the Poggio Semproniano plateau lies on top of Plio-Quaternary marine deposits. (b) Southern margin of the Poggio Semproniano travertine plateau. (c) Sub-horizontal travertine beds forming the Poggio I Piani plateau. (d) Detail of a laminated bedded travertine from Poggio I Piani plateau. (e) Close-up view of the bedded travertine occurring at Poggio i Piani**.**

The Semproniano ridge is separated from the Poggio Semproniano and Poggio I Piani deposits by a narrow NW-SE-trending valley with a minimum elevation of about 500 m (Fig. 3.3). The Semproniano ridge crops out from the top of a NW-SE-elongate domed hill with maximum altitude around 620 m a.s.l. and about 1000 m long and 400 m wide. The central part of the Semproniano ridge, constituted by banded sparry travertine with a total thickness of more than 50 m, is characterized by complex geometries such as V-like-shaped (Fig. 3.5e) or crosscutting carbonate bands that are up to about 2 cm thick. The sparry subvertical bands of carbonate form a unique, composite and uninterrupted vein that we call the Semproniano giant vein for its large thickness of more than 50 m. The southwestern flank of the ridge is characterized by the presence of sub-horizontal

bedded travertine leaning over the sub-vertical banded travertine (Fig. 3.5f). The bedded travertine is characterized by sub-horizontal brownish centimeters-thick beds (Fig. 3.5g), shrubs, and laminations affected, in places, by millimeters-to-centimeters-sized cavities of depositional and post-depositional (karst) origin. In some cases, the porous bedded travertine appears to be pervaded by bed-parallel veins (Fig. 3.5h, i). In the external part of the southwestern flank of the giant vein, at an altitude of about 580 m a.s.l, a set of sub-vertical centimeters-thick carbonate veins cut through the marly carbonates of the Scaglia Toscana Fmt. (Fig. 3.5j, k), which is the host rock of the giant vein travertine (Fig. 3.2).

The I Vignacci deposit crops out about 800 m to the northwest of the Semproniano ridge, exactly along the NW-SE prolongation of the Semproniano hill and ridge (Figs. 3.2 and 3.3). I Vignacci travertine is located at an altitude of about 430 m a.s.l., the lowest reached of the studied travertines. I Vignacci travertine deposit is small and it is characterized by banded travertine with subvertical NW-SE-striking bands. These bands cut through the surrounding sub-horizontal beds of the Scaglia Toscana Fmt. Geometrical attitude and location of I Vignacci outcrop suggest a structural and geometric continuity with the Semproniano ridge (Figs. 3.2 and 3.3).

Figure 3.5. (on the next page) (a) Panoramic view of the Semproniano giant vein and travertine plateau (Poggio Semproniano). (b) Attitude of the sparry bands (banded travertine) forming the Semproniano giant vein (NE flank). This exposure is located below the fortress of the Aldobrandeschi family (X century) in the Semproniano village. (c) The Semproniano giant vein (banded travertine) is mainly oriented NW-SE and characterized by high dip values (see the stereoplot: Schmidt net, lower hemisphere, showing poles to travertine subvertical bands forming the giant vein). (d) Detail from the Semproniano giant vein (banded travertine) with indication of the vein growth. (e) The central part of the Semproniano giant vein shows a V-like shape and is characterized by a rhythmic sequence of crystallized subvertical bands of sparry carbonate. Sample SP12, used for fluid inclusion analysis, was collected here. (f) Spatial relationships between banded and bedded travertine along the flank of the Semproniano giant vein. (g) Sub-horizontal, bedded travertine exposed on the south-western flank of the Semproniano giant vein. (h) Sub-horizontal, bedded travertine cut through by bedded parallel travertine veins (Semproniano village). (i) Bedded travertine fabric characterized by laminations, shrubs, and karst-dissolution cavities (Semproniano village). (j) and (k) Travertine veins cutting through carbonate rocks (Tuscan Domain) along the SW flank of the Semproniano giant vein. Cross-cutting relationships between travertine veins show multiple phases of veining.

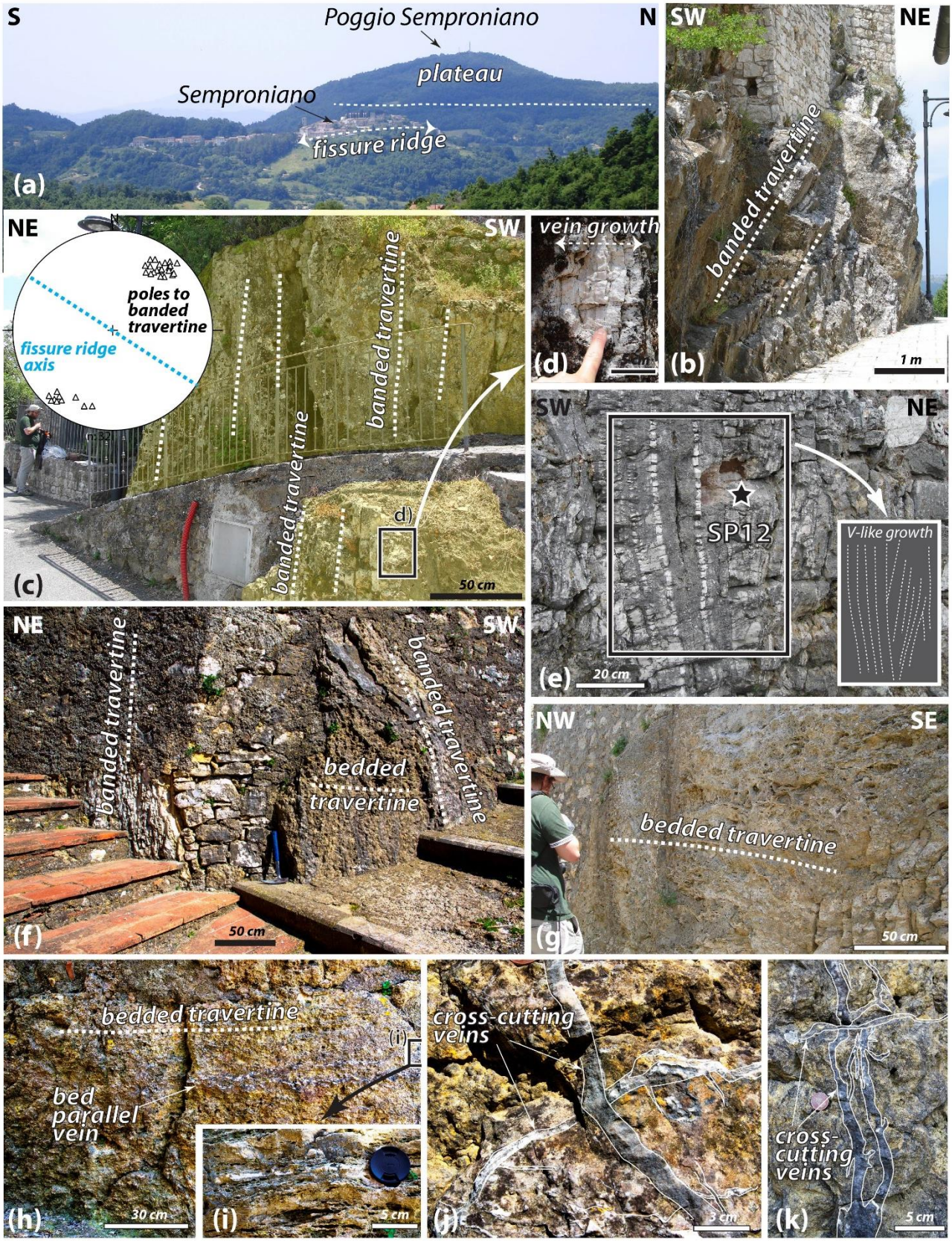

From a tectonic point of view, the travertine deposits are cross-cut by two main subvertical fault systems, one striking ca. E-W and one striking N-S (Figs. 3.2 and 3.6). In particular, we recognized

that the E-W-striking fault system cuts through the northern portion of the Poggio Semproniano travertine plateau (Fig. 3.6a). It consists of meter-thick damage zone defined by fault slip surfaces and secondary, subparallel, fracture network (Fig. 3.6b). A pitch smaller than 15° or greater than 165° have been measured for most slickenlines and abrasive striations occurring on fault planes (Fig. 3.6c). The kinematic indicators observed on the fault surfaces are mainly represented by synthetic shear fractures within the damage zone (Riedel shear planes) and they are consistent with right-lateral strike-slip movements. The N-S-striking fault system passes along the valley that separates the Poggio Semproniano and Poggio i Piani travertine deposits (Fig. 3.2). We identified this set of faults as affecting the travertine deposits of the Semproniano ridge and cut through the banded travertine of the Semproniano fissure ridge (Fig. 3.6a). Within the ridge, the fault system is characterized by a 0.5 m-thick damage zone and several speleothem-filled fracture networks cutting through the banded travertine (Fig. 3.6d). When observed, abrasive striations on fault planes show a pitch of about 60-70°. Geometrical relationships between faults and secondary fractures are consistent with an extensional movement (associated to a left-lateral movement) lowering the Poggio Semproniano travertine deposit.

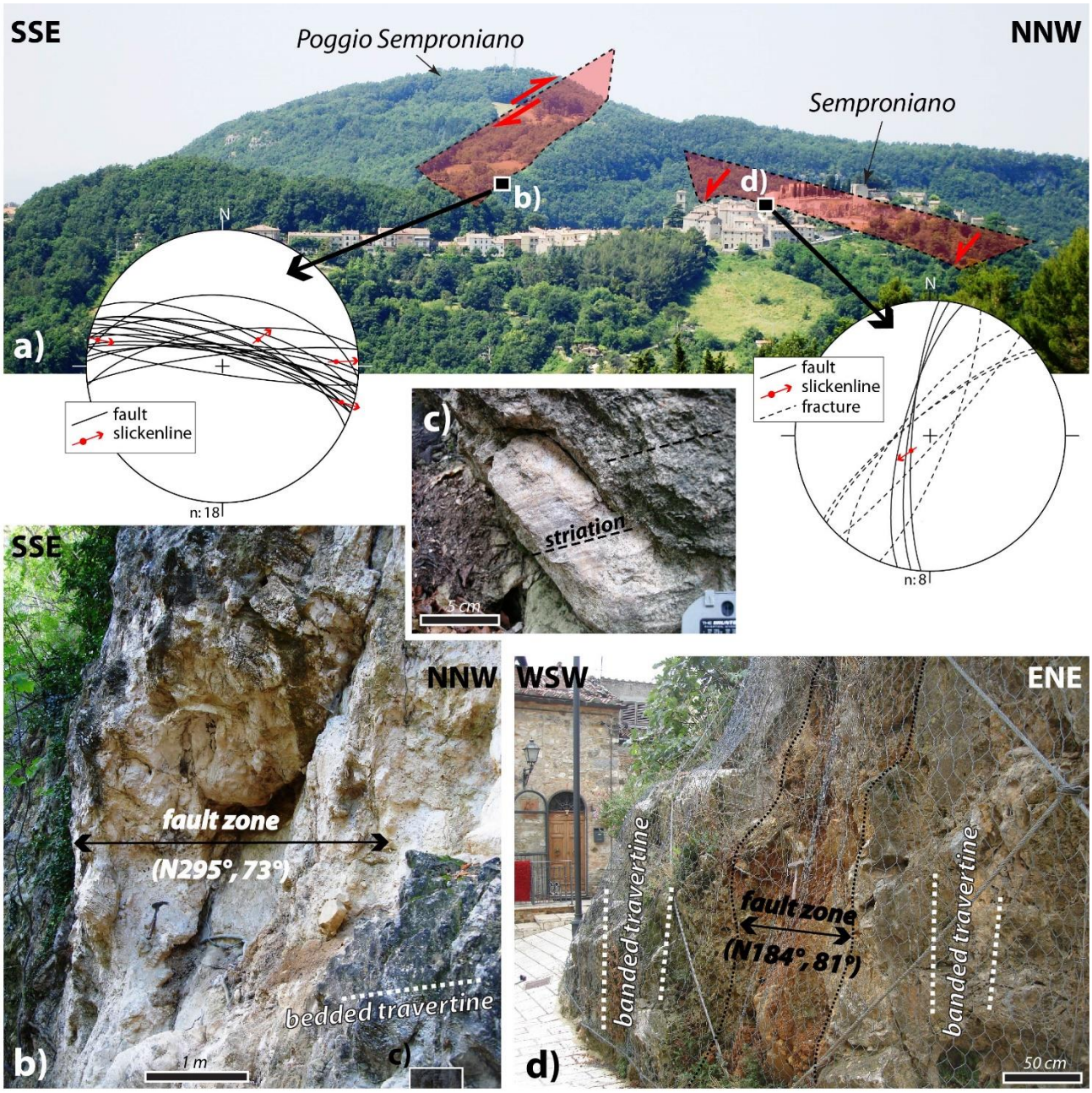

Figure 3.6 - (a) Panoramic view of the Semproniano-Poggio Semproniano area where the traces of the main fault systems (ca. E-W- and N-S-striking) are indicated. The stereoplots (Schmidt net, lower hemisphere) show attitude of the measured structural features. (b) The E-W-striking fault system affecting the bedded travertine at Poggio Semproniano is characterized by meter-thick damage zone and narrowly-spaced fault surfaces. (c) Fault surfaces are equipped with oblique- to strike-slip striations (pitch is generally higher than 160° or lesser than 20°; see the stereoplot). Right-lateral strike-slip kinematics has been documented for this fault system. (d) The N-S-striking fault across the banded travertine of the Semproniano village is defined by a half-meter-thick damage zone and secondary fracture network. Extensional kinematics (associated to a left-lateral movement) has been documented for this fault system.

3.3.2. U/Th geochronology

We dated nineteen samples from the $CaCO_3$ mineralizations in the study area (Tables 3.1, 3.2, and S3.1), namely from Semproniano (thirteen samples from the giant banded vein, bedded travertines, and one subordinate vein), I Vignacci (one sample from the banded travertine), Poggio Semproniano (three samples from bedded travertines and veins), and Poggio I Piani (one sample from bedded travertines). The analytical methods (α spectrometry and mass spectrometry) are described in the Appendix.

Table 3.1 - Samples, sampling sites, and laboratory analyses.

Sample	**Locality**	**Rock Type**	**$\delta^{13}C$ (‰ V-PDB)**	**$\delta^{18}O$ (‰ V-PDB)**	**$^{87}Sr/^{86}Sr$**	**$^{143}Nd/^{144}Nd$**	**REE**	**U/Th**
SP1	Semproniano Village	Banded Travertine	X	X				X
SP5	Semproniano Village	Banded Travertine	X	X				
SP6	Semproniano Village	Banded Travertine	X	X				
SP7	Semproniano Village	Banded Travertine	X	X				
SP8	Semproniano Village	Banded Travertine	X	X				
SP11	Semproniano Village	Bedded Travertine	X	X	X			X
SP12*	Semproniano Village	Banded Travertine	X	X	X			X
SP12B	Semproniano Village	Banded Travertine	X	X				
SP15	Semproniano Village	Banded Travertine	X	X				X
SP16	Semproniano Village	Calcite Vein	X	X				X
SP17	Semproniano Village	Bedded Travertine			X			
SP14/03	Semproniano Village	Banded Travertine	X	X				
SP14/04	Semproniano Village	Banded Travertine	X	X				

SP14/05	Semproniano Village	Bedded Travertine	X	X				
SP14/06	Semproniano Village	Bedded Travertine	X	X	X	X	X	
SP14/08	Semproniano Village	Banded Travertine	X	X				
SP14/09	Semproniano Village	Banded Travertine	X	X				
SP14/10	Semproniano Village	Banded Travertine	X	X				
SP14/11	Semproniano Village	Banded Travertine	X	X				
SP14/11 B	Semproniano Village	Banded Travertine	X	X				
SP14/12	Semproniano Village	Banded Travertine	X	X				
SP14/13	Semproniano Village	Banded Travertine	X	X				
SP14/14	Semproniano Village	Banded Travertine	X	X				
SP14/15	Semproniano Village	Banded Travertine	X	X				X
SP14/16	Semproniano Village	Banded Travertine	X	X				
SP14/17	Semproniano Village	Banded Travertine	X	X				
SP14/18	Semproniano Village	Banded Travertine	X	X	X		X	X
SP14/19	Semproniano Village	Banded Travertine	X	X				
SP14/20	Semproniano Village	Banded Travertine	X	X				X
SP14/21	Semproniano Village	Banded Travertine	X	X				
SP14/22	Semproniano Village	Banded Travertine	X	X				
SP14/23	Semproniano Village	Banded Travertine	X	X				X
SP14/24	Semproniano Village	Banded Travertine	X	X				
SP14/25	Semproniano Village	Banded Travertine	X	X				X

SP14/26	Semproniano Village	Banded Travertine	X	X				
SP14/27	Semproniano Village	Banded Travertine	X	X				
SP14/28	Semproniano Village	Banded Travertine	X	X	X			X
SP14/29	Semproniano Village	Banded Travertine	X	X				
SP14/30	Semproniano Village	Banded Travertine	X	X				X
SP14/31	Semproniano Village	Banded Travertine	X	X				
SP14/32	Semproniano Village	Banded Travertine	X	X				X
SP14/33	Semproniano Village	Banded Travertine	X	X				
SP14/34	Semproniano Village	Banded Travertine	X	X				X
VI1	I Vignacci	Banded Travertine	X	X	X	X	X	X
SP3	Poggio Semproniano	Calcite Vein	X	X	X	X	X	X
SP9	Poggio Semproniano	Bedded Travertine	X	X	X			
SP10	Poggio Semproniano	Calcite Vein	X	X	X			X
PS1	Poggio Semproniano	Bedded Travertine	X	X				
PS2	Poggio Semproniano	Bedded Travertine	X	X				
PS3	Poggio Semproniano	Bedded Travertine	X	X				
PO1	Poggio Semproniano	Bedded Travertine	X	X	X		X	
PO2	Poggio Semproniano	Bedded Travertine	X	X	X			X
PP1	Poggio i Piani	Bedded Travertine	X	X				X

* In addition to the reported analyses, geothermometric determinations through fluid inclusion and clumped isotope analyses were done on this sample (SP12).

Banded travertine samples from Semproniano Village (SP1) and I Vignacci (VI1) are characterized by a $^{230}Th/^{234}U$ activity ratio higher than 1 and, therefore, by ages higher than the limit of the U/Th method in α spectrometry (c. 350 ka). The bedded travertine exposed on the south-western flank of the Semproniano giant vein (SP11) is characterized by a moderate detrital contamination ($^{230}Th/^{232}Th$ activity ratio = 7.148 ± 0.251) and by a corrected $^{230}Th/^{234}U$ activity ratio of 0.878 ± 0.051, indicating an age of 214 +50/-37 ka. A subordinate carbonate vein (SP16) cutting through the Scaglia Toscana Fmt. (Tuscan Nappe) in the external south-western flank of the Semproniano giant vein is characterized by a $^{230}Th/^{232}Th$ activity ratio of 12.564 ± 1.987 and by a corrected $^{230}Th/^{234}U$ activity ratio of 0.641 ± 0.064. Calculated age for this sample is 104 ± 16 ka. A bedded travertine sample collected in the southern part of Poggio Semproniano plateau (PO2; Fig. 3.4b) is characterized by a $^{230}Th/^{234}U$ activity ratio of 0.818 ± 0.039. The resulting age is 171 ± 19 ka. Two samples of calcite-filled veins (SP3 and SP10) cutting through the bedded travertine of Poggio Semproniano and the underlying Scaglia Toscana Fmt. are characterized by a $^{230}Th/^{234}U$ activity ratio of 0.340 ± 0.052 and 0.299 ± 0.023, respectively. The related ages are 43 ± 8 ka and 39 ± 4 for the SP3 and SP10 samples, respectively. A sample of bedded travertine from Poggio I Piani plateau (PP1; Fig. 3.4e) is characterized by a $^{230}Th/^{234}U$ activity ratio of 0.857 ± 0.028 and a resulting age of 198 ± 18 ka.

To understand the spatio-temporal growth of the Semproniano giant banded vein, we dated eleven samples from this vein along a 5m transect across the vein (Fig. 3.6), and one sample (SP12) from the upper part of the transect (Figs. 3.5e and 7) by mass spectrometry (Fig. 3.7 and Tables 3.2 and S3.1). We obtained, ages between 86 ka to 646 ka (Fig. 3.7), with only one sample being older than the resolution of the method (> c. 800 ka). Radiometric ages along the transect do not vary systematically. In other words, the oldest samples are not located within the inner or external portions of the vein to indicate its antitaxial or syntaxial growth. The three oldest samples (i.e., c. 646, 613, and >800 ka) occur in separate inner portions of the vein and are divided by younger carbonates. (Fig. 3.7). The oldest samples have lager errors caused by proximity to secular equilibrium, whereas the youngest ages are characterized by smaller errors (Table 3.2).

Table 3.2 - U/Th Age of travertines sampled in the study area. See Table S1 for a complete list of data. Samples indicated with * were analyzed through MC-ICP-MS at the HISPEC lab of the National Taiwan University (errors quoted as 2σ), whereas samples indicated with ** were analyzed through α spectrometry at the Laboratorio di Geochimica Ambientale.

Sample	Location	Rock type	Age corrected (ka)
SP15*	Semproniano Village	Banded travertine	**347 ± 22**
SP14/15*	Semproniano Village	Banded travertine	***>800***
SP14/18*	Semproniano Village	Banded travertine	**86 ± 1**
SP14/20*	Semproniano Village	Banded travertine	**231 ± 9**
SP14/23*	Semproniano Village	Banded travertine	**314 ± 11**
SP14/25*	Semproniano Village	Banded travertine	**419 ± 39**
SP14/28*	Semproniano Village	Banded travertine	**613 ± 200**
SP14/30*	Semproniano Village	Banded travertine	**105 ± 1**
SP14/32*	Semproniano Village	Banded travertine	***646***
SP14/34*	Semproniano Village	Banded travertine	**495 ± 99**
SP1**	Semproniano Village	Banded travertine	**>350**
SP12**	Semproniano Village	Banded travertine	**128 ± 19**
SP16**	Semproniano Village	Calcite vein	**104 ± 16**
SP11**	Semproniano Village	Bedded travertine	**214 +50/-37**
SP3**	Poggio Semproniano	Calcite vein	**43 ± 8**
SP10**	Poggio Semproniano	Calcite vein	**39 ± 4**
PO2**	Poggio Semproniano	Bedded travertine	**171 ± 19**
PP1**	Poggio i Piani	Bedded travertine	**198 ± 18**
VI1**	Vignacci	Banded travertine	**>350**

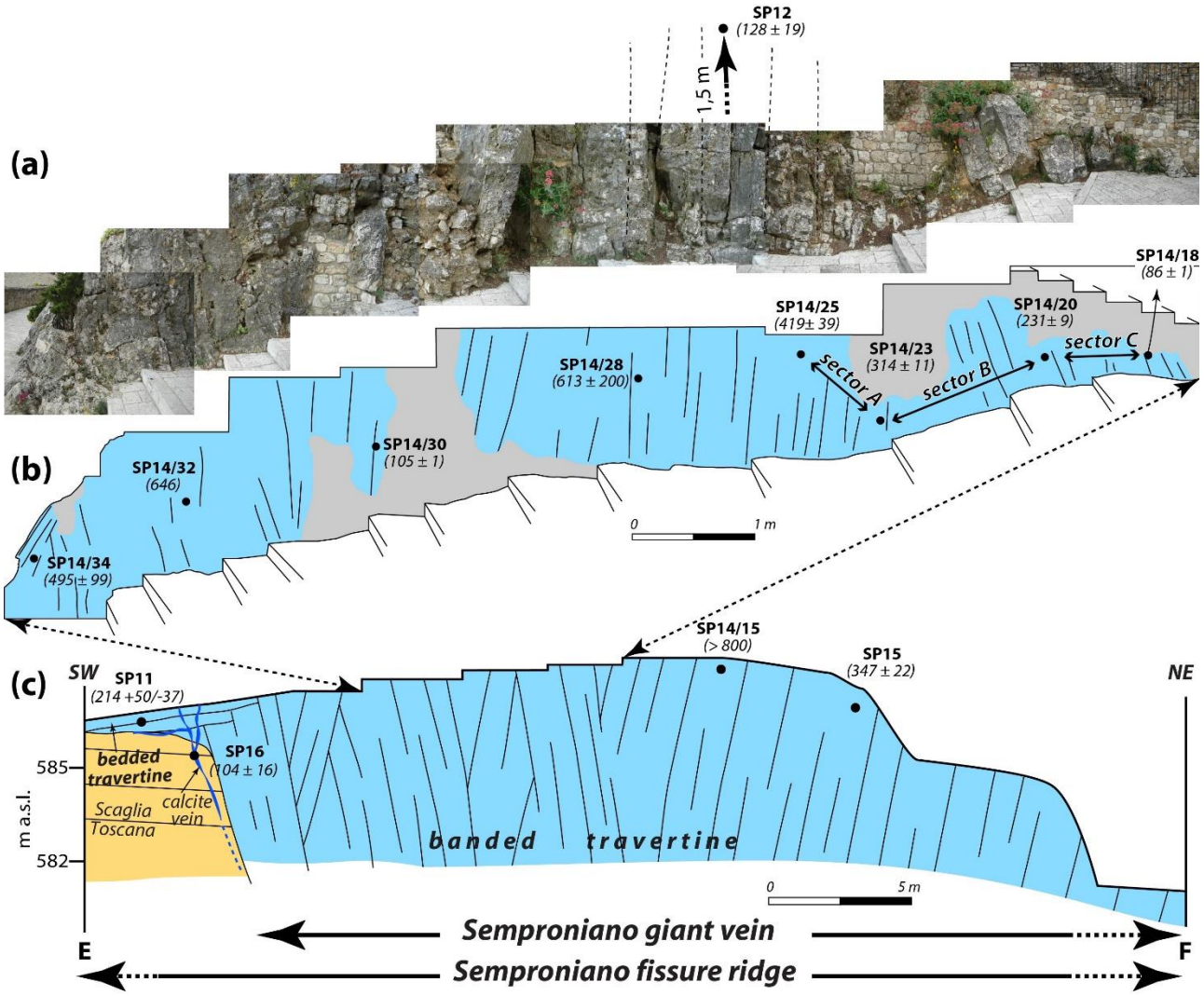

Figure 3.7 - (a) Photomosaic (above) and related line drawing (below) of the Sempronian giant vein as it is exposed in the upper part of the Sempronian village. (b) Conceptual cross-sectional sketch of the Sempronian giant vein that is made of an uninterrupted swarm of sparry bands (banded travertine). Sample location and related radiometric ages are shown both in (a) and in (b).

3.3.3. C- and O-isotopes and parental fluid thermometry from O-isotopes

We performed $\delta^{13}C$ and $\delta^{18}O$ analyses on fifty-one samples (banded and bedded travertines, calcite veins) from the Sempronian area (Tables 3.1 and 3.3). Details on the analytical procedure are provided in the Appendix. Oxygen and carbon isotopes are reported with respect to V-PDB. All analyzed samples are characterized by positive values of $\delta^{13}C$ (between 3.2 and 10.5‰) and negative values of $\delta^{18}O$ (between -14.6 and -7.6‰) (Table 3.3). Results, in particular, are clustered around 8‰ for $\delta^{13}C$ and around -11‰ for $\delta^{18}O$ (Fig. 3.8b).

Semproniano Village. Samples of banded travertine from the Semproniano veins are characterized by $\delta^{13}C$ values between 3.2 and 10.5‰ (V-PDB) and by $\delta^{18}O$ values between -14.6 and -7.6‰ (V-PDB). Samples from the associated bedded travertine are characterized by $\delta^{13}C$ values between 5.3 and 9.9‰ (V-PDB) and by $\delta^{18}O$ values between -9.8 and -8.2‰ (V-PDB).

I Vignacci. The sample from the banded travertine of I Vignacci (sample VI1) is characterized by a $\delta^{13}C$ of 3.7‰ (V-PDB) and a $\delta^{18}O$ of -9.6‰ (V-PDB).

Poggio Semproniano. Samples of bedded travertine from Poggio Semproniano are characterized by values of $\delta^{13}C$ between 5.7 and 7.1‰ (V-PDB) and values of $\delta^{18}O$ between -11.4 and -8.1‰ (V-PDB). Calcite-filled veins pervading the bedded travertine and the underlying underlying Scaglia Toscana Fmt. (Samples SP3, SP10) at the bottom of the Poggio Semproniano travertine plateau are characterized by $\delta^{13}C$ values between 7.1 and 8.4‰ (V-PDB) and $\delta^{18}O$ values between -11.5 and -10.7‰ (V-PDB).

Poggio i Piani. One sample from the bedded travertine (sample PP1) of Poggio i Piani is characterized by a $\delta^{13}C$ of 6.5‰ (V-PDB) and a $\delta^{18}O$ of -11.6‰ (V-PDB).

We focused particular attention to the Semproniano giant vein by collecting two transects across it (samples SP14/03 to SP14/04 and SP14/08 to SP14/34) and three further samples in the adjacent bedded travertine (samples SP11, SP14/05, SP14/06) (Table 3.3). Banded travertines collected along the two transects show a wide variability. Samples from the first transect (samples SP14/03 to SP14/16), in particular, are characterized by $\delta^{13}C$ values comprised between 5.3 and 9.7‰ (and $\delta^{18}O$ values comprised between -12.8 and -9.0‰. Samples from the second transect (samples SP14/17 to SP14/34) are characterized by $\delta^{13}C$ values comprised between 3.2 and 10.2‰ and $\delta^{18}O$ values comprised between -12.6 and -7.6‰. Samples from the bedded travertine located along the flanks of the Semproniano giant vein are characterized by $\delta^{13}C$ values comprised between 5.3 and 9.9‰ and $\delta^{18}O$ values comprised between -9.8 and -8.2 ‰. Samples from the two transects do not show any pattern in O and C isotopic values along the Semproniano giant vein.

We calculated the paleo-temperature of the mineralizing parental fluids applying the equation of Kele et al. (2015) to the entire $\delta^{18}O$ dataset (Table 3.3 and Fig. 3.8c) and using the present $\delta^{18}O$ of the the Saturnia spring hydrothermal waters (-6.4‰ V-SMOW), whose active source is located 9 km to the south of the Semproniano giant vein. We assume that the oxygen isotope composition of the palaeosprings was similar to those of the current Saturnia spring. The banded travertines of the Semproniano giant vein yield temperatures between 34 ± 2 and 71 ± 7 °C, with the majority in the range comprised between 45 and 60 °C. The bedded travertines associated with the giant vein give temperatures between 35 ± 2 and 43 ± 3 °C, whereas the banded travertine sample from I Vignacci sample yields a temperature of 42 ± 3°C. The Poggio Semproniano plateau samples yield temperatures of 36 ± 2 and 53 ± 5 °C, for the bedded travertine, and 49 ± 4 and 53 ± 5 °C, for the calcite veins. The bedded travertine from Poggio I Piani a temperature of 53 ± 5 °C. There is no correlation scheme between ages and temperature of precipitation (Fig. 3.8d). In particular, there is no systematic trend of decreasing temperature with younger ages of deposition.

Table 3.3 - Stable oxygen and carbon isotope composition, and paleotemperature of banded travertine, bedded travertine, and calcite veins from the study area. Isotope compositions are expressed in ‰ against Vienna Pee Dee Belemnite standard (V-PDB) and in ‰ against Vienna Standard Mean Ocean Water (V-SMOW). Temperature of parental fluids derive from $\delta^{18}O$ through the equation of Kele et al. (2015). $\delta^{13}C_{Co2}$* have been calculated using the empirical equation of Panichi and Tongiorgi. (1976). $\delta^{13}C_{Co2}$** have been calculated using the theoretical equation of Bottinga (1968).

Sample	Locality	Rock Type	$\delta^{13}C$ (‰ V-PDB)	$\delta^{18}O$ (‰ V-PDB)	$\delta^{18}O$ (‰ V-SMOW)	$T_{calculated}$ (°C)	$\delta^{13}C_{Co2}$* (‰ V-PDB)	$\delta^{13}C_{Co2}$** (‰ V-PDB)
SP1	Semproniano Village	Banded Travertine	9.5	-12.7	17.8	60 ± 6	0.9	3.2
SP5	Semproniano Village	Banded Travertine	8.9	-10.8	19.8	49 ± 4	0.2	1.5
SP6	Semproniano Village	Banded Travertine	10.0	-12.2	18.3	57 ± 5	1.4	3.3
SP7	Semproniano Village	Banded Travertine	10.5	-11.6	19.0	53 ± 5	2.1	3.5
SP8	Semproniano Village	Banded Travertine	9.7	-12.3	18.2	58 ± 5	1.2	3.1
SP11	Semproniano Village	Bedded Travertine	9.9	-8.2	22.4	36 ± 2	1.4	1.1
SP12	Semproniano Village	Banded Travertine	4.9	-14.6	15.9	71 ± 7	-4.6	-0.5
SP12B	Semproniano Village	Banded Travertine	4.7	-13.5	17.0	64 ± 6	-4.9	-1.3
SP16	Semproniano Village	Calcite Vein	8.9	-12.0	18.6	56 ± 5	0.2	2.1
SP14/03	Semproniano Village	Banded Travertine	9.6	-12.3	18.2	58 ± 5	1.0	3.0
SP14/04	Semproniano Village	Banded Travertine	9.2	-12.7	17.8	60 ± 5	0.6	2.9
SP14/05	Semproniano Village	Bedded Travertine	5.8	-9.7	20.9	44 ± 3	-3.5	-2.2
SP14/06	Semproniano Village	Bedded Travertine	5.3	-9.8	20.9	44 ± 3	-4.2	-2.7
SP14/08	Semproniano Village	Banded Travertine	6.0	-9.8	20.8	44 ± 3	-3.3	-1.9
SP14/09	Semproniano Village	Banded Travertine	9.8	-11.1	19.5	51 ± 4	1.2	2.5
SP14/10	Semproniano Village	Banded Travertine	9.3	-10.9	19.7	50 ± 4	0.7	1.9
SP14/11	Semproniano Village	Banded Travertine	7.1	-11.1	19.5	51 ± 4	-2.1	-0.2

SP14/11B	Semproniano Village	Banded Travertine	6.0	-11.6	19.0	54 ± 5	-3.3	-1.0
SP14/12	Semproniano Village	Banded Travertine	9.2	-12.8	17.7	60 ±6	0.6	2.9
SP14/13	Semproniano Village	Banded Travertine	8.6	-12.3	18.3	57 ± 5	-0.2	2.0
SP14/14	Semproniano Village	Banded Travertine	7.7	-9.0	21.6	40 ± 3	-1.2	-0.7
SP14/15	Semproniano Village	Banded Travertine	8.0	-11.3	19.3	52 ± 5	-0.9	0.9
SP14/16	Semproniano Village	Banded Travertine	9.7	-10.1	20.5	46 ± 4	1.1	1.9
SP14/17	Semproniano Village	Banded Travertine	10.2	-10.7	19.9	49 ± 4	1.7	2.7
SP14/18	Semproniano Village	Banded Travertine	9.9	-10.6	20.0	48 ± 4	1.3	2.4
SP14/19	Semproniano Village	Banded Travertine	8.5	-10.7	19.9	49 ± 4	-0.3	1.1
SP14/20	Semproniano Village	Banded Travertine	8.2	-9.6	21.0	43 ± 3	-0.6	0.1
SP14/21	Semproniano Village	Banded Travertine	8.4	-12.1	18.5	56 ± 5	-0.4	1.7
SP14/22	Semproniano Village	Banded Travertine	10.1	-12.0	18.5	56 ± 5	1.6	3.3
SP14/23	Semproniano Village	Banded Travertine	7.0	-11.6	19.0	53 ± 5	-2.1	0.0
SP14/24	Semproniano Village	Banded Travertine	6.8	-11.3	19.2	52 ± 5	-2.3	-0.3
SP14/25	Semproniano Village	Banded Travertine	8.9	-9.9	20.7	45 ± 3	0.2	1.0
SP14/26	Semproniano Village	Banded Travertine	6.7	-11.4	19.2	52 ± 5	-2.5	-0.4
SP14/27	Semproniano Village	Banded Travertine	8.8	-10.7	19.9	49 ± 4	0.1	1.3
SP14/28	Semproniano Village	Banded Travertine	7.6	-10.0	20.6	45 ± 3	-1.4	-0.2
SP14/29	Semproniano Village	Banded Travertine	3.2	-8.8	21.8	39 ± 3	-6.7	-5.4
SP14/30	Semproniano Village	Banded Travertine	8.6	-11.2	19.4	51 ± 4	-0.2	1.4
SP14/31	Semproniano Village	Banded Travertine	6.5	-11.1	19.5	51 ± 4	-2.7	-0.8
SP14/32	Semproniano Village	Banded Travertine	9.0	-10.1	20.5	46 ± 4	0.3	1.2
SP14/33	Semproniano Village	Banded Travertine	6.3	-7.6	23.1	34 ± 2	-2.9	-2.9

SP14/34	Semproniano Village	Banded Travertine	6.5	-12.6	17.9	59 ± 5	-2.7	0.0
VI1	I Vignacci	Banded Travertine	3.7	-9.6	21.0	43 ± 3	-6.0	-4.4
SP3	Poggio Semproniano	Calcite Vein	7.1	-11.5	19.0	53 ± 5	-2.0	0.0
SP9	Poggio Semproniano	Bedded Travertine	6.8	-9.6	21.0	43 ± 3	-2.4	-1.3
SP10	Poggio Semproniano	Calcite Vein	8.4	-10.7	19.9	49 ± 4	-0.5	0.9
PS1	Poggio Semproniano	Bedded Travertine	6.9	-10.2	20.4	46 ± 4	-2.2	-0.8
PS2	Poggio Semproniano	Bedded Travertine	6.7	-8.1	22.6	36-± 2	-2.5	-2.3
PS3	Poggio Semproniano	Bedded Travertine	5.8	-10.1	20.5	46 ± 4	-3.6	-2.0
PO1	Poggio Semproniano	Bedded Travertine	5.6	-11.4	19.2	53 ± 5	-3.8	-1.5
PO2	Poggio Semproniano	Bedded Travertine	7.1	-9.8	20.8	44 ± 3	-2	-0.8
PP1	Poggio i Piani	Bedded Travertine	6.5	-11.6	19.0	53 ± 5	-2.7	-0.5

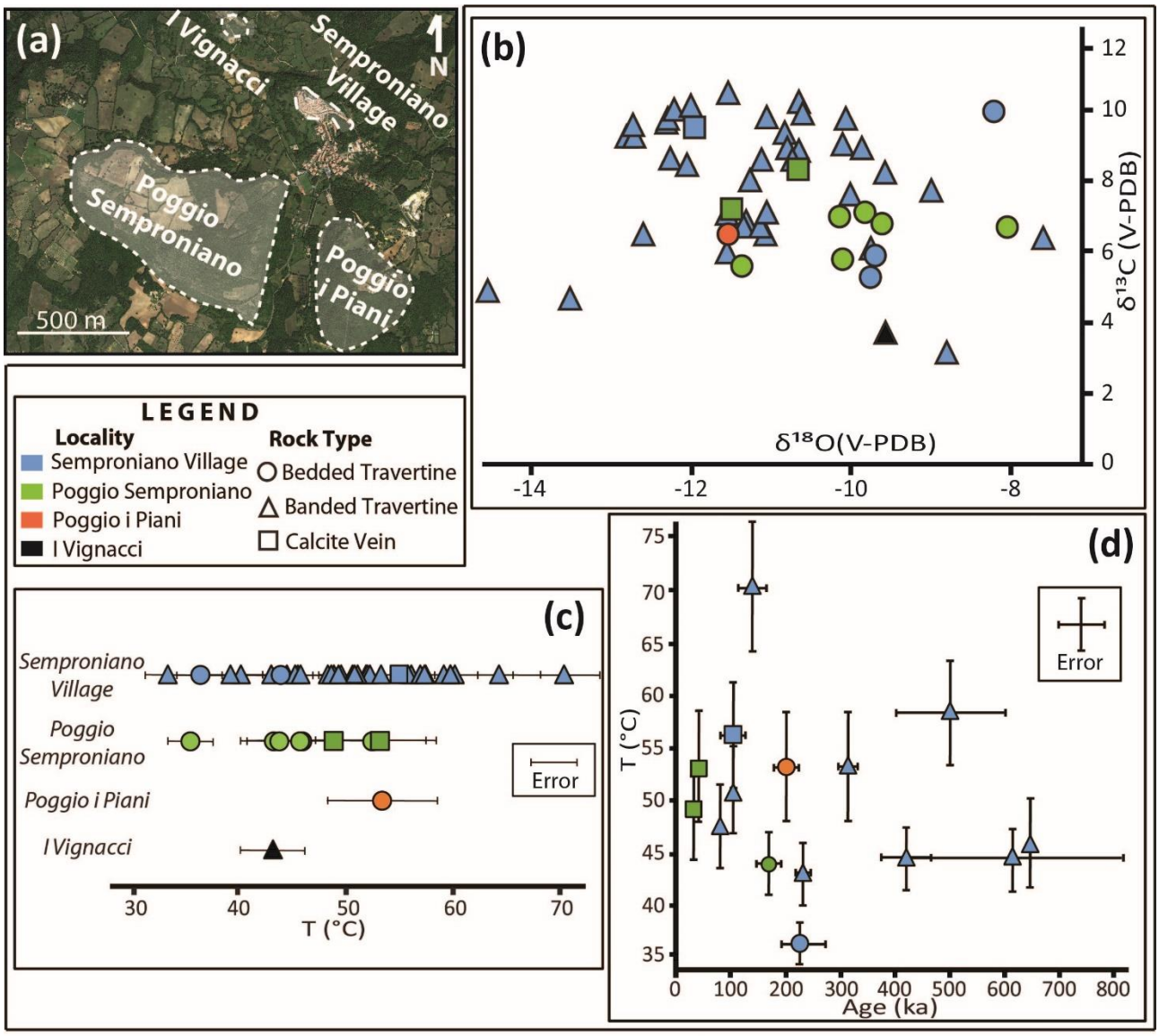

Figure 3.8 - (a) Panoramic view (Google Earth image) with localization of the studied travertine deposits (same as Fig. 3.3a). (b) Combined plot of $\delta^{13}C$ (‰ V-PDB) and $\delta^{18}O$ (‰ V-PDB) isotope values derived from samples of bedded and banded travertines and calcite veins (Table 3.3). (c) Plot of calculated temperatures for the parental fluids of the studied travertines and CaCO3 precipitates (Table 3.3). (d) Combined plot of parental fluid temperatures and U/Th ages determined on the same samples.

3.3.4. Sr- and Nd-Isotopes and rare Earth elements

We performed Strontium, REE, and Yttrium (Y; REE + Yttrium = REY) concentration analyses, and Strontium and Neodymium isotope measurements to understand the subsurface circuit of hydrothermal fluids (e.g., Ederfield and Greaves, 1982; McLennan, 1989; Webb et al., 2000; Uysal et al., 2007; 2009). The analytical procedures and protocols are detailed in the Appendix; results are reported in Tables 3.4, S3.2, and Fig. 3.9.

We observed a variable Sr concentration, comprised between 105.3 to 4956.3 mg/kg. The mean value (3200 mg/kg) is in the range of Sr contents of most travertines in central Italy (Minissale, 2004). Sr-isotope ratios range from 0.708277 to 0.708527. The banded travertine from the Semproniano giant vein (SP12, SP14/18 and SP14/28), the banded travertine from I Vignacci (VI1), and the calcite vein from Poggio Semproniano (SP3 and SP10) are characterized by the highest Sr concentrations, between 1125.9 and 4956.3 mg/kg. On the contrary, the bedded travertine from the flanks of the Semproniano giant vein (SP11, SP14/06, SP17) and the bedded travertines from Poggio Semproniano (SP9, PO1, PO2) are have the lowest Sr concentrations, between 105.3 and 787.3 mg/kg.

The Nd-isotope composition of one bedded travertine from the flanks of the Semproniano giant vein (SP14/06), one banded travertine from I Vignacci (VI1), and one calcite vein from Poggio Semproniano (SP3) show values comprised in a narrow range between 0.512253 and 0.512330 (Table 3.4).

We determined REY concentrations of the banded travertine from the Semproniano giant vein (SP14/18), of the bedded travertine sample from the flanks of the Semproniano giant vein (SP14/06), of the banded travertine sample from I Vignacci (VI1) of the bedded travertine sample (PO1) and of calcite vein (SP3) from Poggio Semproniano. We normalized the REY concentrations against PAAS (Post-Archean Austrian Shale; McLennan, 1989; Fig. 3.9 and Table S3.2). The REY concentrations are highly variable (ΣREE = 0.08-18.6), resulting significantly lower than PAAS (Fig. 3.9). The main features of REY patterns are (Fig. 3.9): (i) relative depletion of the light rare Earth elements (LREE = 0.1-0.71, with the exclusion of sample VI1); (ii) variable enrichment of the heavy rare Earth elements (HREE as NdN/YbN = 1.9- 0.07, according to Webb and Kamber, 2000); (iii) strongly superchondritic Y/Ho ratio (38.3 -221.3) characterized by a huge positive Y spike in the pattern; (iv) positive Gd anomaly for sample SP14/06 and VI1; (v) consistent negative Ce anomaly (Ce/Ce* = 0.30-0.94; Table S3.2).

Table 3.4 - Strontium, Strontium isotopes and Neodymium isotopes measured on selected samples from travertines of the study area.

Sample	Locality	Rock Type	Sr (mg/kg)	$^{87}Sr/^{86}Sr \pm 2se^*$	$^{143}Nd/^{144}Nd \pm 2se^*$	εNd i
SP12	Semproniano Village	Banded travertine	1189.46	0.708277 ± 11		
SP14/18	Semproniano Village	Banded travertine	1223.70	0.708395 ± 9		
SP14/28	Semproniano Village	Banded travertine	1125.91	0.708368 ± 10		
SP11	Semproniano Village	Bedded travertine	105.31	0.708491 ± 10		
SP14/06	Semproniano Village	Bedded travertine	652.35	0.708470 ± 5	0.512253 ± 18	-6.50
SP17	Semproniano Village	Bedded travertine	592.74	0.708437 ± 6		
SP9	Poggio Semproniano	Bedded travertine	734.74	0.708326 ± 7		
PO1	Poggio Semproniano	Bedded travertine	502.19	0.708334 ± 5		
PO2	Poggio Semproniano	Bedded travertine	787.25	0.708366 ± 7		
SP3	Poggio Semproniano	Calcite Vein	4763.20	0.708527 ± 7	0.512330 ± 39	-2.41
SP10	Poggio Semproniano	Calcite Vein	4154.77	0.708488 ± 9		
VI1	I Vignacci	Banded travertine	4956.30	0.708456 ± 6	0.512275 ± 20	-9.93

*Uncertainties are 2se mean, within-run precision and refer to the last digits

** ε_{Nd} has been calculated at 200Ma.

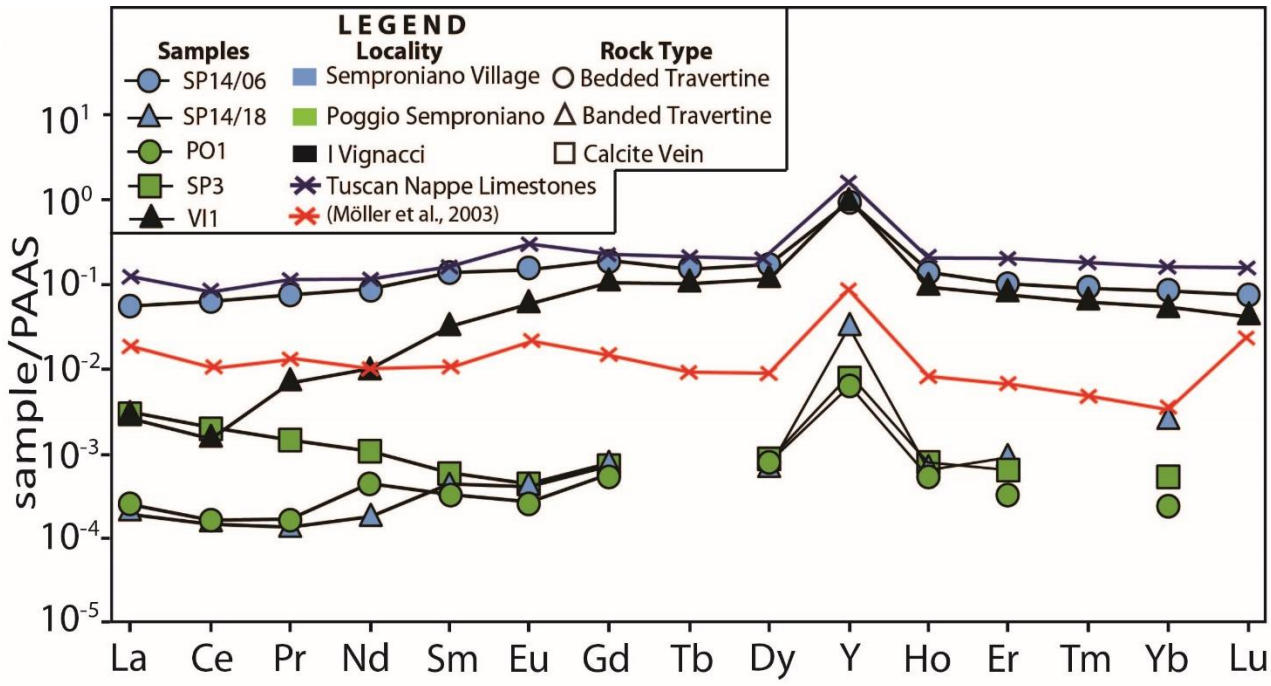

Figure 3.9 - Post Archean Australian shale (PAAS) – normalized REY pattern (rare Earth elements + Yttrium) for: the Semproniano giant vein (banded travertine); the bedded travertine flanking the giant vein; bedded travertine and calcite vein from Poggio Semproniano; and banded travertine from I Vignacci. For comparison, REE data from the Tuscan Nappe limestone are also shown (data from Möller et al., 2003).

3.3.5. Fluid inclusion microthermometry

Fluid inclusion microthermometry is the best direct technique to understand and reconstruct the physical and chemical properties of the mineralizing fluids; however, fluid inclusion studies on travertines are rare (Słowakiewicz 2003; Gibert et al., 2009; El Desouky et al., 2015; Raimondi et al., 2015) due to some difficulties inherent to travertines such as: (1) scarce occurrence and small size of inclusions (Pentecost 2005); (2) inclusion metastability often causing failing in bubble nucleation upon cooling from the trapping conditions to room temperature (Diamond, 2003); and (3) inclusion anelastic stretching and decrepitation that can cause difficulties in performing microthermometric analyses; (4) double refraction of calcite (Bodnar, 2003).

Unfortunately only one sample contained fluid inclusions suited for microthermometry (Fig. 3.10a). It consists of elongate calcite crystals, containing numerous two-phase (Liquid + Vapor or L+V) liquid-rich fluid inclusions 5 to 50 μm long and a constant V/L ratio for all the analyzed structures (Figs. 3.10b-3.10d). Fluid inclusions occur both as primary isolated and as pseudosecondary in small planes that do not cross the crystal rims. The inclusion shape is variable. We recognized, in particular, two main types of inclusions: (1) flat irregular (Figs. 3.10c and 3.10d) and (2) polygonal (Fig. 3.10b).

As it is shown in Fig. 3.10(f), Tm_{ice} values (i.e., the temperature of ice melting from which salinity is deduced) range between 0.0 and +4.8 °C, but are mostly concentrated around 0-1 °C. Being very small systems, fluid inclusions may exhibit metastable behavior and metastable ice crystals can persist at temperatures as high as +6,5°C (Roedder, 1967) (Fig. 3.10f). From these data we can conclude that the fluid consists of pure water. Homogenization temperature (Th) values range between 57 and 105°C, with a maximum around 70-90 °C (Fig. 3.9g). No pressure correction is

required for these homogenization temperature values as the analyzed sample precipitated in a very shallow environment represented by the giant vein. Our microthermometric results (Fig. 3.10e) are consistent with the ones obtained by Capezzuoli et al. (2013), who obtained temperatures between 65 and 95 °C and 0.2 wt% NaCl eq.

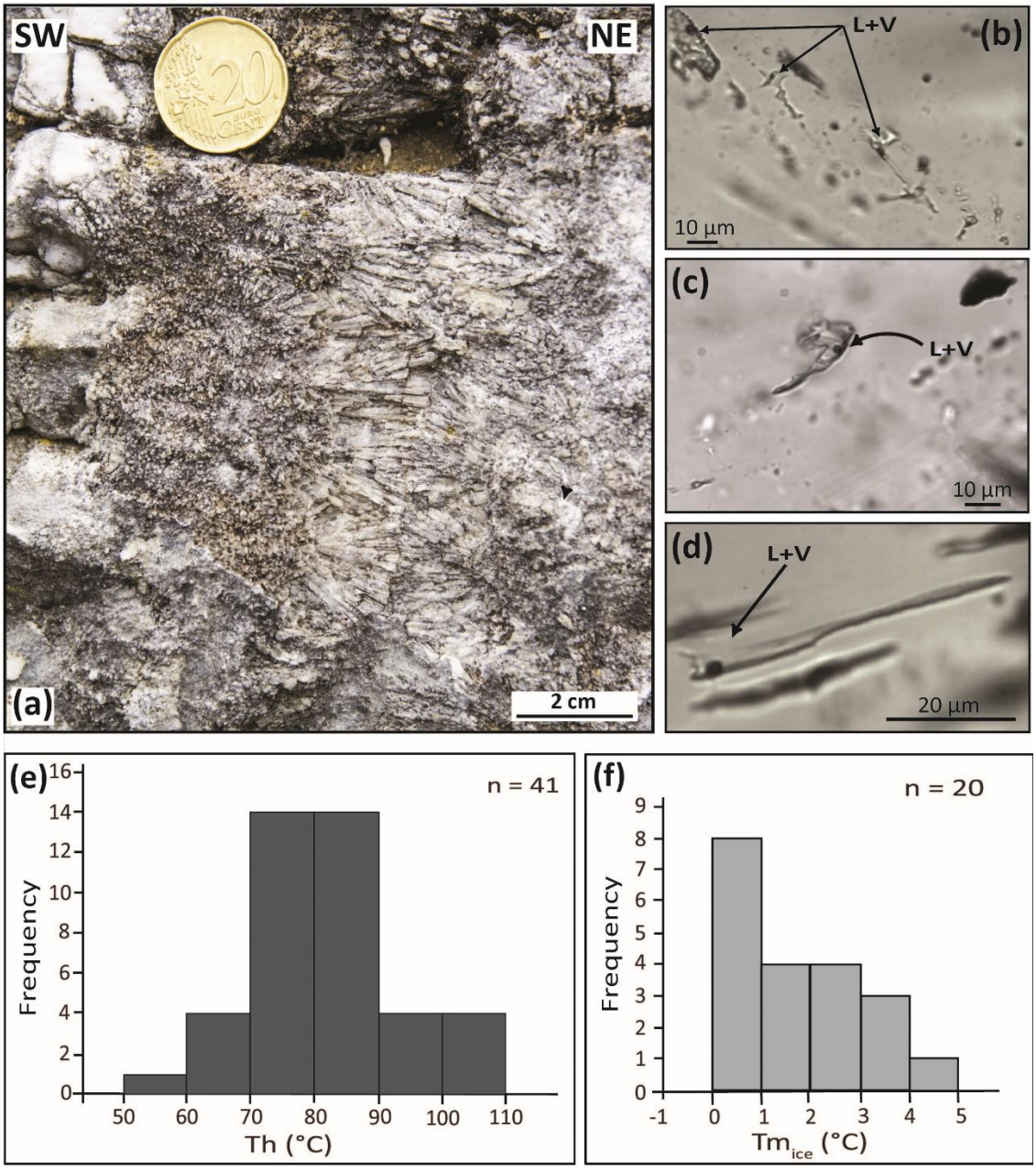

Figure 3.10 - (a) Close up photograph of banded travertine from the central part of the Semproniano giant vein. The sample studied for fluid inclusions comes exactly from the spot shown in the photograph. (b), (c), and (d) Microphotographs (transmitted light, parallel nicols) of liquid-rich fluid inclusions hosted in the banded travertine shown in the previous close-up photograph. L and V are for liquid and vapor phases, respectively, within the studied inclusions. (e) and (f) results of microthermometry on fluid inclusions hosted in elongate calcite crystals. Th is the temperature (°C) of homogenization whereas Tmice (°C) is the temperature of last melting of ice.

3.4. Discussion

3.4.1. A long-lived giant vein

The thick and continuous sequence of travertine sparry subvertical bands (the giant vein) in the Semproniano village accompanied by bedded travertine on its flanks and by veins in the Tuscan Nappe host rock suggest that the Semproniano giant vein represent the central portion of a fossil fissure ridge travertine larger than, but similar to those known in several other hydrothermal areas such as Turkey (e.g. Denizli Basin; Altunel and Hancock 1993a,1993b, 1996; Uysal et al., 2007,2009; De Filippis et al., 2012, 2013a), U.S.A. (e.g. Mammoth Hot Springs and Bridgeport; Hancock et al., 1999; De Filippis and Billi, 2012), Italy (e.g. Rapolano, Castelnuovo dell'Abate, and Tivoli; Guo and Riding, 1999; Brogi, 2004a; Brogi and Capezzuoli, 2009; De Filippis et al., 2013b; Rimondi et al., 2015), and elsewhere (De Filippis et al., 2012). Most fissure ridge travertines are volumetrically dominated by bedded travertines occurring mainly along the flanks and partially along the axial portion of the ridges, whereas the banded travertine is normally confined within a narrow band along the ridge axis. In the Semproniano case, although we have no record on the amount of eroded bedded travertine over time (since about 650 ka), the ridge seems to be characterized by a predominance of banded travertine (i.e., the giant vein) with only small slabs (at present) of bedded travertine on its flanks.

We consider the Semproniano vein as a giant structure characterized by a minimum thickness of 50 m larger than any one we found in the published literature. Thus the Semproniano giant vein is probably the thickest continuous vein (i.e., no relics of host rock are interspersed across the Semproniano giant vein) so far documented in the geological literature. Very thick veins (i.e., banded travertine) are common in many fissure ridge travertines (e.g. Uysal et al., 2007, 2009; De Filippis et al., 2012), but their thickness (at least that of the continuous portion of banded travertine) is normally at least one order of magnitude smaller than that of Semproniano. For instance, the Akköy fissure ridge in the Denizli basin (Turkey) is known as one of the largest and thickest fissure ridges on the Earth. This fossil structure is well visible in its inner portion thanks to the presence of numerous

quarries. In the quarries, the Akköy ridge is characterized by inner veins that are less than 10 m thick (i.e., considering only continuous veins; De Filippis et al., 2012).

Very thick veins pervading rocks are common in different settings (e.g., metamorphic rocks), but all these occurrences are characterized by non-continuous veins, with relics of host rock interspersed across the veins. Quartz veins of a thickness comparable to the one of Semproniano were described by Bons (2001) and Yilmaz et al. (2014). In both instances, the veins have thicknesses close to 50 m but, unlike the Semproniano structure, these quartz veins are characterized by wall rock inclusions.

We interpret the giant thickness of the Semproniano vein as due to two main factors: (1) the shallow emplacement of this vein and therefore the limited confining pressure, which would have otherwise limited the lateral expansion of the vein in a deeper case. Although we do not know the exact depth of formation, most veins along fissure ridge travertines are typically formed only at a few meters depth at the most (De Filippis et al., 2012, 2013a); (2) the second factor is the unique longevity of the hydrothermal activity, which lasted at least 600 ka. This is much longer than what is reported by other studies of fissure ridge travertines which are typically around 10^4 a (e.g., Altunel and Karabacak, 2005; Uysal et al., 2007, 2009).

3.4.2. Rate and mode of vein growth

The Semproniano giant vein grew between about >650 and 85 ka. Considering 50 m as the vein total thickness, the average growth rate around can be estimated to be 8×10^{-2} mm/a. The three inner sectors of the giant vein can also be considered separately according to age groups: sector A, between samples SP14/25 and SP14/23; sector B, between samples SP14/23 and SP14/20; and sector C, between samples SP14/20 and SP14/18 (Fig. 3.7b). With distance between the dated samples in each sector and the age difference, we obtain average growth (i.e., thickening) rates of about 7×10^{-3}, 2×10^{-2}, and 6×10^{-3} mm a^{-1} for sectors A, B, and C, respectively. We therefore assume that the Semproniano giant vein grew with average rates ranging between ca. 10^{-2} and 10^{-3} mm a^{-1}. These rates are consistent with previously-estimated rates for banded travertines within fissure ridges

located elsewhere (about 10^{-2} mm/a; Uysal et al., 2007; Mesci et al., 2008; Gratier et al., 2012; De Filippis e al., 2013a; Frery et a., 2015). This result confirm that the giant thickness of the Semproniano vein is not related to a fast growth rate but rather to the duration of hydrothermal activity, which is significantly larger than veins in other fissure ridges (e.g., Altunel and Karabacak, 2005; Uysal et al., 2007, 2009).

The age distribution along the transect shows that the oldest samples are located neither at the lateral ends of the giant vein nor at its central part indicating that the vein did not grow in a syntaxial or antitaxial fashion (Bons et al., 2012). The three oldest samples (i.e., c. 646, 613, and >800 ka; Fig. 3.7b) occur in separate inner portions of the vein showing that it grew asymmetrically and ataxially (Passchier and Trouw, 1996; Bons et al., 2012) with no systematic growth direction and no systematic age sequence. Based on our data, we hypothesize an accordion-like mode of growth through multiple events of crack-and-seals pulses, which is well supported by the U/Th ages. This growth mode for the Semproniano giant vein is somewhat different from models proposed for fissure ridge structures (e.g., Hancock et al., 1999; Brogi and Capezzuoli, 2009) characterized by banded travertine forming injection veins and sill-like structures filling diffused fractures within the bedded travertine. The Semproniano giant vein, in fact, defines a singular structure that grew within the same horst rock over a long time, maintaining the same orientation.

3.4.3. Hydrothermal parental fluids

C- and O-isotope data show that the Semproniano giant vein is of thermogene origin (Pentecost, 2005). All analyzed samples are characterized by positive $\delta^{13}C$ and negative $\delta^{18}O$ values (Table 3.3, Fig. 3.7b), indicating mixing between hydrothermal parental fluids and meteoric waters and with a significant contribution of CO_2 originating from limestone decarbonation (Gonfiantini et al., 1968; Guo et al., 1996: Billi et al., 2007). Our stable isotope data are in the range typical of thermogene travertines deposited by present-day thermal springs of central Italy (Minissale, 2004; Gandin and Capezzuoli, 2008).

$\delta^{13}C$ values of travertines have been used to determinate the original signal of $\delta^{13}C_{CO2}$ applying the empirical equation of Panichi and Tongiorgi (1976) and the theoretical equation of Bottinga (1968) (Table 3.3). According to the equation of Panichi and Tongiorgi (1976), the $\delta^{13}C_{CO2}$ values are comprised between -6.7 and 2.1 ‰ (V-PDB), while according to the equation of Bottinga (1968), the $\delta^{13}C_{CO2}$ values are comprised between -5.4 and 3.5 ‰ (V-PDB). Those results confirm a mixing between CO_2 originated from limestone decarbonation with CO_2 of igneous origin (e.g. Turi, 1986; Minissale, 2004; Kele et al., 2011).

The O-isotope composition allowed us to estimate the parental fluid temperatures using the water oxygen isotopic composition of modern springs. In the case of the Semproniano giant vein, calculated temperatures span between about 34 ± 2 and 71 ± 7°C, with the majority of data comprised between 46 and 60 °C (Table 3.3, Fig. 3.8c). The validity of these temperature estimates are confirmed by the fluid inclusion microthermometric data on sample SP12 yielding temperatures between 70 and 90 °C (Fig. 3.10). This supports the assumption that the oxygen isotope composition of the hydrothermal fluid did not change substantially through time. Fluid inclusion data also show that the giant vein parental fluid was constituted by almost pure water.

The lack of correlation between ages and precipitation temperatures in the giant vein (Fig. 3.8d), indicate no systematic and linear cooling of hydrothermal parental fluids with time. This differ from the study of Rimondi et al. (2015), on the Pleistocene Castelnuovo dell'Abate travertines on the northern flank of the Mt. Amiata volcano which showed a cooling of the hydrothermal fluid of about 70 °C in 300-400 ka. Therefore, while the Castelnuovo dell'Abate travertines were strictly and directly connected with the Mt. Amiata geothermal anomaly, the Semproniano system, which is located about 20 km to the south, was influenced not only by the Mt. Amiata geothermal anomaly, but also by further paleoenvironmental and/or paleoclimate factors (see below).

The Sr- and Nd-isotopes as well as the REE patterns help to characterize the origin of the hydrothermal fluids. The rather homogeneous Sr- and Nd-isotope values are indicative of a unique reservoir for the deposition of travertines and calcite veins. Sr- and Nd- isotope values are different

from isotopic signature of Mt. Amiata volcanic rocks (Conticelli et al. 2015). In particular, our Sr-isotope values are in the range of those obtained for the Mesozoic sedimentary units of central Italy (e.g., Barbieri et al., 1979; Cortecci and Lupi, 1994; Barbieri and Morotti, 2003; Gasparrini et al., 2013) and for the hydrothermal springs of Saturnia (Barbagli et al., 2013). This suggests no contamination through volcanic units during underground circulation of these fluids. This interpretation is compatible with the REE patterns that are similar to those obtained from the Tuscan Nappe limestone from the Larderello-Travale geothermal area (Möller et al., 2003; Fig. 3.9). Accordingly, we consider the Mesozoic limestones of the Albegna area (e.g., Bonciani et al., 2005; Brogi, 2008; Guastaldi et al., 2014) as the main reservoir of the hydrothermal system and the probable source for the chemical signature of the studied carbonates. Eventually, the best scenario explaining the entire hydrothermal fluid circuit should involve variable mixing of meteoric waters with fluids characterized by water-rock isotopic exchange similar to the broad field of endogeneous fluids (e.g., Crossey et al., 2009).

3.4.4. Estimation of CO_2 outflow

Minimum value of total CO_2 volume leaked during the formation of the Semproniano giant vein can be estimated from the volume of $CaCO_3$ precipitated (Crossey et al., 2009; Frery, 2012; Karlstrom, 2013). It has been shown that the volume of leaked CO_2 precipitated in travertine/vein deposits is only a minor part of the total leakage, representing between 6.6% and 10% (Shipton et al., 2005) of the total dissolved CO_2. According to Frery (2012), it is possible to calculate only the minimum value of CO_2 leakage during $CaCO_3$ vein formation for two reasons: (i) the proportion between precipitated CO_2 and total leaked CO_2 includes only the dissolved part of the CO_2 at the surface, thus disregarding the CO_2 escaping as free phase (i.e., degassing); (ii) after formation, the vein or travertine deposit may have undergone erosional processes, which are difficult to accurately quantify.

For fossil travertines or $CaCO_3$ veins, the total mass of precipitated CO_2 ($m_{CO2}^{precipitated}$) can be calculated using the calcium carbonate precipitation equation:

$$m_{CO2}^{precipitated} = \rho_{CaCO3} \cdot V_{CaCO3}\{M_{CO2}|M_{CaCO3}\} \qquad \text{(Eq. 1)}$$

where ρ_{CaCO3} and$\{M_{CO2}|M_{CaCO3}\}$ are considered as constant parameters: ρ_{CaCO3}= $2.7 \cdot 10^3$ kg m^{-3}; M_{CO2} = 44g mol^{-1}, and M_{CaCO3} = 100.1 g mol^{-1}.

Based on field observations, we estimate the volume of the Semproniano giant vein assuming a length of 500 m and a width of 50 m. for the thickness of the vein, we consider two alternative end members: 10 m (the observable vein exposed in the field), and 50 m (estimated through geological cross-sectioning; Fig. 3.2b). For a thickness of 10 m, the estimated total mass of CO_2 leakage are 3 x 10^6 and 5 x 10^6 tons, for total dissolved CO_2 masses of 10 and 6.6%, respectively. For a depth of 50 m 14 x 10^6 and 22 x 10^6 tons are calculated. Collectively, all these values provide a CO_2 leakage between 5 ton/a and 37 tons/a over the 600 ka longevity of the Semproniano giant vein, corresponding to a CO_2 flux between 5 x 10^6 mol a^{-1} km^{-2} and 3 x 10^7 mol a^{-1} km^{-2}. These estimates are of the same order of magnitude of measured average CO_2 flux discharged by present-day thermal springs in central Italy (between 1×10^4 mol a^{-1} km^{-2} and 5×10^7 mol a^{-1} km^{-2}, Minissale, 2004; Frondini et al., 2008) and it is two order of magnitude lower than the CO_2 flux (3.7×10^9 mol a^{-1}) in present-day thermal springs on the Colorado Plateau, USA (Crossey et al., 2009). For comparison, the estimated CO_2 flux during the formation of the Semproniano giant vein is about four order of magnitude lower than the deeply sourced (endogenic) CO_2 in non-volcanic areas of Italy (10^{11} mol a^{-1}, Rogie et al., 2000) and represent about one millionth of the present-day CO_2 released from volcanic areas at the global scale (Gerlach, 2011).

3.4.5. Paleoclimate influence

To determine a possible influence of paleoclimate on the growth of the Semproniano giant vein, in Fig. 3.11 we matched our U/Th ages (Tables 3.2 and S3.1) with Quaternary glacial cycles, using the curve extracted from the deep sea oxygen isotope trend elaborated by Zachos et al. (2001), and the pollen record of the Valle di Castiglione, located about 150 km to the south of the study area (Fig. 3.1a), elaborated by Tzedakis et al. (2001).

We note that, except for two points, most samples from the giant vein fall within the inter-glacial stages. Also the host rock of the giant vein and the bedded travertine on the vein flanks match well with interglacial stages (Fig. 3.11). It is noteworthy that six samples fall within marine isotope stages MIS 5 and MIS 7, which are suggested to be humid times by the pollen curve (Fig. 3.11).

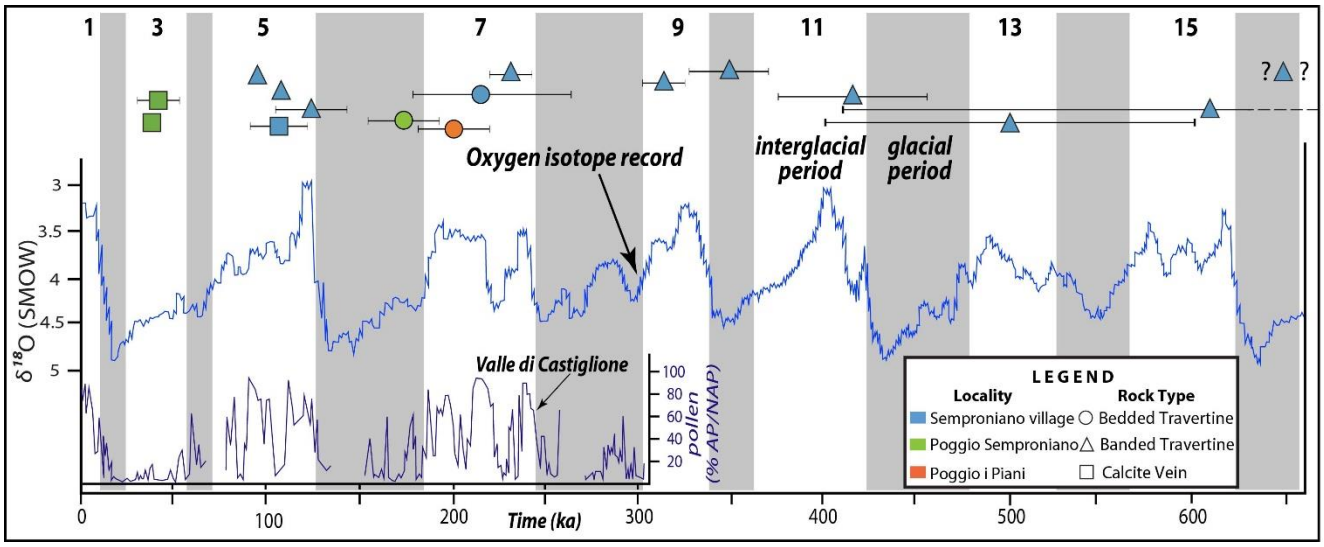

Figure 3.11 - Comparison between U/Th ages of bedded travertine, banded travertine, and calcite veins from the study area and major paleoclimate indicators represented by the deep sea oxygen isotope trend (Zachos et al., 2001) and by the pollen dataset from Valle di Castiglione (Tzedakis et al., 2001). Global glacial/interglacial periods are redrawn and modified after Priewish et al (2014).

The dating, thus suggests that the Semproniano giant vein formed preferentially during warm and humid climate periods characterized by high stands of the water table promoting a greater fluid discharge. Similar patterns have been suggested for other Quaternary travertine deposits (e.g., Dramis

et al., 1999; Frank et al., 2000; Rihs et al., 2000; Soligo et al., 2002; Pentecost, 2005; Luque and Julià, 2007; Faccenna et al., 2008; Kampman et al., 2012; Priewisch et al. 2014).

This scenario is different from the one proposed by Uysal et al. (2007, 2009) for banded travertines precipitated in co-seismic fissures of the Denizli basin (Turkey) which was based on U/Th ages and REE data. These authors, proposed that carbonate precipitation was controlled by seismic-related CO_2 exsolution from a depressed water table during glacial stages. Ages obtained for Turkish travertines by Özkul et al., (2013) and Toker et al., (2015) show that deposition was active during glacial and interglacial time, indicating that travertine precipitation during late Quaternary was not strongly influenced by climatic variation. In particular, we found similarities with Toker et al., (2015) whose recognized that the highest amount travertine precipitation in Kocabas (Denizli basin, Turkey) occurred during MIS 5 (interglacial) and proposed that active fault systems favored the rise of hydrothermal fluids and travertine deposition,

Finally, our results for the Semproniano giant vein suggest that high stand of the water table was a primary influencing factor in the vein formation.

3.4.6. Relationships between the giant vein and nearby travertine deposits: the fluid circuit

The Poggio Semproniano and Poggio I Piani travertine plateaus constitute the largest travertine deposits in the Semproniano area (Fig. 3.3a). Although the dataset for these deposits is smaller than that of the giant vein, the C- and O-isotope values are comparable (Fig. 3.8b), showing that the hydrothermal parental fluids were very similar. The Sr-, Nd-isotopes, and REE data (Table 3.4 and Fig. 3.9) confirm that the parental fluid circuit and reservoir was mainly the Mesozoic limestones of the Albegna basin.

U/Th ages for the bedded travertine samples from the plateaus (Table 3.2), 171 ± 14 ka for Poggio Semproniano, 198 ± 18 ka for Poggio I Piani) indicate that the formation of the two plateaus was at least in part contemporaneous with that of the Semproniano giant vein. Moreover, also the activity of the nearby Mt. Amiata volcanic district (300-190 ka, Cadoux and Pinti, 2009; 300-225 ka, Laurenzi

et al., 2015) was partly contemporaneous with the $CaCO_3$ mineralizations of the Semproniano area, with the giant vein being partly older and partly younger than the volcanic district.

From previous studies we know that while fissure ridges such as the Semproniano giant vein are aggradational systems that tend to grow vertically due to the scarcity of feeding fluids (i.e., $CaCO_3$ precipitates contributing to the vertical grow of the deposit), travertine plateaus are progradational systems where the abundance of feeding fluids contribute to the horizontal grow (progradation) of the deposit (Faccenna et al., 2008; De Filippis et al. 2013a). We also know that fissure ridges and plateaus can coexist, in space and time, in geothermal areas where the abundance of geothermal fluids primarily feeds the plateau whereas the fissure ridge(s) constitutes a remote apophysis of the plateau with a scarcity of fluids that provokes the aggradation development of the fissure ridge (e.g., Tivoli travertines; De Filippis et al., 2013b).

The possible scenario for the genesis of the Semproniano giant travertine vein is a structurally-controlled pathway (faults and fractures) for the circulating mineralising fluids during the Quaternary. Dominant meteoric fluids interacted with the carbonate reservoir of the Mt. Amiata volcano and were heated at depth, where the heat source is maintained by the regional geothermal anomaly (Fig. 3.12a). In this scenario, the Semproniano giant vein resulted as an epithermal fluid discharge area after convective circulation of the CO_2-enriched hydrothermal fluids (Fig. 3.12b). In particular, we can assume a fluid pressure cycling in a long-lived fault-valve behavior setting (Cox et al., 2001; Sibson, 2004; Cox, 2010), assisted by fracture network generation and maintenance that could have been provided by the well-known N-S-striking fault zone system active during Quaternary time in the Mt Amiata-Albegna basin region (Zanchi and Tozzi, 1987; Brogi, 2004b; Bellani et al., 2004; Brogi and Fabbrini, 2009). In this model, the Semproniano giant vein (i.e., the fissure ridge) is interpreted as an apophysis of a large geothermal field characterized by the deposition of big travertine plateaus.

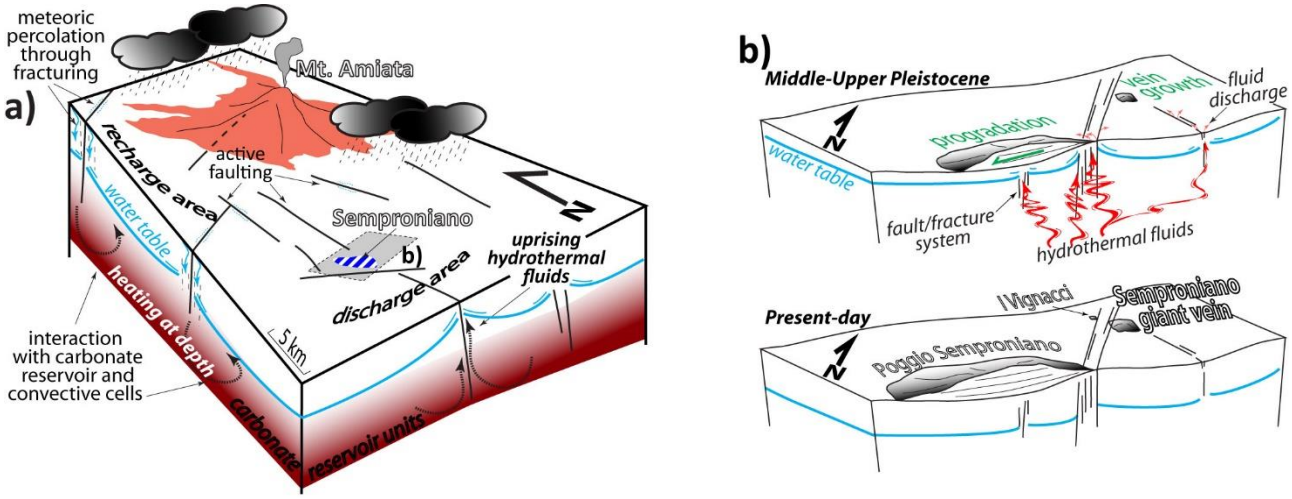

Figure 3.12 - (a) Schematic 3D-block diagram interpreting the hydrothermal settingin the Mt. Amiata-Semproniano area. Active faulting and related fracturation have primary role in controlling meteoric percolation within the carbonate reservoir at depth, and the uprise of hydrothermal fluids. (b) Two-step scenario illustrating the mode of travertine deposition (by veining at Semproniano fissure ridge and by dominant progradation at the Poggio Semproniano plateau) supplied by hydrothermal fluid discharge at the fault/fracture tips. The fault architecture is indicative.

3.5. Conclusions

(1) The thickest continuous vein hitherto documented in the literature (50 m) is found and studied within a fissure ridge travertine exposed in the Semproniano village, in the hydrothermal area surrounding the Pleistocene Mt. Amiata volcano in southern Tuscany, Italy.

(2) The thickness of the Semproniano vein is connected with its probable shallow emplacement and with the unusual longevity of the hydrothermal activity between at least 650 and 85 ka.

(3) The epithermal fluid supply feeding the Semproniano giant vein is not directly connected with the main volcanic paroxysmal activity of the Mt. Amiata volcano (which is younger than the early growth of the vein), rather with the positive geothermal anomaly associated with its pre-eruptive stages (Cadoux et al., 2009) through structurally-controlled fluid pathways which created and maintained active convection and supply of CO_2-enriched meteoric fluids.

(5) The growth of the Semproniano giant vein was modulated by by Pleistocene climate oscillations, with warm humid interglacial periods being the preferential phases of vein accretion, due to the higher fluid discharge.

(6) Structures such as the Semproniano giant vein can be used to estimate the long-term release of CO_2 from geothermal/volcanic provinces, thus improving our knowledge of the CO_2 cycle on Earth.

3.6. Appendix

3.6.1. $^{230}Th/^{234}U$ dating

As reported in Tables 3.2 and S3.1, we performed U/Th dating analyses using two different methods, namely (1) through α spectrometry performed at the Laboratorio di Geochimica Ambientale e Isotopica of Roma Tre University (Italy), or (2) through a Thermo Electron Neptune multi-collector inductively coupled mass spectrometer (MC-ICP-MS) (Shen et al., 2012) hosted at the High-Precision Mass Spectrometry and Environment Change Laboratory (HISPEC) of the National Taiwan University, Taipei (Taiwan ROC).

For MC-ICP-MS dating, we covered about 0.05 g of each sample with H_2O and dissolved it gradually with double distilled 14 N HNO_3. After dissolution, we added a ^{229}Th-^{233}U-^{236}U spike (Shen et al., 2003) to the sample, followed by 10-20 drops of $HClO_4$ to clear the organic matter. We then followed the chemical procedure described in Shen et al. (2003) for the separation of Uranium and Thorium. We calculated the age correction using an estimated atomic $^{230}Th/^{232}Th$ ratio of 4 ± 2 ppm. These latter values are the ones typical for a material at secular equilibrium with the crustal $^{232}Th/^{238}U$ value of 3.8. We arbitrarily assumed a 50% error.

For α spectrometry dating, we dissolved about 60 g of each sample in 7 N HNO_3 and filtered the solution to separate the leachates from the insoluble residue. We heated the leachate at 200 °C after adding a few millilitres of hydrogen peroxide to clear the organic matter, and then spiked the solution with a ^{228}Th-^{232}U tracer. We extracted the isotopic complexes of U and Th following the procedure described in Edwards et al. (1988) and then analyzed the solution by an alpha-counted using high-resolution ion-implanted Ortec silicon-surface barrier detectors. Due to the presence of non-radiogenic ^{230}Th related to detrital ^{232}Th, ages obtained for samples with a $^{230}Th/^{232}Th$ activity ratio less than or equal to 80 required a proper correction, which we performed assuming that all the detrital Th had an average $^{230}Th/^{232}Th$ activity ratio of 0.85 ± 0.36 (Wedepohl, 1995), which is the crustal thorium mean composition. We then calculated the ages using ISOPLOT, a plotting and regression program for radiogenic-isotope data (Ludwig, 2003).

3.6.2. C- and O-isotope determination

The isotopic composition of carbonate was measured according to the method described in detail in Breitenbach and Bernasconi (2011). Briefly, approximately 100 µg of powder were filled in 12 ml Exetainers (Labco, High Wycombe, UK) and flushed with pure Helium. The samples were reacted with 3-5 drops of 100% phosphoric acid at 70°C with a ThermoFisher GasBench device connected to a ThermoFisher Delta V mass spectrometer. The average long term reproducibility of the measurements based on replicated standards was ±0.05‰ for $\delta^{13}C$ and ±0.06‰ for $\delta^{18}O$. The instrument is calibrated with the international standards NBS19 ($\delta^{13}C$= 1.95 and $\delta^{18}O$ = -2.2‰) and NBS18 ($\delta^{13}C$= -5.01 and $\delta^{18}O$ = -23.01‰). The isotope values are reported in the conventional delta notation with respect to VPDB (Vienna Pee Dee Belemnite).

3.6.3. Thermometry of mineralizing parental fluids from O-isotopes

We calculated the paleo-temperature of mineralizing parental fluids using the equation of Kele et al. (2015) specifically developed for travertine parental fluids and calibrated through clumped isotope thermometer. This empirical equation is expressed as:

$$1000\ln \alpha_{(calcite\text{-}water)} = (20 \pm 2)\ 1000/T - (36 \pm 7) \qquad \text{(Eq.3)}$$

where (1) $\alpha_{(calcite\text{-}water)} = (\delta^{18}O_{calcite} + 1000) / (\delta^{18}O_{water} + 1000)$, (2) T is the temperature of the mineralizing $CaCO_3$-rich fluids expressed in K and (3) $\delta^{18}O_{calcite}$ and $\delta^{18}O_{water}$ are expressed in parts ‰ relative to V-SMOW. As benchmark ($\delta^{18}O_{water}$), we measured and used the present $\delta^{18}O$ isotopic value from the Saturnia spring hydrothermal waters (-6.4‰ V-SMOW), whose active source is located 9 km to the south of the Semproniano giant vein. We assume that the oxygen isotope composition of the paleosprings was similar to those of the current springs.

3.6.4. Sr- and Nd-isotope and REE determination

We determined the Strontium (Sr) and Neodymium (Nd) isotope ratios as well as Strontium, rare Earth elements (REE) and Yttrium (Y) concentrations on fragments of handpicked travertine and vein samples. We crushed the chips of travertine in a stainless steel mortar and then we dissolved about 200 mg of each sample with ultrapure HNO_3 (3%). We splitted 100 ml of solution from each sample into two aliquots. We used one of the two aliquots for REE, Y, and Sr concentrations and the other aliquot for Sr and Nd isotopes. The aliquot for REE, Y and Sr concentration were analyzed via ICP-MS (Agilent mod. 7500ce) equipped with collision cell at the Chemical Laboratory of Istituto di Chimica Agraria ed Ambientale, Catholic University of Piacenza and Cremona (Italy). We evaporated the aliquot for isotope analysis, converted it into chloride form, and loaded it onto standard Bio-Rad AG50W-X12 cation exchange resin to separate Sr from matrix. The very low REE and Y (REY) contents in travertine required the procedure of Sharma and Wasserburg (1996): we added ultrapure NH_3 to the solution diluted with MilliΩ water up to ionic strength of about 1.0 to shift pH to 9.0 for precipitating REY with Fe oxide-hydroxides. We then mixed both the precipitate and the supernatant with a vortex overnight and separated from each other by filtration. We dissolved the oxide-hydroxides with 4M HCl and separated them from the matrix via ion-exchange chromatography. We separated Nd from the other REE with Ln. Spec resin (Triskem-international) following the procedure of Pin and Zalduegui (1997).

We carried out the isotopic analyses at Istituto di Geologia Ambientale e Geoingegneria – Consiglio nazionale delle Ricerche (IGAG-CNR) laboratory c.o. Dipartimento di Scienze della Terra, Sapienza University of Rome (Italy) using a FINNIGAN MAT 262RPQ multicollector mass spectrometer. We loaded all samples on a Re double filament as nitrate and analyzed them in static mode. We normalized Sr analyses to $^{86}Sr/^{88}Sr = 0.1194$. We fixed Sr analytical blank at 1 ng. Internal precision ("within-run" precision) of a single analytical result is given as two standard error of the mean (2se) and is obtained as a mean of more than 200 ratios collected on each sample with a stable bean of 2.0 V.

Repeated analyses of NIST-987 during the period of the analyses gave a mean value of $^{87}Sr/^{86}Sr$ = 0.710235 ± 9 (n = 20) and La Jolla $^{143}Nd/^{144}Nd$ = 0.511851 ± 10 (n=20), $^{146}Nd/^{144}Nd$ normalized to 0.7219. Total procedural blanks were below 2 ng of Sr and 1 ng of Nd for all the samples. The measured $^{143}Nd/^{144}Nd$ ratios are presented as fractional deviation in parts in 10^4 (ε-units) from $^{143}Nd/^{144}Nd$ in a Chondritic Uniform Reservoir (CHUR) as measured today:

$$\varepsilon_{Nd\,(0)} = [(^{143}Nd/^{144}Nd)_{sample} / (^{143}Nd/^{144}Nd)_{CHUR} - 1] \times 10^4 \qquad \text{(Eq.4)}$$

where $(^{143}Nd/^{144}Nd)_{sample}$ is the ratio measured in the sample today and $(^{143}Nd/^{144}Nd)_{CHUR}$ is the ratio in the reference reservoir today, i.e. 0.511847 (DePaolo and Wasserburg, 1976).

3.6.5. Fluid inclusion analysis

We performed microthermometric measurements at Istituto di Geologia Ambientale e Geoingegneria – Consiglio nazionale delle Ricerche (IGAG-CNR) Fluid Inclusion Laboratory c/o Dipartimento di Scienze della Terra, Sapienza University of Rome (Italy), using a freezing-heating stage Linkam THMSG600 (from -196 to +600 °C). The stage is adapted to a Nikon Optiphot-Pol transmitted-light microscope equipped with long-working distance objectives (5X, 10X, 20X, and 40X) and a video camera. We performed the analysis of fluid inclusions on a 150 μm thick double-polished slice of calcite vein (Fig. 3.10). Due to the physical properties of calcite minerals, we took particular care in maintaining as low as possible the temperature during grinding, polishing, and, in general, during all the sample preparation (Goldtsein and Reynolds, 1994; Bodnar, 2003). A low-temperature sample preparation is fundamental to avoid phenomena of stretching and decrepitation of the inclusions, which may affect the microthermometric measurements. In those fluid inclusions where decrepitation and stretching phenomena due to the volume expansion during ice formation (Bodnar, 2003) were visible, we perform Tm_{ice} measurements separately from Th measurements. Salinity contents (expressed in wt% NaCl eq.) of fluid inclusions has been calculated through the

Tm_{ice} values using the equation proposed by Bodnar and Vityk (1994). Data reproducibility is of ± 0.2 °C for cooling runs and of ± 1 °C for heating run

3.6.6. Additional Tables

Sample	Travertine type	Location	U (ppb)	$\delta^{234}U$ measured	$[^{230}Th/^{238}U]$ activity	$[^{230}Th/^{232}Th]$ ppm	$\delta^{234}U_{initial}$ corrected	$^{230}Th/^{232}Th$	$^{234}U/^{238}U$	$^{230}Th/^{234}U$	$(^{230}Th/^{234}U)$ corrected	Age corrected (ka)
SP15*	Banded	Semproniano Village	15.063 ± 0.021	45.5 ± 4.3	1.0171 ± 0,0077	1058 ± 46	121 ± 14					**347 ± 22**
SP14/15*	Banded	Semproniano Village	8.155 ± 0.013	89.1 ± 8.6	1.138 ± 0.010	966 ± 63	— —					***>800***
SP14/18*	Banded	Semproniano Village	29.783 ± 0.054	77.8 ± 2.4	0.5924 ± 0.0036	2619 ± 81	99.1 ± 3.1					**86 ± 1**
SP14/20*	Banded	Semproniano Village	7.287 ± 0.013	42.7 ± 4.6	0.9324 ± 0.0094	93.02 ± 0.97	82.1 ± 9.1					**231 ± 9**
SP14/23*	Banded	Semproniano Village	12.908 ± 0.021	15.8 ± 2.7	0.9635 ± 0.0046	8688 ± 977	38.3 ± 6.7					**314 ± 11**
SP14/25*	Banded	Semproniano Village	7.451 ± 0.014	47.5 ± 4.4	1.0428 ± 0.0062	280.3 ± 3.6	155.2 ± 25.0					**419 ± 39**
SP14/28*	Banded	Semproniano Village	22.212 ± 0.037	38.3 ± 2.5	1.0507 ± 0.0041	2129 ± 36	216 ± 292					**613 ± 200**
SP14/30*	Banded	Semproniano Village	65.13 ± 0.11	179.9 ± 2.3	0.7458 ± 0.0040	475.0 ± 2.8	241.8 ± 3.1					**105 ± 1**
SP14/32*	Banded	Semproniano Village	12.408 ± 0.018	62.8 ± 4.8	1.0866 ± 0.0062	390.0 ± 3.9	— —					**646**
SP14/34*	Banded	Semproniano Village	30.647 ± 0.054	23.4 ± 2.1	1.0218 ± 0.0083	273.1 ± 2.4	95 ± 44					**495 ± 99**
SP1**	Banded	Semproniano Village	12.4 ± 0.9					23.746 ± 2.639	1.138 ± 0.107	1.014 ± 0.087		**>350**
SP12**	Banded	Semproniano Village	77 ± 0.2					2.425 ± 0.131	1.017 ± 0.028	0.757 ± 0.030	0.693 ± 0.053	**128 ± 19**
SP16**	Calcite vein	Semproniano Village	10.5 ± 6.0					12.564 ± 1.987	1.471 ± 0.107	0.658 ± 0.045	0.641 ± 0.064	**104 ± 16**
SP11**	Bedded	Semproniano Village	53 ± 0.2					7.148 ± 0.251	1.094 ± 0.026	0.892 ± 0.027	0.878 ± 0.051	**214 +50/-37**
SP3**	Calcite vein	Poggio Semproniano	3.7 ± 0.3					6.244 ± 0.711	3.804 ± 0.294	0.372 ± 0.024	0.340 ± 0.052	**43 ± 8**
SP10**	Calcite vein	Poggio Semproniano	32 ± 2					110.353 ± 20.338	0.978 ± 0.061	0.299 ± 0.023		**39 ± 4**

PO2**	Bedded	Poggio Semproniano	53 ± 2					169.884 ± 26.205	1.198 ± 0.036	0.818 ± 0.039		**171 ± 19**
PP1**	Bedded	Poggio i Piani	77 ± 3					171.43 ± 23.82	1.112 ± 0.031	0.857 ± 0.028		**198 ± 18**
VI1**	Banded	Vignacci	77 ± 0.6					2.277 ± 0.112	1.012 ± 0.071	1.578 ± 0.093		**>350**

Table S3.2. - Concentration or rare earth elements and yttrium for travertine samples of the study area (in μg/kg).

Sample	Travertine Type	Location	La	Ce	Pr	Nd	Sm	Eu	Gd	Tb	Dy	Y	Ho	Er	Tm	Yb	Lu	SREE	Y/Ho	Eu/Eu*	Ce/Ce*	Gd/Gd*	LaN/YbN	LaN/SmN	NdN/YbN
SP14/06	Bedded travertine	Semproniano Village	2059.61	4839.19	625.23	2951.00	760.60	166.20	858.48	114.78	734.29	4797.94	125.27	287.54	36.65	234.18	31.45	18622.41	38.30	0.97	0.94	0.21	0.65	0.39	1.05
SP14/18	Banded travertine	Semproniano Village	7.41	11.57	1.18	6.20	2.40	0.43	3.31		3.19	144.54	0.65	2.39		6.90		190.17	221.33	0.71	0.76		0.08	0.45	0.07
PO1	Bedded travertine	Poggio Semproniano	9.06	12.20	1.48	14.63	1.85	0.29	2.74		3.05	32.79	0.55	1.02		0.70		80.35	59.85	0.61	0.51		0.96	0.71	1.74
SP3	Calcite vein	Poggio Semproniano	110.57	147.15	12.43	34.40	3.09	0.46	3.23		4.00	38.60	0.75	1.97		1.46		358.12	51.23	0.69	0.82	0.13	5.58	5.20	1.96
VI1	Banded travertine	I Vignacci	114.35	125.91	56.64	340.23	173.16	62.69	479.34	80.03	567.04	4562.58	98.47	217.34	25.93	150.45	18.39	7072.56	46.34	1.02	0.30		0.06	0.10	0.19

Eu anomaly denoted as Eu/Eu calculated using the equation $Eu/Eu^* = Eu_N/(Sm_N \times Gd_N)^{1/2}$ (Taylor and McLennan, 1985); Ce anomaly denoted as Ce/Ce* calculated using the equation: $Ce/Ce^* = 3Ce_N/(2La_N + Nd_N)$ (Ederfield and Greaves, 1982; McLennan, 1989); Gd anomaly denoted as Gd/Gd* calculated using the equation: Gd/Gd* = GdN/(0.33SmN+ 0.67TbN) (Bau and Dulski, 1996).

3.7. References

Altunel E., Hancock P.L., 1993a. Active fissuring and faulting in Quaternary travertines at Pamukkale, western Turkey. In: Stewart, I.S., Vita-Finzi, C., Owen, L.A. (Eds.), Neotectonics and Active Faulting: Zeitschrift fuer Geomorphologie Supplement, 94, 285–302.

Altunel E., Hancock P.L., 1993b. Morphology and structural setting of Quaternary travertines at Pamukkale, Turkey. Geological Journal, 28, 335–346.

Altunel E., Hancock P.L., 1996. Structural attributes of travertine-filled extensional fissures in the Pamukkale plateau, western Turkey. International Geology Review, 38, 768–777.

Altunel E., Karabacak V., 2005. Determination of horizontal extension from fissure-ridge travertines: a case study from the Denizli Basin, southwestern Turkey. Geodinamica Acta, 18, 333–342.

Annunziatellis A., Beaubien S.E., Bigi S., Ciotoli G., Coltella M., Lombardi S., 2008. Gas migration along fault systems and through the vadose zone in the Latera caldera (central Italy): implications for CO2 geological storage. International Journal of Greenhouse Gas Control, 2, 353-372.

Barbagli A., Brogna F.N.A., Callegari I., Guastaldi E., Liali G., Marsico N., Rezza C., Trotta M., 2013. Approccio multi-isotopico ed idrogeochimico per la caratterizzazione di acque termali: il caso di Saturnia (GR). Italian Journal of Groundwater, AS07029, 025-040, DOI 10.7343/AS-049-13-0076.

Barberi F., Buonasorte G., Cioni R., Fiordelisi A., Foresi L., Iaccarino S., Laurenzi M.A., Sbrana A., Vernia L., Villa I.M., 1994. Plio-Pleistocene geological evolution of the geothermal area of Tuscany and Latium. Memorie Descrittive della Carta Geologica d'Italia, 49, 77–133.

Barbieri M. and Morotti M., 2003. Hydrogeochemistry and strontium isotopes of spring and mineral waters from Monte Vulture volcano, Italy. Applied Geochemistry, 18, 117-125.

Barbieri M., Masi U., Tolomeo L., 1979. Origin and distribution of strontium in the travertines of Latium (central Italy). Chemical Geology, 24, 181-188.

Barchi M., Minelli G., Pialli G., 1998. The CROP-03 profile: a synthesis of results on deep structures of the Northern Apennines. Memorie della Società Geologica Italiana, 52, 383-400.

Batini F., Brogi A., Lazzarotto A., Liotta D., Pandeli E. 2003. Geological features of the Larderello–Travale and Monte Amiata geothermal areas (southern Tuscany, Italy). Episodes, 26, 239-244.

Beasley C.J., Fiduk J.C., Bize E., Boyd A., Frydman M., Zerilli A., Dribus J.R., Moreira J.L.P., Capeliero Pinto A.C., 2010: Brazil's subsalt play. Oilfield Review, 22, No. 3, 28-37.

Bellani S., Brogi A., Lazzarotto A., Liotta D., Ranalli G., 2004. Heat flow, deep temperatures and extensional structures in the Larderello geothermal field (Italy). Constraints on geothermal fluid flow. Journal of Volcanology and Geothermal Research, 132, 15–29.

Bickle M., Kampman N., 2013. Lessons in carbon storage from geological analogues. Geology, 41, 525-526.

Billi A., Tiberti M.M., Cavinato G.P., Cosentino D., Di Luzio E., Keller J.V.A., Kluth C., Orlando L., Parotto M., Praturlon A., Romanelli M., Storti F., Wardell N., 2006. First results from the CROP-11 deep seismic profile, central Apennines, Italy: evidence of mid-crustal folding. Journal of Geological Society London, 163, 583-586.

Billi A., Valle A., Brilli M., Faccenna C., Funiciello R., 2007. Fracture-controlled fluid circulation and dissolutional weathering in sinkhole-prone carbonate rocks from central Italy. Journal of Structural Geology, 29, 385-395.

Bodnar R.J., Vytik M.O., 1994. Interpretation of microthermometric data for H_2O–NaCl fluid inclusions. In: De Vivo B., Frezzotti M.L. (eds) Fluid inclusions in minerals: methods and applications. Virginia Polytechnic Institute, Blacksburg, 117-130.

Bodnar R.J., 2003. Reequilibration of fluid inclusions In: Samson IM, Anderson AJ, Marshall DD (Eds.) Fluid Inclusions: Analysis and Interpretation. Mineralogical Association of Canada, Short Course, 32, 213-230.

Bonazzi U., Fazzini P., Gasperi G., 1992. Note alla carta geologica del Bacino del Fiume Albegna. Bollettino della Società Geologica Italiana, 111, 341-354.

Bonciani F., Callegari I., Conti P., Cornamusini G., Carmignani L., 2005. Neogene post-collisional evolution of the internal Northern Apennines: insights from the upper Fiora and Albegna valleys (Mt. Amiata geothermal area, southern Tuscany). Bollettino della Società Geologica Italiana, Special Volume 3, 103-118.

Bons P.D., 2001. The formation of large quartz veins by rapid ascent of fluids in mobile hydrofractures. Tectonophysics, 336, 1-17.

Bons P.D., Elburg M.A., Gomez-Rivas, E., 2012. A review of the formation of tectonic veins and their microstructures. Journal of Structural Geology, 43, 33-62

Bosi C., Messina P., Rosati M., Sposato A., 1996. Età dei travertini della Toscana meridionale e relative implicazioni neotettoniche. Memorie della Società Geologica Italiana, 51, 293-304.

Bossio A., Foresi L.M., Mazzei R., Salvatorini G., Sandrelli F., Bilotti M., Colli A., Rossetto R., 2004. Geology and stratigraphy of the southern sector of the Neogene Albegna River Basin (Grosseto, Tuscany, Italy): Geologica Romana, 37, 165-173.

Bottinga Y., 1968. Calculation of fractionation factors for carbon and oxygen isotopic exchange in the system calcite–carbon dioxide–water. Journal of Physical Chemistry, 72, 800–808

Breitenbach S.F:M. and Bernasconi S.M. 2011. Carbon and oxygen isotope analysis of small carbonate samples (20 to 100 µg) with a GasBench II preparation device. Rapid Communications in Mass Spectrometry, 25, 1910-1914.

Brogi, A., 2004a. Faults linkage, damage rocks and hydrothermal fluid circulation: tectonic interpretation of the Rapolano Terme travertines (southern Tuscany, Italy) in the context of the Northern Apennines Neogene–Quaternary extension. Eclogae Geologicae Helvetiae, 97, 307–320.

Brogi A., 2004b. Miocene extension in the inner Northern Apennines: the Tuscan Nappe megaboudins in the Mt. Amiata geothermal area and their influence on Neogene sedimentation. Bollettino della Società Geologica Italiana, 123, 513-529.

Brogi A., 2008. The structure of the Monte Amiata volcano-geothermal area (Northern Apennines, Italy): Neogene-Quaternary compression versus extension. International Journal of Earth Sciences, 97, 677-703. DOI 10.1007/s00531-007-0191-1

Brogi A., Liotta, D., 2008. Highly extended terrains, lateral segmentation of the substratum, and basin development: the Middle–Late Miocene Radicondoli Basin (inner northern Apennines, Italy). Tectonics, 27, TC 5002.

Brogi A., Fabbrini L, 2009. Extensional and strike-slip tectonics across the Monte Amiata–Monte Cetona transect (Northern Apennines, Italy) and seismotectonic implications. Tectonophysics, 476, 195-209.

Brogi A., Capezzuoli E., 2009. Travertine deposition and faulting: the fault-related travertine fissure-ridge at Terme S. Giovanni, Rapolano Terme (Italy). International Journal of Earth Sciences (Geologische Rundschau), 98, 931–947.

Brogi A., Capezzuoli E., Ague R., Branca M., Voltaggio M., 2010. Studying travertines for neotectonics investigations: middle–late Pleistocene syn-tectonic travertine deposition at Serre di Rapolano (Northern Apennines, Italy). International Journal of Earth Sciences, 99, 1382–1398.

Brogi A., 2011. Bowl-shaped basin related to low-angle detachment during continental extension: The case of the controversial Neogene Siena Basin (central Italy, Northern Apennines). Tectonophysics, 499, 54-76.

Brogi A., Capezzuoli E., Buracchi E., Branca M., 2012. Tectonic control on travertine and calcareous tufa deposition in a low-temperature geothermal system (Sarteano, Central Italy). Journal of the Geological Society, 169, 461–476.

Brogi A., Fidolini F., Liotta D., 2013. Tectonic and sedimentary evolution of the Upper Valdarno Basin: new insights from the lacustrine S. Barbara Basin. Italian Journal of Geosciences, 132/1, 81-97.

Brogi A., Capezzuoli E., Martini I., Picozzi M., Sandrelli F., 2014. Late Quaternary tectonics in the inner Northern Apennines (Siena Basin, southern Tuscany, Italy) and their seismotectonic implication. Journal of Geodynamics, 76, 25-45.

Brogi A., Capezzuoli, E., Liotta D., Meccheri M., 2015. The Tuscan Nappe structures in the Monte Amiata geothermal area (central Italy): a review. Italian Journal of Geosciences, 134-2, 219-236.

Buonasorte G., Cataldi R., Ceccarelli A., Costantini A., D'Offizi S., Lazzarotto A., Ridolfi A., Baldi P., Barelli A., Bertini G., Bertrami R., Calamai A., Cameli G., Corsi R., D'Acquino C., Fiordelisi A., Gezzo A. & Lovari F., 1988. Ricerca ed esplorazione nell'area geotermica di Torre Alfina (Lazio – Umbria). Bollettino della Società Geologica Italiana, 107, 265-337.

Burnside, N.M., Shipton, Z.K., Dockrill, B., Ellam, R.M., 2013. Man-made versus natural CO_2 leakage: A 400 k.y. history of an analogue for engineered geological storage of CO_2. Geology, 41, 471–474.

Cadoux A., Pinti D.L., 2009. Hybrid character and pre-eruptive events of Mt Amiata volcano (Italy) inferred from geochronological, petro-geochemical and isotopic data. Journal of Volcanology and Geothermal Research, 179, 169-190.

Çakır Z., 1999. Along-strike discontinuity of active normal faults and its influence on Quaternary travertine deposition; examples from western Turkey. Turkish Journal of Earth Sciences, 8, 67–80.

Calvo P. and Regueiro M., 2010. Carbonate rocks in the Mediterranean region, from classical to innovative uses of building stone. Geological Society, London, Special Publication, 331, 27-35.

Capezzuoli E., Ruggieri G., Brogi A., Liotta D., 2013. Fluid inclusion analyses in hydrothermal veins associated to travertine: insights from the Semproniano fissure-ridge type travertine deposits (southern Tuscany, Italy). Fist Geoitalia 2013, IX Forum di Scienze della Terra, Pisa 16-18 Settembre 2013.

Carmignani L., Decandia F.A., Fantozzi P.L., Lazzarotto A., Liotta D. & Meccheri M., 1994. Tertiary extensional tectonics in Tuscany (Northern Apennines, Italy). Tectonophysics, 238, 295-315.

Carmignani L., Conti P., Cornamusini G., Pirro A. 2013. Geological map of Tuscany (Italy). Journal of Maps, 9:4, 487-497, DOI:10.1080/17445647.2013.820154

Cavinato G.P., De Celles P.G., 1999. Extensional basins in the tectonically bimodal central Apennines fold-thrust belt, Italy: response to corner flow above a subducting slab in retrograde motion. Geology, 27, 955-958.

Chafetz H.S., Folk R.L., 1984. Travertines: depositional morphology and the bacterially constructed constituents. Journal of Sedimentary Petrology, 54, 289–316.

Chiarabba C., Amato A., Fiordelisi A., 1995. Upper crustal tomographic images of the Amiata–Vulsini geothermal region, central Italy. Journal of Geophysical Research, 100, 4053–4066.

Cipollari P., Cosentino D., 1995. Miocene unconformities in the Central Apennines: geodynamic significance and sedimentary basin evolution. Tectonophysics, 252, 375-389.

Collettini C., De Paola N., Holdsworth R.E., Barchi M.R., 2006. The development and behavior of low-angle normal faults during Cenozoic asymmetric extension in the Northern Apennines, Italy. Journal of Structural Geology, 28, 333-352.

Conticelli S., Boari E., Burlamacchi L., Cifelli F., Moscardi F., Laurenzi M.A., Ferrari Pedraglio L., Francalanci L., Benvenuti M.G., Braschi E., Manetti P., 2015. Geochemistry and Sr–Nd–Pb isotopes of Monte Amiata Volcano, Central Italy: evidence for magma mixing between high-K calc-alkaline and leucititic mantle-derived magmas. Italian Journal of Geosciences 134, 266–290.

Cortecci G., Lupi L., 1994. Carbon, oxygen and strontium isotope geochemistry of carbonate rocks from the Tuscan Nappe, Italy. Mineralogia et Petrographica acta, 37, 63-80.

Cox S.F., Knackstedt M.A., Braun J., 2001. Principles of structural controls on permeability and fluid flow in hydrothermal systems. Reviews in Economic Geology, 14, 1–24.

Cox S.F., 2010. The application of failure mode diagrams for exploring the roles of fluid pressure and stress states in controlling styles of fracture-controlled permeability enhancement in faults and shear zones. Geofluids, 10, 217–233.

Crossey L.J., Fischer T.P., Patchett P.J., Karlstrom K.E., Hilton D.R., Newell D.L., Huntoon P., Reynolds A.C., de Leeuw G.A.M., 2006. Dissected hydrologic system at the Grand Canyon: interaction between deeply derived fluids and plateau aquifer waters in modern springs and travertine. Geology, 34, 25-28.

Crossey L.J., Karlstrom K.E., Springer A.E., Newell D., Hilton D.R., Fischer T., 2009. Colorado Plateau region - Neotectonic connections and implications for groundwater systems. Geological Society of America Bulletin, 121 (7/8), 1034-1053.

Crossey L.C., Karlstrom K.E., Dorsey R., Pearce J., Wan E., Beard L.S., Asmerom Y., Polyak., Crow R.S., Cohen A., Bright J., Pecha, M.E, 2015. Importance of groundwater in propagating downward integration of the 6-5 Ma Colorado River system: Geochemistry of springs,

travertines and lacustrine carbonates of the Grand Canyon region over the past 12 Ma. Geosphere, 11, 3, 1-23.

De Filippis L., Billi A., 2012. Morphotectonics of fissure ridge travertines from geothermal areas of Mammoth Hot Springs (Wyoming) and Bridgeport (California). Tectonophysics, 548-549, 34-38.

De Filippis L., Faccenna C., Billi A., Anzalone E., Brilli M., Özkul M., Soligo M., Tuccimei P., Villa I.M., 2012. Growth of fissure ridge travertines from geothermal springs of Denizli basin, western Turkey. Geological Society of America Bulletin, 124, 1629–1645.

De Filippis L., Faccenna C., Billi A., Anzalone E., Brilli M., Soligo M., Tuccimei P., 2013a. Plateau versus fissure ridge travertines from Quaternary geothermal springs of Italy and Turkey: Interactions and feedbacks between fluid discharge, paleoclimate, and tectonics. Earth-Science Reviews, 123, 35-52.

De Filippis L., Anzalone E., Billi A., Faccenna C., Poncia P.P., Sella P., 2013b. The origin and growth of a recently-active fissure ridge travertine over a seismic fault, Tivoli, Italy. Geomorphology, 195, 13-26.

Dewey J.F., 1988. Extensional collapse of orogens. Tectonics, 7, 1123-1139.

DePaolo D.J., Wasserburg G.J., 1976. Nd isotopic variations and petrogenetic models. Geophysical Research Letters, 3, 249–252.

Diamond L. W., 2003. Systematics of H2O inclusions. In: Samson IM, Anderson AJ, Marshall DD (eds.) Fluid inclusions: analysis and interpretation. Mineralogical Association of Canada, Short Course, 32, 55–80.

Dini A., Granelli G., Puxeddu M., Ruggirei G., 2005. Origin and evolution of Pliocene–Pleistocene granites from the Larderello geothermal field (Tuscan Magmatic Province, Italy). Lithos, 81, 1-31.

Dramis F., Materazzi M., Cilla G., 1999. Influence of climatic changes on freshwater travertine deposition: A new hypothesis. Physics and Chemistry of the Earth, Part A: Solid Earth and Geodesy, 24, 893-897, doi: 1127 10.1016/S1464-1895(99)00132-5.

Ederfield H., Greaves M.J., 1982. The rare-elements in seawater. Nature, 296, 214–219.

Edwards R.L., Chen J.H., Wasserburg, G.J., 1988. ^{238}U–^{234}U–^{230}Th systematics and the precise measurement of time over the last 500,000 years. Earth and Planetary Science Letters, 81, 175–192.

El Desouky H., Soete J., Claes H., Özkul M., Vanhaecke F., Swennen R., 2015. Novel applications of fluid inclusions and isotope geochemistry in unravelling the genesis of fossil travertine systems. Sedimentology, 62, 27-57.

Faccenna C., Soligo M., Billi A., De Filippis L., Funiciello R., Rossetti C., Tuccimei P., 2008. Late Pleistocene depositional cycles of the Lapis Tiburtinus travertine (Tivoli, central Italy): possible influence of climate and fault activity. Global and Planetary Change, 63, 299–308.

Ford T.D., Pedley H.M., 1996. A review of tufa and travertine deposits of the world. Earth-Science Reviews 41, 117–175.

Frank N., Braum M., Hambach U., Mangini A., Wagner G., 2000. Warm period growth of travertine during the last 1150 interglaciation in Southern Germany. Quaternary Research, 54, 38–48. doi:10.1006/qres.2000.2135.

Frery E., 2012. Episodic circulation of reactive fluids along faults. From travertine- to basin-scale based on the Colorado Plateau natural example (USA). PhD Thesis, Université Joseph Fourrier Grenoble (France), 247pp.

Frery E., Gratier J.P., Ellouz-Zimmerman N., Loiselet C., Braun J., Deschamps P., Blamart D., Hamelin B., Swennen R., 2015. Evolution of fault permeability during episodic fluid circulation: Evidence for the effects of fluid–rock interactions from travertine studies (Utah–USA). Tectonophysics, http://dx.doi.org/10.1016/j.tecto.2015.03.018.

Frondini F., Caliro S., Cardellini C., Chiodini G., Morgantini N., Parello F., 2008. Carbon dioxide degassing from Tuscany and Northern Latium (Italy). Global and Planetary Change 61, 89–102.

Gandin A., Capezzuoli E., 2008. Travertine versus Calcareous tufa: distinctive petrologic features and related stable isotopes signature. Il Quaternario Italian Journal of Quaternary Science, 21, 125-136.

Gerlach T., 2011. Volcanic versus anthropogenic carbon dioxide. Eos, 92 no. 24, 201-202.

Gianelli G., Manzella A., Puxeddu M., 1997. Crustal models of southern Tuscany (Italy). Tectonophysics, 281, 221–239.

Gibert R.O., Taberner C., Sáez A., Giralt S., Alonso R.N., Edwards R.L., Pueyo J.J., 2009. Igneous origin of CO_2 in ancient and recent hot-spring waters and travertines from the northern Argentinean Andes. Journal of Sedimentary Research, 79, 554-567.

Goldtsein R.H., Reynolds T.J., 1994. Fluid inclusion microthermometry. In: Systematics of fluid inclusions in diagenetic minerals. Society for Sedimentation Geology, short course 31, 7-121.

Gonfiantini R., Panichi C., Tongiorgi E., 1968. Isotopic disequilibrium in travertine deposition. Earth and Planetary Science Letters, 5, 55-58.

Gradziński M., Wróblewski W., Duliński M., Hercman H., 2014. Earthquake-affected development of a travertine ridge. Sedimentology, 61, 238–263.

Gratier J. P., Frery E., Deschamps P., Røyne A., Renard F., Dysthe D., Ellouz-Zimmerman N., Hamelin B., 2012. How travertine veins grow from top to bottom and lift the rocks above them: the effect of crystallization force. Geology, 40, 1015–1018.

Guastaldi E., Graziano L., Liali G., Nunzio F., Brogna A., Barbagli A., 2014. Intrinsic vulnerability assessment of Saturnia thermal aquifer by means of three parametric methods: SINTACS, GODS and COP. Environmental Earth Sciences, DOI 10.1007/s12665-014-3191-z.

Guo L., Andrews J., Riding R., Dennis P., Dresser, Q., 1996. Possible microbial effects on stable carbon isotopes in hot travertine. Journal of Sedimentary Research, 66, 468-473.

Guo L., Riding R., 1999. Rapid facies changes in Holocene fissure ridge hot spring travertines, Rapolano Terme, Italy. Sedimentology, 46, 1145-1158. doi:10.1046/j.1365-3091.1999.00269.x

Hancock P.L., Chalmers R.M.L., Altunel E., Çakir Z., 1999. Travitonics: using travertine in active fault studies. Journal of Structural Geology, 21, 903–916.

Jolivet L., Faccenna C., Goffé B., Mattei M., Rossetti F., Brunet C., et al., 1998. Midcrustal shear zones in post-orogenic extension: example from the northern Tyrrhenian Sea (Italy). Journal of Geophysical Research, 103, 12123–12160.

Kampman N., Burnside N.M., Shipton Z.K., Chapman H.J., Nicholl J.A., Ellam R.M., Bickle M.J., 2012. Pulses of carbon dioxide emissions from intracrustal faults following climatic warming. Nature Geoscience, 5, 352-358.

Karlstrom K.E., Crossey L.J., Hilton D.R., Barry P.H., 2013.Mantle ^{3}He and CO_2 degassing in carbonic and geothermal springs of Colorado and implications for neotectonics of the Rocky Mountains. Geology, 41, 495-498.

Kele S., Özkul M., Fórizs I., Gökgöz A., Baykara M.O., Alçiçek M.C., Németh T., 2011. Stable isotope geochemical study of Pamukkale travertines: new evidences of lowtemperature non-equilibrium calcite-water fractionation. Sedimentary Geology, 238, 191–212.

Kele S., Breitenbach S.F.M., Capezzuoli E., Meckler A.N., Ziegler M., Millan I.M., Kluge T., Deák J., Hanselmann K., John C., Yan H., Liu Z., Bernasconi S.M., 2015. Temperature dependence of oxygen- and clumped isotope fractionation in carbonates: a study of travertines and tufas in the 6-95°C temperature range. Geochimica et Cosmochimica Acta, 168, 172-192.

Keller J.V.A., Minelli G., Pialli G., 1994. Anatomy of a late orogenic extension: the Northern Apennines case. Tectonophysics, 238, 275–294.

Laurenzi M.A., Braschi E., Casalini M., Conticelli S., 2015. New $^{40}Ar/^{39}Ar$ dating and revision of geochronology of the Monte Amiata Volcano, Central Italy. Italian Journal of Geosciences, 134-2, 255-265.

Liotta D., 1994. Structural features of the Radicofani basin along the Piancastagnaio (Mt. Amiata) - S. Casciano dei Bagni (Mt. Cetona) cross section. Memorie della Società Geologica, Italiana 48, 401–408.

Liotta, D., Ruggieri, G., Brogi, A., Fulignati, P., Dini, A., Cardini, I., 2010. Migration of geothermal fluids in extensional terrains: the ore deposits of the Boccheggiano-Montieri area (southern Tuscany, Italy). International Journal of Earth Sciences, 99, 623–644

Locardi E., Nicolich R., 1988. Geodinamica del Tirreno e dell'Appennino centro-meridionale: la nuova carta della Moho (Geodynamic of the Thyrrenian Sea and of Central-Southern Apennine: the new map of Moho). Memorie della Societa Geologica Italiana, 41, 121–140.

Ludwig K.R., 2003. Isoplot/Ex version 3.00, A Geochronological Toolkit for Microsoft Excel. Berkeley Geochronology Center Special Publication, 4.

Luque J.A. and Julià R., 2007. U/Th dating of Quaternary travertines at the middle River Llobregat (NE Iberian Peninsula, Northwestern Mediterranean). Correlation with sea-level changes. Geologica Acta, 5, 109-117.

Maggi M., Cianfarra P., Salvini F., de Lima C.C., 2015. Staircase fractures in microbialites and the role of lamination-related mechanical anisotropy: the example of the Acquasanta Terme travertine deposits (central Italy). Geological Society of America Bullettin, 127, no. 5-6, 879-896.

Malinverno A., Ryan W., 1986. Extension in the Tyrrhenian sea and shortening in the Apennines as result of arc migration driven by sinking of the lithosphere. Tectonics, 5, 227-245.

Marroni M., Moratti G., Costantini A., Conticelli S., Benvenuti M.G., Pandolfi L., Bonini M., Cornamusini G., Laurenzi M.A., 2015. Geology of the Monte Amiata region, Southern Tuscany, Central Italy. Italian Journal of Geosciences, 134-2, 171-199.

Martelli L., Moratti G., Sani F., 1989. Analisi strutturale dei travertini della Toscana meridionale (Valle dell'Albegna). Bollettino della Società Geologica Italiana, 108, 197-205.

Martini I.P., Sagri M., 1993. Tectono-sedimentary characteristics of Late Miocene –Quaternary extensional basins of the northern Apennines, Italy. Earth Science Reviews, 34, 197 – 233

Massoli D., Koyi H.A., Barchi M.R., 2006. Structural evolution of a fold and thrust belt generated by multiple décollements: Analogue models and natural examples from the Northern Apennines (Italy). Journal of Structural Geology, 28, 185-199.

McLennan S.M., 1989. Rare earth elements in sedimentary rocks. Influence of provenance and sedimentary processes. In: Lipin, B.R., McKay, G.A. (Eds.), Geochemistry and Mineralogy of Rare Earth Elements. Reviews in Mineralogy, 21. Mineralogical Soc. America, Washington, pp. 169–200.

Mesci L.B., Gürsoy H., Tatar O., 2008. The evolution of travertine masses in the Sivas area (central Turkey) and their relationships to active tectonics: Turkish Journal of Earth Sciences, 17, 219–240.

Minissale A., 2004. Origin, transport and discharge of CO2 in central Italy. Earth-Science Reviews, 66, 89-141.

Möller P., Dulsky P., Morteani G., 2003. Partitioning of rare earth elements, yttrium, and some major elements among source rocks, liquid and vapor of Larderello-Travale Geothermal Field, Tuscany (Central Italy). Geochimica et Cosmochimica Acta, 67 (2), 171–183.

Nappi G., A. Renzulli, P. Santi and P.Y. Gillot, 1995. Geological evolution and geochronology of the Vulsini Volcano District (Central Italy). Bollettino della Società Geologica Italiana, 114, 599-613.

Özkul M., Kele S., Gökgöz, A., Shen C.C., Jones B., Baykara M.O., Fórizs I., Nemeth T., Chang Y.-W., Alçiçek M.C., 2013. Comparison of the Quaternary travertine sites in the Denizli Extensional Basin based on their depositional and geochemical data. Sedimentary Geology, 294, 179–204.

Panichi C., Tongiorgi E., 1976. Carbon isotopic composition of CO_2 from springs, fumaroles, mofettes and travertines of central and southern Italy: a preliminary prospection method of geothermal area. Proc. 2nd UN Symposium on the Development and Use of Geothermal Energy. San Francisco, U.S.A, 815–825.

Pascucci V., Costantini A., Martini P.I., Dringoli R., 2006. Tectono-sedimentary analysis of a complex, extensional, Neogene basin formed on thrust-faulted, Northern Apennines hinterland: Radicofani Basin, Italy. Sedimentary Geology, 183, 71–97.

Passchier C.W., Trouw R.A.J., 1996. Microtectonics. Springer Verlag, Berlin.

Patacca E., Sartori R., Scandone P., 1990. Tyrrhenian basin and Apenninic arcs: kinematic relation since late Tortonian times. Memorie della Società Geologica Italiana, 45, 425-451.

Pauselli C., Barchi M.R., Federico C., Magnani B., Minelli G., 2006. The crustal structure of the Northern Apennines (central Italy): an insight by the CROP03 seismic line. American Journal of Science, 306, 428-450.

Peccerillo A., 2003. Plio-Quaternary magmatism in Italy. Episodes, 26, 222-226.

Pentecost A., 1995. The Quaternary travertine deposits of Europe and Asia Minor. Quaternary Science Reviews, 14, 1005–1028.

Pentecost A., 2005. Travertine. Springer-Verlag, Berlin Heidelberg, 445 pp.

Pin C., Zalduegui J.F.S., 1997. Sequential separation of light rare-earth elements, thorium and uranium by miniaturized extraction chromatography: Application to isotopic analyses of silicate rocks. Analytica Chimica Acta, 339, 79-89.

Priewisch A., Crossey L.J., Karlstrom K.E., Polyak V.J., Asmerom Y., Nereson A., Ricketts J.W., 2014. U-series geochronology of large-volume Quaternary travertine deposits of the southeastern Colorado Plateau: Evaluating episodicity and tectonic and paleohydrologic controls. Geosphere, 10, 401-423.

Rimondi V., Costagliola P., Ruggieri G., Benvenuti M., Boschi C., Brogi A., Capezzuoli E., Morelli G., Gasparon M., Liotta D., 2015. Investigating fossil hydrothermal systems by means of fluid inclusions and stable isotopes in banded travertine: an example from Castelnuovo dell'Abate (southern Tuscany, Italy). International Journal of Earth Sciences, 1-21.

Rezende M.F., Pope M.C., 2015. Importance of depositional texture in pore characterization of subsalt microbialite carbonates, offshore Brazil. Geological Society, London, Special Publication, 418, doi:10.1144/SP418.2.

Ricketts J.W., Karlstrom K.E., Priewisch A., Crossey L.J., Polyak V.J., Asmerom Y., 2014. Quaternary extension in the Rio Grande rift at elevated strain rates recorded in travertine deposits, central New Mexico. Lithosphere, 6, 3–16.

Rihs S., Condomines M., Poidevin J.L., 2000. Long-term behaviour of continental hydrothermal systems: U-series study of hydrothermal carbonates from the French Massif Central (Allier Valley). Geochimica et Cosmochimica Acta, 64 (18), 3189-3199.

Roedder E. 1967. Metastable Superheated Ice in Liquid-Water Inclusions under High Negative Pressure. Science, 155, No. 3768, 1413-1417.

Rogie J. D., Kerrick D. M., Chiodini G., Frondini F., 2000. Measurements of non-volcanic CO_2 emission from some vents in central Italy, Journal of Geophysical Research, 105, 8435–8445.

Ronchi P., Cruciani F., 2015. Continental carbonates as a hydrocarbon reservoir, an analog case study from the travertine of Saturnia, Italy. AAPG Bulletin, 99, 711–734.

Rossetti F., Balsamo F., Villa I.M., Bouybaouenne M., Faccenna C., Funiciello R., 2008. Pliocene–Pleistocene HT–LP metamorphism during multiple granitic intrusions in the southern branch of the Larderello geothermal field (southern Tuscany, Italy). Journal of the Geological Society, London, 165, 247-262.

Rossetti F., Aldega L., Tecce F., Balsamo F., Billi A., Brilli M., 2011. Fluid flow within the damage zone of the Boccheggiano extensional fault (Larderello–Travale geothermal field, central Italy): structures, alteration and implications for hydrothermal mineralization in extensional settings. Geological Magazine, 148 (4), 558–578.

Serri G., Innocenti F., Manetti P., 1993. Geochemical and petrological evidence of the subduction of delaminated Adriatic continental lithosphere in the genesis of the Neogene-Quaternary magmatism in central Italy. Tectonophysics, 223, 117– 147.

Serri G., 1997. Neogene–Quaternary magmatic activity and its geodynamic implications in the Central Mediterranean region. Annals of Geophysics, 40, 681–703.

Sharma M. and Wasserburg G.J., 1996. The neodymium isotopic compositions and rare earth patterns in highly depleted ultramafic rocks. Geochimica et Cosmochimica Acta, 60, 4537–4550.

Shen C.-C., Cheng H., Edwards R.L., Moran S.B., Edmonds H.N., Hoff J.A., Thomas R.B., 2003. Measurement of attogram quantities of ^{231}Pa in dissolved and particulate fractions of seawater by isotope dilution thermal ionization mass spectroscopy. Analytical Chemistry, 75, 1075-1079.

Shen C.-C., Wu C.-C., Cheng H., Edwards R.L., Hsieh Y.-T., Gallet S., Chang C.-C., Li T.-Y., Lam D.D., Kano A., Hori M., Spötl C., 2012. High-precision and high resolution carbonate ^{230}Th dating by MC-ICP-MS with SEM protocols. Geochimica et Cosmochimica Acta, 99, 71–86.

Shipton Z.K., Evans J.P., Kirchner D., Kolesar P.T., Williams A.P., Heath J., 2004. Analysis of CO_2 leakage through "low-permeability" faults from natural reservoirs in the Colorado Plateau, southern Utah. Geological Society, London, Special Publications, 233, 43-58.

Shipton Z.K., Evans J.P., Dockrill B., Heath J., Williams A., Kirchner D., Kolesar P.T., 2005. Natural leaking CO_2-charged systems as analogs for failed geologic storage reservoirs. Carbon dioxide capture for storage in deep geological formations, 2, 699-712.

Sibson R. H., 2004. Controls on maximum fluid overpressure defining conditions for mesozonal mineralization. Journal of Structural Geology, 26, 1127–1136

Słowakiewicz M., 2003. Fluid inclusion data from the Upper Triassic hot-spring travertines in southern Poland. Journal of Geochemical Exploration, 78–79, 123-126.

Soligo M., Tuccimei P., Barberi R., Delitala M.C., Miccadei E., Taddeucci A., 2002. U/Th dating of freshwater travertine from Middle Velino Valley (Central Italy): paleoclimatic and geological implications. Palaeogeography, Palaeoclimatology, Palaeoecology, 184, 147-161.

Sturchio, N.C., Pierce, K.L., Murrell, M.T., Sorey, M.L., 1994. Uranium-series ages of travertines and timing of the last glaciation in the northern Yellowstone area, Wyoming– Montana. Quaternary Research, 41, 265–277.

Toker E., Kayseri-Özer M. S., Özkul M., Kele S., 2015. Depositional system and palaeoclimatic interpretations of Middle to Late Pleistocene travertines: Kocabaş, Denizli, south-west Turkey. Sedimentology, 62, 1360-1383.

Turi B., 1986: Stable isotope geochemistry of travertines: chapter 5. In: Fritz, P., Fontes, J.C (Eds.). The Terrestrial Environment, B, Handbook of Environmental Isotope Geochemistry, vol. 2. Elsevier, Amsterdam, pp 207–238.

Tzedakis P.C., Andrieu V., de Beaulieu J.-L., Birks H.J.B., Crowhurst S., Follieri M., Hooghiemstra H., Magri D., Reille M., Sadori L., Shackleton N.J., Wijmstra T.A., 2001. Establishing a terrestrial chronological framework as a basis for biostratigraphical comparisons. Quaternary Science Reviews, 20, 1583-1592.

Uysal I.T., Feng Y., Zhao J.X., Altunel E., Weatherley D., Karabacak V., Cengiz O., Golding S.D., Lawrence M.G., Collerson K.D., 2007. U-series dating and geochemical tracing of late Quaternary travertine in co-seismic fissures: Earth and Planetary Science Letters, 257 (3–4), 450–462.

Uysal I.T., Feng Y., Zhao J.X., Isik V., Nuriel P., Golding S.D., 2009. Hydrotermal CO_2 degassing in seismically active zones during the late Quaternary. Chemical Geology, 265, 442–454.

Vignaroli G., Pinton A., De Benedetti A.A., Giordano G., Rossetti F., Soligo M., Berardi G., 2013. Structural compartmentalisation of a geothermal system, the Torre Alfina field (central Italy). Tectonophysics, 608, 482-498.

Webb G.E., Kamber B.S. , 2000 Rare earth elements in Holocene reefal microbialites: a shallow seawater proxy. Geochimica et Cosmochimica Acta, 64, 1557–1565.

Wedepohl K., 1995. The composition of the continental crust. Geochimica et Cosmochimica Acta, 59, 1217–1239.

Yilmaz T.I., Prosser G., Liotta D., Kruhl J.H., Gilg H.A., 2014. Repeated hydrothermal quartz crystallization and cataclasis in the Bavarian Pfahl shear zone (Germany). Journal of Structural Geology, 68, 158-174

Zanchi A., Tozzi M., 1987. Evoluzione paleogeografica e strutturale recente del bacino del fiume Albegna (Toscana meridionale). Geologica Romana 26, 305–325.

Chapter 4

This chapter consists of a paper submitted to Geological Society of America Bulletin (Billi A., Berardi G., Rossetti F., Vignaroli G., Baykara M.A., Bernasconi S.M., Kele S., Soligo M., De Filippis L., Shen C.C. "Syn-diagenetic non-tectonic buckle folding of thermogene travertines caused by progressive hydrothermal veining"), focusing on thermogene travertine diagenetic processes, that can modify pristine properties of primary deposited travertine.

Syn-diagenetic non-tectonic buckle folding of thermogene travertines caused by progressive hydrothermal veining

Abstract

Two Pleistocene thermogene travertine deposits in the late Miocene-Pleistocene Tuscan extensional-hydrothermal province, central Italy, consist of primary porous beds hosting secondary bed-parallel carbonate veins. The deposits are generally flat-lying, but the veined travertine beds form undulated structures (eventually interpreted as folds) that are up to a few meters-sized and usually confined within the lower-middle section of the studied deposits. Evidence such as the downward growth of vein crystals, flattening and obliteration of pristine pores in the fold thickened hinges, U/Th ages of veins and host rock, domal shape of folds, and O-isotope-deduced parental fluid temperatures shows that the undulated travertines can be interpreted as syn-diagenetic non-tectonic (buckle-)folds. The non-tectonic origin of the studied folds is also supported by the absence of contractional deformation in the adjacent marine-to-continental sediments host extensional basin (the Albegna basin). In the proposed interpretation, the travertine folds were generated by layer-parallel shortening caused by a

laterally-confined volume increase during syn-diagenetic circulation of mineralizing fluids and related incremental veining. Modeling the folds with the Biot-Ramberg's buckling equation, a vein-to-host travertine viscosity ratio between 1.5 and 8 is found, confirming the syn-diagenetic origin of veins and folds. Veining and folding changed some original rock properties such as fabric, porosity, stratigraphic-chronological sequence, and rheology. Those presented are the first records of syn-diagenetic non-tectonic contractional deformations in thermogene travertines. The identification of these structures and related changes of rock properties is relevant for the frequent use of thermogene travertines as proxy in paleoclimate, neotectonic, paleohydrological, paleoseismic, and hydrocarbon or CO_2 reservoir/storage studies. The occurrence of similar structures in other thermogene travertine deposits corroborates the relevance of the presented results.

4.1. Introduction

Recent discoveries of hydrocarbon major reserves in subsalt porous travertine-like rocks along the Atlantic Brazilian and Angolan margins impose a better understanding not only of deposition, but also of diagenetic (porosity vs. cementation) history of these non-marine carbonates (Beasley et al., 2010; Seard et al., 2013; Rezende and Pope, 2015; Ronchi and Cruciani, 2015; Soete et al., 2015). Also, the identification and understanding of travertine diagenetic processes and related changes of rock properties will impact the frequent use of this rock as proxy for paleoclimate, neotectonic, paleoseismic, paleohydrological, and CO_2 storage studies (e.g., Hancock et al., 1999; Rihs et al., 2000; Crossey et al., 2006; Uysal et al., 2007, 2009; Brogi et al., 2012; Kampman et al., 2012; Bickle and Kampman, 2013; Burnside et al., 2013; De Filippis et al., 2013b; Karlstrom et al., 2013; Brogi and Capezzuoli, 2014; Frery et al., 2015; Toker et al., 2015).

In this paper, focusing on thermogene travertine diagenetic processes, we aim at responding to two main questions: what can happen to the freshly deposited porous travertines with a continuous syn-diagenetic supply of mineralizing fluids? Can this supply diagenize the primary travertine modifying some of its original properties such as sedimentary fabric, porosity, stratigraphic-chronological sequence, and rheology?

Using a multidisciplinary approach including structural observations, U/Th geochronology, and stable isotope determinations, we analyze two deposits of Pleistocene thermogene travertine from Tuscany, central Italy (Fig. 4.1). We provide, in particular, the first record of syn-diagenetic non-tectonic contractional deformation in thermogene travertines. The studied structures are compared with others observed in previously studied thermogene travertine deposits. A syn-diagenetic non-tectonic buckling mechanism is proposed for the travertine folding. Eventually, some implications for the use of thermogene travertines in the geosciences are synthetically drawn and commented.

4.2. Geological Setting

The studied deposits are located and excellently exposed in the Pianetti and Pian di Palma quarries within the late Miocene-Pleistocene Albegna extensional basin, southern Tuscany (Figs. 4.1 and 4.2). This latter region is located in the hinterland (west) of the Paleogene-Quaternary northern Apennines fold-thrust belt, which developed through an eastward migration of thrust fronts and foredeep basins in a classical piggy-back sequence of thrust propagation toward the Adriatic foreland (Patacca et al., 1990; Cipollari and Cosentino, 1995; Pauselli et al., 2006).

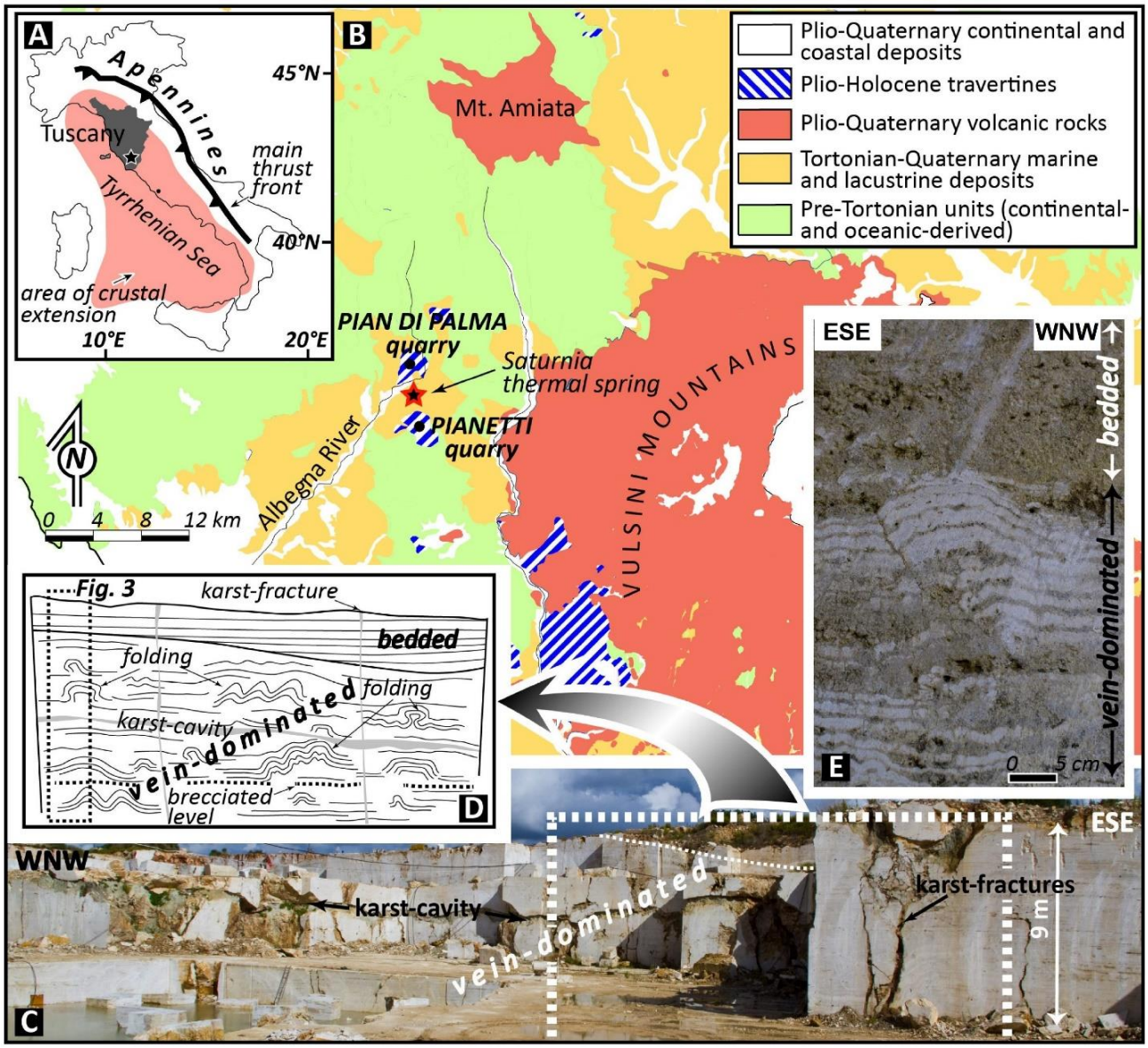

Figure 4.1 - (A) Location of the study area (Albegna basin) in southern Tuscany, Italy. (B) Geological map of the upper Albegna basin, where the studied Pianetti and Pian di Palma travertine deposits are located. Coordinates of the two study quarries are as follows: Pianetti quarry, 42°37'59.69''N, 11°30'39.76''E; Pian di Palma quarry, 42°41'21.11''N, 11°29'52.88''E. (C) Panoramic view of the travertine deposit exposed in the Pianetti quarry. (D) Conceptual sketch of the Pianetti travertine deposit characterized by vein-dominated folded rocks in the lower and intermediate sections and poorly-veined flat rocks (bedded travertine) in the upper section. (E) Photograph from the Pian di Palma quarry showing the transition from vein-dominated folded (below) and non-veined flat host (above) travertines. The Pian di Palma travertine (Fig. 4.2A) is characterized by a depositional architecture very similar (vein-dominated folded and poorly-veined flat travertines) to that drawn for the Pianetti travertine in (D).

The Neogene-Quaternary extensional tectonics in Tuscany is connected with the opening of the adjacent Tyrrhenian basin and with post-orogenic stretching mechanisms acting at the rear (west) of the eastward migrating compressional front (Malinverno and Ryan, 1986; Doglioni, 1991; Carmignani et al., 1994; Jolivet et al., 1998; Collettini et al., 2006). In the study region, these tectonic processes led to the formation of extensional basins usually controlled by NW-striking extensional faults and laterally bounded by perpendicular transfer zones (Acocella and Funiciello, 2006). The post-orogenic stretching mechanisms originated also wide magmatic provinces of late Miocene-Quaternary age all along the Tyrrhenian margin including Tuscany (Peccerillo, 2003; Conticelli et al., 2015 Rossetti et al., 2007), where endogenic fluid circulation up to the surface occurred and still occurs, in places, mainly along active extensional faults and associated damage zones (Brogi, 2008; Liotta et al., 2010; Billi et al., 2007; Rossetti et al., 2008, 2011; Brogi et al., 2012; 2015; Vignaroli et al., 2015).

In southern Tuscany and nearby peri-Tyrrhenian regions, active and fossil Quaternary travertine deposits occur with variable size and shape often in proximity of the main volcanic districts (e.g., Faccenna et al., 2008; Rimondi et al., 2015). For instance, the fossil travertine deposits studied in this paper are located in the Albegna basin in the peri-volcanic rings of the middle-late Pleistocene Amiata and Vulsini volcanic districts (Nappi et al., 1995; Cadoux and Pinti, 2009; Carmignani et al., 2013; Laurenzi et al., 2015; Marroni et al., 2015). The Albegna basin is a NE-SW-trending tectonic depression filled by late Miocene to Quaternary marine and transitional sediments consisting of clays,

sands, gravels, and conglomerates covered by aeolian sands and fluvial clays and silts. The basin formed under the control of main NE-SW-striking extensional and transtensional faults. No contractional deformations are observed in this basin at least in the youngest portion (Pliocene-Quaternary) of the basin-filling sediments. The Pianetti and Pian di Palma travertine deposits, which are studied in this paper, unconformably lie on top of and are hosted by the Neogene-Quaternary sediments of the Albegna basin (Zanchi and Tozzi, 1987; Bosi et al., 1996; Bossio et al., 2003; Carmignani et al., 2013).

4.3. Structures

The Pianetti and Pian di Palma quarries (Figs. 4.1 and 4.2) host large exposures of travertine for a maximum depth of 25-30 m and horizontal length up to 200 m. In both quarries, we recognized two main types of chemical carbonate rock (Figs. 4.1D, 4.1E, 4.2, and Data Repository): (1) primary (host) porous bedded travertine and (2) secondary sparry veins. In these rocks, Ronchi and Cruciani (2015) measured bulk porosities between less than 3% and ~35% without distinguishing between veins and host travertine.

The main observed structures are shown in Figs. 4.1 and 4.2; however, the investigated quarries are characterized by exposures of a large number of veins and folds at different scales within the studied travertine beds. A thorough documentation of these structures is the first step to properly interpret them. All these structures cannot be photographically documented in the main article and are therefore shown in a photographic atlas with 40 panels in the Data Repository (Figs. DR1-DR40).

Veins usually form bed-parallel banded patterns, but, more often, are arranged to form complex undulated structures (Figs. 4.1E, 4.2, and Data Repository), which we will eventually interpret as folds. The folds are numerous and restricted to the lower and middle portions of the investigated exposures, whereas no or very rare folds occur in the shallowest portion (Figs. 4.1D and 4.2A). Folds are between about 1 cm and less than 10 m in wavelength and are made of undulated veins or veins

alternated with bedded travertine (Fig. 4.2 and Data Repository). We synthesize as follows the main field and microscopic observations made on these undulated structures (folds) to understand their origin: (1) folds overprint and deform originally flat travertine beds with shape as diverse as those of chimney-like, convolute, chevron, and thrust-related structures. (Figs. 4.1E, 4.2B, and Data Repository); (2) the vein crystals are frequently characterized by a downward radiating pattern, indicating that they grew from a pre-existing top travertine bed toward the bottom bed (Figs. 4.2F and Data Repository); (3) the vein crystals usually tend to invade (cut through) the pre-existing overlying or underlying bedded travertine (Figs. 4.2F, 4.2G, and Data Repository); (4) the folded veins and travertine beds are often associated with axial-planar foliations and small-scale (parasitic) folds.

Figure 4.2 – (next page) Photographs of bedded travertine and veins either flat or folded from the Pianetti and Pian di Palma quarries. (A) Panoramic view of the travertine deposit exposed in the Pian di Palma quarry. (B) Chimney-like folded veins across bedded travertine (Pian di Palma). (C) Flattening of original travertine pores in fold thickened hinges (Pianetti). (D) Travertine pore flattening and bed upward dragging across the transition between flat bedded travertine and folded veins (Pian di Palma). (E) Travertine bed and vein upward dragging along the upright limb of an antiformal fold (Pianetti). (F) Downward growth of vein crystals (Pianetti). (G) Vein crystals upward invading the overlying travertine beds (Pianetti). (H) and (I) Fan-patterned foliations and small parasitic folds across a large antiformal fold (Pianetti). (J) Thickening of fold hinge and small parasitic folds along fold limbs (Pianetti). (K) Bird's eye view of chimney-like folded veins that are laterally confined by porous bedded travertine (Pian di Palma). The 2D rounded shape of folds in this photograph suggests a 3D domal shape. (L) and (M) Flattening and obliteration of original travertine pores in fold thickened hinges (Pianetti). (N) Flat and folded (buckled) veins. Note the occurrence of voids at the cores of folds right at the transition between flat and folded veins (Pian di Palma).

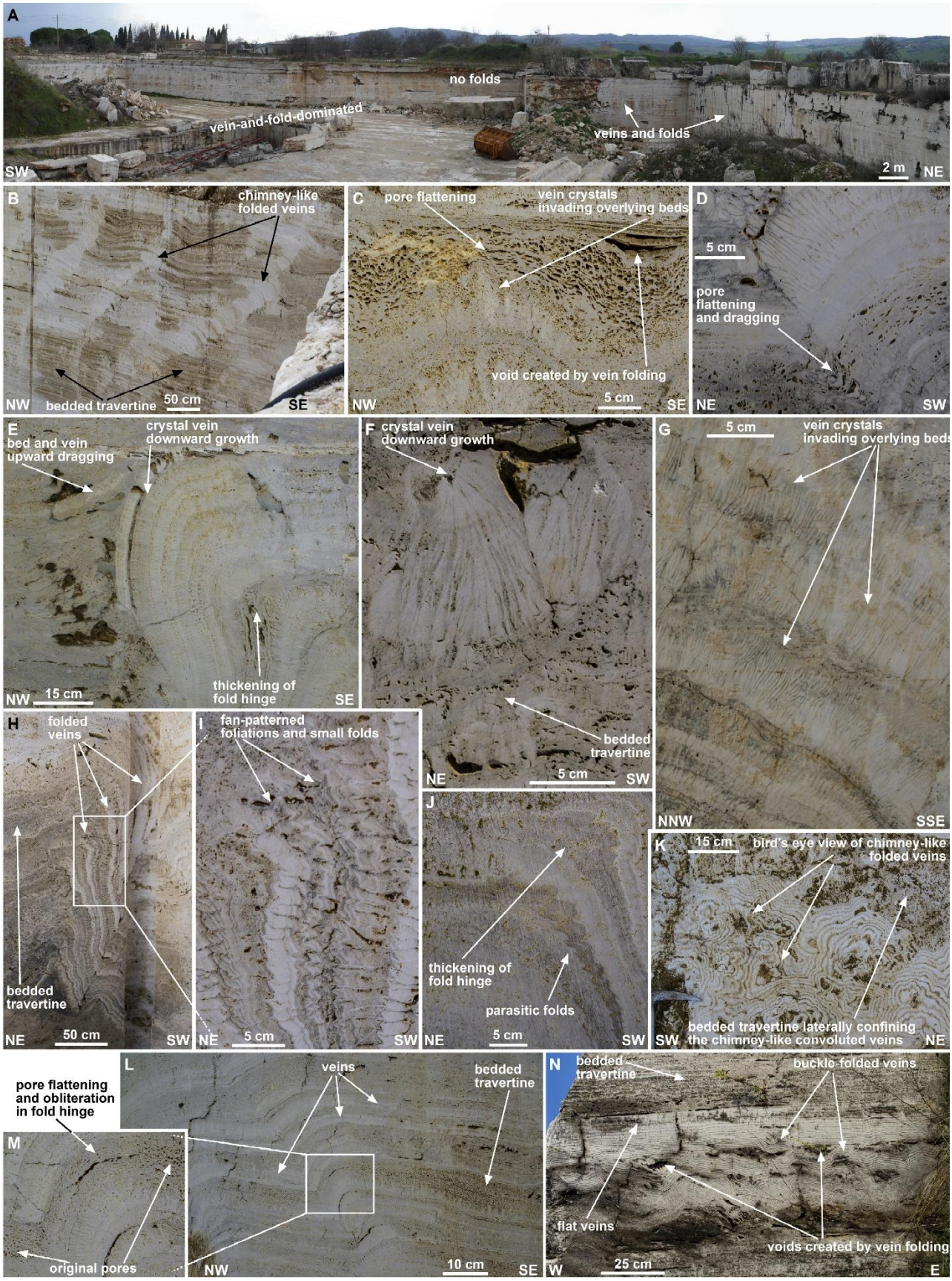
A
no folds
vein-and-fold-dominated
veins and folds
SW
2 m
NE
B
chimney-like folded veins
NW
bedded travertine
50 cm
SE
C
pore flattening
vein crystals invading overlying beds
void created by vein folding
NW
5 cm
SE
D
5 cm
pore flattening and dragging
NE
SW
E
bed and vein upward dragging
crystal vein downward growth
thickening of fold hinge
NW
15 cm
SE
F
crystal vein downward growth
bedded travertine
NE
5 cm
SW
G
5 cm
vein crystals invading overlying beds
NNW
SSE
H
folded veins
bedded travertine
NE
50 cm
SW
I
fan-patterned foliations and small folds
NE
5 cm
SW
J
thickening of fold hinge
parasitic folds
NE
5 cm
SW
K
15 cm
bird's eye view of chimney-like folded veins
bedded travertine laterally confining the chimney-like convoluted veins
SW
NE
pore flattening and obliteration in fold hinge
M
original pores
L
veins
bedded travertine
NW
10 cm
SE
N
bedded travertine
buckle-folded veins
flat veins
voids created by vein folding
W
25 cm
E

The foliation fans across the folded layers so that it tends to remain perpendicular to the fold limbs (Figs. 4.2H, 4.2I, 4.2J, and Data Repository); (5) the pristine subcircular pores typical of the bedded travertine appear as flattened, squeezed, dragged, or totally obliterated when approaching the fold hinges and the veins (Figs. 4.2C, 4.2D, 4.2E, 4.2L, 4.2M, and Data Repository); (6) the folds are usually characterized by hinge thickening as compared with the limbs (Figs. 4.2H and Data Repository); (7) when observed on subhorizontal natural pavements, the folds are not elongate and cylindrical but sub-circular, suggesting a 3D domal shape (Figs. 4.2K); and (8) when the vein arrays contain both flat and undulated veins, voids occur at the contact between these two types of veins, specifically in the cores of folds or undulations (Figs. 4.2C and 4.2N).

4.4. Geochronology

4.4.1. Method

To understand the temporal relationship between veins, folds, and host travertine, we performed a set of U/Th geochronological determinations on 11 samples (Table 4.1). As reported in Table DR4.1, we performed U/Th dating analyses using two alternative different methods, namely: (1) through α spectrometry performed at the Laboratorio di Geochimica Ambientale e Isotopica of Roma Tre University, Italy (Soligo et al., 2002), or (2) through a Thermo Electron Neptune multi-collector inductively coupled mass spectrometer (MC-ICP-MS; Shen et al., 2012) hosted at the High-Precision Mass Spectrometry and Environment Change Laboratory (HISPEC) of the National Taiwan University, Taipei, Taiwan ROC.

For MC-ICP-MS dating, we covered about 0.1 g of each sample with H_2O and dissolved it gradually with double distilled 14N HNO_3. After dissolution, we added a ^{229}Th-^{233}U-^{236}U spike (Shen et al., 2003) to the sample, followed by 10-20 drops of $HClO_4$ to clear the organic matter. We then followed the chemical procedure described in Shen et al. (2003) for the separation of Uranium and Thorium. We calculated the age correction using an estimated atomic ^{230}Th/^{232}Th ratio of 4 ± 2 ppm.

These latter values are the ones typical for a material at secular equilibrium with the crustal $^{232}Th/^{238}U$ value of 3.8. We arbitrarily assumed a 50% error.

For α spectrometry dating, we dissolved about 60 g of each sample in 7N HNO_3 and filtered the solution to separate the leachates from the insoluble residue. We heated the leachate at 200 °C after adding a few milliliters of hydrogen peroxide to clear the organic matter, and then spiked the solution with a ^{228}Th-^{232}U tracer. We extracted the isotopic complexes of U and Th following the procedure described in Edwards et al. (1987) and then analyzed the solution by an alpha-counter using high-resolution ion-implanted Ortec silicon-surface barrier detectors. Due to the presence of non-radiogenic ^{230}Th related to detrital ^{232}Th, ages obtained for samples with a $^{230}Th/^{232}Th$ activity ratio less than or equal to 80 required a proper correction, which we performed assuming that all the detrital Th had an average $^{230}Th/^{232}Th$ activity ratio of 0.85 ± 0.36 (Wedepohl, 1995). We then calculated the ages using ISOPLOT, a plotting and regression program for radiogenic-isotope data (Ludwig, 2003).

4.4.2. Results

Results from our radiometric analyses are reported in Table 4.1 and synthesized in the stratigraphic column of Fig. 4.3. We mainly dated vein samples (8 out of 11 samples) as they usually provide results more accurate and reliable than bedded travertines (Uysal et al., 2007, 2009; De Filippis et al., 2013b). Yet, we carefully selected two samples of bedded travertine (ST4 and CP14_25) so to obtain reliable results also from this type of rock. Results (Fig. 4.3) show a general bottom-up younging series between about 368 and 107 ka (CP14_5 and ST4 samples, respectively). The oldest sample (CP14_5 = 368±14 ka), in particular, comes from a vein, hence indicating that the host travertine at the same stratigraphic level should be older than 368±14 ka. A speleothem sampled within an intra-travertine karst cavity (Fig. 4.3) and dated at about 15 ka (ST1_sp1) indicates that the travertine deposit was undergoing weathering at that time. We noted that at least four dated vein samples do not respect the law of stratigraphic superposition, namely ST3, ST1, CP14_2, and

CP15_8. Each of these latter samples are younger than at least one overlying dated sample (either vein or host travertine) as shown in Fig. 4.3.

Table 4.1 - U/Th radiometric age of travertine samples from the Pianetti quarry (Fig. 4.3). Complete results are in Table DR1.

Sample	Rock Type	Age (ka)
ST4	bedded travertine	107 ± 15
ST3	vein	90 ± 11
CP13_1-5	vein	163 ± 19
CP13_1-4	vein	169 ± 14
ST1_sp1	speleothem	15 ± 6
ST1	vein	130 ± 23
CP14_25	bedded travertine	274 ± 6
CP14_5	vein	368 ± 14
CP14_2	vein	269 ± 5
CP15_1	vein	332 ± 9
CP15_8	vein	238 ± 2

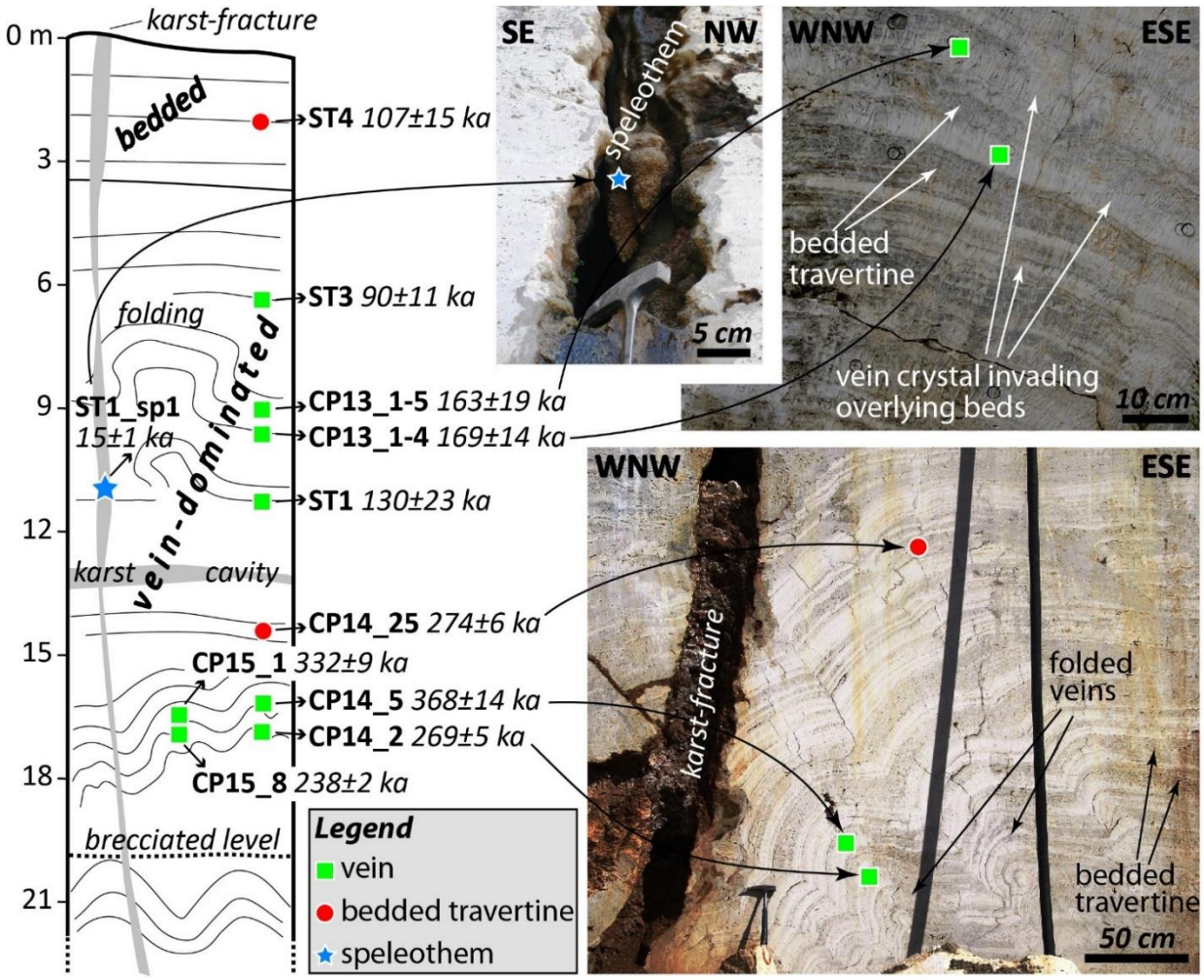

Figure 4.3 - Synthesis and stratigraphy of radiometric dating results for the Pianetti travertine samples. Complete results are in Tables 1 and DR1.

4.5. Stable Isotopes

4.5.1. Method

To investigate the origin of the studied travertines, understand the differences between primary travertines (bedded porous travertines) and hosted veins, and calculate the temperature of the mineralizing parental CO_2-rich fluids (e.g., Crossey et al., 2006, 2009; Uysal et al., 2007, 2009; Demeny et al., 2010; Kele et al., 2011, 2015; Karlstrom et al., 2013; Frery et al., 2015), we analyzed C- and O-isotopes ($\delta^{13}C$ and $\delta^{18}O$) from 61 samples collected in the Pianetti quarry and from 18 samples collected in the Pian di Palma quarry (Table 4.2 and Figs. 4.4, 4.5, DR41, and DR42). The samples, in particular, come from the folded veins and related host bedded travertines for a total of seven analyzed structures (veins or folded veins and host bedded travertine), namely five structures in the Pianetti quarry (Fig. DR41) and two structures in the Pian di Palma quarry (Fig. DR42).

We measured the isotopic composition of carbonate samples following the method described in detail in Breitenbach and Bernasconi (2011). Briefly, we filled approximately 100 µg of powder in 12 ml Exetainers (Labco, High Wycombe, UK) and flushed it with pure Helium. The samples were then reacted with 3-5 drops of 100% phosphoric acid at 70°C with a ThermoFisher GasBench device connected to a ThermoFisher Delta V mass spectrometer. The average long term reproducibility of the measurements based on replicated standards is better than 0.1‰. The instrument is calibrated with the international standards NBS19 ($\delta^{13}C$= 1.95 and $\delta^{18}O$= -2.2‰) and NBS18 ($\delta^{13}C$= -5.01 and $\delta^{18}O$ = -23.01‰). The isotope values (Table 2) are reported in the conventional delta notation with respect to V-PDB (Vienna Pee Dee Belemnite) or, in the case of $\delta^{18}O$, also with respect to V-SMOW (Vienna Standard Mean Ocean Water).

We calculated the mineralizing fluid temperatures using the equation of Kele et al. (2015) specifically developed for travertines. This empirical equation is expressed as:

$$1000 \ln \alpha_{(calcite\text{-}water)} = (20 \pm 2)\ 1000/T - (36 \pm 7) \qquad (1)$$

where $\alpha_{(calcite\text{-}water)} = (\delta^{18}O_{calcite} + 1000) / (\delta^{18}O_{water} + 1000)$, and T is the temperature of the mineralizing CO_2-rich fluids expressed in K, whereas $\delta^{18}O_{calcite}$ and $\delta^{18}O_{water}$ are expressed in parts ‰ relative to V-SMOW. As benchmark, we used the present $\delta^{18}O$ isotopic value from the Saturnia Spring hydrothermal waters (-6.4‰ V-SMOW), where thermogene travertines are being actively precipitated in a locality that is between the Pianetti (1.7 km distant) and Pian di Palma (5 km distant) quarries (Fig. 4.1).

4.5.2. Results

$\delta^{13}C$ values are positive for all analyzed samples (bedded travertine and veins), spanning between 5.0 and 6.5‰ (V-PDB) for the Pianetti samples and between 5.8 and 7.4‰ (V-PDB) for the Pian di Palma samples. $\delta^{18}O$ values span between -8.9 and -6.1‰ (V-PDB) for the Pianetti samples and between -6.0 and -5.1‰ (V-PDB) for the Pian di Palma samples (Table 4.2 and Fig. 4.4). $\delta^{13}C$ and $\delta^{18}O$ values are all consistent with a general thermogene origin of the analyzed travertines and veins (Pentecost, 2005) and with the C- and O-isotope range typical of thermogene travertines deposited by numerous fossil (Pleistocene-Holocene) and active thermal springs in Tuscany and central Italy (Manfra et al., 1976; Gandin and Capezzuoli, 2008; De Filippis et al., 2013b). In the $\delta^{13}C$ vs. $\delta^{18}O$ diagrams (Fig. 4.4), we observe that the bedded travertines are generally characterized by $\delta^{18}O$ values slightly more negative than the veins. This pattern is connected with parental fluid temperatures (as calculated from Equation 1) for the bedded travertine slightly warmer than the parental fluid temperatures for the veins at the time of $CaCO_3$ precipitation. In particular, the difference between the fluid temperatures of bedded travertines (average temperatures of 35.4 and 24.5 °C for the Pianetti and Pian di Palma bedded travertines, respectively) and veins (average temperatures of 33.2 and 22.3 °C for the Pianetti and Pian di Palma veins, respectively) ranges between 1.1 and 3.0 °C and is

on average 2.2 °C for both the Pianetti and the Pian di Palma samples (Table 4.2). The total data of parental fluid temperatures against $\delta^{18}O$ values (V-SMOW) are plotted in Figs. 4.5(A) and 4.5(B) for the Pianetti and Pian di Palma samples, respectively. The same data divided for each of the seven analyzed structures in the two quarries are shown in Figs. DR41 and DR42.

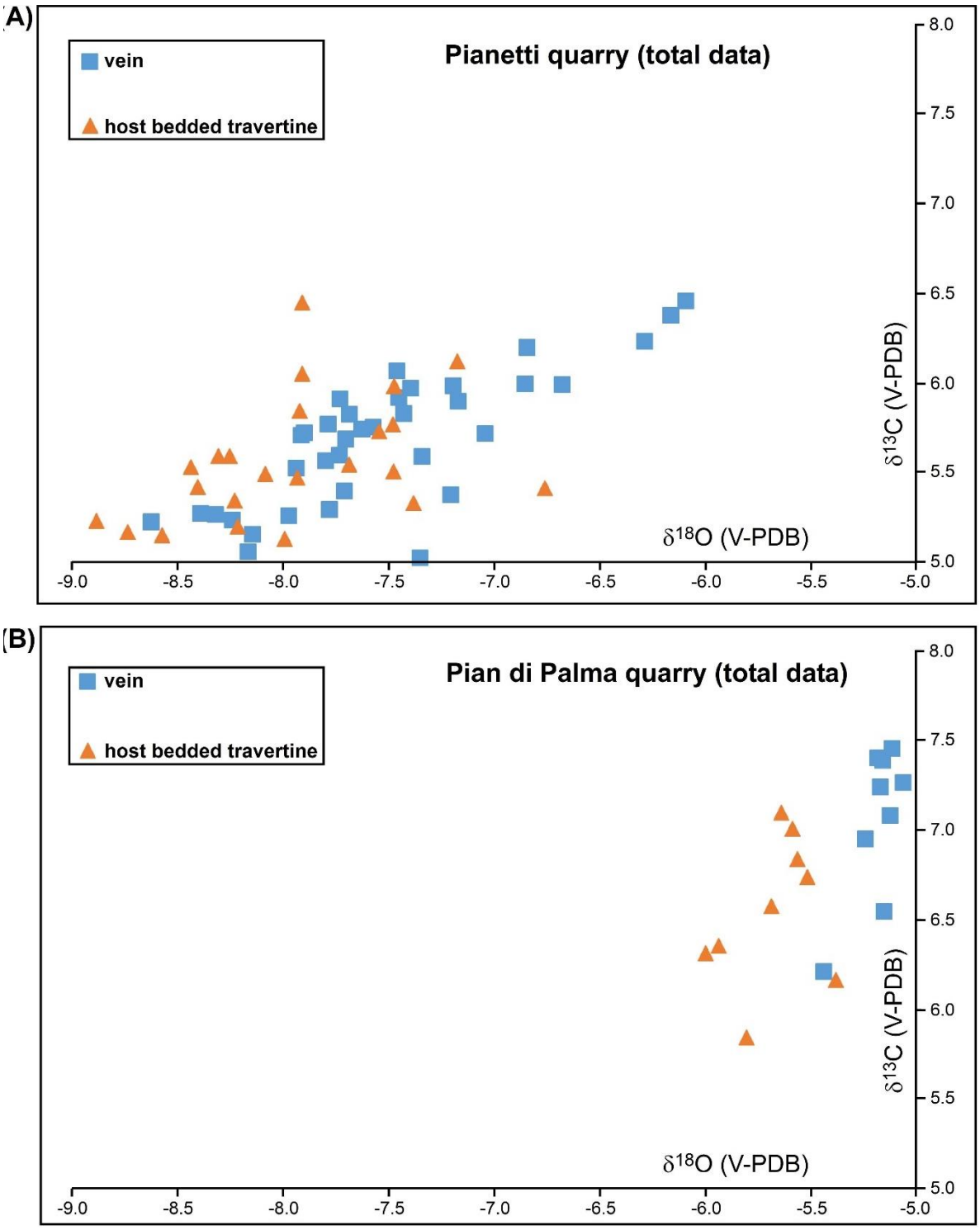

Figure 4.4 - C- vs. O-isotope ($\delta^{13}C$ vs.$\delta^{18}O$) diagrams for samples from the (A) Pianetti and (B) Pian di Palma quarries.

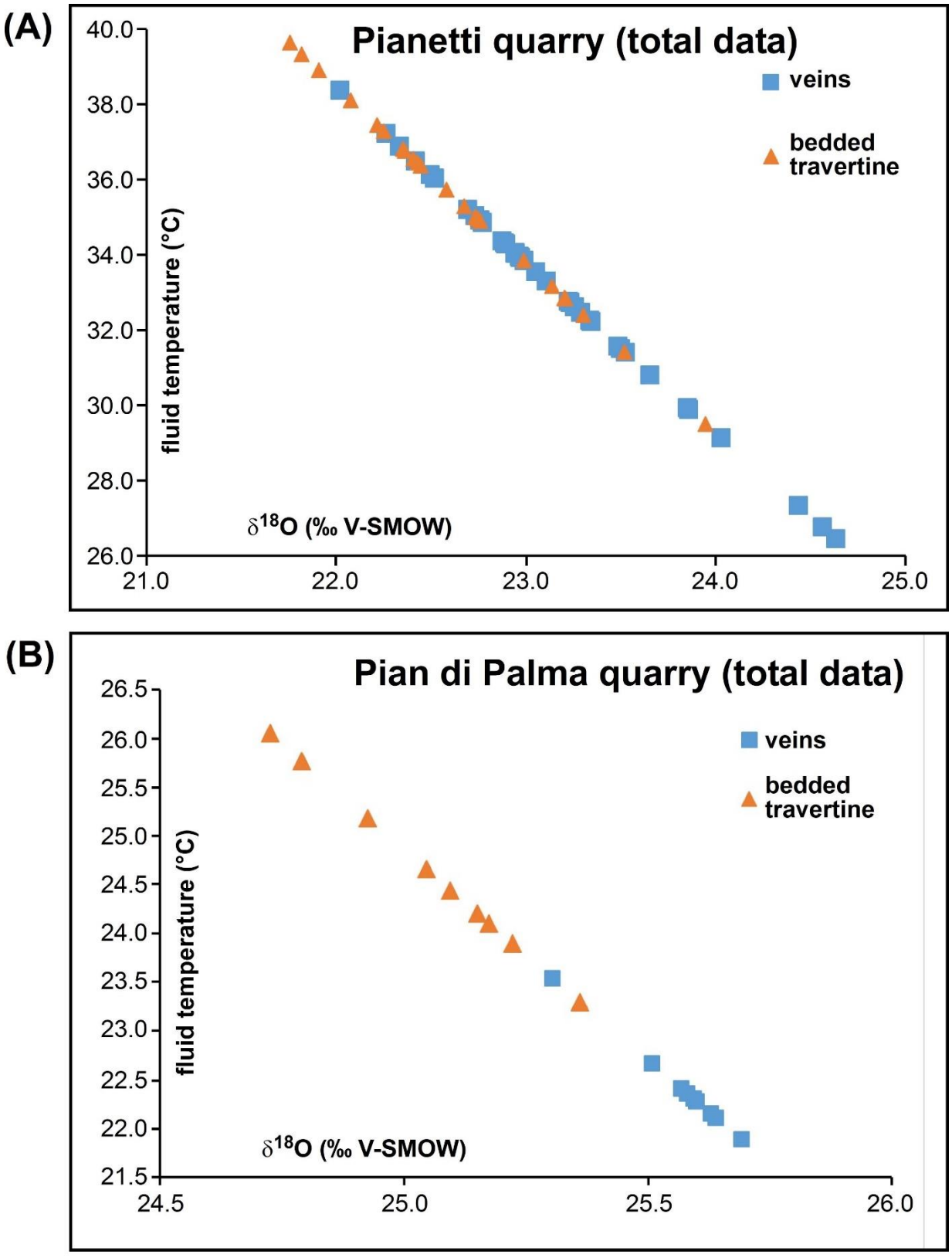

Figure 4.5 - Parental fluid temperature vs. O-isotope($\delta^{18}O$) diagrams for samples from the (A) Pianetti and (B) Pian di Palma quarries. Data are in Table 4.2. Parental fluid temperatures were calculated using the equation of Kele et al. (2015).

Table 4.2 - C- and O-isotope data ($\delta^{13}C$ and $\delta^{18}O$) for travertine samples (veins and host bedded travertine) from the Pianetti and Pian di Palma quarries. The parental fluid temperatures were calculated using the equation of Kele et al. (2015).

Sample	Locality (quarry)	Rock Type	$\delta^{13}C$ (‰ V-PDB)	$\delta^{18}O$ (‰ V-PDB)	$\delta^{18}O$ (‰ V-SMOW)	$T_{calculated}$ (°C)
CP 13-1-1	Pianetti	vein	6.5	-6.1	24.6	26 ± 1
CP 13-1-2	Pianetti	vein	6.2	-6.3	24.4	27 ± 1
CP 13-1-3	Pianetti	vein	6.4	-6.2	24.6	27 ± 1
CP 13-1-4	Pianetti	vein	6.2	-6.8	23.9	30 ± 2
CP 13-1-5	Pianetti	vein	6.0	-7.2	23.5	32 ± 2
CP 13-1-6	Pianetti	bedded travertine	6.1	-7.2	23.5	31 ± 2
CP 13-1-7	Pianetti	vein	6.0	-7.4	23.3	32 ± 2
CP 14-1	Pianetti	vein	5.1	-8.2	22.5	36 ± 2
CP 14-2	Pianetti	vein	5.2	-8.2	22.4	36 ± 2
CP 14-3	Pianetti	vein	5.2	-8.1	22.5	36 ± 2
CP 14-4	Pianetti	vein	5.8	-7.6	23.1	33 ± 2
CP 14-5	Pianetti	vein	5.7	-7.7	23.0	34 ± 2
CP 14-11	Pianetti	bedded travertine	5.4	-6.8	24.0	30 ± 2
CP 14-12	Pianetti	bedded travertine	5.5	-8.1	22.6	36 ± 2
CP 14-13	Pianetti	bedded travertine	5.8	-7.5	23.2	33 ± 2
CP 14-14	Pianetti	bedded travertine	5.5	-7.7	23.0	34 ± 2
CP 14-16	Pianetti	vein	5.6	-7.8	22.9	34 ± 2
CP 14-17	Pianetti	vein	5.7	-7.9	22.8	35 ± 2
CP 14-18	Pianetti	vein	5.8	-7.4	23.3	33 ± 2
CP 14-19	Pianetti	vein	5.9	-7.2	23.5	31 ± 2
CP 14-20	Pianetti	vein	5.7	-7.6	23.1	34 ± 2
CP 14-21	Pianetti	bedded travertine	5.2	-8.9	21.8	40 ± 3
CP 14-22	Pianetti	vein	5.9	-7.5	23.2	33 ± 2
CP 14-23	Pianetti	vein	5.6	-7.3	23.3	32 ± 2
CP 14-24	Pianetti	vein	6.0	-6.7	24.0	29 ± 1
CP 14-25	Pianetti	bedded travertine	5.5	-7.9	22.7	35 ± 2

CP 15-1	Pianetti	vein	5.3	-8.4	22.3	37 ± 2
CP 15-2	Pianetti	vein	5.3	-8.0	22.7	35 ± 2
CP 15-3	Pianetti	vein	5.3	-8.3	22.3	37 ± 2
CP 15-4	Pianetti	vein	5.6	-7.7	22.9	34 ± 2
CP 15-5	Pianetti	vein	5.2	-8.6	22.0	38 ± 3
CP 15-6	Pianetti	bedded travertine	5.0	-8.8	21.8	39 ± 3
CP 15-7	Pianetti	bedded travertine	5.2	-8.6	22.1	38 ± 3
CP 15-8	Pianetti	vein	5.2	-8.7	21.9	39 ± 3
CP V	Pianetti	vein	5.5	-7.9	22.7	35 ± 2
CP 16-01	Pianetti	bedded travertine	5.2	-8.2	22.4	36 ± 2
CP 16-02	Pianetti	vein	6.0	-6.9	23.9	30 ± 2
CP 16-03	Pianetti	vein	5.4	-7.2	23.5	32 ± 2
CP 16-04	Pianetti	bedded travertine	5.3	-8.2	22.4	36 ± 2
CP 16-05	Pianetti	vein	5.0	-7.4	23.3	32 ± 2
CP 16-07	Pianetti	vein	5.4	-7.7	23.0	34 ± 2
CP 16-08	Pianetti	bedded travertine	5.0	-8.3	22.4	37 ± 2
CP 16-09	Pianetti	bedded travertine	5.5	-7.5	23.2	33 ± 2
CP 16-10	Pianetti	vein	5.7	-7.0	23.7	31 ± 2
CP 16-11	Pianetti	vein	5.3	-7.8	22.9	34 ± 2
CP 16-12	Pianetti	bedded travertine	5.7	-7.5	23.1	33 ± 2
CP 17-01	Pianetti	vein	5.8	-7.7	23.0	34 ± 2
CP 17-02	Pianetti	vein	5.7	-7.9	22.8	35 ± 2
CP 17-03	Pianetti	vein	5.9	-7.7	22.9	34 ± 2
CP 17-04	Pianetti	vein	5.8	-7.8	22.9	34 ± 2
CP 17-05	Pianetti	vein	6.1	-7.5	23.2	32 ± 2
CP 17-06	Pianetti	bedded travertine	5.6	-8.3	22.4	37 ± 2
CP 17-07	Pianetti	bedded travertine	5.6	-8.3	22.4	37 ± 2
CP 17-08	Pianetti	bedded travertine	5.5	-8.4	22.2	37 ± 2
CP 17-09	Pianetti	bedded travertine	5.4	-8.4	22.3	37 ± 2

CP 18-01	Pianetti	bedded travertine	6.5	-7.9	22.8	35 ± 2
CP 18-02	Pianetti	bedded travertine	5.1	-8.0	22.7	35 ± 2
CP 18-03	Pianetti	bedded travertine	6.1	-7.9	22.8	35 ± 2
CP 18-04	Pianetti	bedded travertine	5.8	-7.9	22.7	35 ± 2
CP 18-05	Pianetti	bedded travertine	5.3	-7.4	23.3	32 ± 2
CP 18-06	Pianetti	bedded travertine	6.0	-7.5	23.2	33 ± 2
USI 13-1-1	Pian di Palma	vein	7.4	-5.2	25.6	22 ± 1
USI 13-1-2	Pian di Palma	vein	7.4	-5.2	25.6	22 ± 1
USI 13-1-3	Pian di Palma	bedded travertine	5.8	-5.8	24.9	25 ± 1
USI 13-1-4	Pian di Palma	vein	6.2	-5.4	25.3	24 ± 1
USI 13-1-5	Pian di Palma	bedded travertine	6.2	-5.4	25.4	23 ± 1
USI 13-1-6	Pian di Palma	vein	7.1	-5.1	25.6	22 ± 1
USI 13-1-7	Pian di Palma	bedded travertine	6.8	-5.6	25.2	24 ± 1
USI 13-1-8	Pian di Palma	bedded travertine	7.1	-5.6	25.1	24 ± 1
USI 13-1-9	Pian di Palma	bedded travertine	6.6	-5.7	25.1	25 ± 1
USI 13-2-1	Pian di Palma	bedded travertine	7.2	-5.2	25.6	22 ± 1
USI 13-2-2	Pian di Palma	vein	6.9	-5.2	25.5	23 ± 1
USI 13-2-3	Pian di Palma	vein	7.3	-5.1	25.7	22 ± 1
USI 13-2-4	Pian di Palma	bedded travertine	6.7	-5.5	25.2	24 ± 1
USI 13-2-5	Pian di Palma	bedded travertine	7.0	-5.6	25.2	24 ± 1
USI 13-2-6	Pian di Palma	vein	7.4	-5.1	25.6	22 ± 1
USI 13-2-7	Pian di Palma	vein	6.5	-5.2	25.6	22 ± 1
USI 13-2-8	Pian di Palma	bedded travertine	6.3	-6.0	24.7	26 ± 1
USI 13-2-9	Pian di Palma	bedded travertine	6.4	-5.9	24.8	26 ± 1

4.6. Discussion

4.6.1. Comparison with Travertine Structures from Elsewhere

Before discussing our results and proposing a model for the development of the observed travertine structures, it is worth understanding whether these structures are unique or otherwise similar ones exist elsewhere (De Filippis et al., 2012 and references therein). Analogously to the Pianetti and Pian di Palma deposits, primary porous travertine beds and secondary (banded) veins have been frequently recognized in thermogene travertines elsewhere. In particular, thick banded veins often cut through the axial portion of fissure ridge travertines (Bargar, 1978; Hancock et al., 1999; Brogi and Capezzuoli, 2009; De Filippis and Billi, 2012). From these axial veins, lateral ramifications often depart and develop along the host travertine beds in a sill-like fashion, lifting up the overlying beds and forming, in places, (gently) arched structures (Figs. 4.6A-4.6E; Uysal et al., 2009; De Filippis et al., 2012, 2013a; Gratier et al., 2012). Most of these instances, which are observed in travertine deposits from Denizli (Turkey), Tivoli (Italy), Crystal Geyser (Utah), Bridgeport (California), and elsewhere, have been interpreted as post-depositional veining processes occurred in shallow environments (a few meters or few tens of meters depth) possibly on occasions of seismic events (Uysal et al., 2007, 2009), with the vein uplifting the overlying beds thanks to the crystallization force induced by incremental veining rather than crack-and-seal mechanisms (Gratier et al., 2012). Although these veins can form arched structures (Fig. 4.6), they appear as substantially different from the undulated veins studied in the Pianetti and Pian di Palma deposits, where, in contrast to single (banded) or discrete veins observed in previously-studied travertines (Figs. 4.6A-4.6E), veins are much more pervasive and, in places, hard to distinguish from the host porous travertine, which is usually deeply overprinted by veins and diffuse mineralization (compare Fig. 4.2 with Figs. 4.6A-6E). However, it is also interesting to observe that Özkul et al. (2013) showed a specimen of travertine from Denizli (Turkey) with a complex array of veins (Fig. 4.6F). Some of these veins are undulated at the centimetric scale similarly to many veins observed in the Pianetti and

Pian di Palma travertines. Also, during a recent field survey in the Tivoli travertine quarries (central Italy; Faccenna et al., 2008; De Filippis et al., 2013b), two of us (AB and LDF) observed undulated bed-parallel veins hosted within the late Pleistocene Tivoli travertine beds. These veins are shown in Figs. 4.6G-4.6I, where they appear as very similar to those observed in the Pianetti and Pian di Palma deposits (Fig. 4.2 and Data Repository). This evidence let us think that veins and undulated structures such as those from the Pianetti and Pian di Palma deposits may be common to other thermogene travertine deposits such as the Tivoli and Denizli travertines. To this end, it is interesting to mention that the large thermogene deposit of travertine in the Tivoli area is characterized by an uppermost deposit of a very porous travertine locally named testina (Faccenna et al., 2008; De Filippis et al., 2013a, 2013b). The testina travertine is a few meters thick and contrasts with the underlying travertine that is very compact and far less porous. Manfra et al. (1976), based on chemical and isotopic analyses on the testina and the underlying travertines, concluded that the testina porous layer may represent a pristine poorly- to non-diagenized travertine with respect to the diagenized underlying compact deposit.

Eventually, it is important to mention that, in many evaporitic environments, undulated veins similar to those observed in the Pianetti and Pian di Palma travertines are common in veins of gypsum, anhydrite, halite, and also carbonate. These folds form in syn-diagenetic non-tectonic environments thanks to a volume increase (veining fed by mineralizing fluids) in shallow but laterally-constrained environments (Hussain and Warren, 1989; Aref et al., 1997; Jin and Bergman 1999, 2001; Gündogan et al., 2005; Ortí et al., 2012). These folded veins are commonly named enterolithic and the most common mechanism of formation is connected with volume increase as anhydrite veins hydrate to gypsum so that they become contorted (Kinsman, 1969). Based on these previous experiences and on the data presented in this paper, below, we propose a similar mechanism of development for the contorted structures observed in the study travertines of southern Tuscany.

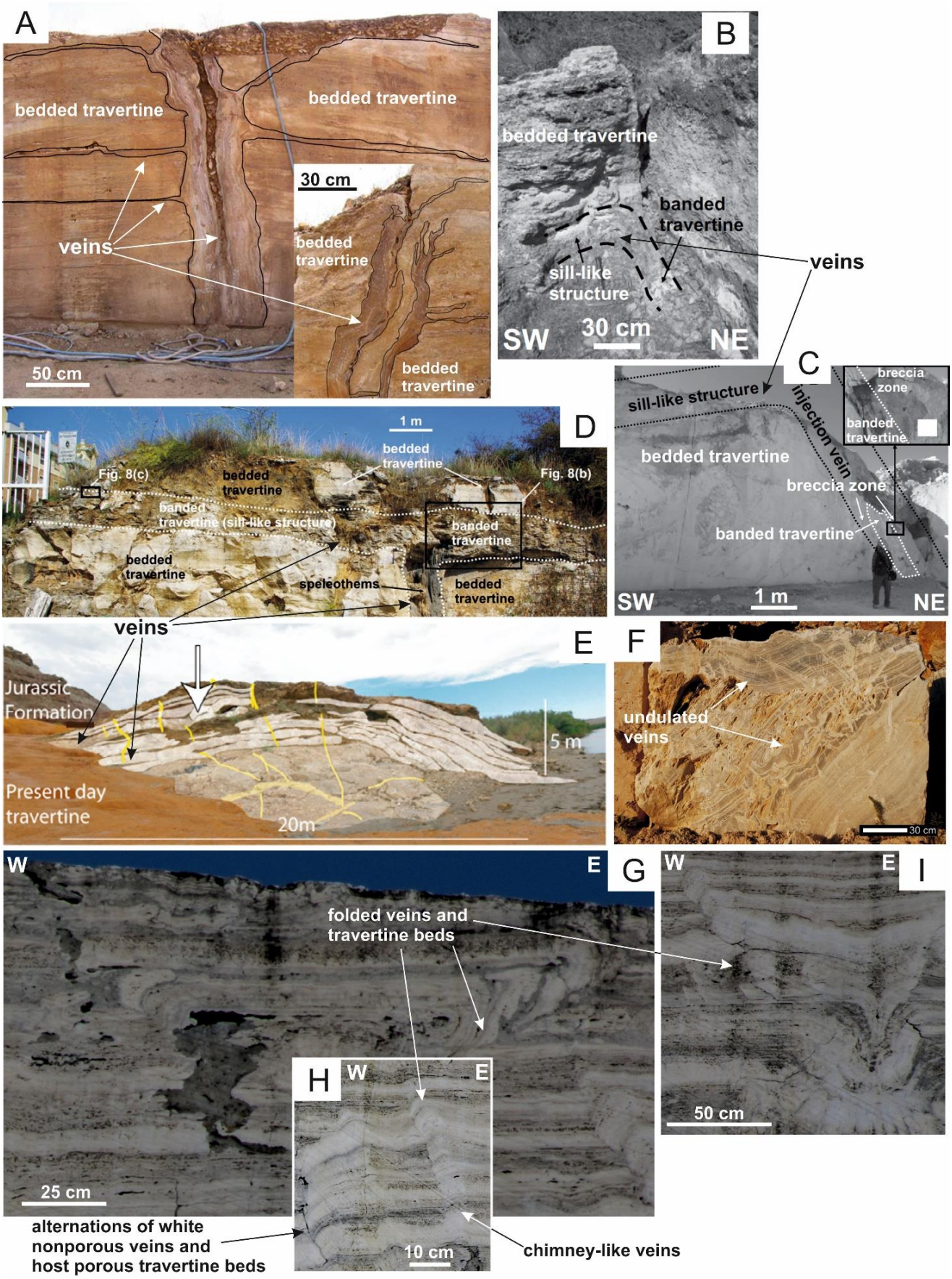
A
bedded travertine
bedded travertine
30 cm
veins
bedded travertine
50 cm
bedded travertine
B
bedded travertine
banded travertine
veins
sill-like structure
SW
30 cm
NE
C
breccia zone
sill-like structure
injection vein
banded travertine
bedded travertine
breccia zone
banded travertine
SW
1 m
NE
D
1 m
bedded travertine
Fig. 8(c)
bedded travertine
Fig. 8(b)
banded travertine (sill-like structure)
banded travertine
bedded travertine
speleothems
bedded travertine
veins
E
Jurassic Formation
5 m
Present day travertine
20m
F
undulated veins
30 cm
W
E
G
folded veins and travertine beds
H
W
E
25 cm
alternations of white nonporous veins and host porous travertine beds
10 cm
chimney-like veins
W
E
I
50 cm

Figure 4.6 - (A) Veins within Pamukkale (Deniszli, Turkey) travertines (Uysal et al., 2009). (B) Veins within Kamara (Denizli, Turkey) travertines (De Filippis et al., 2012). (C) Veins within Kocabaş (Denizli, Turkey) travertines (De Filippis et al., 2012). (D) Veins within Colle Fiorito (Tivoli, Italy) travertines (De Filippis et al., 2013s). (E) Veins within Crystal Geiser (Utah, USA) travertines (Gratier et al., 2012). (F) Specimen of travertine veins from Denizli (Turkey). Note the presence of undulated veins (Özkul et al., 2013). (G), (H), and (I) Folded bed-parallel veins alternated with porous bedded travertine from Tivoli (central Italy). Note the similarity between these structures and those from the Pianetti and Pian di Palma travertines shown in Figs.4.2 and DR1-DR40.

4.6.2. Travertine Veining and Folding

The presented evidence from the Pianetti and Pian di Palma travertines shows that both the veins and their folds are secondary (post-depositional) structures with respect to the primary porous beds. We refer, in particular, to evidence such as the radiometric ages (Fig. 4.3), downward growth of some vein crystals (Fig. 4.2F), and travertine deformation including porosity reduction close to fold hinges and veins (Figs. 4.2C, 4.2D, and 4.2M). Also some non-karstic voids located at the core of folds (Figs. 4.2C and 4.2N) indicate that the folds cannot be syn-depositional, otherwise the voids would have been immediately mineralized and filled. Radiometric dating shows that, during Pleistocene time, vein emplacement occurred progressively from bottom to top in the bedded travertine deposits while the primary travertine beds were still forming in the upper portion of the deposit (Figs. 4.3 and 4.7). Isotope data confirm that the mineralizing thermogene fluids at the origin of veins and bedded travertine are about the same (Fig. 4.4); however, the O-isotope signature indicates a temperature of mineralizing fluids slightly lower (c. 1-3 °C) for the veins than for the bedded travertine (Fig. 4.5 and Table 4.2). We interpret this temperature difference as connected with the rapid vs. slow $CaCO_3$ precipitation for bedded travertine and veins, respectively. In an open air environment (bedded travertine), the fast pressure drop and CO_2 volatilization provoke immediate $CaCO_3$ precipitation from the thermal fluids. In contrast, in an enterolithic environment (veins), the CO_2 degassing and consequent $CaCO_3$ precipitation are slowed processes possibly implying a slight cooling of the mineralizing fluids.

Collectively, the structural, isotope, and geochronological evidence (Figs. 4.1-4.5) indicates that the freshly deposited bedded travertines were soon diagenized through incremental polyphase veining

from the same hydrothermal fluids that had generated and were still generating the primary travertine beds (Fig. 4.7). In this view, we interpret the studied travertine and vein undulations as enterolithic folds (i.e., the product of post-depositional syn-diagenetic deformation) that cannot be thought as of tectonic origin both for their non-cylindrical (domal) shape and for the substantial absence of other compressional structures in the late Miocene-Pleistocene host sediments of the Albegna basin (Zanchi and Tozzi, 1987; Bosi et al., 1996; Carmignani et al., 2013). The travertine folds must have therefore originated through syn-diagenetic progressive and incremental vein growth (Fig. 4.7). We believe that, in a laterally-confined environment offered by the host sediments and travertines, the syn-diagenetic volume increase caused by the vein growth resulted into a regime of layer-parallel shortening, which caused the progressive folding of the vein-host assembly as shown in Fig. 4.2 and outlined in Fig. 4.7. Fold amplification and general doming was likely driven by the crystallization force (Wiltschko and Morse, 2001; Hilgers and Urai, 2005; Noiriel et al., 2010; Gratier et al., 2012) associated with the continuous hydrothermal fluid supply and related veining. This mechanism is similar to that previously proposed for enterolithic contorted veins developed in buried evaporitic environments (Kinsman, 1969; Hussain and Warren, 1989; Aref et al., 1997; Jin and Bergman 1999, 2001; Gündogan et al., 2005; Ortí et al., 2012). Evidence such as the fold hinge thickening and the occurrence of parasitic folds and fan-patterned foliations across the studied folds (Figs. 4.2H-4.2J) suggests that at least part of these folds developed, in a two dimensional view, through a mechanism of buckling. Assuming a Newtonian viscosity, the Biot-Ramberg's buckling equation states that the arc length-thickness (L/t) relationship for a thin folded bed with viscosity η_B surrounded by a matrix with viscosity η_M is (Biot, 1964; Ramberg, 1964):

$$L/t = 2\pi\,(\eta_B/6\eta_M)^{1/3} \qquad (1)$$

Measuring L and t of the veins folded to form the parasitic small folds observed in Figs. 4.2H-4.2J, DR11, DR12, DR13, and DR21, we estimate η_B/η_M as being between 1.5 and 8. In other words, the host travertine was non- or poorly-diagenized and therefore about 1.5-8 times less viscous than

the veins at the time of fold formation. Although this estimate provides only an approximate idea of the rheological contrast between single veins and host bedded travertine at the time of folding, it supports the hypothesis of a syn-diagenetic origin of veins and folds.

The above discussed process of travertine diagenesis evidently changed some important properties of the pristine (pre-diagenesis) travertine deposits, including sedimentary fabric, porosity, stratigraphic-chronological sequence, and rheology. Some of these properties are fundamental in studies where thermogene travertines are considered as suitable proxies of some geological processes. For instance, also due to their radiometric datability, travertines have been frequently used for Quaternary environmental and climatic studies. Results from our study indicate that the stratigraphic-chronological sequence of travertines can be significantly altered by diagenetic processes. Evidently, the lack of recognition and full comprehension of these processes may bias environmental and climatic processes based on travertine geochronology. Our results indicate as well that the travertine original porosity was significantly reduced by syn-diagenetic veining and folding (Figs. 4.2C-4.2D, 4.2L-4.2M; possibly about 35 to 3% according to data by Ronchi and Cruciani, 2015). Also in this case, the lack of recognition of diagenetic processes may render false some porosity and permeability models of hydrocarbon reservoirs hosted in subsalt porous travertine-like rocks (e.g. Atlantic Brazilian and Angolan margins).

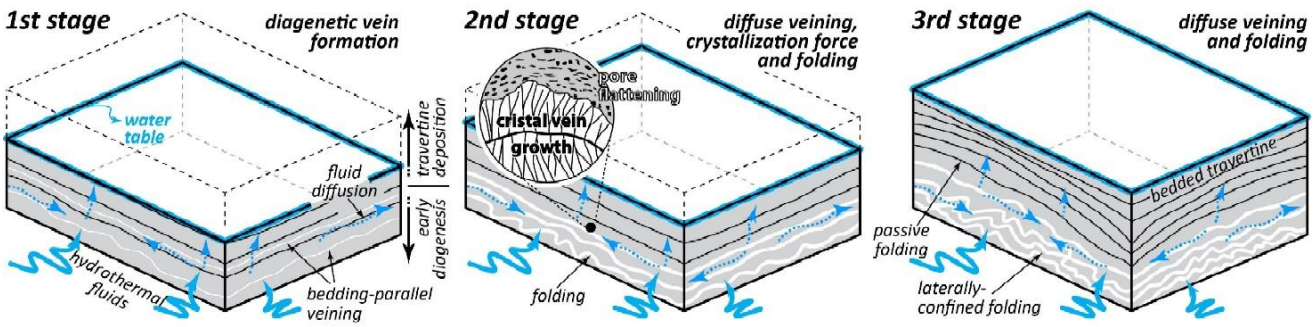

Figure 4.7 - Conceptual model of travertine deposition and post-depositional progressive formation of bed-parallel veins and non-tectonic folds. Domal folds are driven by laterally-constrained syn-diagenetic mineralization (volume increase) induced by a continued hydrothermal supply coming out from under the travertine.

4.7. Conclusions

(1) Non-tectonic syn-diagenetic contractional deformations are observed, depicted, and interpreted for the first time in thermogene travertines.

(2) Travertine syn-diagenetic veining and folding changed radically some pristine rock properties such as fabric, porosity, stratigraphic-chronological sequence, and rheology.

(3) These changes, if disregarded or unrecognized, may significantly impact or even bias studies and assessments on paleoclimate, neotectonics, paleohydrology, and also hydrocarbon reservoirs, based on the absolute chronology of travertines and on the pristine porosity of bedded travertines.

(4) Similar structures in other thermogene travertine deposits suggest that those reported in this paper from southern Tuscany may be travertine structures more common than previously thought.

4.7. Data Repository

4.7.1. Photographic Atlas of Travertine Structures

The investigated quarries (Pianetti and Pian di Palma; Fig. 4.1) in the Tuscan extensional province (Italy) are characterized by exposures of a large number of veins and folds at different scales within Pleistocene thermogene travertine beds. A thorough documentation of structures is the first step to properly interpret them.

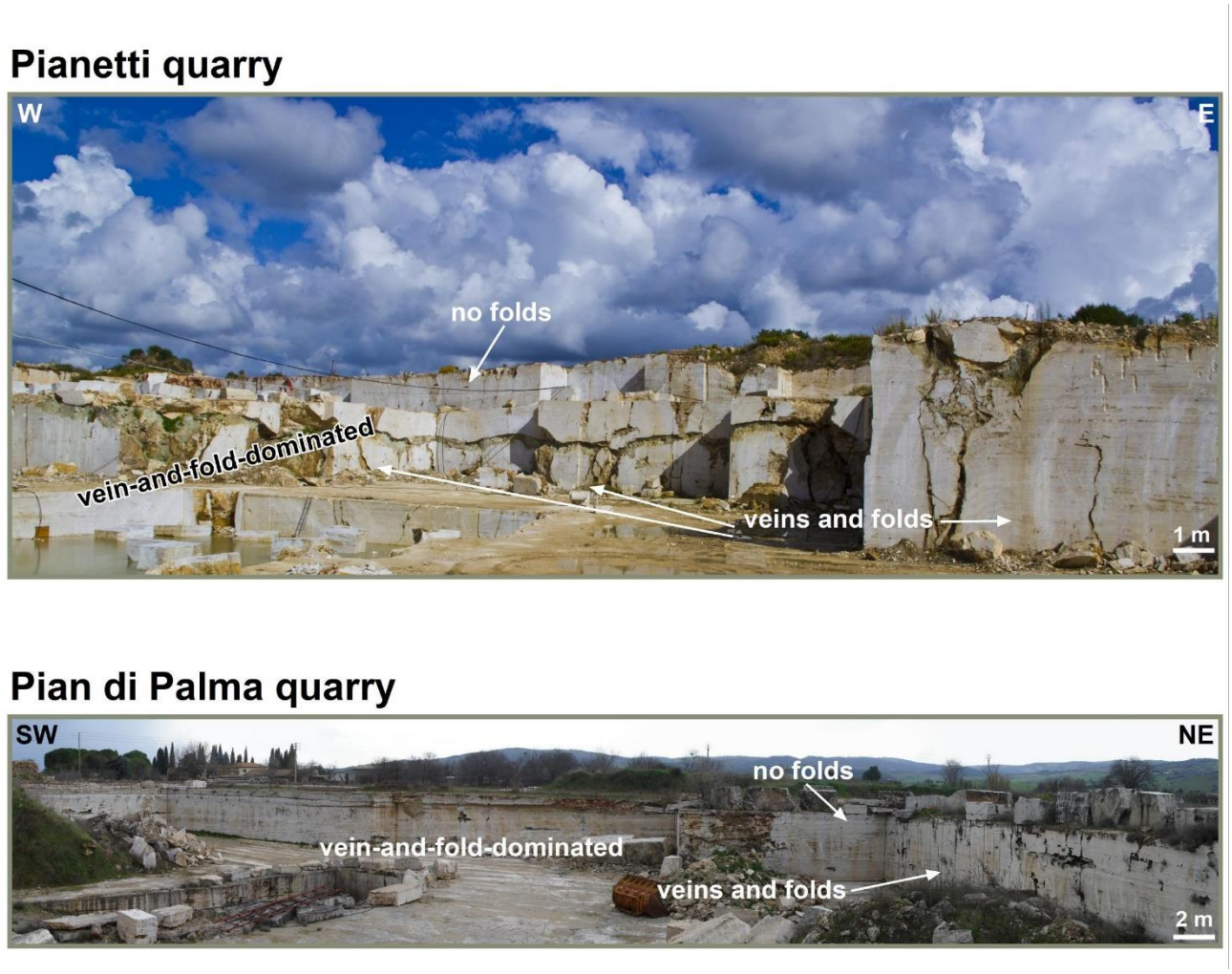

Figure DR1 – Panoramic view of the Pianetti quarry (above). Veins and folds are present in the lower and middle part of the quarry, whereas these structures are absent or rare in the upper part. Panoramic view of the Pian di Palma quarry (below). Also in this case, veins and folds are present in the middle-lower part of the quarry and absent or rare in the very upper part.

Figure DR2 – Panoramic view of the upper portion of the Pianetti quarry. Note the presence of horizontal bedded travertine with no folds.

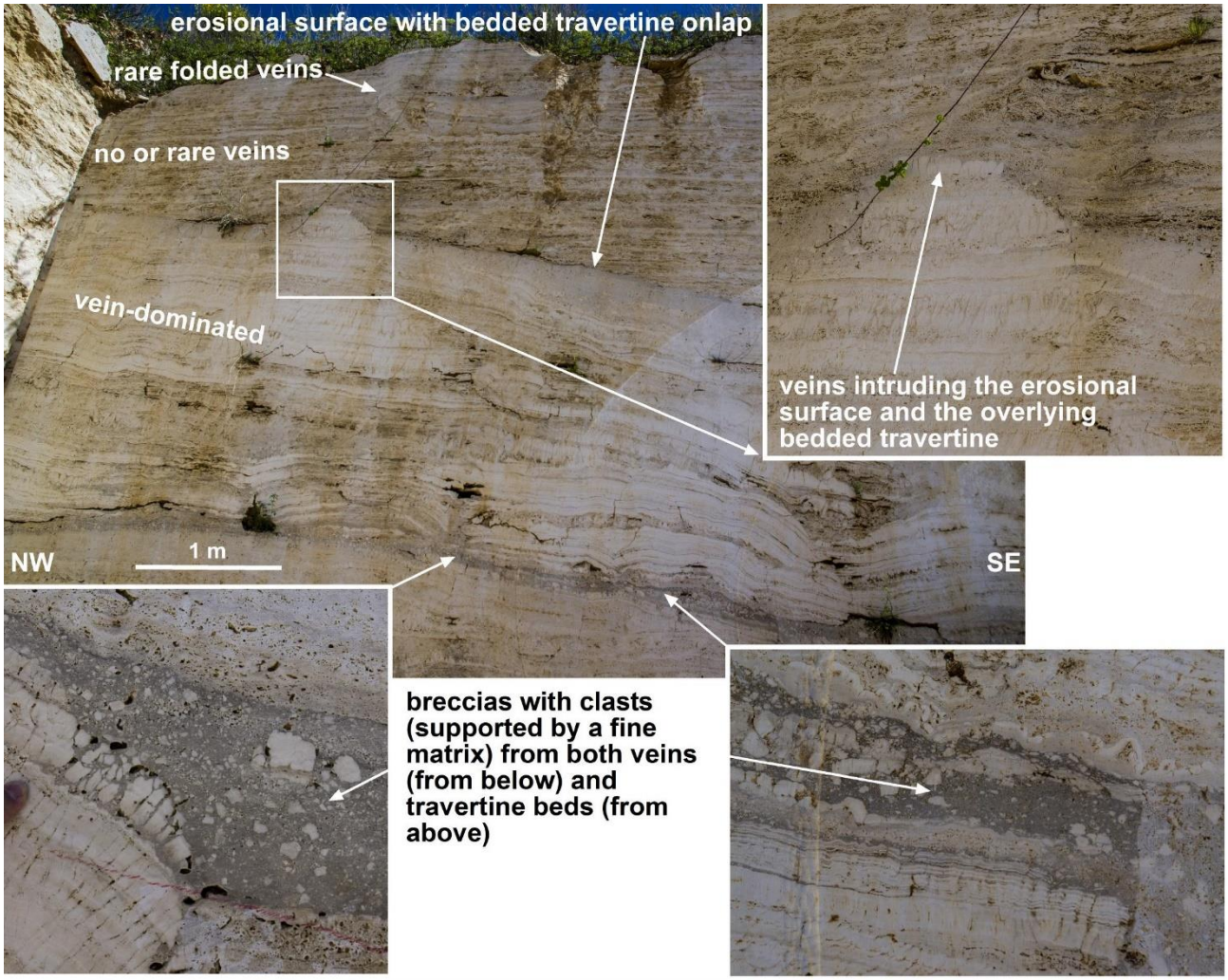

Figure DR3 – Photograph (with close ups in insets) of the upper section of the Pianetti quarry. An erosional surface marks the boundary between vein-dominated travertines (below) and onlapping travertine beds with no or rare veins (above). The veins intrude the overlying travertine beds and erosional surface. Below, a breccia layer contains clasts (which are surrounded and supported by fine matrix) deriving from the layers that restrict the breccia itself above and below (Pianetti quarry).

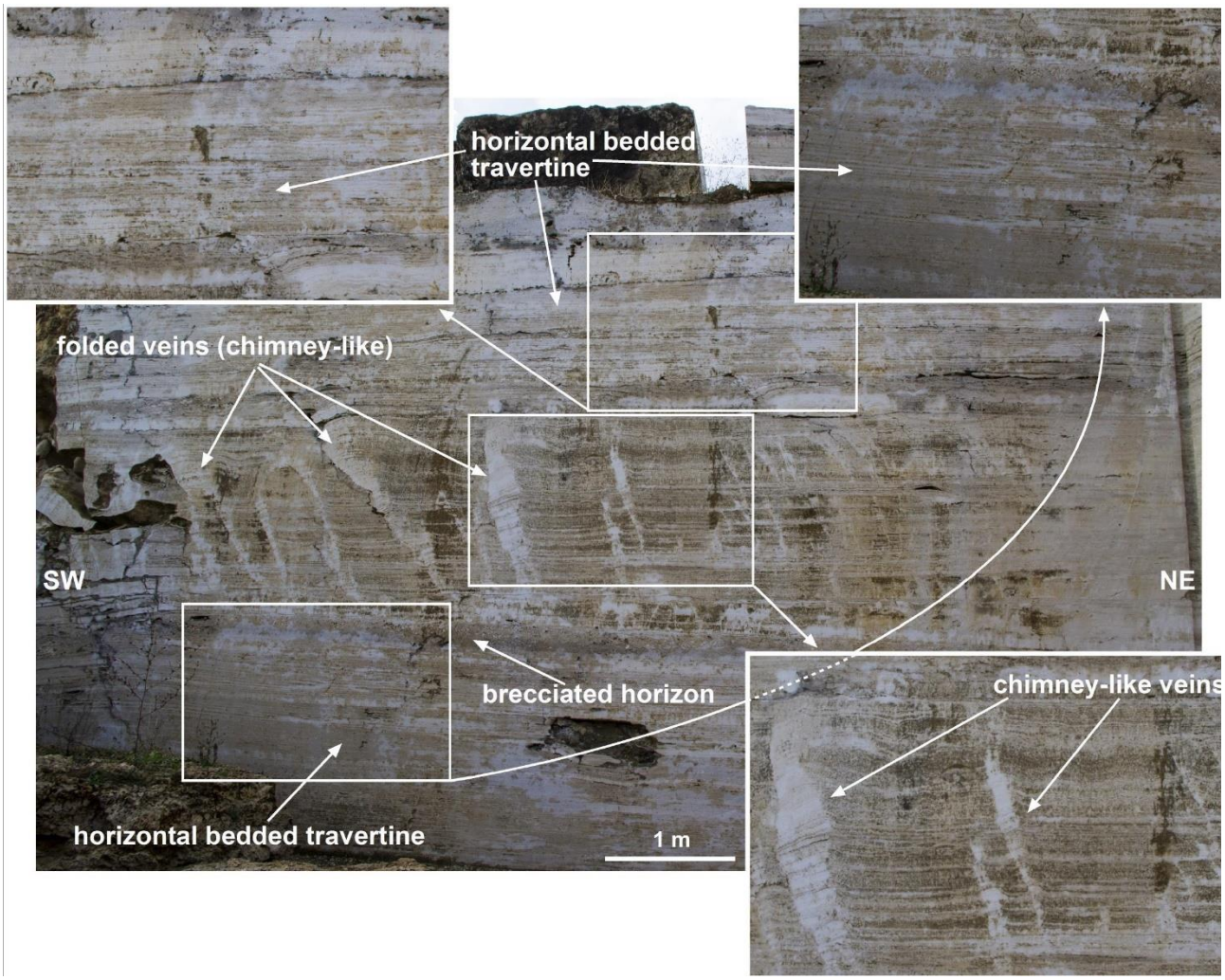

Figure DR4 – Photograph (with three close ups in insets) of the middle-upper portion of the Pian di Palma quarry. Note the presence of horizontal bedded porous travertine, which is affected by chimney-like veins (nonporous, white veins) cutting through and folding the pre-existing bedded travertine. The chimney-like veins seem to originate from a dark-grey brecciated horizon at their base. These veins are restricted to particular stratigraphic intervals bounded above and below by undisturbed travertine beds.

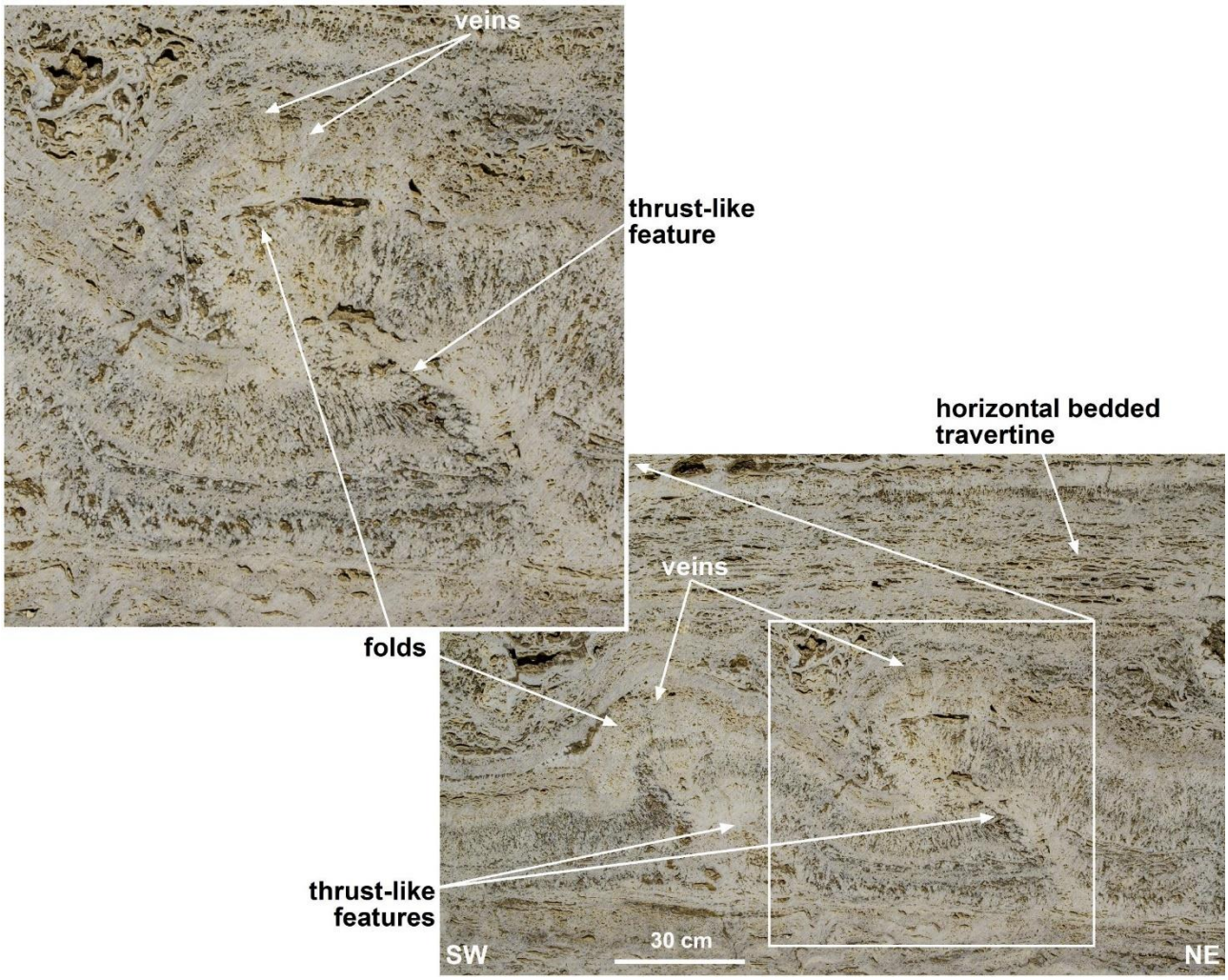

Figure DR5 – Photograph (with close up) of folds and thrust-like features. Note the presence of well-developed veins particularly in the hinge zones, where the growth of secondary crystals contribute to fold the originally-horizontal travertine beds (Pianetti quarry).

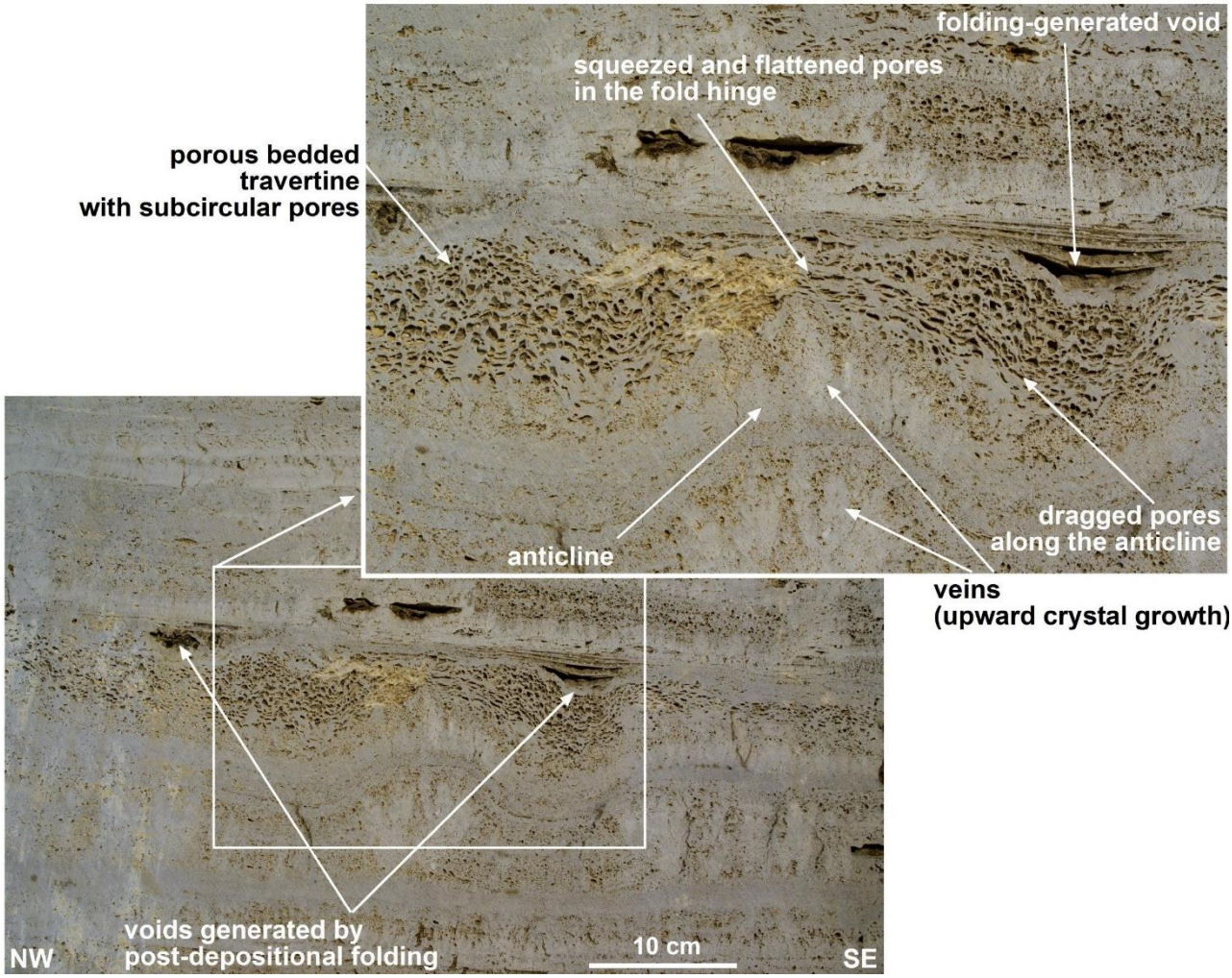

Figure DR6 – Photograph (with close up) of veins that folded the porous bedded travertine. The pores of the bedded travertine are squeezed, flattened and dragged in correspondence of the anticline hinge, which, in turn, corresponds to the occurrence of veins with upward crystal growth. Voids in correspondence of syncline hinges are generated by post-depositional folding (Pianetti quarry).

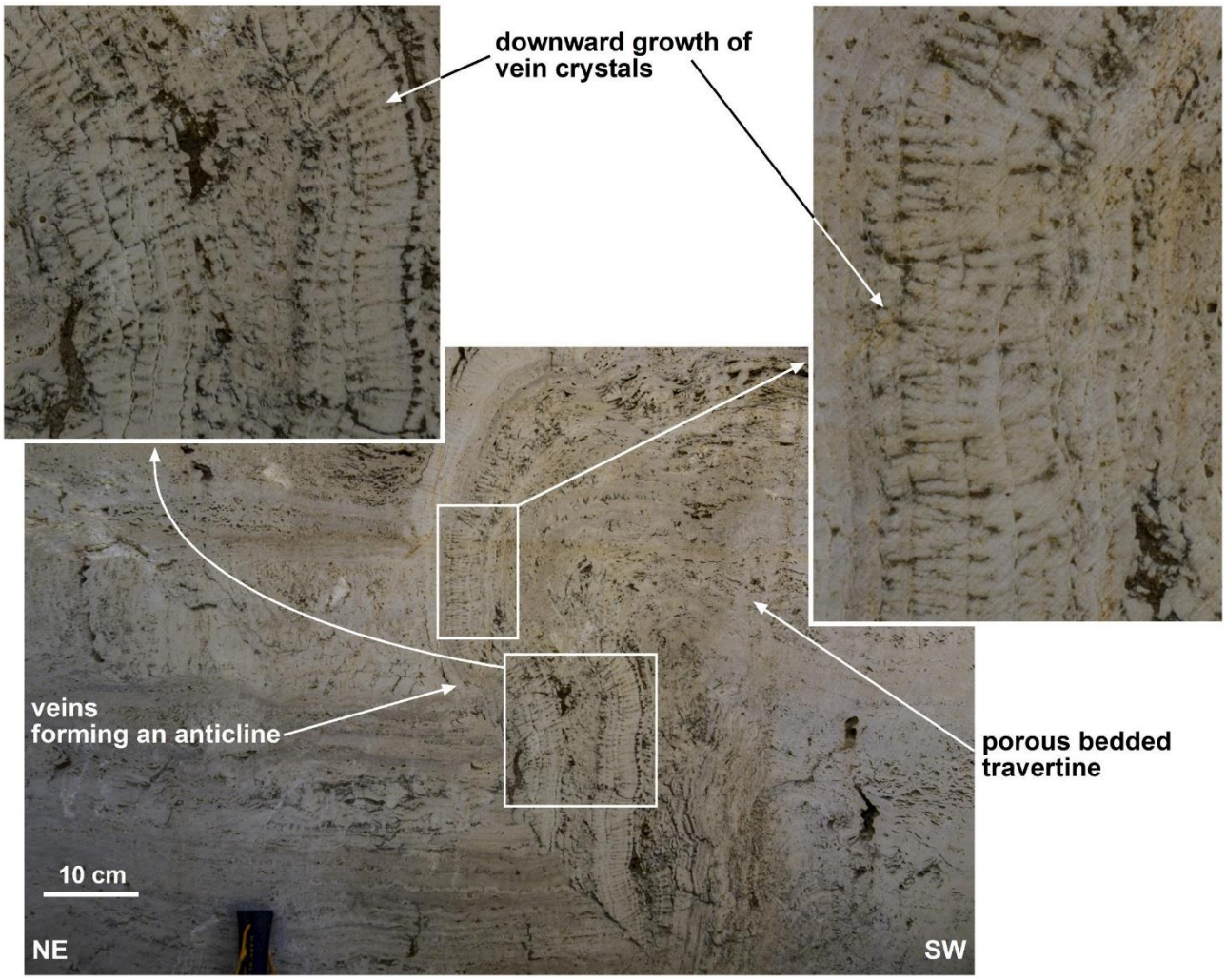

Figure DR7 – Photograph (with close ups in insets) of veins that folded the porous bedded travertine to form an anticline with a vertical limb. The veins in the vertical limb are characterized by crystals that grew downward (before and during the folding and verticalization) (Pianetti quarry).

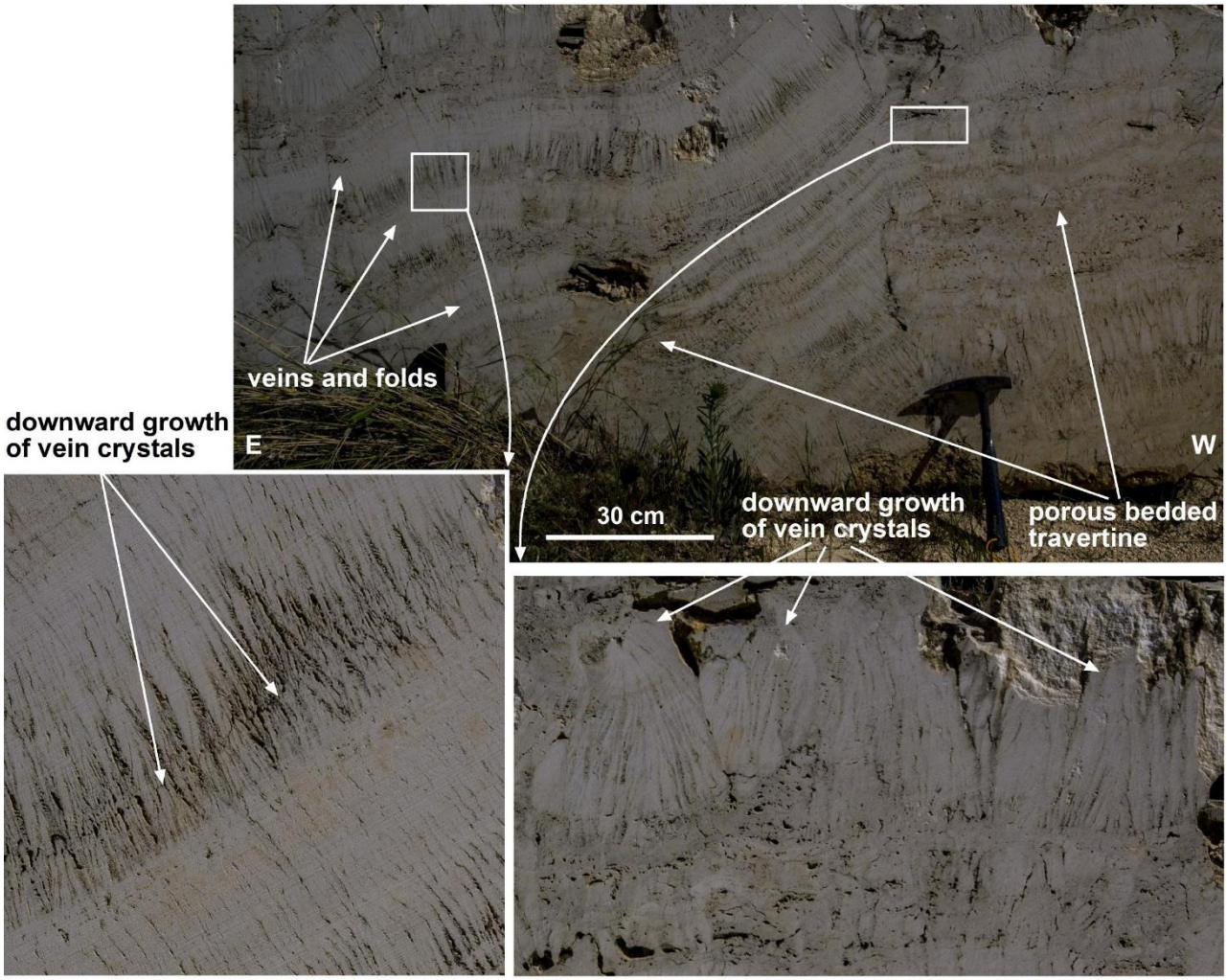

Figure DR8 – Photograph (with close ups in insets) of enterolithic veins to form gentle anticlines and synclines. The veins are often characterized by crystals that grew downward thus demonstrating the secondary development of the veins with respect to the host bedded travertine (Pianetti quarry).

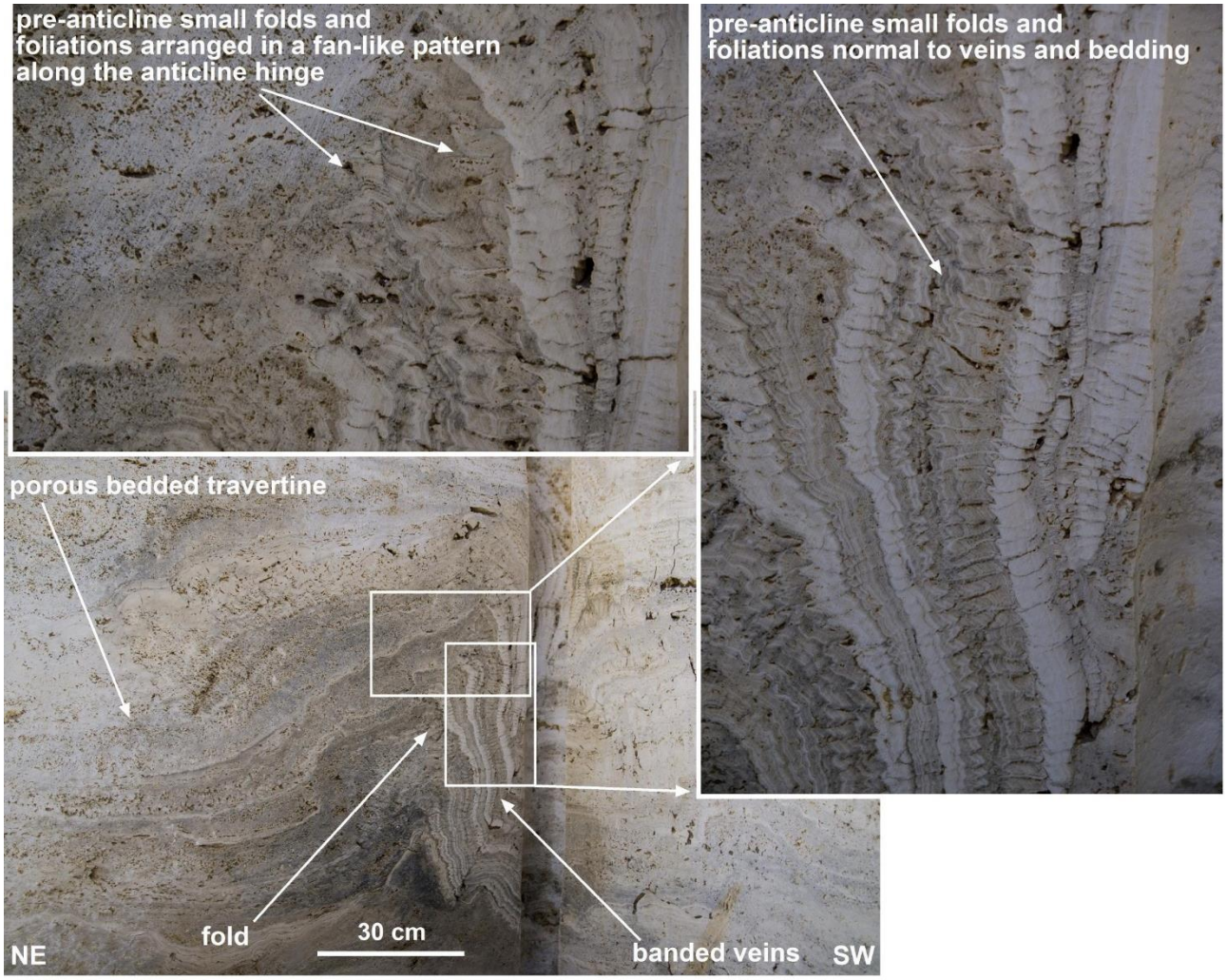

Figure DR9 – Photograph (with close ups in insets) of veins and folds. The steep limb of the anticline includes banded veins that are affected by pre-anticline small parasitic folds and foliations normal to veins and bedding. Along the anticline hinge, the foliation has a bedding-normal fan-like pattern (Pianetti quarry).

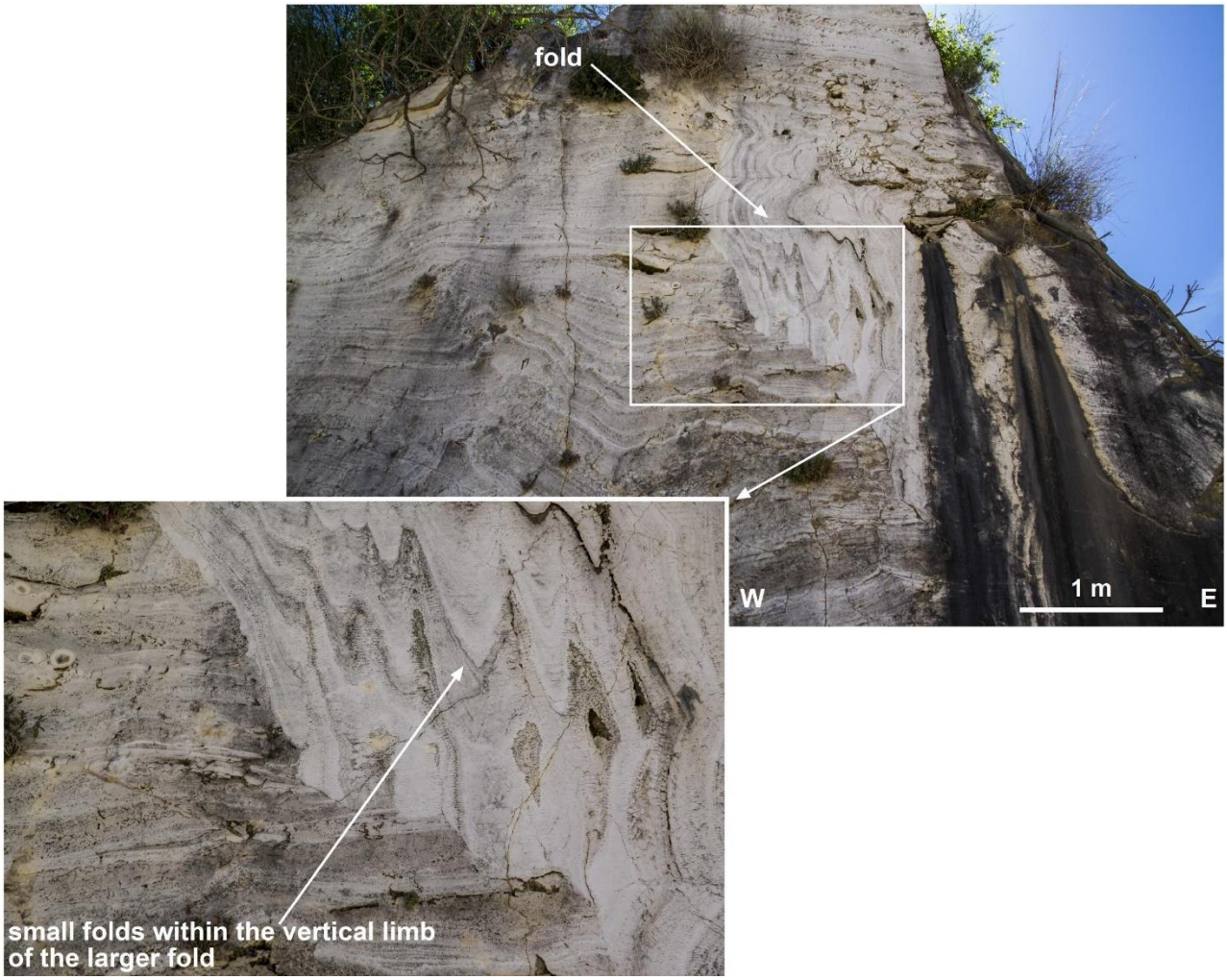

Figure DR10 – Photograph (with close up) of large fold with subvertical limb. The limb is affected by secondary folds with apparent vertical axial planes (Pianetti quarry).

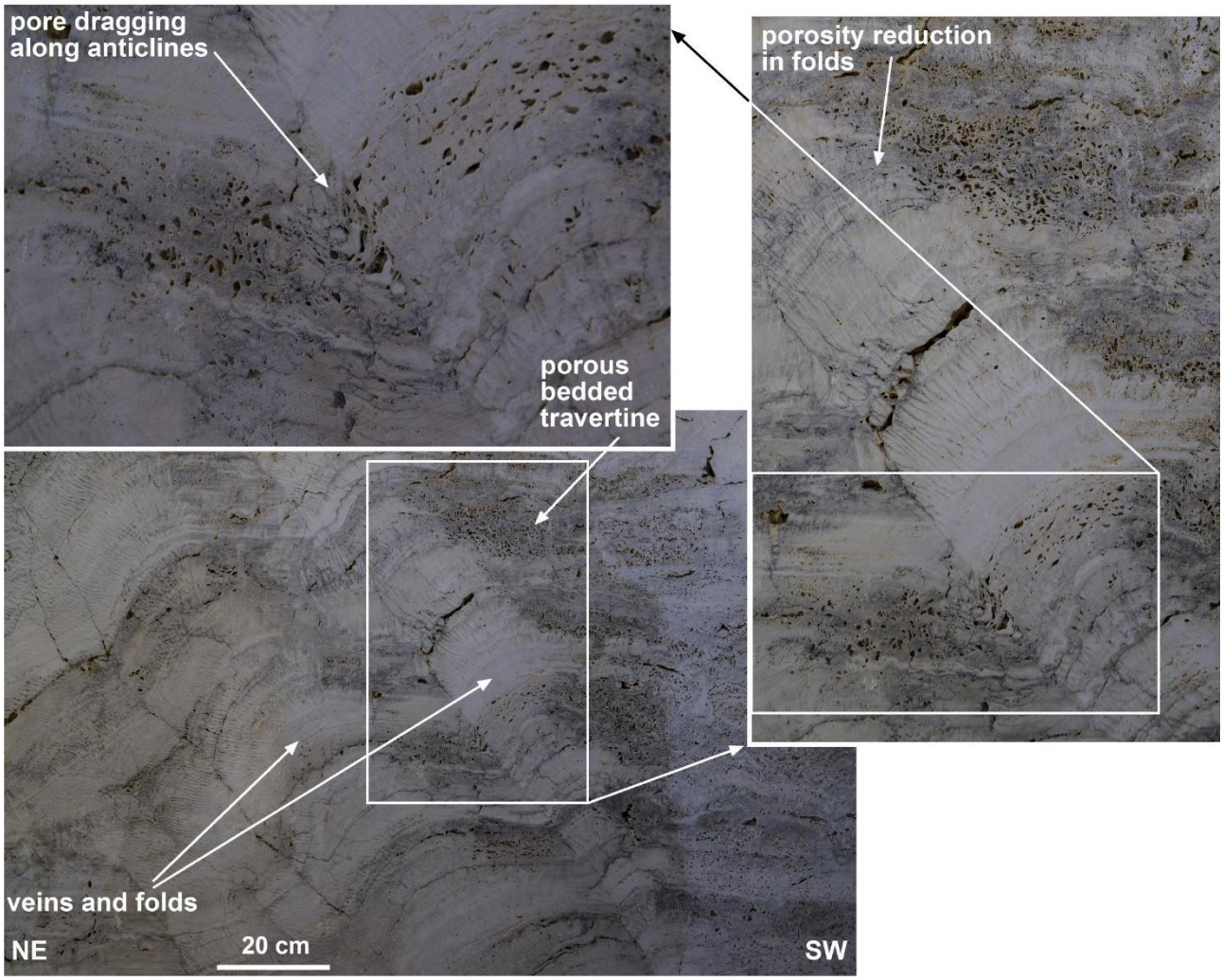

Figure DR11 – Photograph (with close ups in insets) of veins and folds within travertine beds. Note the porosity reduction moving from the porous travertine beds to the veins and folds. Note also the pore upward dragging along the anticlines (Pianetti quarry).

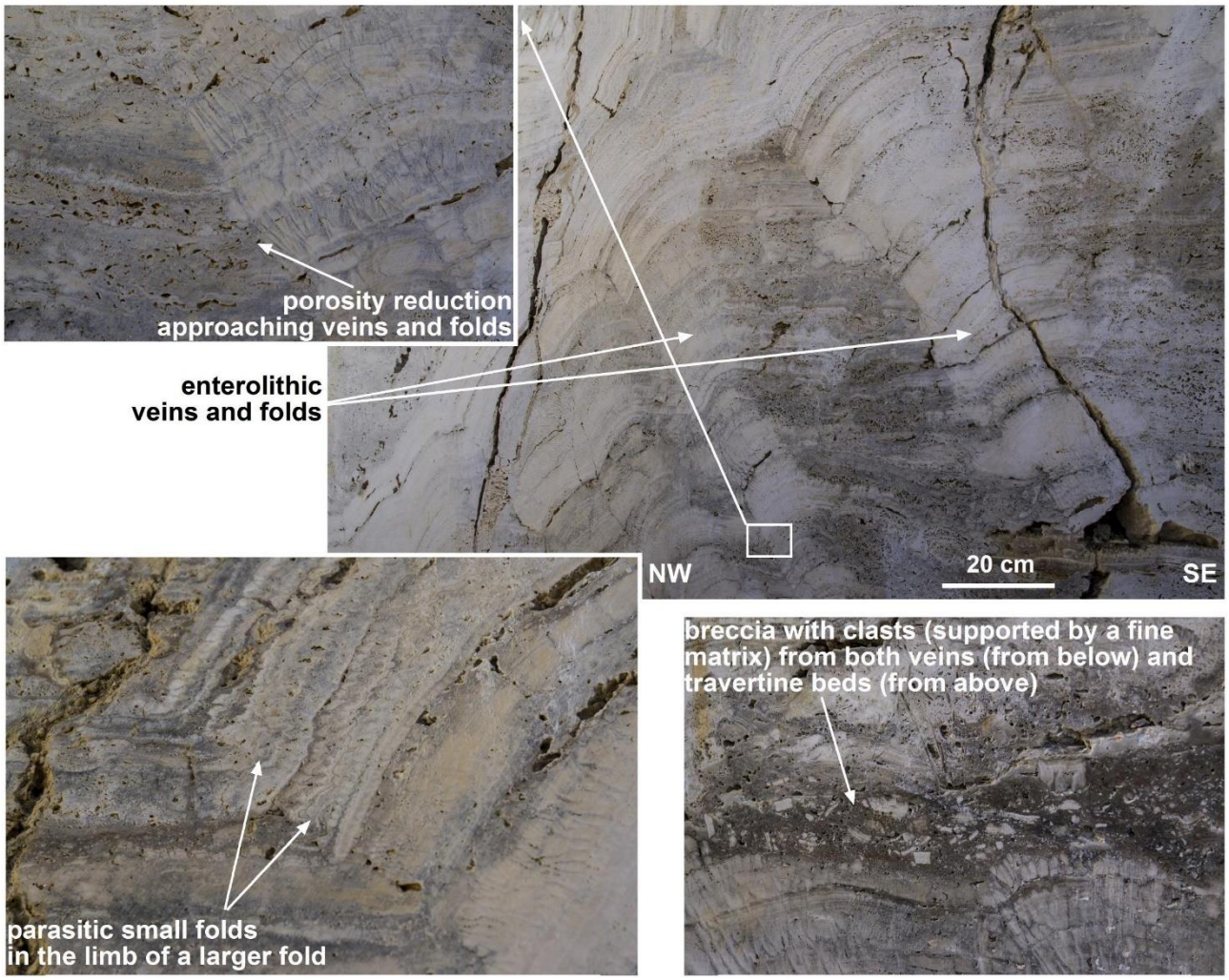

Figure DR12 – Photograph (with close up in inset above and two close up photographs from nearby exposures) of veins and folds within travertine beds. Note the porosity reduction moving from the porous travertine beds to the veins and folds. Note also the breccia restricted between veins (below) and travertine beds (above) and the occurrence of parasitic folds in an anticline limb (Pianetti quarry).

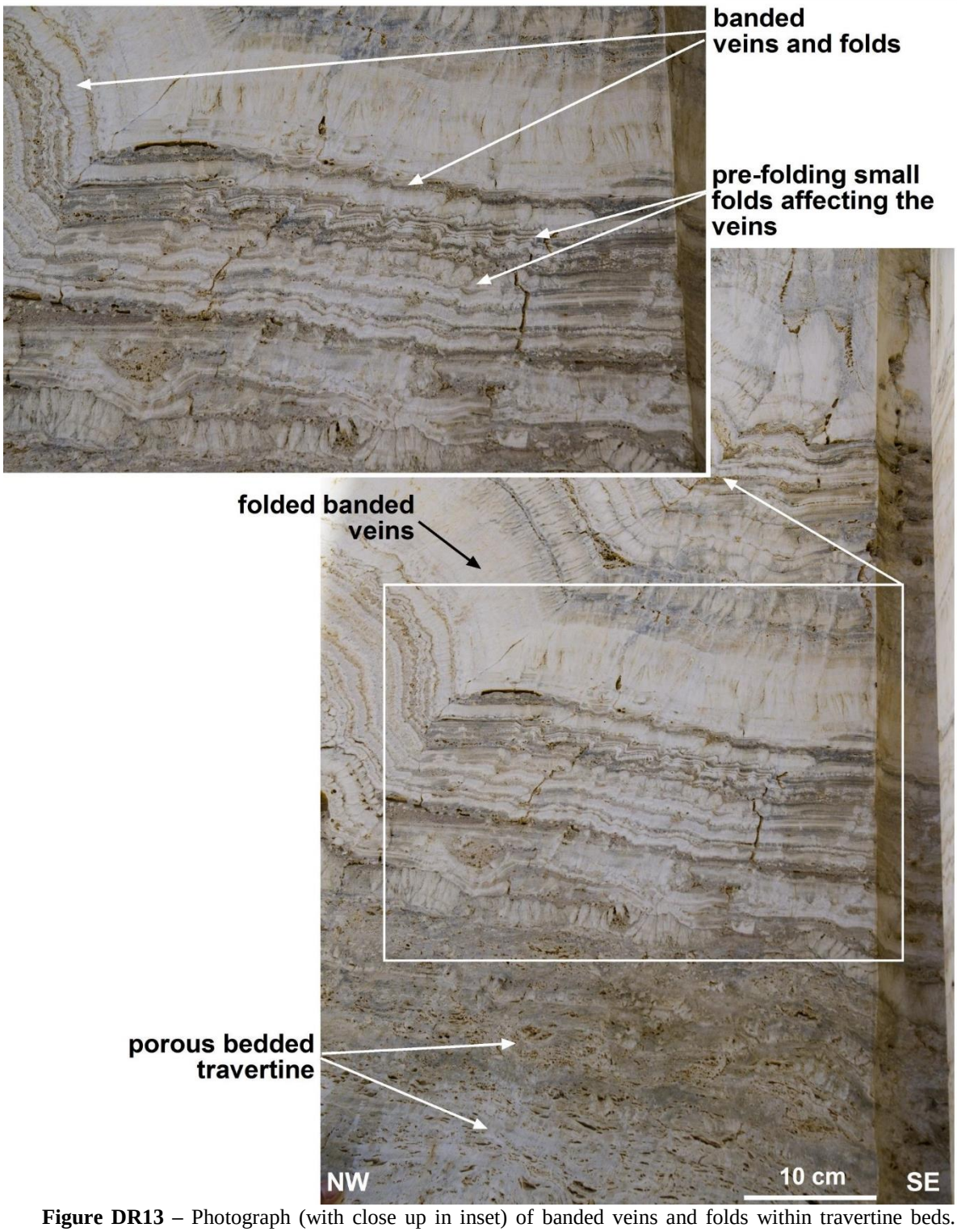

Figure DR13 – Photograph (with close up in inset) of banded veins and folds within travertine beds. Note the occurrence of pre-folding small folds affecting the horizontal veins (Pianetti quarry).

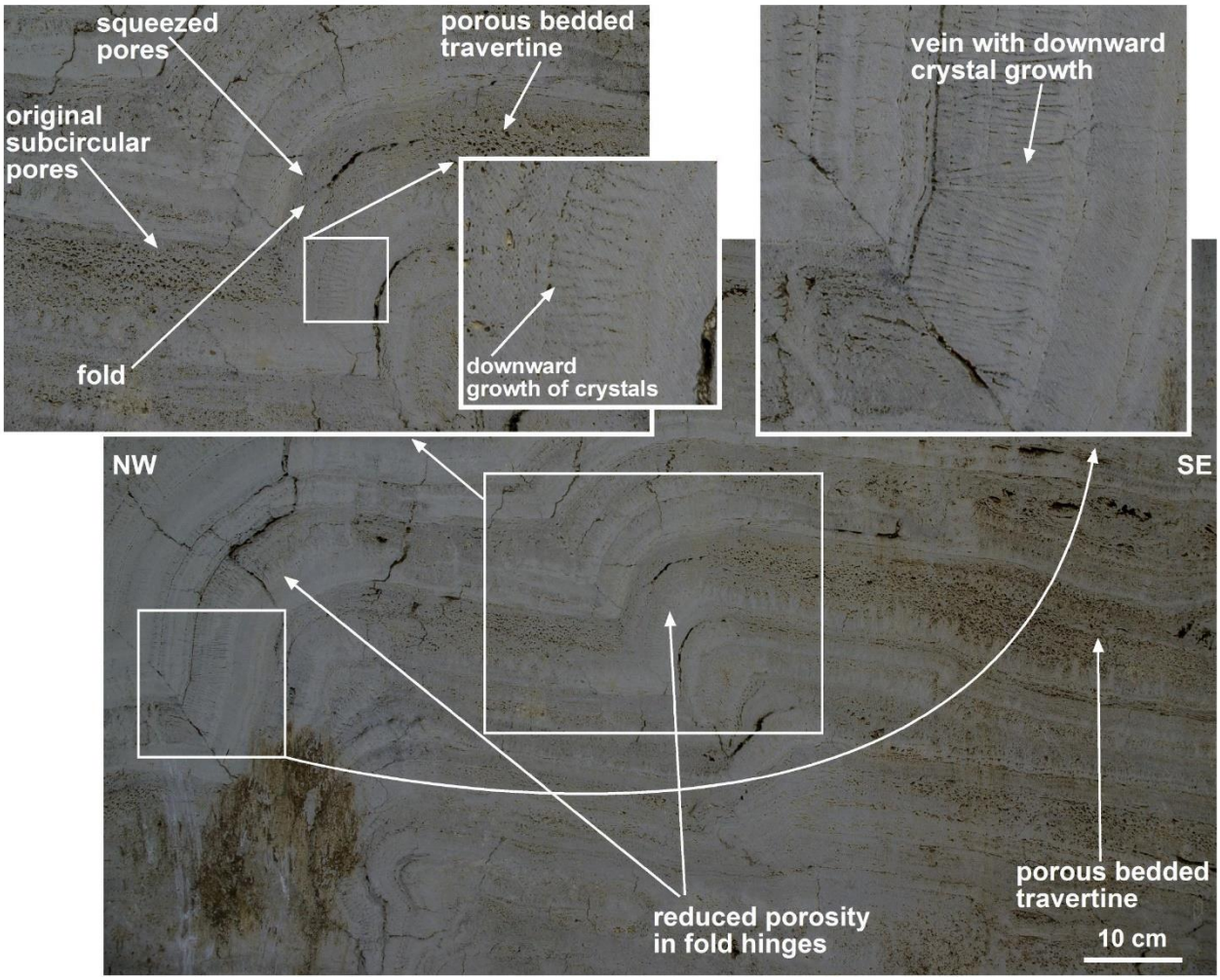

Figure DR14 – Photograph (with close ups in insets) of veins that folded the porous bedded travertine. The pores of the bedded travertine are squeezed and flattened in correspondence of the anticline hinges. Note that in some segments of the folds (upper right inset) the vein crystals grew downward, thus proving the late occurrence of veins with respect to the host bedded travertine. Note also the reduced porosity in the fold hinges with respect to the host bedded travertine in the fore limbs (Pianetti quarry).

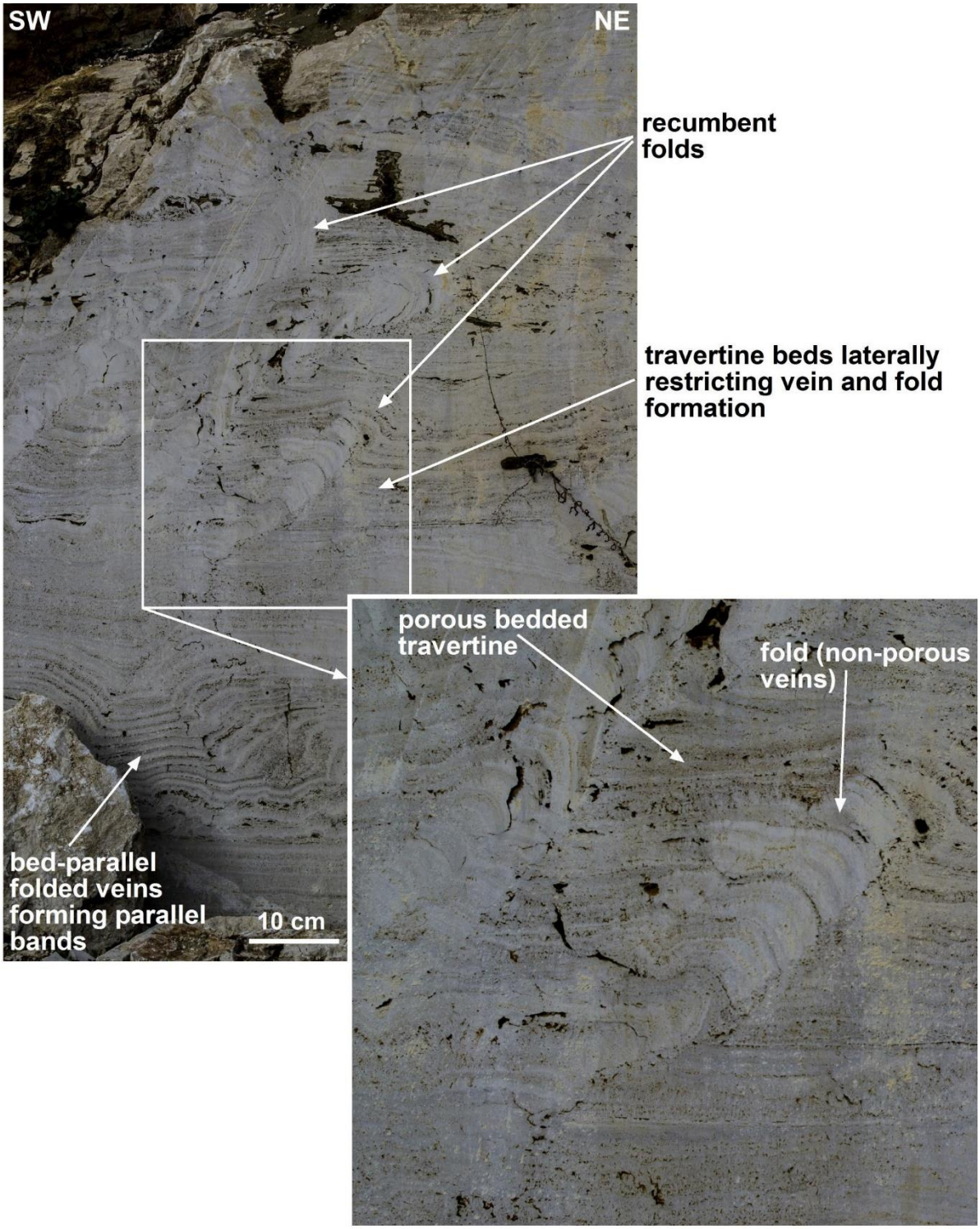

Figure DR15 – Photograph (with close ups in inset) of folds. Note the occurrence of porous bedded travertine that is folded over by non-porous folded veins. In some instances, these folds are even recumbent (Pianetti quarry).

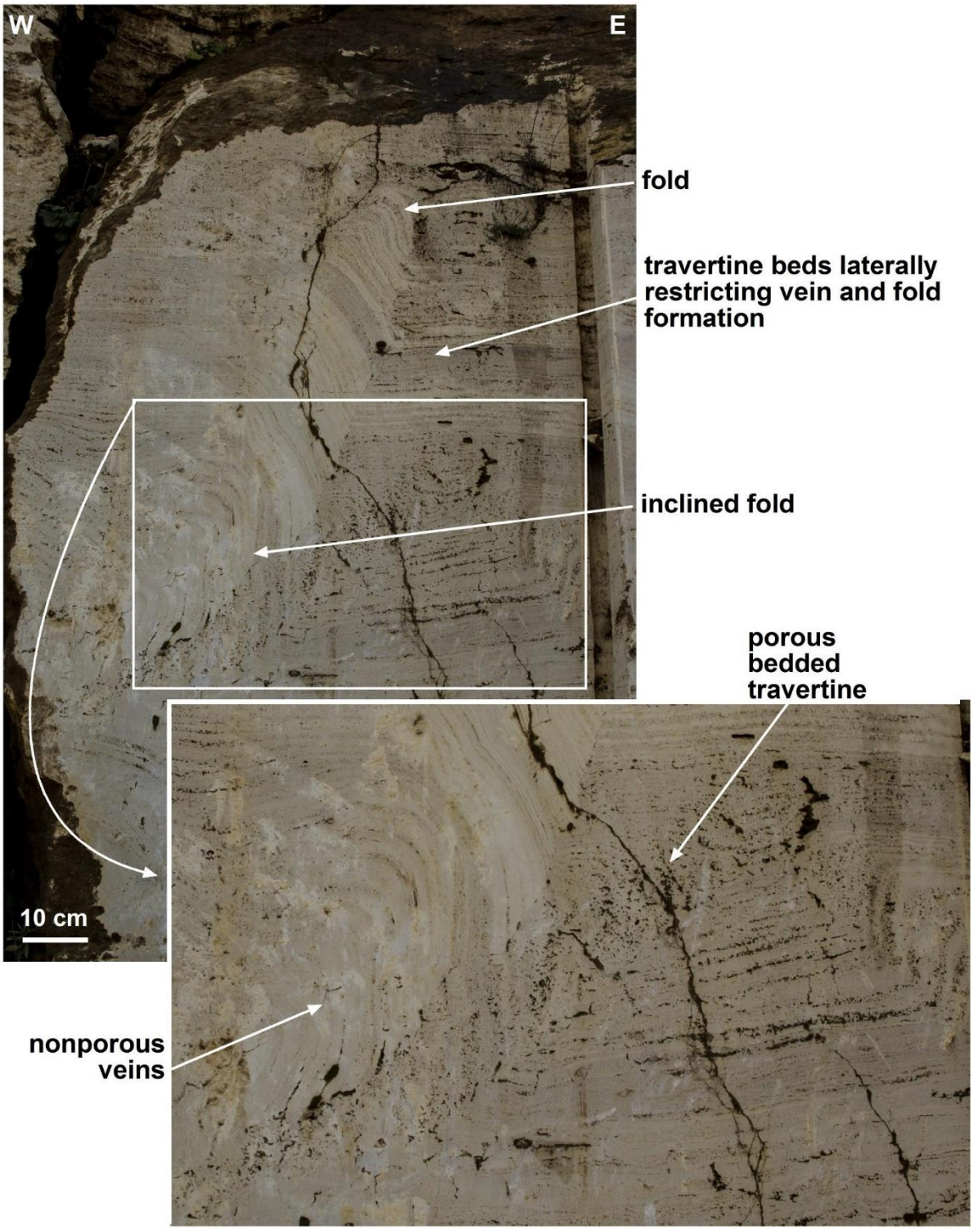

Figure DR16 – Photograph (with close ups in insets) of veins and folds. Note the occurrence of porous bedded travertine that is overlain by an inclined fold formed by nonporous white veins arranged in parallel bands (Pianetti quarry).

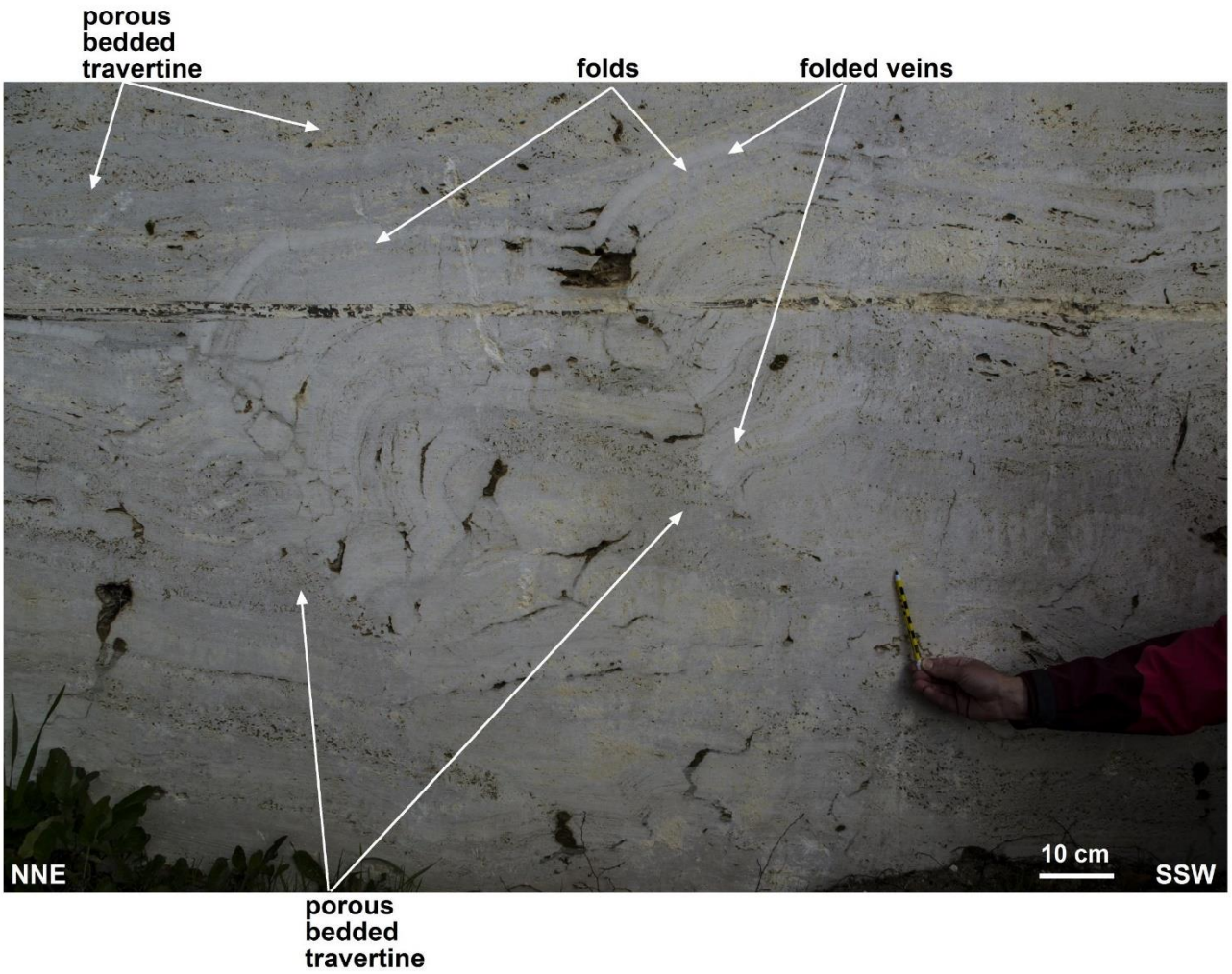

Figure DR17 – Photograph of veins and folds. Note the occurrence of porous bedded travertine that is overlain by folds formed by nonporous folded veins arranged in parallel bands (Pianetti quarry).

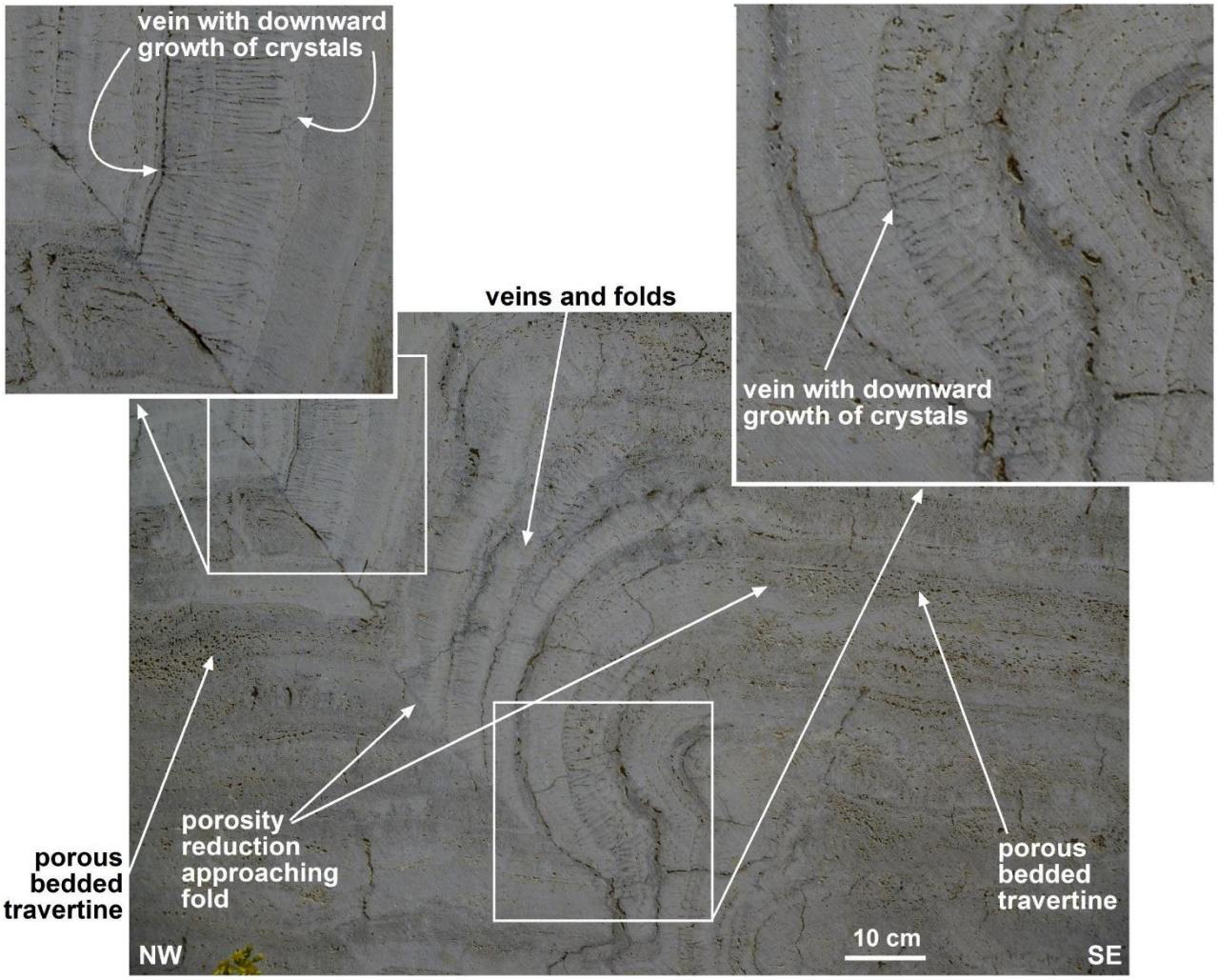

Figure DR18 – Photograph (with close ups in insets) of veins and folds. Note the occurrence of porous bedded travertine that is overlain by nonporous folded veins. Note also that the bedded travertine occurs in the right limb of the recumbent fold. The vein crystals developed at least in part according to a downward growth, demonstrating their late occurrence with respect to the pre-existing bedded travertine (Pianetti quarry).

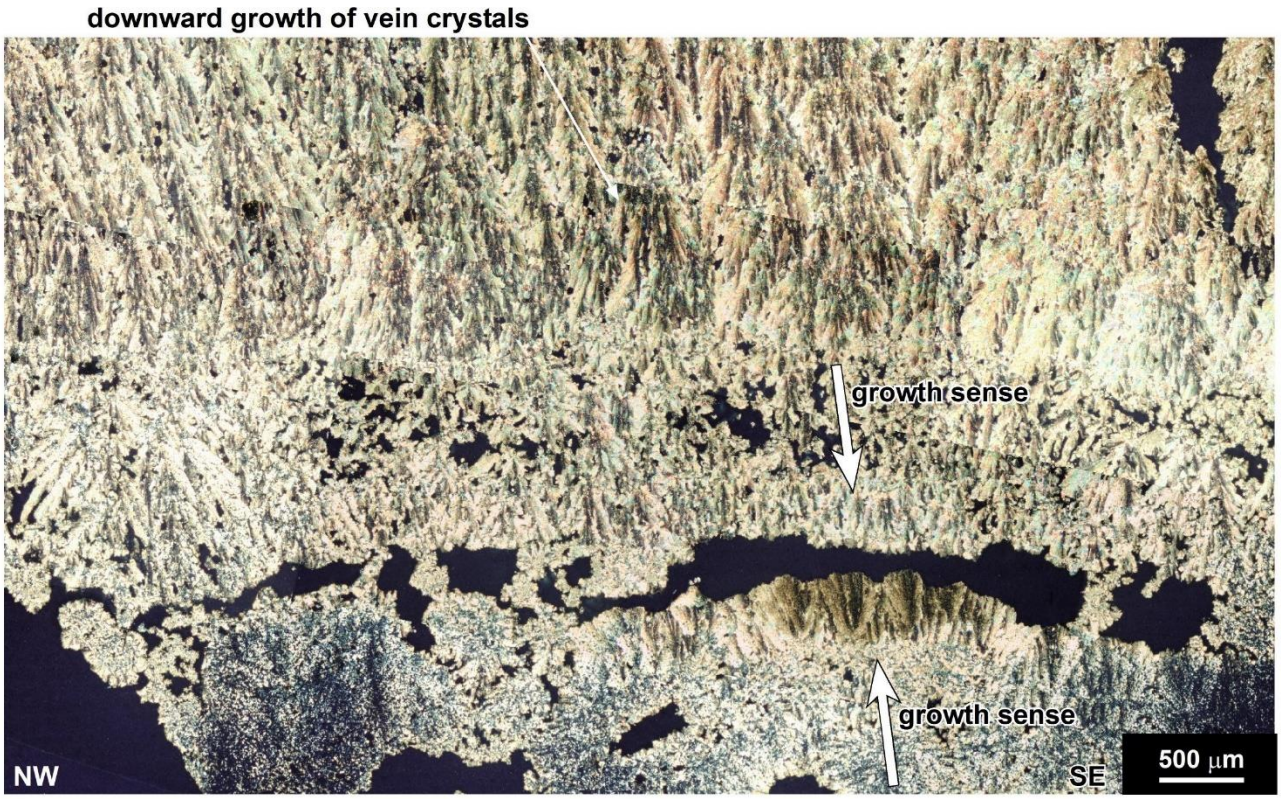

Figure DR19 – Micro-photograph of a subhorizontal folded vein with fan-patterned crystals showing both downward and upward senses of growth (Pianetti quarry). This evidence (downward growth) demonstrates the late occurrence of the vein with respect to the pre-existing host bedded travertine.

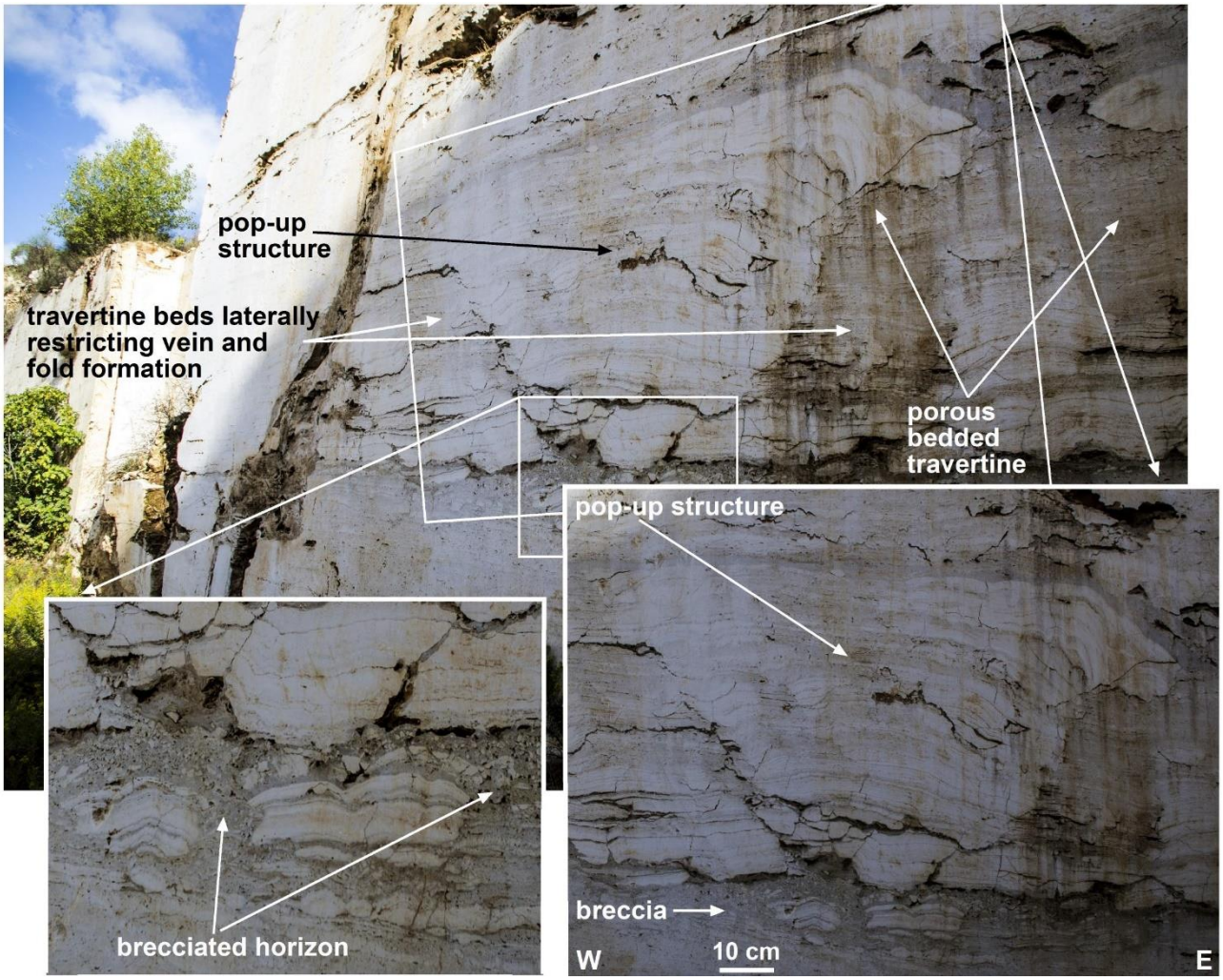

Figure DR20 – Photograph (with close ups in insets) of a pop-up structure consisting of folded veins overlying porous bedded travertines. Note that the pop-up structure seems to originate from a dark-grey brecciated horizon lying at its base (Pianetti quarry).

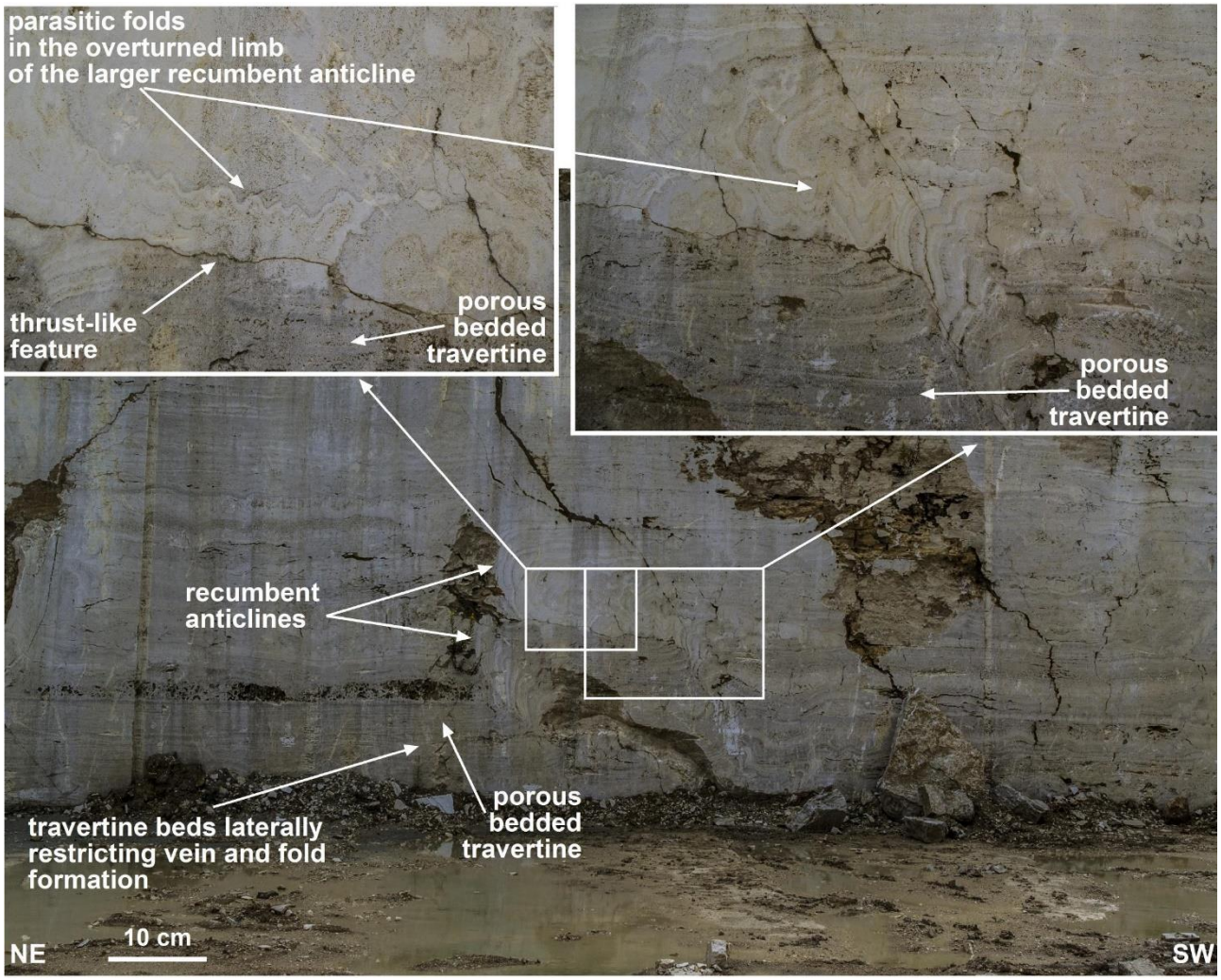

Figure DR21 – Photograph (with close ups in insets) of recumbent anticlines. Note the occurrence of parasitic small folds in the overturned limb of one of the recumbent anticline. The recumbent folds overlie the porous bedded travertine (Pianetti quarry).

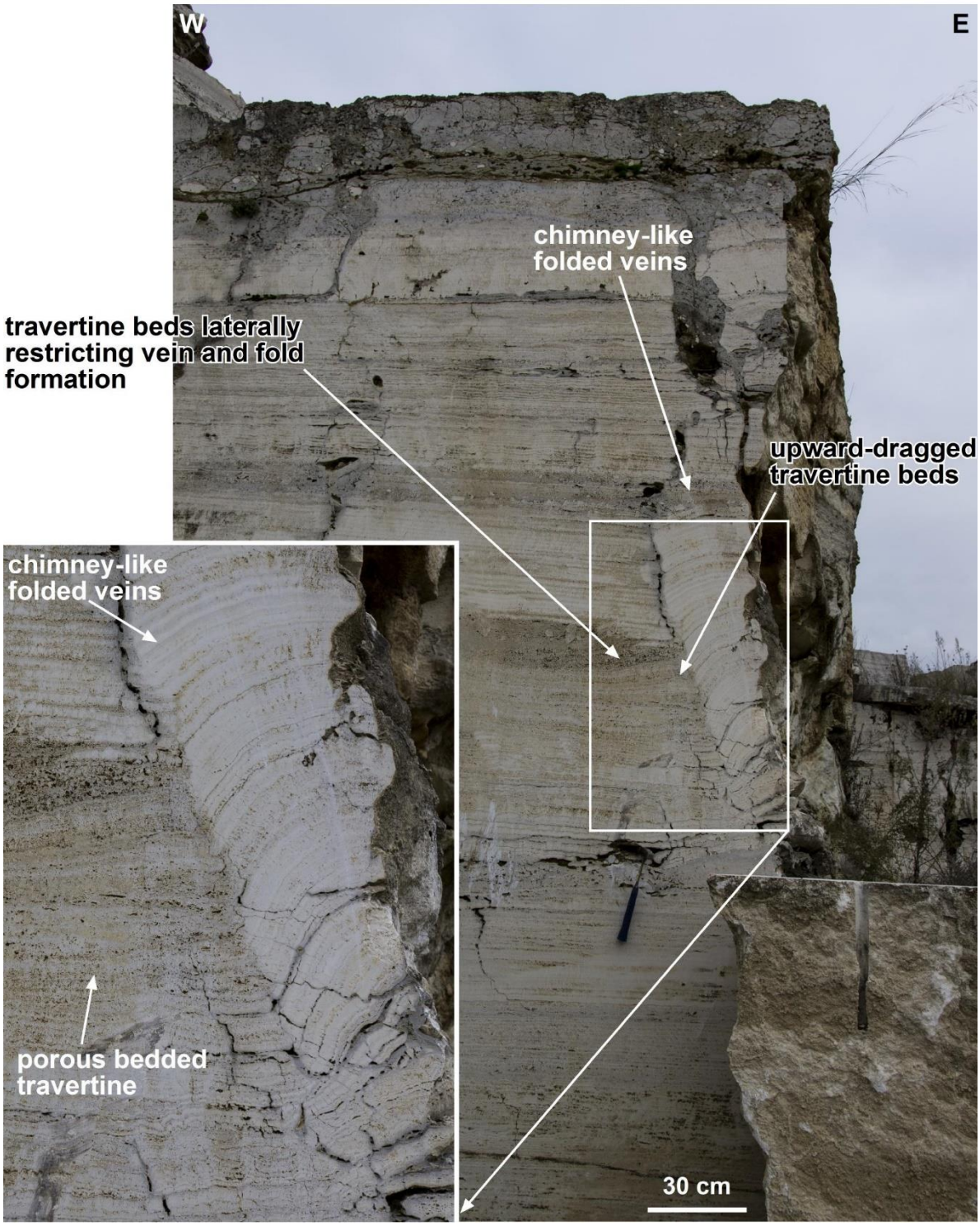

Figure DR22 – Photograph (with close up in insets) of chimney-like veins within porous bedded travertine. The veins are arranged in a banded pattern and are folded to form an anticline that moved up over the pre-existing porous horizontal bedded travertine (Pianetti quarry).

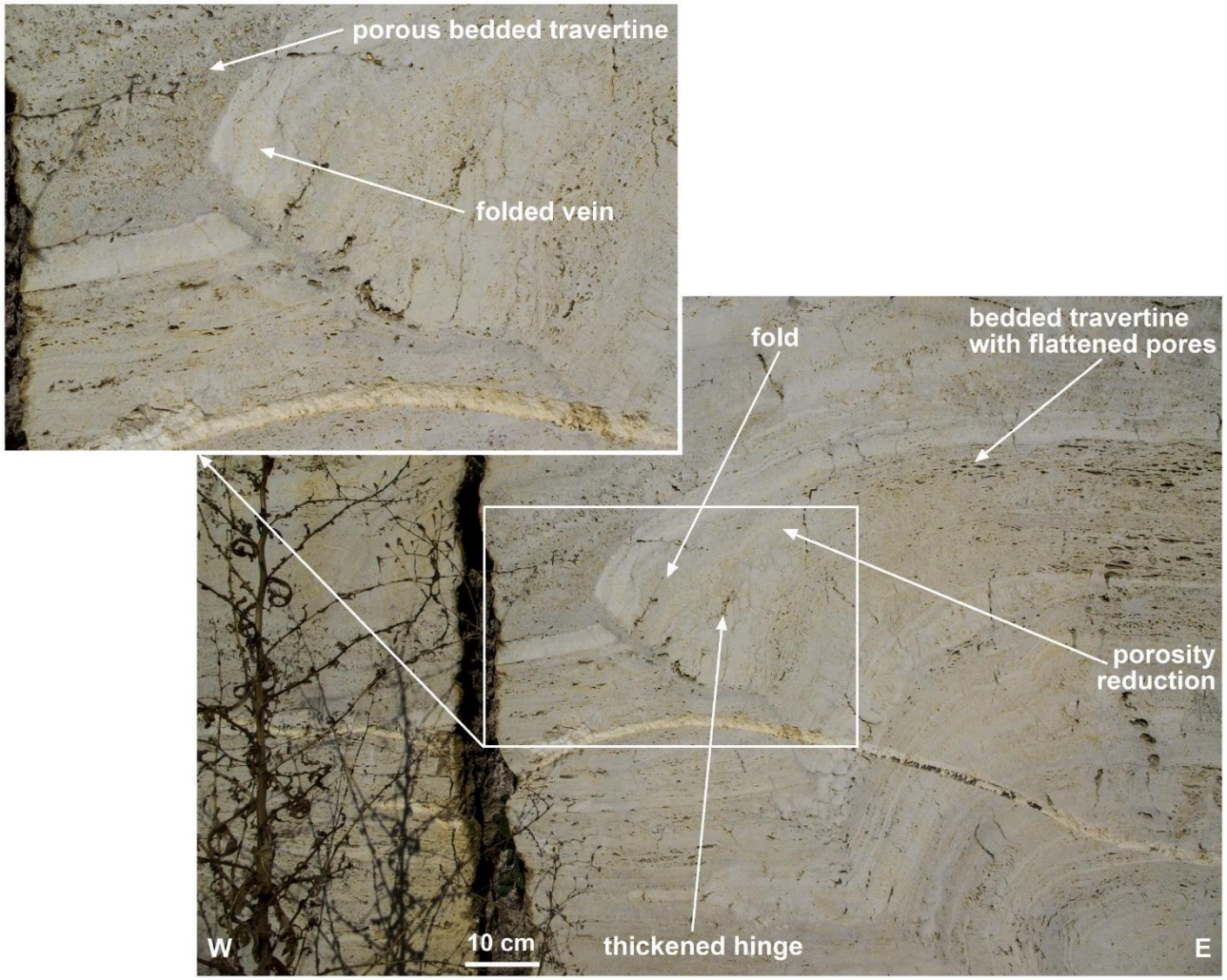

Figure DR23 – Photograph (with close up in inset) of an antiformal body. Note the occurrence of bedded porous travertine with flattened pores in the fold limbs. Note also the occurrence of bedded travertine on top of the fold (Pianetti quarry).

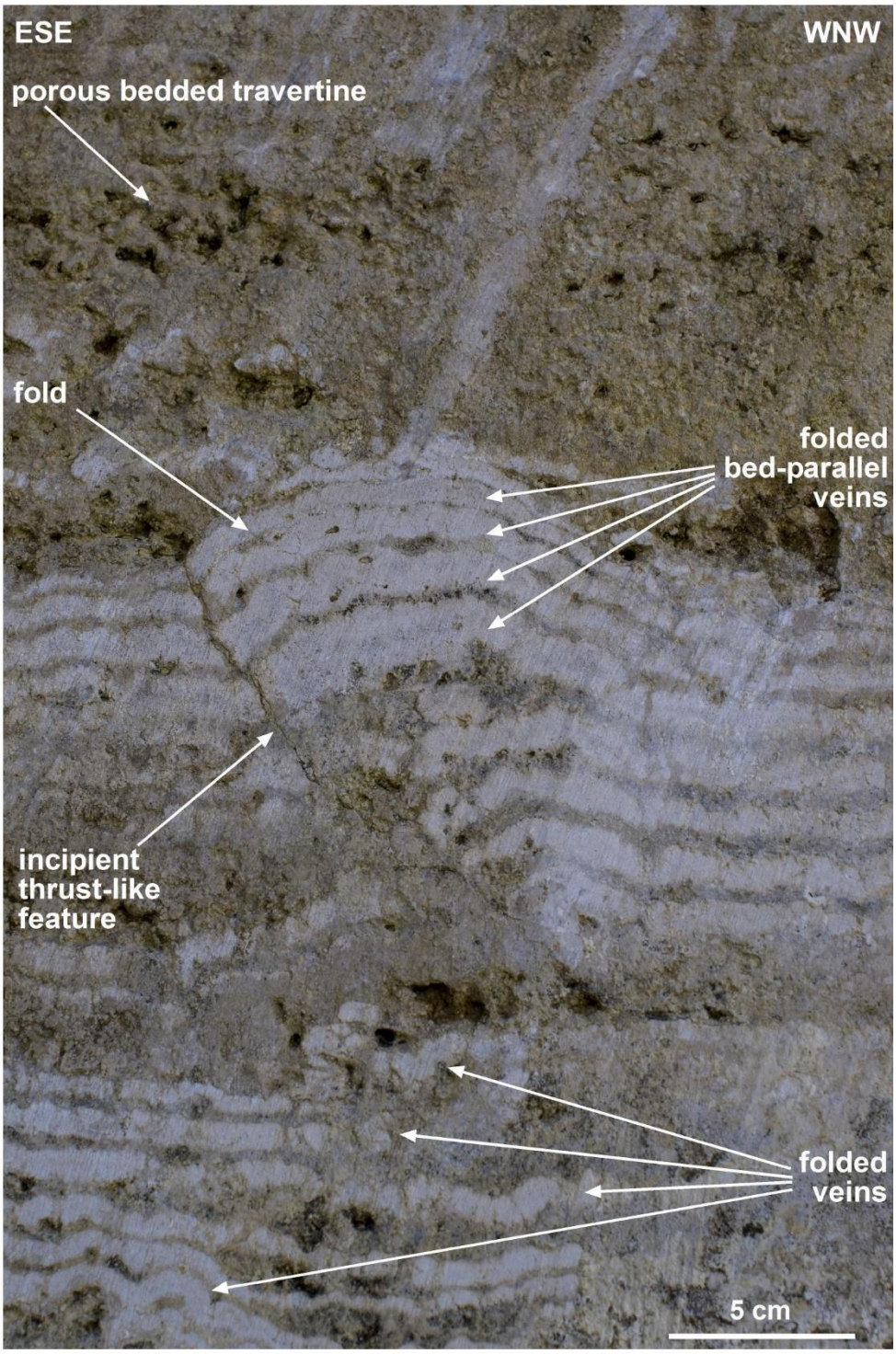

Figure DR24 – Photograph of an antiformal fold with an incipient thrust-like feature at the base. Note the occurrence of folded bed-parallel veins that form a sort of banded pattern. Note also the difference between the veined/banded travertine (below) and the porous bedded one on the top (Pian di Palma quarry).

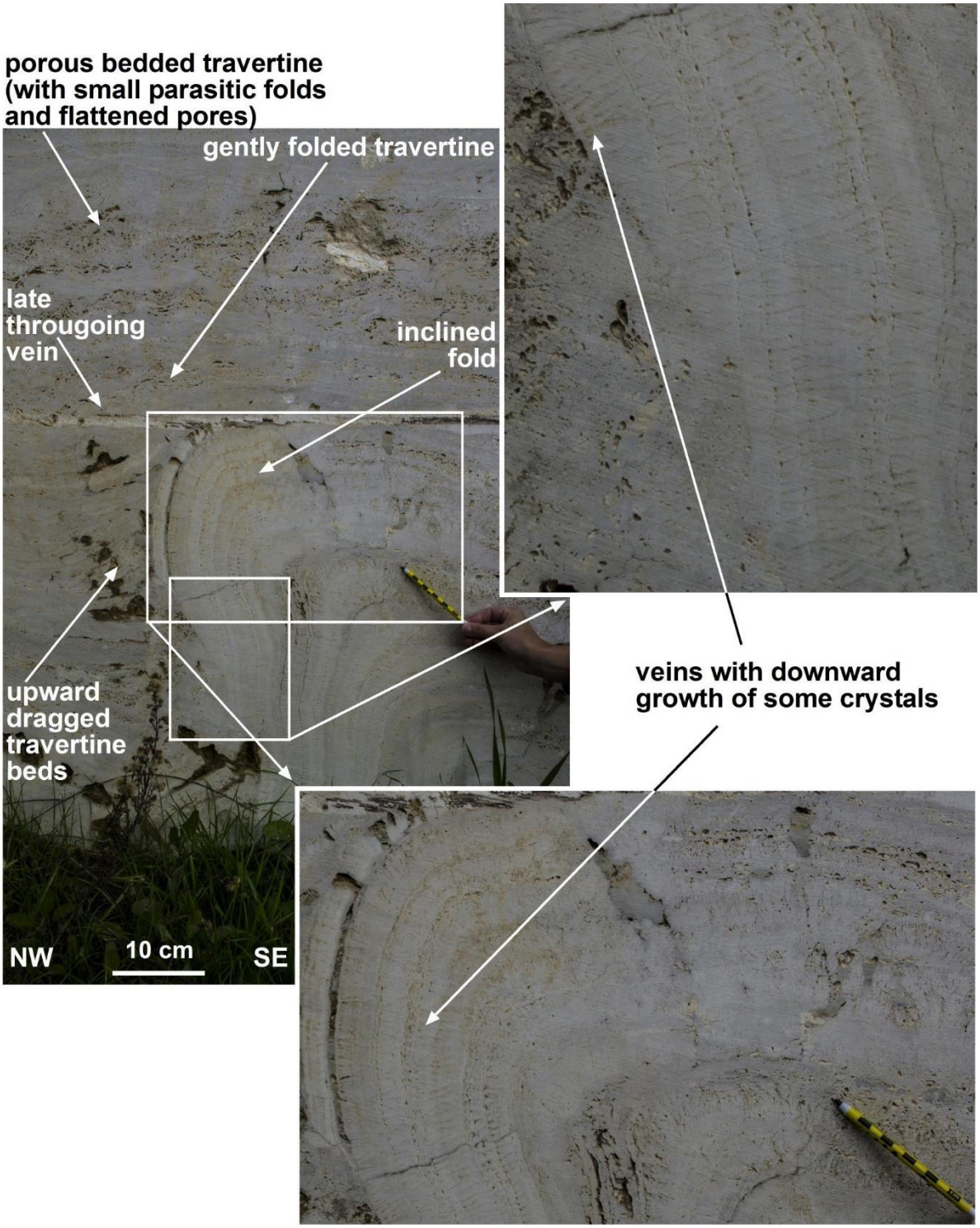

Figure DR25 – Photograph (with close ups in insets) of an overturned enterolithic fold. Note the complex pattern of deformation including upward dragged travertine beds outside the main fold, small parasitic folds in the travertine beds, and the occurrence of a late vein that cuts through the folds and the travertine beds. Note also the occurrence of veins (forming the main fold) characterized by a downward growth of crystals (Pianetti quarry).

Figure DR26 – Photograph of vein and folds. Note the complexity of deformation including also box-like folds and small parasitic folds in the overtunerd limbs of a larger anticline (Pianetti quarry). We thank our collegue G. Fellin (in the photograph) for her help in the field and laboratory.

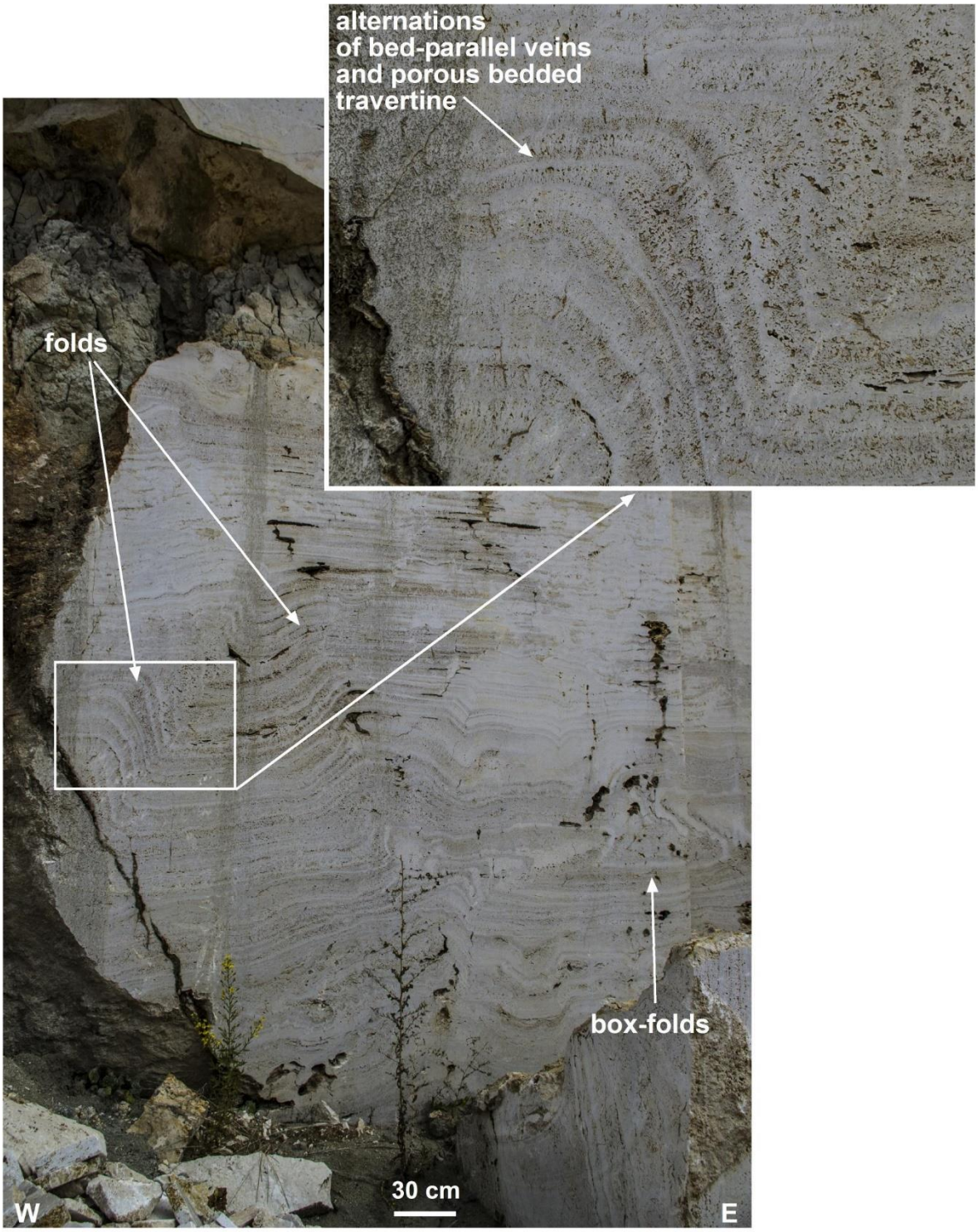

Figure DR27 – Photograph of travertine folds. Note the complexity of deformation including box-folds and alternations of folded porous travertine beds and nonporous bed-parallel white veins (Pianetti quarry).

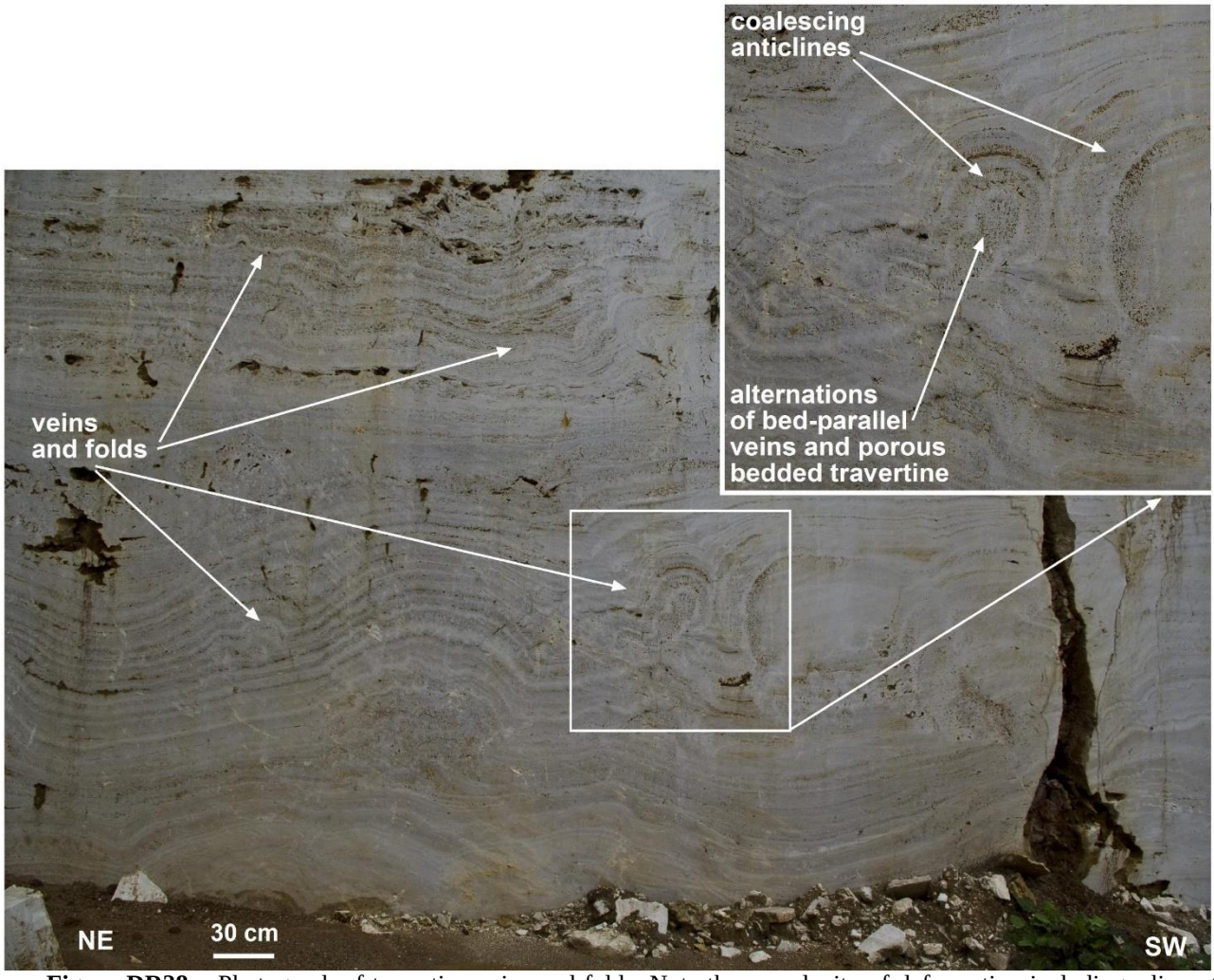

Figure DR28 – Photograph of travertine veins and folds. Note the complexity of deformation including adjacent coalescing anticlines (Pianetti quarry).

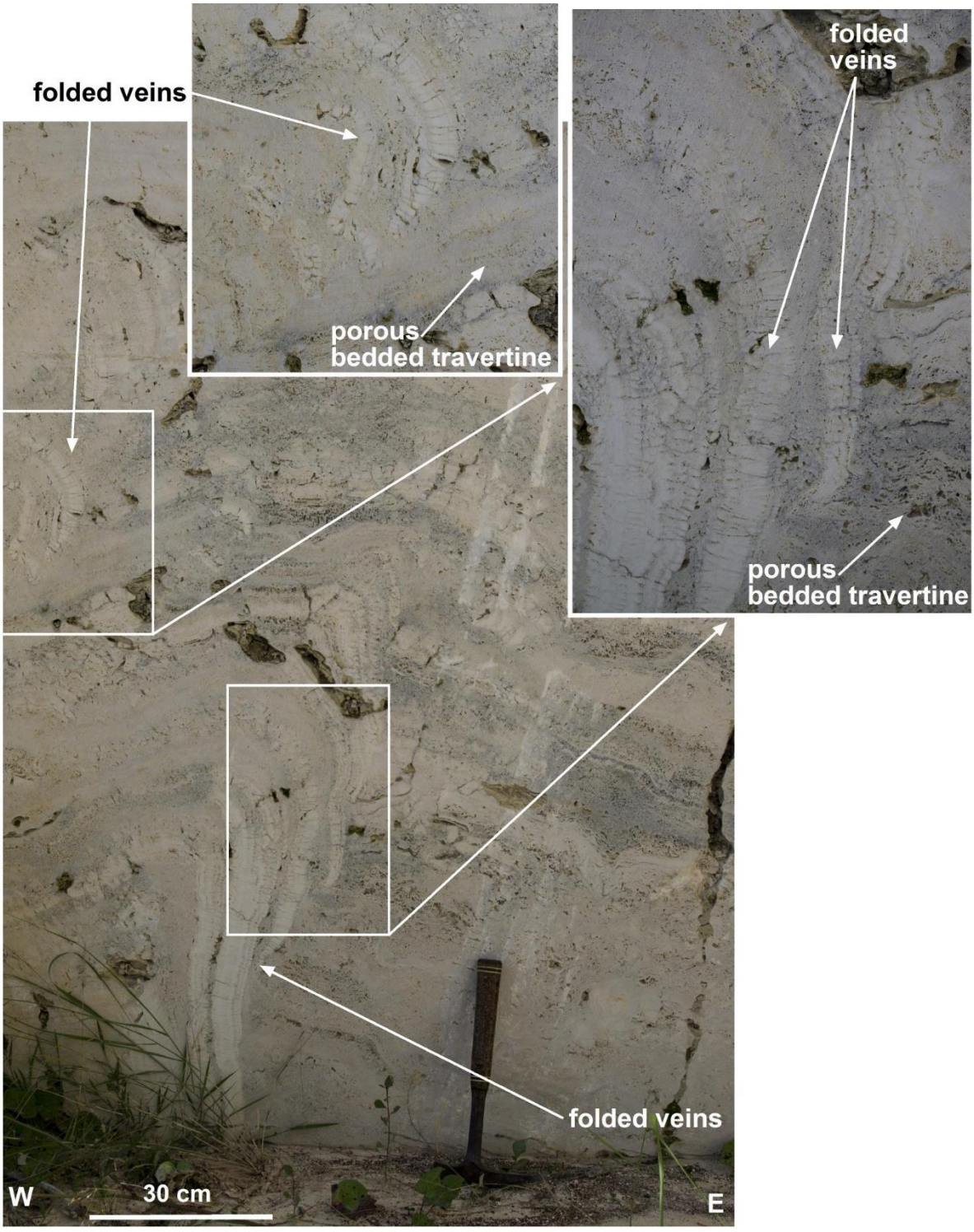

Figure DR29 – Photograph of inclined antiformal folds made of folded veins alternated with porous travertine beds. Fold hinges tend to be remarkably thickened with respect to the limbs. The anticlines tend to be inclined (almost overturned) over pre-existing porous travertine beds (Pianetti quarry).

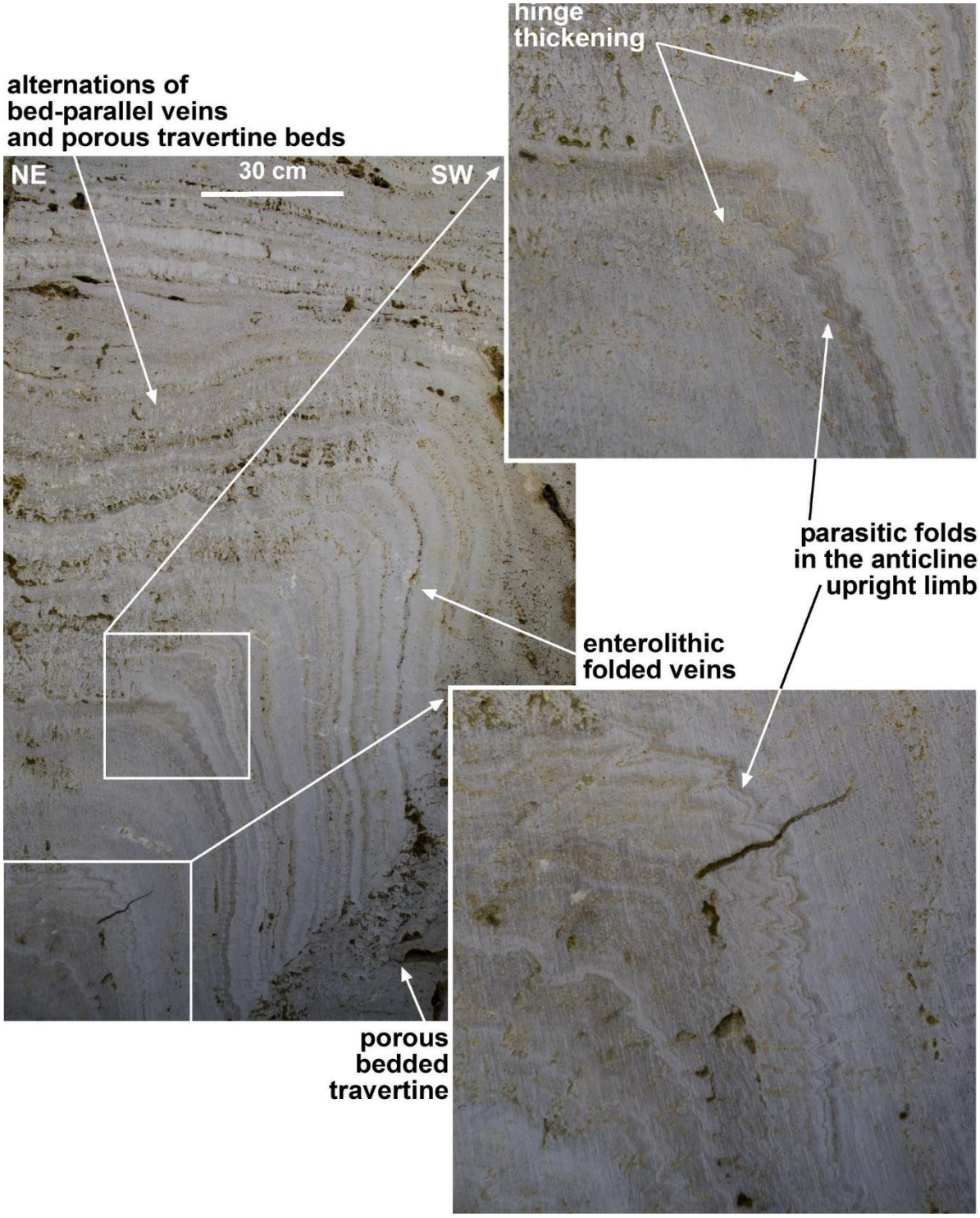

Figure DR30 – Photograph of an inclined antiformal fold made of folded veins. Note the presence of veins in the hinge and in one limb, and the presence of alternating veins and porous travertine bed in the other limb. Small parasitic folds occur in the hinge and limb with veins. The hinge is remarkably thickened with respect to the limbs (Pianetti quarry).

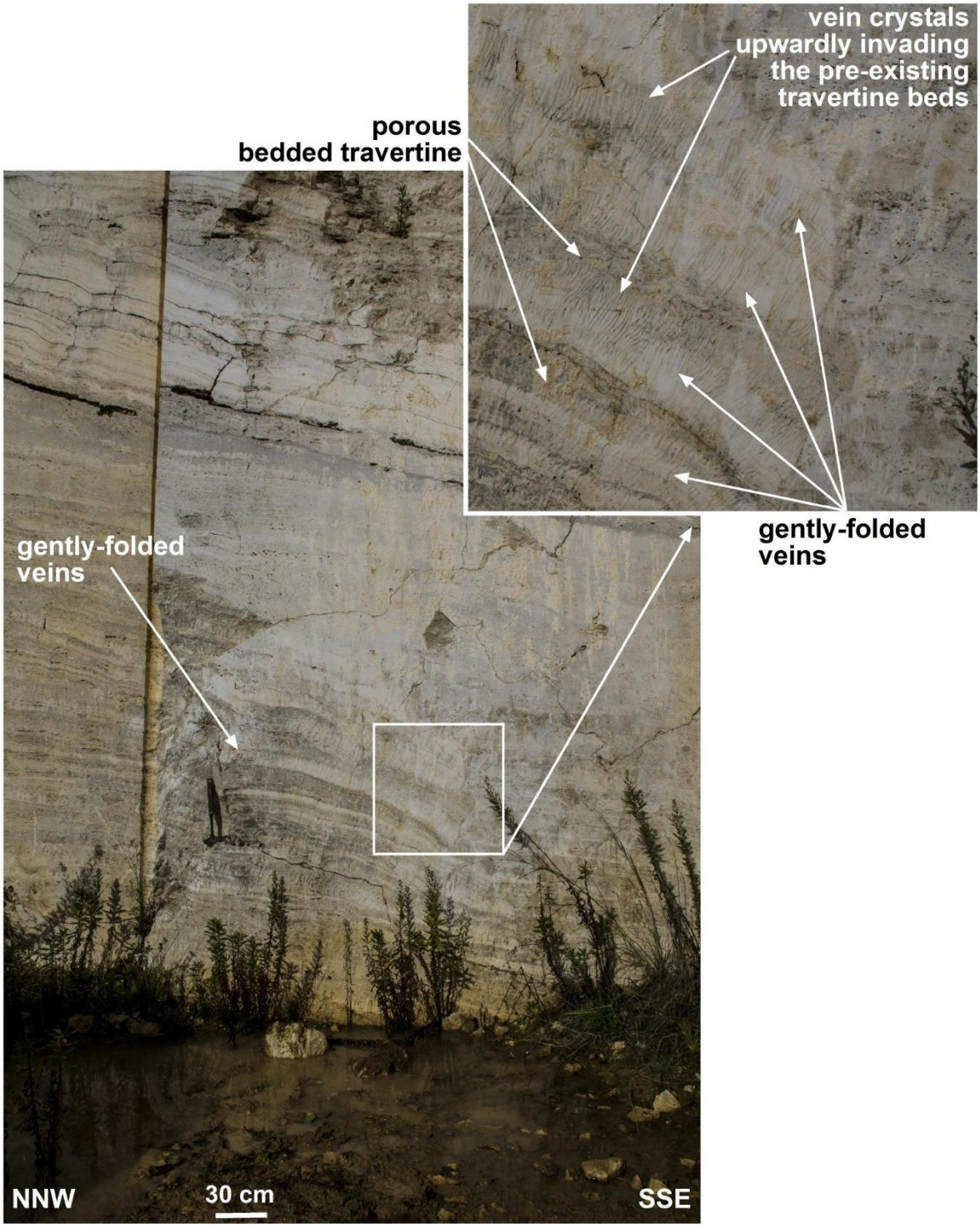

Figure DR31 – Photograph of white veins forming a bed-parallel banded pattern. The vein upward-grown crystals partly overprint and invade the adjacent (overlying) porous travertine beds (Pianetti quarry).

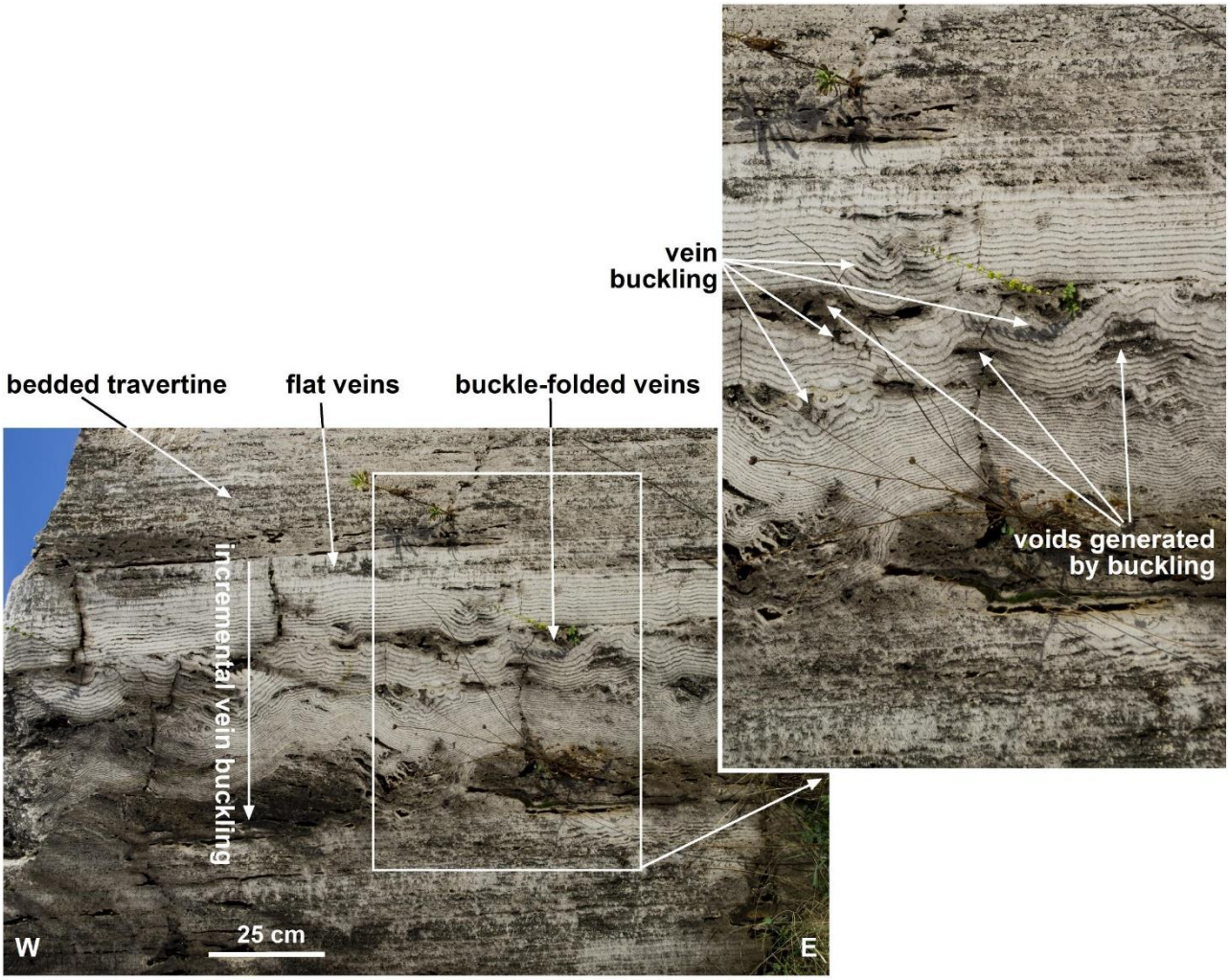

Figure DR32 – Photograph of white veins forming a bed-parallel banded pattern and a series of small buckle folds (Pian di Palma quarry).

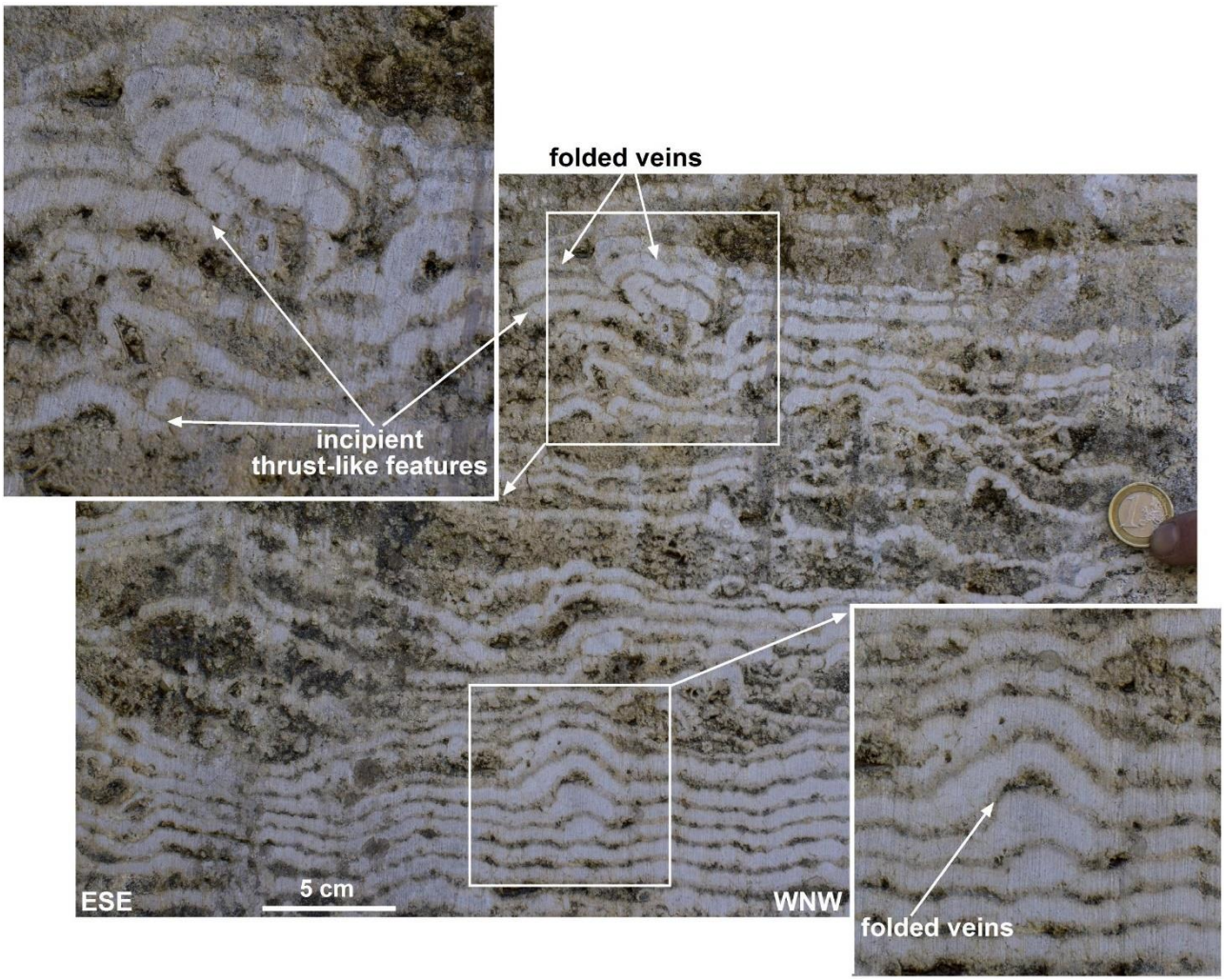

Figure DR33 – Photograph of white veins forming a bed-parallel banded pattern and a series of small folds (Pian di Palma quarry).

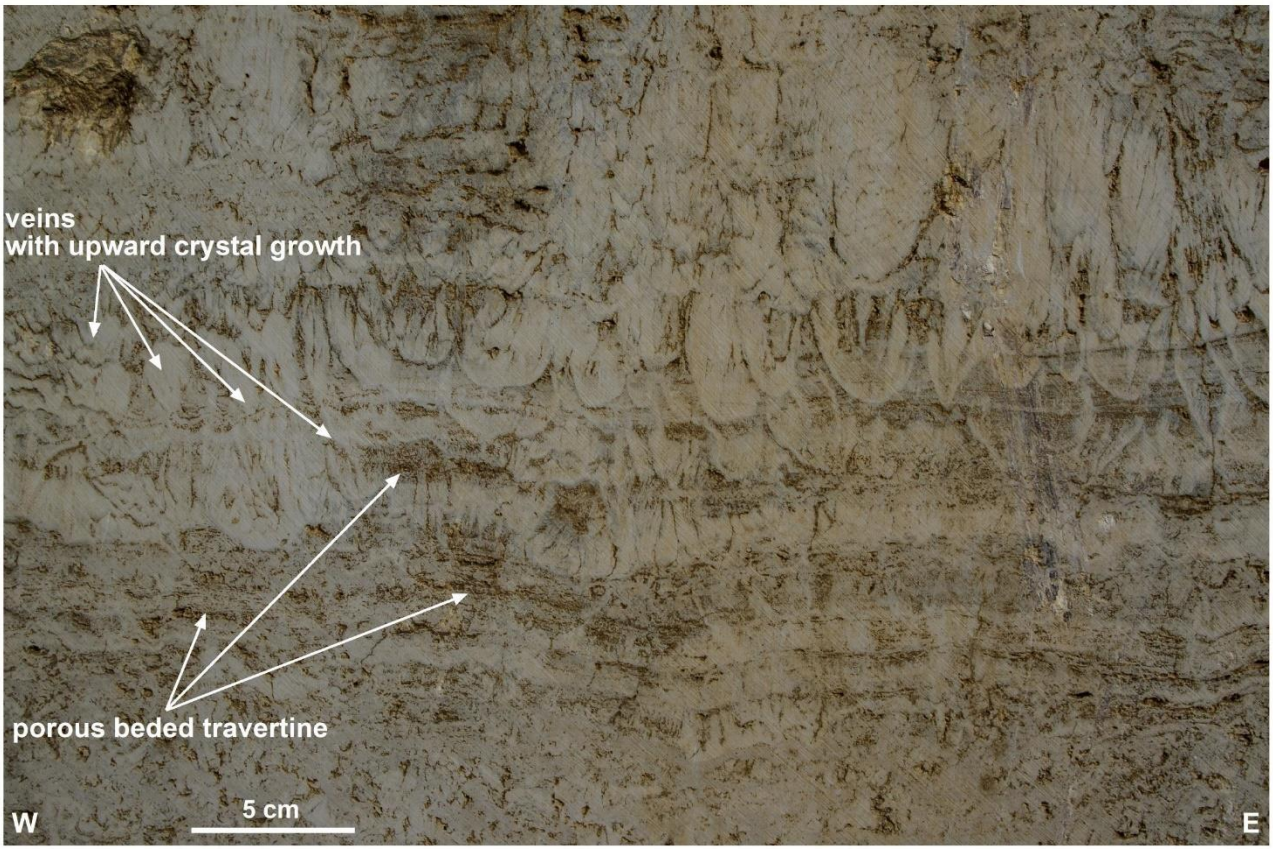

Figure DR34 – Photograph of porous bedded travertine largely overprinted by enterolithic veins characterized by upward growth of crystals. Note the undulating pattern of the originally horizontal travertine beds (Pianetti quarry).

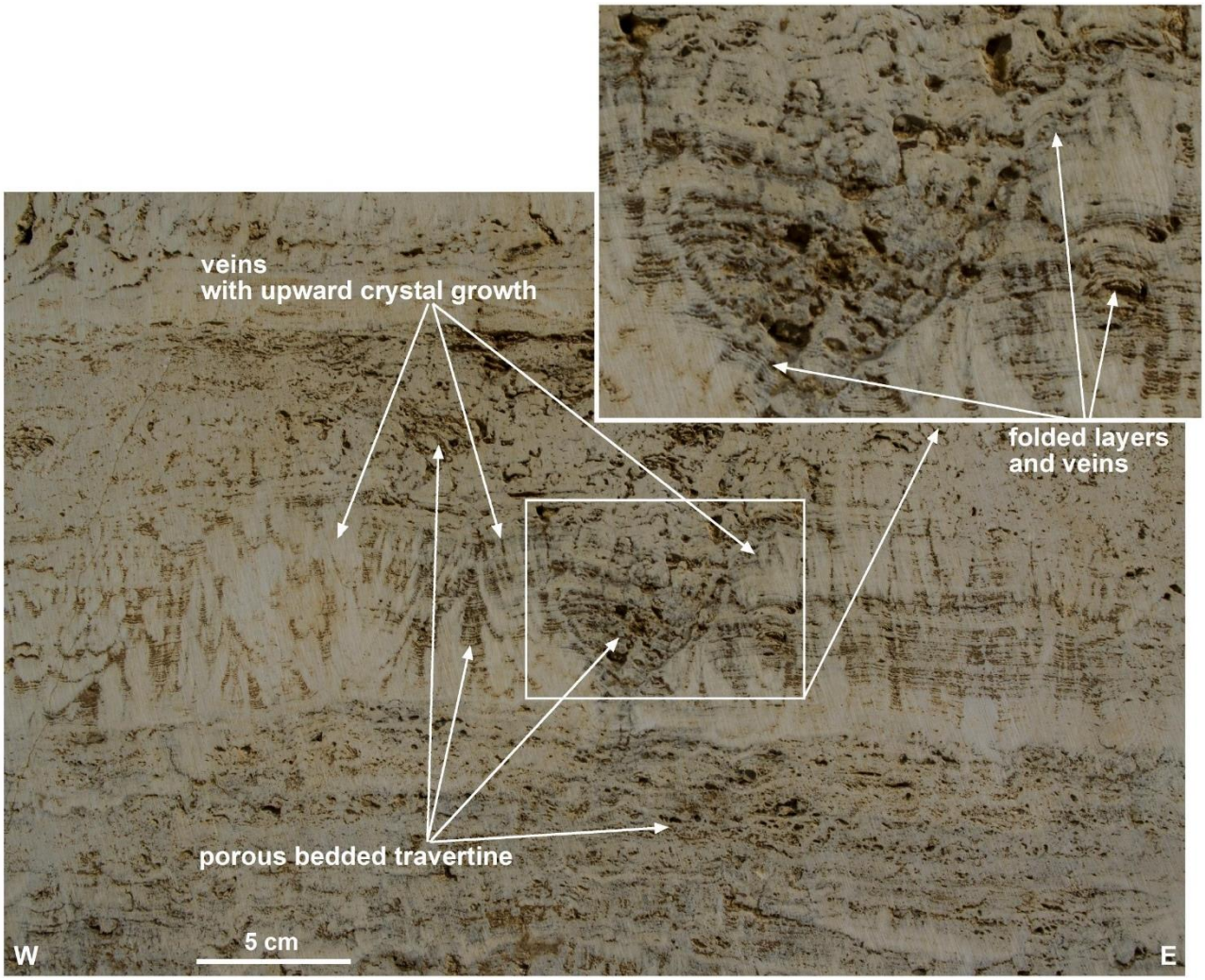

Figure DR35 – Photograph (with close up) of porous bedded travertine largely overprinted by veins characterized by upward growth of crystals. Note the undulating pattern of the originally-horizontal travertine beds (Pianetti quarry).

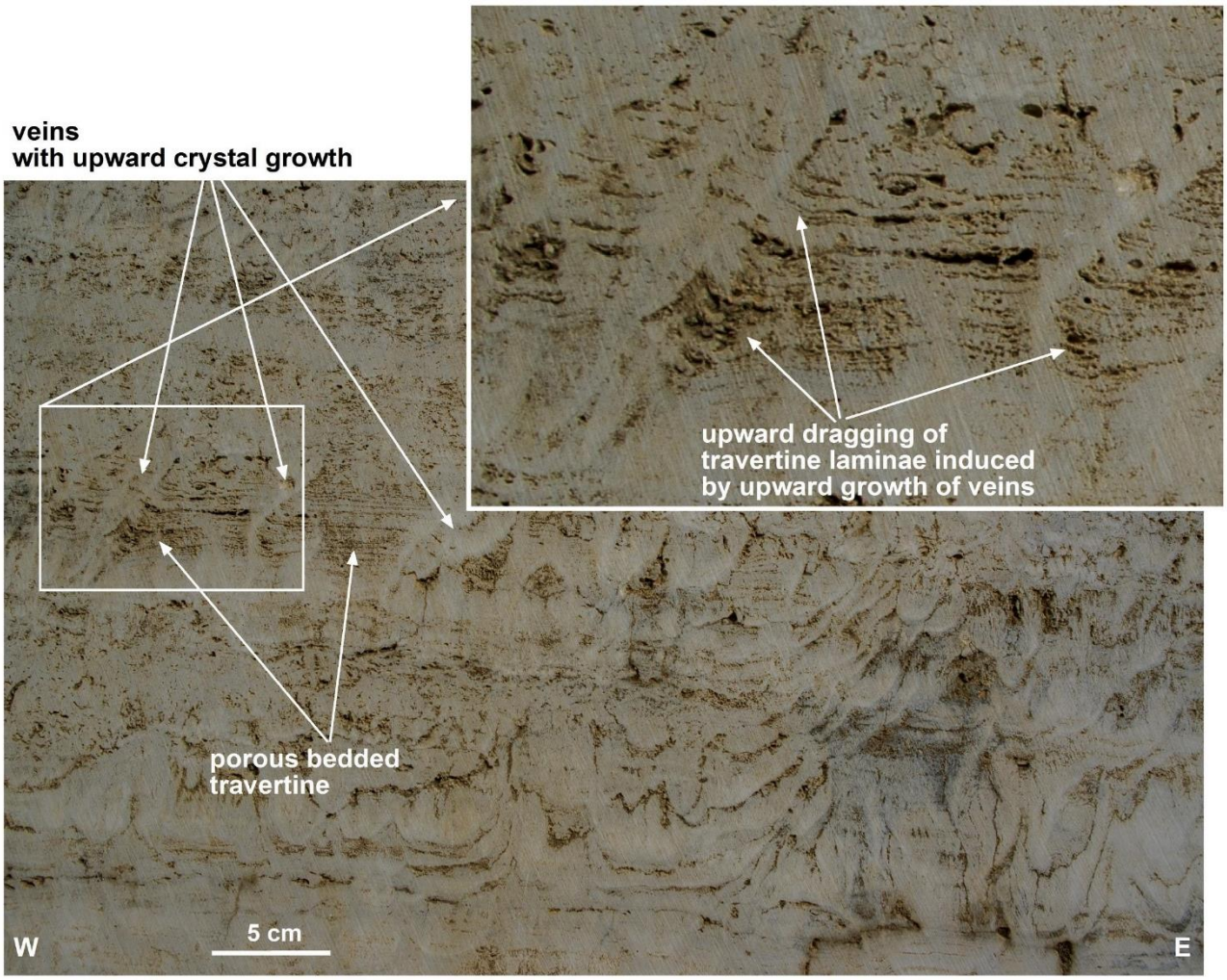

Figure DR35 – Photograph (with close up) of porous bedded travertine largely overprinted by veins characterized by upward growth of crystals. Note the undulating pattern of the originally-horizontal travertine beds (Pianetti quarry).

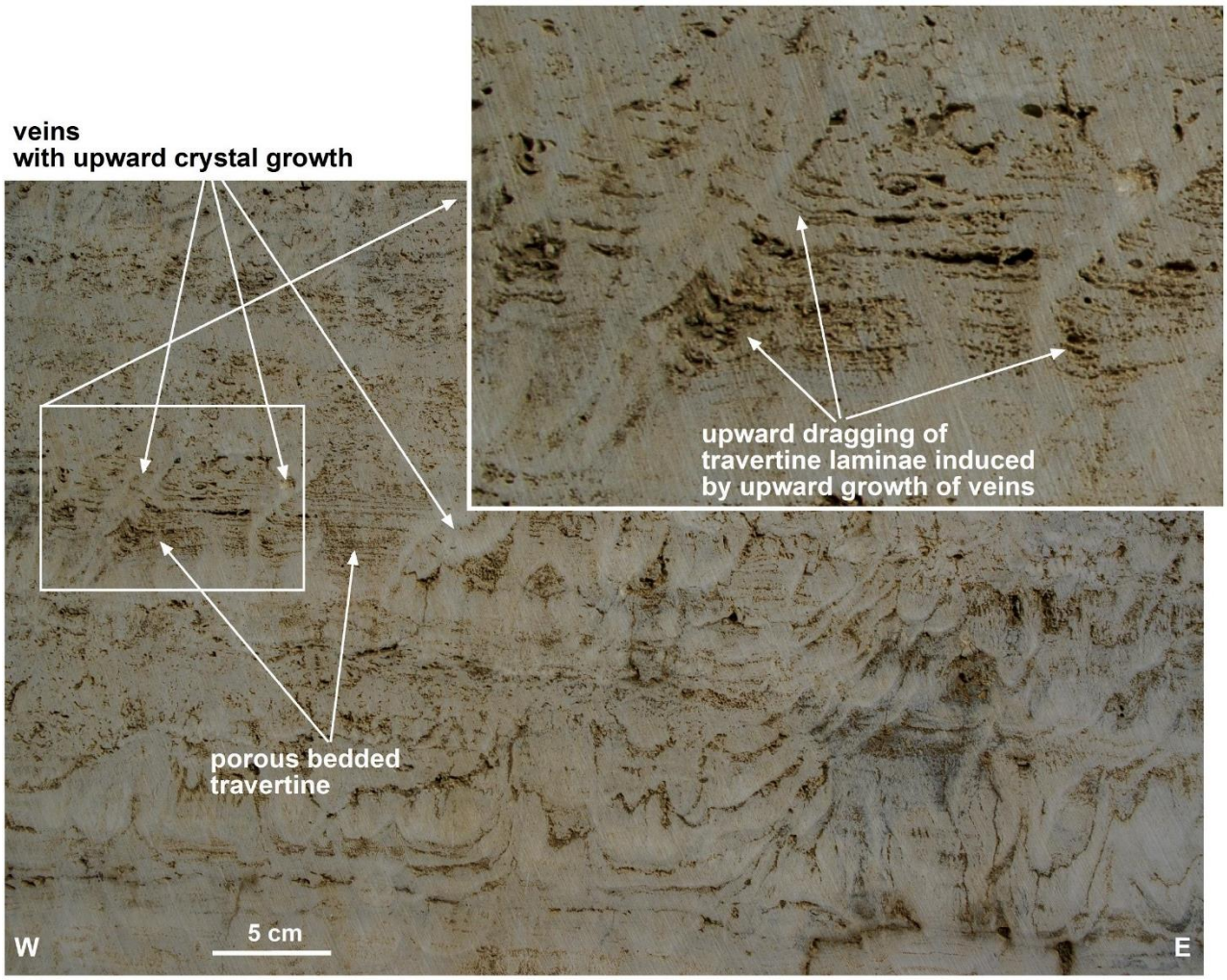

Figure DR36 – Photograph (with close up) of porous bedded travertine largely overprinted by veins characterized by upward growth of crystals. Note the undulating pattern of the originally-horizontal travertine beds. Travertine laminae along the upward-grown veins are upward dragged (Pianetti quarry).

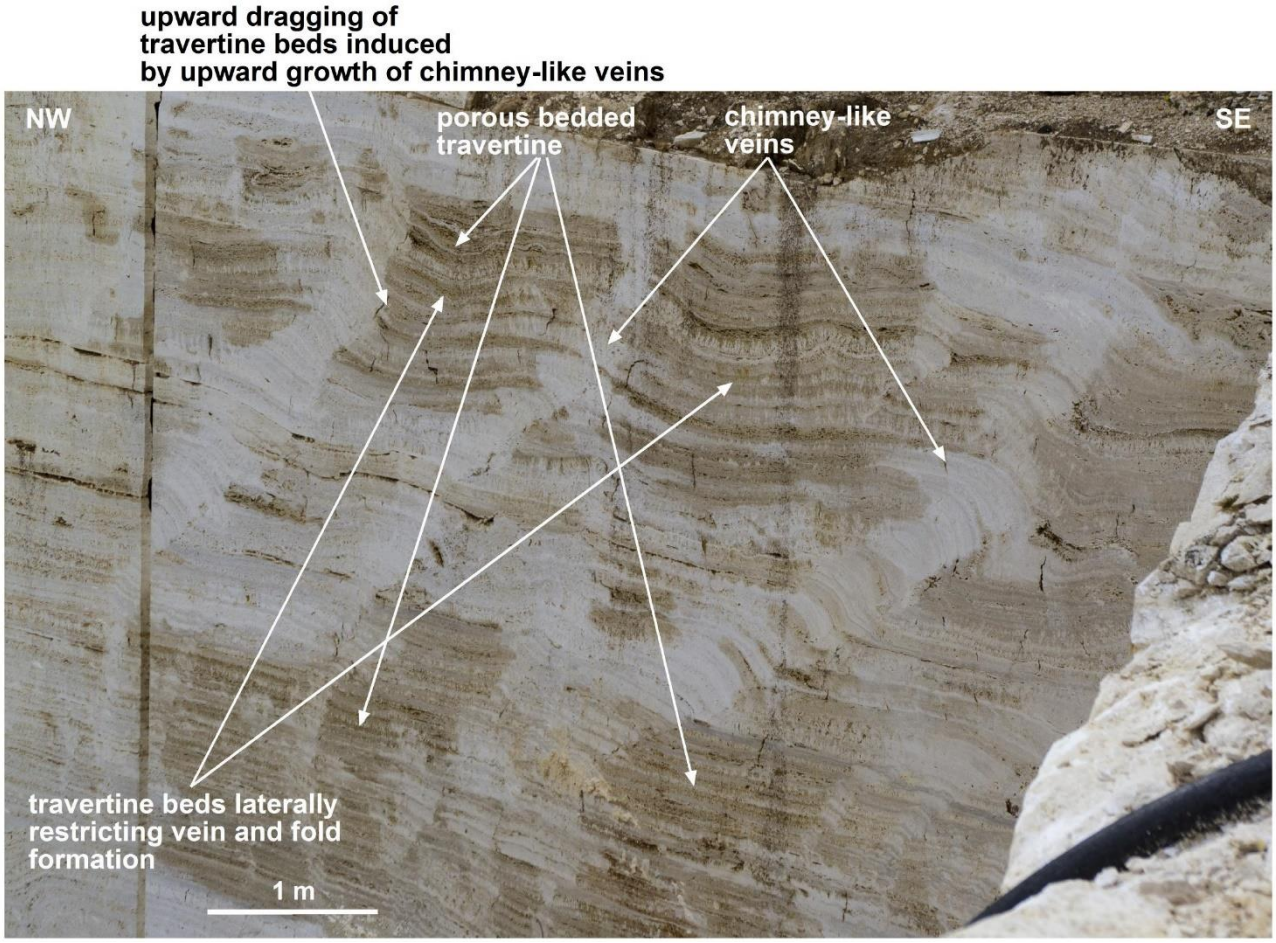

Figure DR37 – Photograph of porous bedded travertine largely overprinted by chimney-like veins. The travertine strata are gently folded and upward dragged along the veins (Pian di Palma quarry).

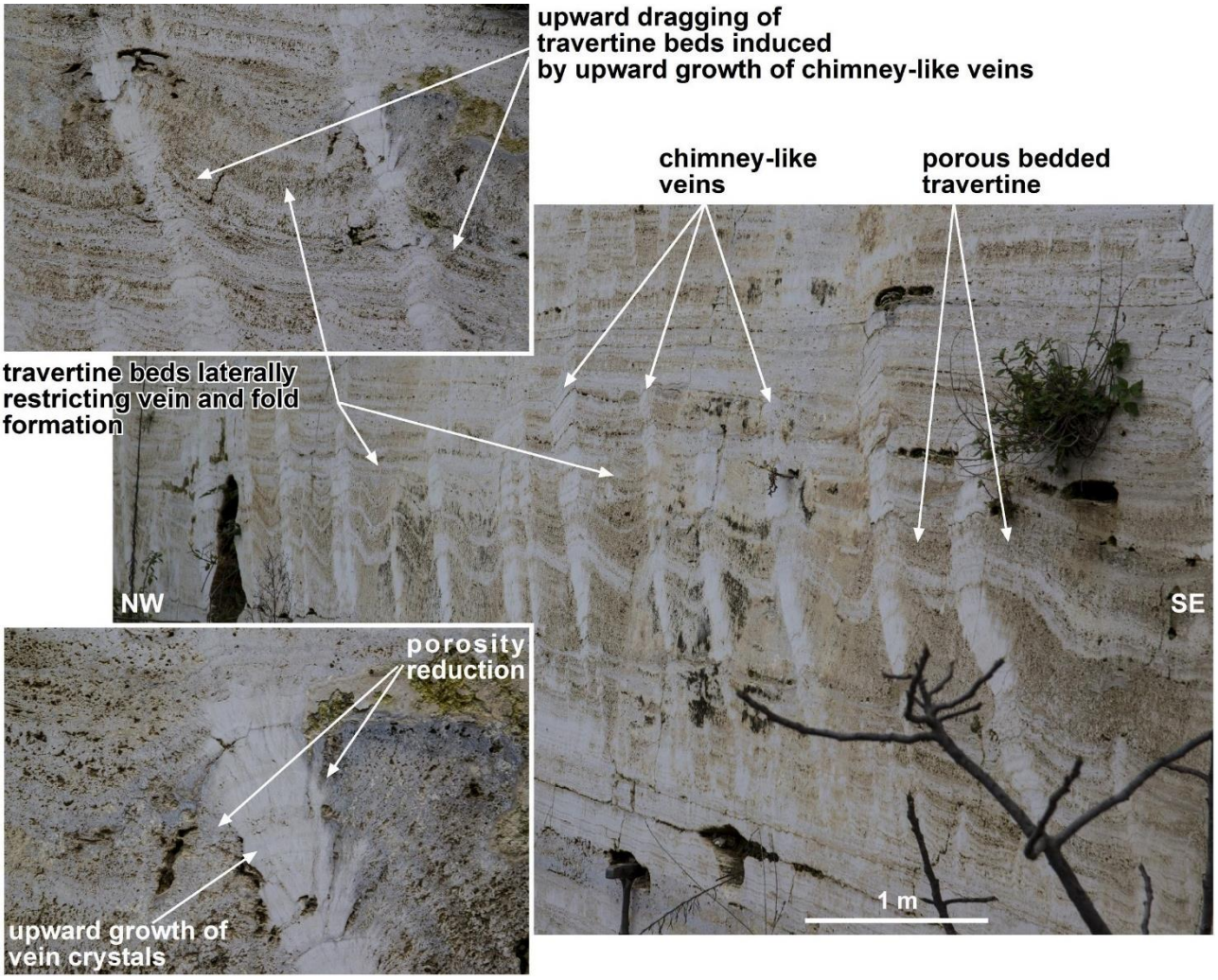

Figure DR38 – Photograph (with close ups in insets) of porous bedded travertine largely overprinted by enterolithic chimney-like veins. The travertine strata are gently folded and upward dragged along the veins. Close ups (insets) are from nearby exposures (Pian di Palma quarry).

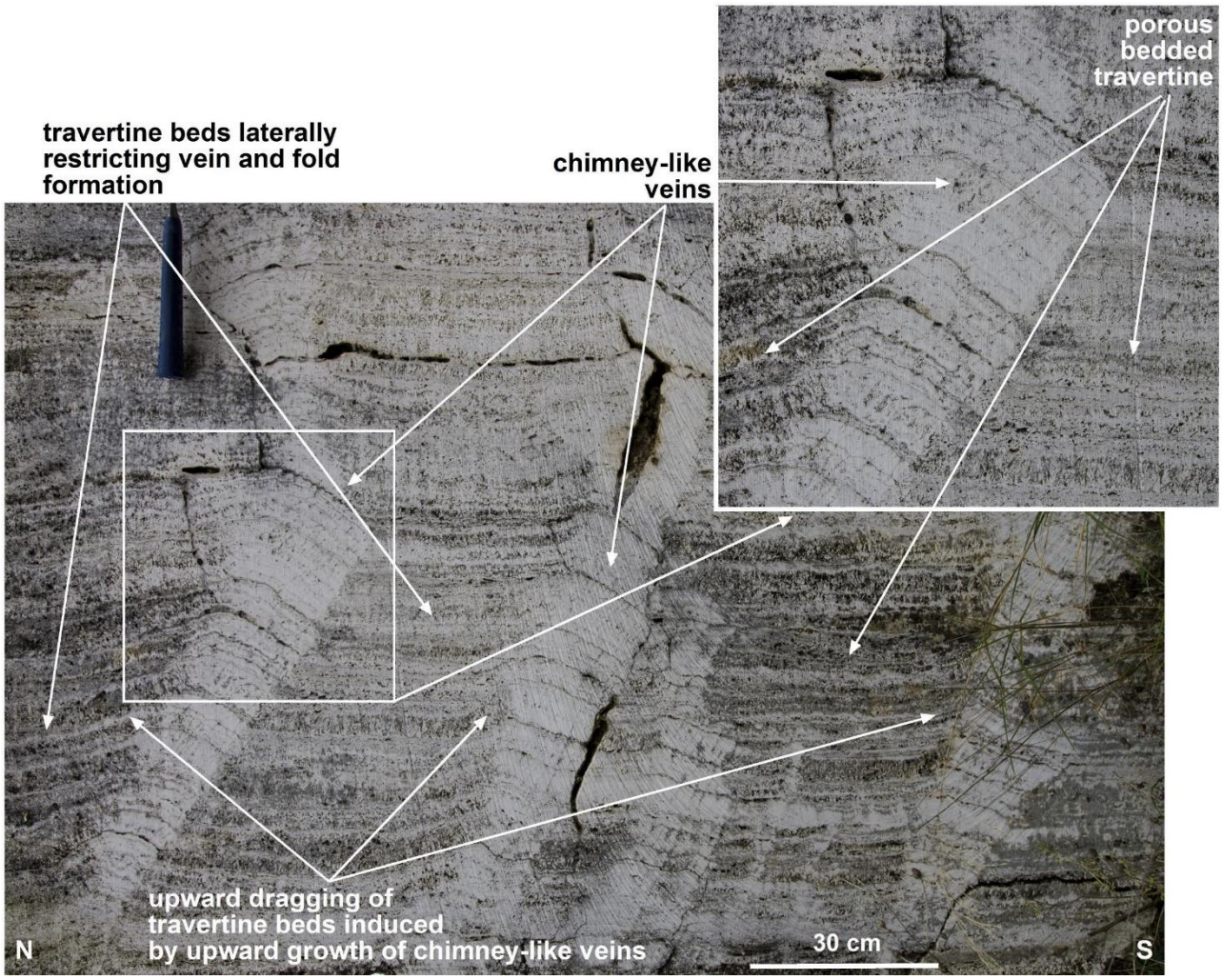

Figure DR39 – Photograph (with close up in inset) of porous bedded travertine largely overprinted by enterolithic chimney-like veins. The travertine strata are gently folded and upward dragged along the vein (Pian di Palma quarry).

Figure DR40 – Photograph (with close up in inset) of porous bedded travertine largely overprinted by enterolithic chimney-like veins. This is a map view (horizontal exposure) showing that the chimney-like veins and folds are sub-circular when viewed over horizontal exposures. Note the coalescence of structures (Pian di Palma quarry).

4.7.2. Additional table

Table DR1 - Uranium isotopic composition and ^{230}Th ages for 11 travertine samples from the Pianetti quarry. Samples are listed from top to bottom of the quarry, respecting their stratigraphic position (Fig. 3). Samples marked with * were analysed through MC-ICP-MS. Age correction were calculated using an estimated atomic $^{230}Th/^{232}Th$ ratio of 4 ± 2 ppm, which is the value typical of a material at secular equilibrium with the crustal $^{232}Th/^{238}U$ value of 3.8. The errors are arbitrarily assumed to be 50%. Samples marked with ** were analysed through alpha spectrometry. The ($^{230}Th/^{234}U$) was corrected using the crustal thorium mean composition of 0.85 ± 0.36 (Wedephol. 1995) for samples with a $^{230}Th/^{232}Th$ activity ratio lower than 80.

Sample	Rock Type	U (ppb)	$\delta^{234}U$ (measured)	$[^{230}Th/^{238}U]$ (activity)	$[^{230}Th/^{232}Th]$ (ppm)	$\delta^{234}U_{initial}$ (corrected)	$[^{230}Th/^{232}Th]$ (activity)	$[^{234}U/^{238}U]$ (activity)	$[^{230}Th/^{234}U]$ (activity)	$[^{230}Th/^{234}U]$ (corrected)	Age (ka)
ST4**	bedded travertine	22 ± 2					1.226 ± 0.081	1.361 ± 0.073	0.785 ± 0.041	0.648 ± 0.056	107 ± 15
ST3**	vein	311 ± 13					139.38 ± 56.28	1.074 ± 0.028	0.566 ± 0.046		90 ± 11
CP13_1-5*	vein	16.092 ± 0.030	176.2 ± 5.4	1.005 ± 0.024	13.93 ± 0.34	279 ± 17					163 ± 19
CP13_1-4*	vein	10.644 ± 0.032	225.2 ± 7.1	1.046 ± 0.024	20.28 ± 0.47	363 ± 18					169 ± 14
ST1_sp1**	speleothem	30.2 ± 2.7					15.027 ± 5.491	1.283 ± 0.132	0.136 ± 0.017	0.130 ± 0.050	15 ± 6
ST1**	vein	45 ± 3					5.832 ± 0.482	1.196 ± 0.035	0.746 ± 0.037	0.716 ± 0.072	130 ± 23
CP14_25*	bedded travertine	197.16 ± 0.41	55.8 ± 2.5	0.9853 ± 0.0036	2476 ± 20	120.8 ± 5.8					274 ± 6
CP14_5*	vein	107.81 ± 0.19	32.7 ± 2.8	1.0084 ± 0.0034	4004 ± 92	92.3 ± 8.8					368 ± 14
CP14_2*	vein	106.64 ± 0.19	42.0 ± 2.5	0.9652 ± 0.0033	2792 ± 37	89.8 ± 5.4					269 ± 5
CP15_1*	vein	83.93 ± 0.12	65.3 ± 2.2	1.0353 ± 0.0033	3678 ± 73	166.6 ± 7.0					332 ± 9
CP15_8*	vein	519.88 ± 0.57	36.8 ± 1.2	0.9290 ± 0.0017	15305 ± 264	72.0 ± 2.5					238 ± 2

4.7.3. Additional figures

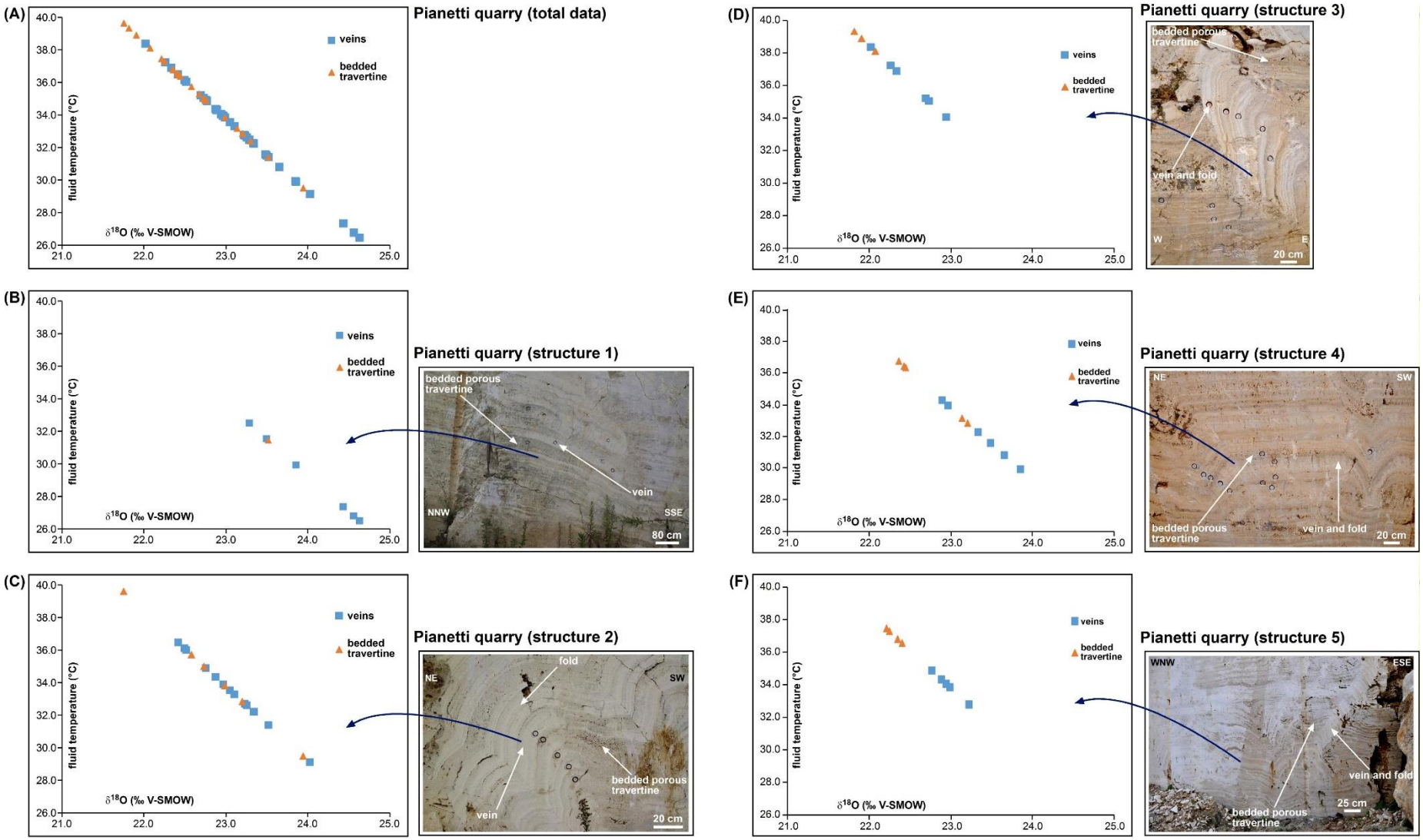

Figure DR41 – Parental fluid temperatures vs $\delta^{18}O$ (V-SMOW) diagrams for samples from the Pianetti quarry. (A) Total data (same as Fig. 4.5A). (B) to (F) Data for samples collected in the structures (veins vs. host bedded travertine) shown in adjacent photograms.

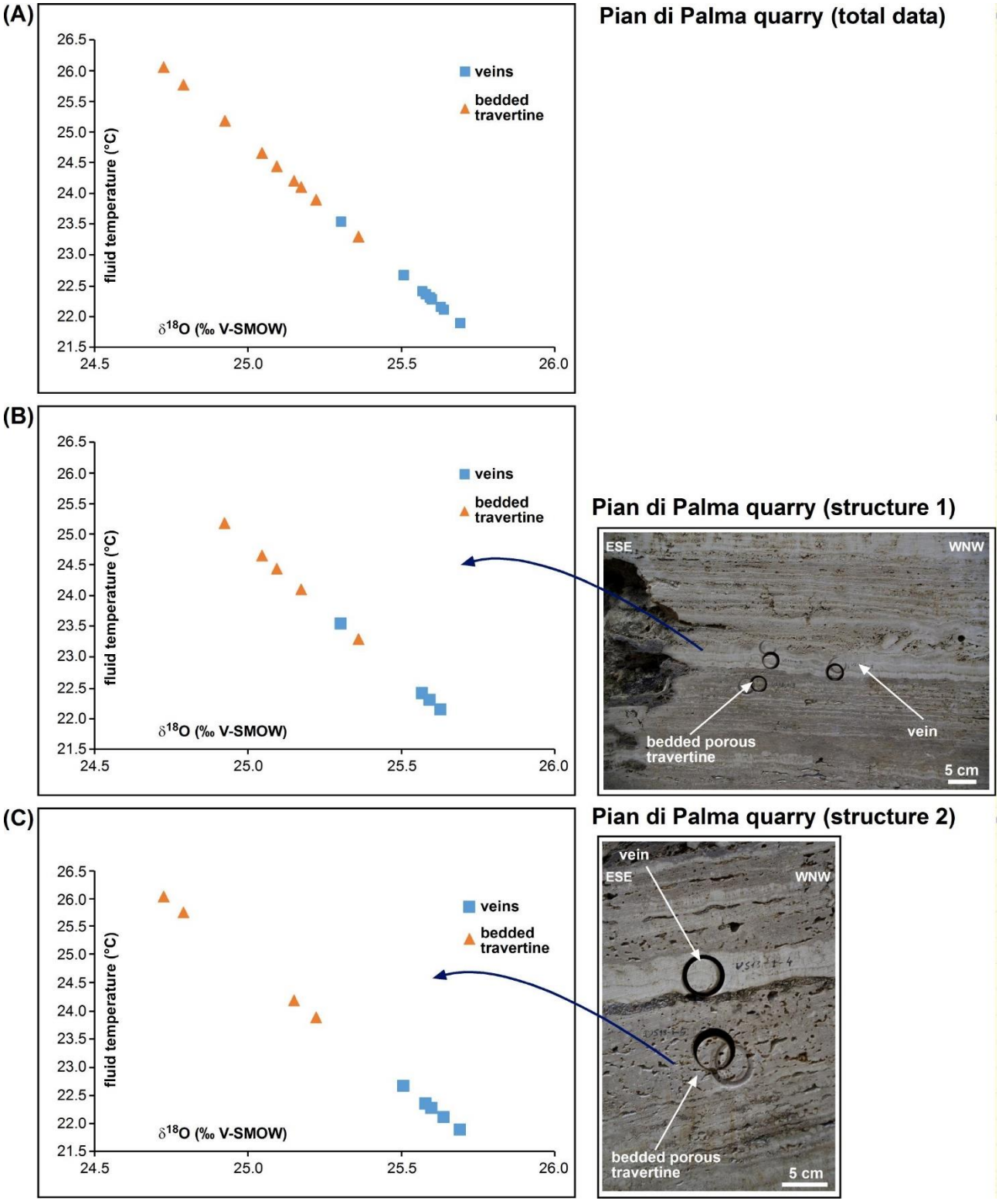

Figure DR42 – Parental fluid temperatures vs $\delta^{18}O$ (V-SMOW) diagrams for samples from the Pian di Palma quarry. (A) Total data. (B) and (C) Data for samples collected in the structures (veins vs. host bedded travertine) shown in adjacent photograms.

4.8. References

Acocella V., Funiciello R., 2006, Transverse systems along the extensional Tyrrhenian margin of central Italy and their influence on volcanism. Tectonics, 25, TC2003, doi: 10.1029/2005TC001845.

Aref M.A.M., Attia O.E.A., Wali A.M.A., 1997, Facies and depositional environment of the Holocene evaporites in the Ras Shukeir area, Gulf of Suez, Egypt: Sedimentary Geology, v. 110, p. 123-145.

Bargar K.E., 1978, Geology and thermal history of Mammoth Hot Springs, Yellowstone National Park, Wyoming: U.S. Geological Survey Bulletin, v. 1444, p. 1-55.

Beasley C.J., Fiduk J.C., Bize E., Boyd A., Frydman M., Zerilli A., Dribus J.R., Moreira J.L.P., Capeliero Pinto, A.C., 2010, Brazil's subsalt play: Oilfield Review, v. 22, p. 28-37.

Bickle M., Kampman N., 2013, Lessons in carbon storage from geological analogues: Geology, v. 41, p. 525-526.

Billi A., Valle A., Brilli M., Faccenna C., Funiciello R., 2007, Fracture-controlled fluid circulation and dissolutional weathering in sinkhole-prone carbonate rocks from central Italy: Journal of Structural Geology, v. 29, p. 385-395.

Biot,M.A., 1964, Theory of internal buckling of a confined multilayered structure: Geological Society of America Bulletin, v. 75, p. 563-568.

Bosi C., Messina P., Rosati M., Sposato A., 1996, Età dei travertini della Toscana meridionale e relative implicazioni neotettoniche: Memorie della Società Geologica Italiana, v. 51, p. 293-304.

Bossio A., Foresi L.M., Mazzei R., Salvatorini G., Sandrelli F., Bilotti M., Colli A., Rossetto R., 2003, Geology and stratigraphy of the southern sector of the Neogene Albegna River Basin (Grosseto, Tuscany, Italy): Geologica Romana, v. 37, p. 165-173.

Breitenbach S.F.M., Bernasconi S.M., 2011, Carbon and oxygen isotope analysis of small carbonate samples (20 to 100 µg) with a GasBench II preparation device: Rapid Communications in Mass Spectrometry, v. 25, p. 1910-1914.

Brogi A., 2008, The structure of the Monte Amiata volcano-geothermal area (Northern Apennines, Italy): Neogene-Quaternary compression versus extension: International Journal of Earth Sciences, v. 97, p. 677-703.

Brogi A., Capezzuoli E., 2009, Travertine deposition and faulting: the fault-related travertine fissure-ridge at Terme S. Giovanni, Rapolano Terme (Italy): International Journal of Earth Sciences, v. 98, p. 931–947.

Brogi A., Capezzuoli E., Buracchi E., Branca M., 2012. Tectonic control on travertine and calcareous tufa deposition in a low-temperature geothermal system (Sarteano, Central Italy): Journal of Geological Society, London, v. 169, p.461-476.

Brogi A., Capezzuoli E., 2014, Earthquake impact on fissure-ridge type travertine deposition: Geological Magazine, v. 151, p. 1135-1143.

Brogi A., Capezzuoli E., Liotta D., Meccheri M., 2015, The Tuscan Nappe structures in the Monte Amiata geothermal area (central Italy): a review: Italian Journal of Geosciences, v. 134, p. 219-236.

Cadoux A., Pinti D.L., 2009, Hybrid character and pre-eruptive events of Mt Amiata volcano (Italy) inferred from geochronological, petro-geochemical and isotopic data: Journal of Volcanology and Geothermal Research, v. 179, p. 169-190.

Burnside N.M., Shipton Z.K., Dockrill B., Ellam R.M., 2013, Man-made versus natural CO_2 leakage: A 400 k.y. history of an analogue for engineered geological storage of CO_2: Geology, v. 41, p. 471-474.

Carmignani L., Decandia F.A., Fantozzi P.L., Lazzarotto A., Liotta D., Meccheri M., 1994, Tertiary extensional tectonics in Tuscany (Northern Apennines, Italy): Tectonophysics, v. 238, p. 295-315.

Carmignani L., Conti P., Cornamusini G., Pirro A., 2013, Geological map of Tuscany (Italy): Journal of Maps, v. 9, p. 487-497.

Cipollari P., Cosentino D., 1995, Miocene unconformities in the Central Apennines: geodynamic significance and sedimentary basin evolution: Tectonophysics, v. 252, p. 375-389.

Collettini C., De Paola N., Holdsworth R.E., Barchi M.R., 2006, The development and behavior of low-angle normal faults during Cenozoic asymmetric extension in the Northern Apennines, Italy: Journal of Structural Geology, v. 28, p. 333-352.

Crossey L.J., Fischer T.P., Patchett P.J., Karlstrom K.E., Hilton D.R., Newell D.L., Huntoon P., Reynolds A.C., de Leeuw G.A.M., 2006, Dissected hydrologic system at the Grand Canyon: interaction between deeply derived fluids and plateau aquifer waters in modern springs and travertine: Geology, v. 34, p. 25–28.

Crossey, L.J., Karlstrom, K.E., Springer, A.E., Newell, D., Hilton, D.R., Fischer, T., 2009, Degassing of mantle-derived CO2 and He from springs in the southern Colorado Plateau region - neotectonic connections and implications for groundwater systems: Geological Society of America Bulletin, v. 121, p. 1034–1053.

De Filippis L., Billi A., 2012, Morphotectonics of fissure ridge travertines from geothermal areas of Mammoth Hot Springs (Wyoming) and Bridgeport (California): Tectonophysics, v. 548–549, p. 34–38.

De Filippis L., Anzalone E., Billi A., Faccenna C., Poncia P.P., Sella P., 2013a, The origin and growth of a recently-active fissure ridge travertine over a seismic fault, Tivoli, Italy: Geomorphology, v. 195, p. 13-26.

De Filippis L., Faccenna C., Billi A., Anzalone E., Brilli M., Soligo M., Tuccimei P., 2013b, Plateau versus fissure ridge travertines from Quaternary geothermal springs of Italy and Turkey: interactions and feedbacks among fluid discharge, paleoclimate, and tectonics: Earth-Science Reviews, v. 123, p. 35-52.

Demeny A., Kele S., Siklosy Z., 2010, Empirical equations for the temperature dependence of calcite-water oxygen isotope fractionation from 10 to 70 degrees C: Rapid Communications in Mass Spectrometry, v. 24, p. 3521-3526.

Doglioni C., 1991, A proposal for the kinematic modelling of W-dipping subduction - possible applications to the Tyrrhenian-Apennines system: Terra Nova, v. 3, p. 423-434.

Faccenna C., Soligo M., Billi A., De Filippis L., Funiciello R., Rossetti C., Tuccimei P., 2008, Late Pleistocene depositional cycles of the Lapis Tiburtinus travertine (Tivoli, central Italy): possible influence of climate and fault activity: Global and Planetary Change, v. 63, p. 299-308.

Edwards R.L., Chen J.H., Wasserburg G.J., 1987, ^{238}U–^{234}U–^{230}Th systematics and the precise measurement of time over the last 500,000 years: Earth and Planetary Science Letters, v. 81, p. 175–192.

Ludwig K.R., 2003, Isoplot/Ex version 3.00. A Geochronological Toolkit for Microsoft Excel. Berkeley Geochronology Center Special Publication, v. 4, 73 p.

Frery E., Gratier J.-P., Ellouz-Zimmerman N., Loiselet C., Braun J., Deschamps P., Blamart D., Hamelin B., Swennen R., 2015, Evolution of fault permeability during episodic fluid circulation: Evidence for the effects of fluid–rock interactions from travertine studies (Utah–USA): Tectonophysics, v. 651–652, p. 121-137.

Gandin A., Capezzuoli E., 2008, Travertine versus calcareous tufa: distinctive petrologic features and stable isotopes signatures: Italian Journal of Quaternary Science, v. 21, p. 125-136.

Gratier J.-P., Frery E., Deschamps P., Røyne A., Renard F., Dysthe D., Ellouz-Zimmerman N., Hamelin B., 2012, How travertine veins grow from top to bottom and lift the rocks above them: the effect of crystallization force: Geology, v. 40, p. 1015–1018.

Güdogan I., Önal M., Depçi T., 2005, Sedimentology, petrography and diagenesis of Eocene–Oligocene evaporites: the Tuzhisar Formation, SW Sivas Basin, Turkey: Journal of Asian Earth Sciences, v. 25, p. 791–803.

Hancock P.L., Chalmers R.M.L., Altunel E., Çakir Z., 1999, Travitonics: using travertine in active fault studies: Journal of Structural Geology, v. 21, p. 903–916.

Hilgers C., Urai J.L., 2005, On the arrangement of solid inclusions in fibrous veins and the role of the crack-seal mechanism: Journal of Structural Geology, v. 27, p. 481–494.

Jin J., Bergman K.M., 1999, Sequence stratigraphy of the Middle Devonian Winnipegosis carbonate-Prairie Evaporite transition, southern Elk Point Basin. Carbonates and Evaporites, v. 14, p. 64-83.

Jin J., Bergman K.M., 2001, Revised stratigraphy of the Middle Devonian (Givetian) Winnipegosis Carbonate-Prairie Evaporite Transition, Elk Point Group, southern Saskatchewan: Bulletin of Canadian Petroleum Geology, v. 49, p. 441-457.

Jolivet L., Faccenna C., Goffé B., Mattei M., Rossetti F., Brunet C., Storti F., Funiciello R., Cadet J.-P., D'Agostino N., Parra T., 1998, Midcrustal shear zones in post-orogenic extension: Example from the northern Tyrrhenian Sea (Italy): Journal of Geophysical Research, v. 103, p. 12123-12160.

Kampman N., Burnsid, N.M., Shipton Z.K., Chapman H.J., Nicholl J.A., Ellam R.A., Bickle M.J., 2012. Pulses of carbon dioxide emissions from intracrustal faults following climatic warming: Nature Geoscience, v. 5, p. 352–358.

Karlstrom K.E., Crossey L.J., Hilton D.R., Barry P.H., 2013, Mantle ^{3}He and CO_2 degassing in carbonic and geothermal springs of Colorado and implications for neotectonics of the Rocky Mountains: Geology, v. 41, p. 495-498.

Kele S., Özkul M., Fórizs I., Gökgöz A., Baykara M.O., Alçiçek M.C., Németh T., 2011, Stable isotope geochemical study of Pamukkale travertines: new evidences of low-temperature non-equilibrium calcite–water fractionation: Sedimentary Geology, v. 238, p. 191–212.

Kele S., Breitenbach S.F.M., Capezzuoli E., Nele Meckler A., Ziegler M., Millan I.M., Kluge T., Deák J., Hanselmann K., John C.M., Yan H., Liu Z., Bernasconi S.M., 2015, Temperature dependence of oxygen- and clumped isotope fractionation in carbonates: a study of travertines and tufas in the 6-95°C temperature range: Geochimica et Cosmochimica Acta, v. 168, p. 172-192.

Kinsman D.J.J., 1969, Modes of formation, sedimentary associations, and diagnostic features of shallow-water and supratidal evaporates: AAPG Bulletin, v. 53, p. 830–840.

Laurenzi M.A., Braschi E., Casalini M., Conticelli S., 2015, New ^{40}Ar-^{39}Ar dating and revision of the geochronology of the Monte Amiata Volcano, Central Italy: Italian Journal of Geosciences, v. 134, p. 255-265.

Liotta D., Ruggieri G., Brogi A., Fulignati P., Dini A., Cardini I., 2010, Migration of geothermal fluids in extensional terrains: the ore deposits of the Boccheggiano-Montieri area (southern Tuscany, Italy): International Journal of Earth Sciences, v. 99, p. 623–644.

Manfr, L., Masi U., Turi B., 1976, La composizione isotopica dei travertini del Lazio: Geologica Romana, v. 15, p. 127–174.

Malinverno A., Ryan W.B.F., 1986, Extension in the Tyrrhenian Sea and shortening in the Apennines as result of arc migration driven by sinking of the lithosphere: Tectonics, v. 5, p. 227-254.

Marroni M., Moratti G., Costantini A., Conticelli S., Benvenuti M.G., Pandolfi L., Bonini M., Cornamusini G., Laurenzi M.A., 2015, Geology of the Monte Amiata region, Southern Tuscany, Central Italy: Italian Journal of Geosciences, v. 134, p. 171-199.

Nappi G., Renzulli A., Santi P., Gillot P.Y., 1995, Geological evolution and geochronology of the Vulsini Volcano District (Central Italy): Bollettino della Società Geologica Italiana, v. 114, p. 599-613.

Noiriel C., Renard F., Doan M.-L., Gratier J.-P., 2010, Intense fracturing and fracture sealing induced by mineral growth in porous rocks. Chemical Geology, v. 269, p. 197–209.

Ortí F., Rosell L., Playà E., Salvany J.M., 2011, Meganodular anhydritization: a new mechanism of gypsum to anhydrite conversion (Palaeogene–Neogene, Ebro Basin, North-east Spain): Sedimentology, v. 59, p. 1257–1277.

Özkul M., Kele S., Gökgöz A., Shen C.-C., Jones B., Baykara M.O., Fórizs I., Németh T., Chang Y.-W., Alçiçek M.C., 2013, Comparison of the Quaternary travertine sites in the Denizli extensional basin based on their depositional and geochemical data: Sedimentary Geology, v. 294, p. 179-204.

Patacca E., Sartori R., Scandone P., 1990, Tyrrhenian basin and Apenninic arcs: kinematic relation since late Tortonian times: Memorie della Società Geologica Italiana, v. 45, p. 425-451.

Pauselli C., Barchi M.R., Federico C., Magnani B., Minelli G., 2006, The crustal structure of the Northern Apennines (central Italy): an insight by the CROP03 seismic line: American Journal of Science, v. 306, p. 428-450.

Pentecost A., 2005. Travertine. Springer-Verlag, Berlin Heidelberg (445 pp.).

Ramberg H., 1964, Selective buckling of composite layers with contrasted rheological properties, a theory for simultaneous formation of several orders of folds: Tectonophysics, v. 1, p. 307-341.

Rimondi V., Costagliola P., Ruggieri G., Benvenuti M., Boschi C., Brogi A., Capezzuoli E., Morelli G., Gasparon M., Liotta D., 2015, Investigating fossil hydrothermal systems by means of fluid inclusions and stable isotopes in banded travertine: an example from Castelnuovo dell'Abate (southern Tuscany, Italy): International Journal of Earth Sciences, doi: 10.1007/s00531-015-1186-y.

Rezende M.F., Pope M.C., 2015, Importance of depositional texture in pore characterization of subsalt microbialite carbonates, offshore Brazil: Geological Society, London, Special Publications, v. 418, p. 193-207.

Rihs S., Condomines M., Poidevin J.L., 2000, Long-term behaviour of continental hydrothermal systems: U-series study of hydrothermal carbonates from the French Massif Central (Allier Valley): Geochimica et Cosmochimica Acta, v. 64, p. 3189–3199.

Ronchi P., Cruciani F., 2015, Continental carbonates as a hydrocarbon reservoir, an analog case study from the travertine of Saturnia, Italy: AAPG Bulletin, v. 99, p. 711–734.

Rossetti F., Tecce F., Billi A., Brilli M., 2007, Patterns of fluid flow in the contact aureole of the late Miocene Monte Capanne pluton (Elba Island, Italy): the role of structures and rheology: Contributions to Mineralogy and Petrology, v. 153, p. 743-760.

Rossetti F., Balsamo F., Villa I.M., Bouybaouenne M., Faccenna C., Funiciello R., 2008, Pliocene–Pleistocene HT–LP metamorphism during multiple granitic intrusions in the southern branch of the Larderello geothermal field (southern Tuscany, Italy): Journal of the Geological Society, London, v. 165, p. 247-262.

Rossetti F., Aldega L., Tecce F., Balsamo F., Billi A., Brilli M., 2011, Fluid flow within the damage zone of the Boccheggiano extensional fault (Larderello–Travale geothermal field, central Italy):

structures, alteration and implications for hydrothermal mineralization in extensional settings: Geological Magazine, v. 148, p. 558-578.

Seard C., Camoin G., Rouchy J.-M., Virgone A., 2013, Composition, structure and evolution of a lacustrine carbonate margin dominated by microbialites: Case study from the Green River formation (Eocene; Wyoming, USA): Palaeogeography Palaeoclimatology Palaeoecology, v. 381–382, p. 128–144.

Shen C.-C., Cheng H., Edwards R.L., Moran S.B., Edmonds H.N., Hoff J.A., Thomas R.B., 2003, Measurement of attogram quantities of ^{231}Pa in dissolved and particulate fractions of seawater by isotope dilution thermal ionization mass spectroscopy: Analytical Chemistry, v. 75, p. 1075-1079.

Shen C.-C., Wu C.-C., Cheng H., Edwards R.L., Hsieh Y.-T., Gallet S., Chang C.-C., Li T.-Y., Lam D.D., Kano A., Hori M., Spötl C., 2012, High-precision and high resolution carbonate 230Th dating by MC-ICP-MS with SEM protocols: Geochimica et Cosmochimica Acta, v. 99, p. 71–86.

Soete J., Kleipool L.M., Claes H., Claes S., Hamaekers H., Kele S., Ozkul M., Foubert A., Reijmer J.J.G., Swennen R., 2015, Acoustic properties in travertines and their relation to porosity and pore types: Marine and Petroleum Geology, v. 59, p. 320-335.

Soligo M., Tuccimei P., Barberi R., Delitala M.C., Miccadei E., Taddeucci A., 2002, U/Th dating of freshwater travertine from Middle Velino Valley (Central Italy): paleoclimatic and geological implications. Palaeogeography Palaeoclimatology Palaeoecology, v. 184, 147-161.

Toker E., Kayseri-Özer M.S., Özkul M., Kele S., 2015, Depositional system and palaeoclimatic interpretations of Middle to Late Pleistocene travertines: Kocabaş, Denizli, south-west Turkey. Sedimentology, v. 62, p. 1360-1383.

Uysal I.T., Feng Y., Zhao J.X., Altunel E., Weatherley D., Karabacak V., Cengiz O., Golding S.D., Lawrence M.G., Collerson K.D., 2007, U-series dating and geochemical tracing of late Quaternary travertine in co-seismic fissures: Earth and Planetary Science Letters, v. 257, p. 450–462.

Uysal I.T., Feng Y., Zhao J.X., Isik V., Nuriel P., Golding S.D., 2009. Hydrotermal CO_2 degassing in seismically active zones during the late Quaternary: Chemical Geology, v. 265, p. 442–454.

Vignaroli G., Aldega L., Balsamo F., Billi A., De Benedetti A.A., De Filippis L., Giordano G., Rossetti F., 2015. A way to hydrothermal paroxysm, Colli Albani Volcano, Italy. Geological Society of America Bulletin, v. 127, p. 672-687.

Wedepohl K., 1995, The composition of the continental crust: Geochimica et Cosmochimica Acta, v. 59, p. 1217–1239.

Wiltschko D.V., Morse J.W., 2001, Crystallization pressure versus "crack seal" as the mechanism for banded veins: Geology, v. 29, p. 79-82.

Zanchi A., Tozzi M., 1987, Evoluzione paleogeografica e strutturale recente del bacino del Fiume Albegna (Toscana meridionale): Geologica Romana, v. 26, p. 305–325.

Chapter 5

Conclusions

This PhD study provides valid tools to clarify and better understand the problematic related to the feedback interaction between travertine deposition, hydrothermal circulation, Quaternary tectonics, and paleoclimate oscillations, presenting also some innovative results. This study on the Quaternary travertine deposits from the Albegna basin, Southern Tuscany, Italy, aimed at providing insights (i) at the scale of the single travertine deposit, (ii) at the scale of the whole Albegna basin hydrothermal setting, (iii) at the regional scale.

The answers to the main aims of this work are here synthetized:

(1) The Albegna basin is characterized by the coexistence of two main types of travertine deposits: plateaus and fissure ridges (which are different in volume and geometry), and the presence of active travertine deposition at the Saturnia spring. The 100 meters thick, travertine deposit of Poggio Semproniano is a good example of travertine plateau, characterized by sub-horizontal bedded travertine, lying on top of the Pliocene-Quaternary marine sequence or of the Scaglia Toscana. On the opposite, the Semproniano giant vein is a good example of fissure ridge travertine, characterized by a 50 m wide sub-vertical sparry banded travertine, in contact with the Scaglia Toscana and Pliocene-Quaternary marine sequence in its north-western part and with Diaspri unit in its south-eastern part. Saturnia village travertine deposit is characterized by the coexistence of banded and bedded travertine, with steeply dipping banded travertine cross-cutting the bedded travertine.

(2) Travertine deposits and the present-day thermal spring are aligned along a N-S structural feature consisting of an articulate pattern of extensional and strike-slip faults. Many travertine deposits and travertine-related structures, like the Semproniano giant vein, the calcite-filled

veins at Poggio Semproniano, the karst-fractures at Poggio Semproniano and Poggio I Piani, and the banded travertine at Saturnia and I Vignacci) are distributed along fault segments and at fault-fault intersections. The N-S-striking fault system, marking the contact between the Tuscan Domain units and the Plio-Quaternary marine deposits, represents the main structure in the region and probably forms part of a major N-S-striking structural system that, toward the north, bounds the Mesozoic carbonate ridge of the Mt. Labbro (e.g. Brogi, 2004). The right-lateral strike-slip to transtensional faults that are oriented between E-W and NW-SE are subordinate with respect to the master N-S-striking fault and affects some of the travertine deposits. The NW-SE orientation of the Semproniano fissure ridge, the calcite-filled veins of Poggio Semproniano, the karstified fractures of Poggio Semproniano and Poggio I Piani, and the banded travertine of Saturnia and I Vignacci suggests that all these structures developed under a NE-SW stretching process during Quaternary time.

(3) Our geochronological data allow dating the beginning of the tectonic-hydrothermal processes as middle Pleistocene. The oldest travertine dated, banded travertine from the Semproniano giant vein provided an age of around 650 ka, whereas the youngest sample, bedded travertine from the Pian di Palma quarry, is about 33 ka old.

(4) All the sample analyzed are characterized by positive to highly-positive $\delta^{13}C$ and negative $\delta^{18}O$ values which are indicative of a hydrothermal fluid source derived by the mixing of deep magmatic fluids and meteoric waters mixed with CO_2 originated from limestone decarbonation (Gonfiantini et al., 1968; Guo et al., 1996). Our $\delta^{13}C$ and $\delta^{18}O$ values are comparable to those reported in previous studies (e.g., Minissale, 2004 and references therein) and are in the range typical of thermogene travertines deposited by present-day thermal springs of central Italy (Minissale, 2004; Gandin and Capezzuoli, 2008). Estimated temperatures for parental fluids span between about 71°C for the banded travertine from the Semproniano village and about 22 °C for the bedded travertine from the Pian di Palma quarry. The rather homogeneous Sr- and Nd-isotope values are indicative of a unique reservoir for

the deposition of travertines and calcite veins. Sr- and Nd- isotope values are different from isotopic signature of Mt. Amiata volcanic rocks (Conticelli et al. 2015). In particular, our Sr isotope values are in the range of those obtained for the Mesozoic sedimentary units of the Tuscan Nappe (e.g. Cortecci and Lupi, 1994) and for the hydrothermal springs of Saturnia (Barbagli et al., 2013). Accordingly, we consider the Mesozoic limestones of the Albegna area as the main reservoir of the hydrothermal system and the probable source for the chemical signature of the studied carbonates.

The major results obtained through this study allowed answering several questions:

(1) Travertines in the Albegna basin formed different morphologies, plateaus and fissure ridges travertines, characterized by different volumes (big volumes for plateau travertines, small volumes for fissure ridge travertines). Detailed geochronological data on the Semproniano giant vein, allowed recognizing no systematic growth direction and no systematic age sequence during its deposition, and that the vein grew with average rates ranging between ca. 10^{-2} and 10^{-3} mm a^{-1}. These rates are consistent with previously-estimated rates for banded travertines within fissure ridges located elsewhere (about 10^{-2} mm a^{-1}; Uysal et al., 2007; Mesci et al., 2008; Gratier et al., 2012; De Filippis e al., 2013; Frery et a., 2015). This result proves that the thickness of the Semproniano vein in not related to a fast growth rate but rather to the duration of the hydrothermal activity, one order of magnitude larger than in other fissure ridges (e.g., Altunel and Karabacak, 2005; Uysal et al., 2007, 2009).

(2) Syn-diagenetic non-tectonic contractional deformation in thermogene travertines have been documented for the first time. This work provides evidences that both the veins and their folds, from the Pianetti and Pian di Palma travertines, are secondary (post-depositional) structures with respect to the primary porous beds. In this view, the studied travertine and vein undulations are interpreted as enterolithic folds (i.e., the product of post-depositional syn-diagenetic deformation) that cannot be thought as of tectonic origin both for their non-

cylindrical (domal) shape and for the substantial absence of other compressional structures in the late Miocene-Pleistocene host sediments of the Albegna basin (Zanchi and Tozzi, 1987; Bosi et al., 1996; Carmignani et al., 2013). These syn-diagenetic processes evidently changed some important properties of the pristine (pre-diagenesis) travertine deposits, including sedimentary fabric, porosity, stratigraphic-chronological sequence, and rheology. In particular, recent discoveries of hydrocarbon major reserves in subsalt porous travertine-like rocks along the Atlantic Brazilian and Angolan margins impose a better understanding not only of deposition, but also of diagenetic (porosity vs. cementation) history of travertines.

(3) The travertine deposits of the Albegna basin are a marker of the hydrothermal activity that evolved in space and time along a N-S structural alignment. The spatio-temporal reconstruction of the hydrothermal system allowed recognizing a longevity of around 650 ka with, moving from north to south, a travertine deposition that becomes younger and at lower altitudes. At the scale of the basin it is evident a change of isotopic signature, with a general decreasing trend of $\delta^{13}C$ and increasing trend of $\delta^{18}O$ from older to younger travertine deposits. The highest $\delta^{13}C$ values belong to the oldest travertines (the Semproniano fissure ridge), whereas the lowest $\delta^{13}C$ are found in the active thermal spring of Bagni di Saturnia. This trend is not evident at the scale of the single deposit. For example, the Semproniano giant vein does not show linear correlations between isotopic signature and age of deposition.

(4) The scenario for the genesis of the travertine deposition in the Albegna basin is a structurally controlled pathway (faults and fractures) for the circulating mineralizing fluids during the Quaternary. Dominant meteoric fluids interacted with the carbonate reservoir of the Tuscan Nappe sequence and were heated at depth, where the heat source is maintained by the regional geothermal anomaly. The main travertine-depositing centers changed its position horizontally (along the N-S structural alignment) and vertically (lowering of the depositional altitudes), reaching the present-day deposition center at the Bagni di Saturnia locality. The travertines

show decreasing $\delta^{13}C$ and increasing of the $\delta^{18}O$, consistent with an increasing dilution of endogenic fluids by meteoric fluids moving away from the Amiata Mt. geothermal field.

(5) Our geochronological dataset, combined with those from other works (e.g., Brogi et al., 2012; Rimondi et al., 2015), suggests a scenario of diffuse hydrothermalism around the Mt. Amiata area during the Upper Pleistocene. In particular, our dataset indicates that travertine deposition predated the onset of the volcanic paroxysm in the Mt. Amiata region.

(6) Our U/Th ages, integrated with recent studies on travertine deposits (e.g., Brogi et al., 2010a) and other hydrothermal-related deposits (Bellani et al., 2004; Brogi and Fabbrini, 2009; Liotta et al., 2010; Rossetti et al., 2011), document that extensional tectonics in Tuscany, previously thought as quiescent since about Pliocene time, is indeed younger (Late Pleistocene time, at least), with extensional-to-transtensional faulting acting a primary role into the endogenic fluid circulation that fed and still feeds some geothermal fields;

(7) The recognition of transverse structures (i.e., transversally to the Apennines trend) found in the Albegna basin impose to reconsider the models claimed for the localization and evolution of several hydrothermal settings along the Tyrrhenian margin. In particular, the (re-)activation of transverse fault systems, perpendicular-to-oblique to the strike of the main orogenic fronts and fault-banded basins, seems to provide preferential pathways for hydrothermal outflow at least since late Pleistocene time. These originally-shallow faults were re-activated and enhanced, due to the change in the stress tensor induced by post-orogenic crustal thinning, so to rupture downward into the crust and generate the pathway for hydrothermal fluid ascension.

(8) Geochronological data compared with major paleoclimate indicators and events at global and regional scale show that the majority of Albegna basin travertine and associated mineralization ages falls within the interglacial periods. This evidence suggests that the travertines and travertine-related structures preferentially formed during warm (and humid) climate periods characterized by high-stand conditions of the water table. Ages of deposition

suggest that high stand of the water table was a primary influencing factor in the travertine deposition.

Long living hydrothermal systems in tectonically active settings, such as the Albegna basin, are key areas to define the feedback relationships between hydrothermal circulation, Quaternary tectonic and paleoclimate oscillations.

Systematic geochronological constraints, geochemical characterization, and the determination of fracture and fault systems controlling the fluid circulation should be investigated in details in future studies on travertine deposits. Nevertheless, higher resolution geochronology, with smaller associated error, is necessary for correlating travertine deposition not only with paloeclimate oscillations, but also with other processes such as eustatism, morphological molding and groundwater level changes.

Finally, future studies on travertine as analogs for hydrocarbon exploration should consider the importance of diagenesis for the study of porosity.

References

Acocella V., Funiciello R., 2006. Transverse systems along the extensional Tyrrhenian margin of central Italy and their influence on volcanism. Tectonics 25, TC2003. http://dx.doi.org/10.1029/2005TC001845.

Altunel E., Karabacak V., 2005. Determination of horizontal extension from fissure-ridge travertines: a case study from the Denizli Basin, southwestern Turkey. Geodinamica Acta, 18, 333–342.

Barbagli A., Brogna F.N.A., Callegari I., Guastaldi E., Liali G., Marsico N., Rezza C., Trotta M., 2013. Approccio multi-isotopico ed idrogeochimico per la caratterizzazione di acque termali: il caso di Saturnia (GR). Italian Journal of Groundwater, AS07029, 025-040, DOI 10.7343/AS-049-13-0076.

Bosi C., Messina P., Rosati M., Sposato A., 1996. Età dei travertini della Toscana meridionale e relative implicazioni neotettoniche. Memorie della Società Geologica Italiana, 51, 293-304.

Brogi A., 2004. Miocene extension in the inner Northern Apennines: the Tuscan Nappe megaboudins in the Mt. Amiata geothermal area and their influence on Neogene sedimentation. Bollettino della Società Geologica Italiana, 123, 513-529.

Carmignani L., Conti P., Cornamusini G., Pirro A. 2013. Geological map of Tuscany (Italy). Journal of Maps, 9:4, 487-497, DOI:10.1080/17445647.2013.820154

Conticelli S., Boari E., Burlamacchi L., Cifelli F., Moscardi F., Laurenzi M.A., Ferrari Pedraglio L., Francalanci L., Benvenuti M.G., Braschi E., Manetti P., 2015. Geochemistry and Sr–Nd–Pb isotopes of Monte Amiata Volcano, Central Italy: evidence for magma mixing between high-K calc-alkaline and leucititic mantle-derived magmas. Italian Journal of Geosciences 134, 266–290.

Cortecci G., Lupi L., 1994. Carbon, oxygen and strontium isotope geochemistry of carbonate rocks from the Tuscan Nappe, Italy. Mineralogia et Petrographica acta, 37, 63-80.

De Filippis L., Faccenna C., Billi A., Anzalone E., Brilli M., Soligo M., Tuccimei P., 2013. Plateau versus fissure ridge travertines from Quaternary geothermal springs of Italy and Turkey: Interactions and feedbacks between fluid discharge, paleoclimate, and tectonics. Earth-Science Reviews, 123, 35-52.

Faccenna C., Funiciello R., Bruni A., Mattei M., Sagnotti L., 1994. Evolution of a transfer-related basin: the Ardea basin (Latium, central Italy). Basin Research, 6, 35-46.

Frery E., Gratier J.P., Ellouz-Zimmerman N., Loiselet C., Braun J., Deschamps P., Blamart D., Hamelin B., Swennen R., 2015. Evolution of fault permeability during episodic fluid

circulation: Evidence for the effects of fluid–rock interactions from travertine studies (Utah–USA). Tectonophysics, http://dx.doi.org/10.1016/j.tecto.2015.03.018.

Gandin A., Capezzuoli E., 2008. Travertine versus Calcareous tufa: distinctive petrologic features and related stable isotopes signature. Il Quaternario Italian Journal of Quaternary Science, 21, 125-136.

Gonfiantini R., Panichi C., Tongiorgi E., 1968. Isotopic disequilibrium in travertine deposition. Earth and Planetary Science Letters, 5, 55-58.

Gratier J. P., Frery E., Deschamps P., Røyne A., Renard F., Dysthe D., Ellouz-Zimmerman N., Hamelin B., 2012. How travertine veins grow from top to bottom and lift the rocks above them: the effect of crystallization force. Geology, 40, 1015–1018.

Guo L., Andrews J., Riding R., Dennis P., Dresser, Q., 1996. Possible microbial effects on stable carbon isotopes in hot travertine. Journal of Sedimentary Research, 66, 468-473.

Jolivet L., Faccenna C., Goffé B., Mattei M., Rossetti F., Brunet C., et al., 1998. Midcrustal shear zones in post-orogenic extension: example from the northern Tyrrhenian Sea (Italy). Journal of Geophysical Research, 103, 12123–12160.

Malinverno A., Ryan W., 1986. Extension in the Tyrrhenian sea and shortening in the Apennines as result of arc migration driven by sinking of the lithosphere. Tectonics, 5, 227-245.

Mesci L.B., Gürsoy H., Tatar O., 2008. The evolution of travertine masses in the Sivas area (central Turkey) and their relationships to active tectonics: Turkish Journal of Earth Sciences, 17, 219–240.

Minissale A., 2004. Origin, transport and discharge of CO_2 in central Italy. Earth-Science Reviews, 66, 89-141.

Uysal I.T., Feng Y., Zhao J.X., Altunel E., Weatherley D., Karabacak V., Cengiz O., Golding S.D., Lawrence M.G., Collerson K.D., 2007. U-series dating and geochemical tracing of late Quaternary travertine in co-seismic fissures: Earth and Planetary Science Letters, 257 (3–4), 450–462.

Uysal I.T., Feng Y., Zhao J.X., Isik V., Nuriel P., Golding S.D., 2009. Hydrotermal CO_2 degassing in seismically active zones during the late Quaternary. Chemical Geology, 265, 442–454.

Zanchi A., Tozzi M., 1987. Evoluzione paleogeografica e strutturale recente del bacino del fiume Albegna (Toscana meridionale). Geologica Romana 26, 305–325.